

# PURDUE UNIVERSITY

RAYMOND VISKANTA  
W.F.M. GOSS DISTINGUISHED  
PROFESSOR OF ENGINEERING

March 9, 1994

Dr. Mohsen Khatib-Rahbar  
Energy Research Inc.  
P.O. Box 2034  
Rockville, MD 20847

Ref: NRC and NRC/Westinghouse AP600 PCCS Scaling Meeting  
Westinghouse Energy Center, Monroeville, PA  
February 22-24, 1994.

Dear Mohsen:

This is a follow-up to the discussion concerning the thermal-hydraulics scaling issues at the referenced meeting. I have spent considerable time in the Purdue University Potter Engineering Library and going through my files looking for up to-date information on turbulent natural, forced and mixed convection heat transfer relevant to external and internal (annular channel) heat and mass (evaporation) transfer. In this letter I will provide a brief summary on my literature review findings and highlight my concerns about Westinghouse's approach in predicting external and internal thermal-hydraulics in the AP600 and the integral test facilities that I expressed at the meeting. For the sake of clarity, I will keep my remarks separately.

## Findings of Review Literature

### External

Reasonably up-to-date discussion of mixed convection heat transfer is given by Chen and Armaly [1] and Pethukhov and Polyakov [2]. Correlations are available for horizontal and vertical plates, but experimental data under turbulent flow conditions are very limited. The data are particularly meager for turbulent free and mixed convection under at high Rayleigh or Grashof numbers for free convection and for high Richardson (Grashof over Reynolds number squared) numbers under mixed convection conditions.

For example, Siebers et al. [3] correlate their experimental data for turbulent free convection from a vertical plate by an equation

$$Nu_x = 0.098 Gr_x^{1/3} (T_w/T_\infty)^{-0.14} \quad (1)$$

9406030087 940429  
PDR ADDCK 05200003  
A PDR

where  $x$  is the vertical distance,  $Gr_x$  is the local Grashof number based on the local coordinate  $x$  and  $T_w$  and  $T_\infty$  are the wall and free-stream temperatures, respectively. Their experimental data extend to  $Gr_x = 1.86 \times 10^{12}$ . These values are higher than the range covered by Vliet (1969) to which Westinghouse referred (see Figure 1 of presentation by Dan Spencer). The data of Vliet were obtained under a constant heat flux boundary condition, and, therefore, he used a Grashof number ( $Gr_x^*$ ) which is based on  $q_w$  and not  $T_w - T_\infty$  to define the Grashof number. Even if the temperature dependence of the thermophysical properties on temperature (i.e., factor  $(T_w/T_\infty)^{-0.14}$ ) is ignored, the coefficient of 0.098 differs from the value of 0.13 used by Westinghouse (see Equation 1 in D. Spencer's notes).

A number of mixed turbulent convection correlations are presented by Chen and Armaly [1, pp. 14-24 to 14-26] and need not be discussed here in detail. Some of these correlations are purely numerical (theoretical) and others have received some experimental validation. In summary, the correlations proposed by Westinghouse (Equation 5 in D. Spencer's notes), is different from those published in the literature. What is probably more significant is that the local Nusselt number for a vertical plate is considerably higher than for a horizontal flat plate, and this suggests that Equation (5) in Spencer's notes can not be used for both orientations. In addition, there is a need to distinguish between the flows where buoyancy aids and where it opposes forced flow.

### Internal

Heat transfer to fluids flowing in vertical tubes under conditions of mixed (forced and free) turbulent convection have shown to exhibit marked departures from the case of purely forced convection. Significant degradation or enhancement of heat transfer can occur, depending on the flow orientation and the degree of buoyancy influence. Several state-of-the-art discussions are available and include those of Pethukhov et al. [4], Aung [5], Gebhart et al. [6], Pethukhov and Polyakov [2], Jackson et al. [7], Cotton and Jackson [8] and Poskas and Vilemas [9]. Some of these reviews are very extensive and may include as many as a hundred references. The review by Aung [5] cites 87 references and the one by Jackson et al. [7] is probably the most complete and cites 99 references. Unfortunately, the extensive experimental data reported are for vertical pipes and not parallel plate channels and fluids other than air.

For ascending flow in a uniformly heated vertical tube, an implicit expression for the Nusselt number ratio,  $Nu/Nu_F$  (Nusselt number for mixed turbulent convection  $Nu$  to Nusselt number for forced convection  $Nu_F$ ) has been recommended by Cotton and Jackson [10] of the form

$$\frac{Nu}{Nu_F} = \left[ \left| 1.0 \pm 8 \times 10^4 B \left[ \frac{Nu}{Nu_F} \right]^{-2} \right| \right]^{0.46} \quad (2)$$

where the + sign applies to descending flow and the - sign to ascending flow. The buoyancy parameter  $B$  is defined as

$$B = \frac{Gr^*}{Re^{3.425} Pr^{0.8}} \quad (3)$$

In Eq.(3)  $Gr^*$  is the Grashof number based on the wall heat flux  $q_w$  (i.e.,  $Gr^* = g\beta q_w D^4 / k_v^2$ ), and  $Re$  is the Reynolds number based on the diameter  $D$  as the characteristic length. The Nusselt number for forced convection,  $Nu_F$ , is calculated from the Dittus-Boelter equation,

$$Nu_F = 0.023 Re^{0.8} Pr^{0.4} \quad (4)$$

Equation (2) has been compared with a body of experimental data for turbulent mixed convection heat transfer to gases in tubes. The details can be found in Cotton and Jackson [10], Jackson et al. [7] and Poskas and Vilemas [9].

The buoyancy parameter  $B$  defined by Eq.(3) in the turbulent mixed convection regime is based on the consideration of the modified shear stress distributions which occur in the near-wall region in response to buoyancy forces. Both the buoyancy parameter  $B$  and the semi-empirical equation for the Nusselt number ratio,  $Nu/Nu_F$ , given by Eq.(2) are derived on the assumption of fully-developed hydrodynamic and thermal conditions; however, in ascending mixed convection flows, very long development lengths ( $\sim 100 D$ ) are found to occur both experimentally and numerically [10]. It should be noted that Eq.(2) gives a discontinuity in Nusselt number for heated upward flow when  $Gr^*/Re^{3.425} Pr^{0.8} = 3 \times 10^{-6}$ . The published results show that in ascending flow heat transfer may be either impaired with respect to forced convection (at moderate wall heat fluxes) or enhanced (at high wall heat fluxes); whereas, in descending flow, heat transfer is enhanced at all imposed heat fluxes. The results reported here raise technical issues concerning the validity of the computational mixed convection heat transfer model employed by Westinghouse to calculate turbulent mixed convection heat transfer in the annulus between the containment shell and the air baffle (see Equation 5 given in the notes of D. Spencer).

I was not successful in identifying any theoretical or experimental results for turbulent mixed convection heat transfer in an axisymmetrically heated vertical duct that is formed by one uniform temperature wall and one adiabatic wall. This physical situation would be quite close to the case of a dry containment wall. For laminar flow the experimental local convective heat transfer results in a two-dimensional axisymmetrically heated vertical channel where represented by an empirical correlation [11],

$$Nu_x / Re_x^{1/2} = \left[ (0.296)^n + (0.359 Ri_x^{1/4})^n \right]^{1/n} \quad (5)$$

where  $Ri_x = Gr_x / Re_x^2$  is the local Richardson number. The value of  $n = 2.0$  gave the best correlation for the experimental data. The experimental local Reynolds number  $Re_x$  was based on  $u_0$  which is the center line velocity at the inlet section of the duct. Note that according to Eq.(5) the relevant scaling parameters for local heat transfer along the heated vertical wall of a vertical parallel-plate channel are the local Reynolds number  $Re_x$  and the local Richardson number  $Ri_x$  and not the Reynolds number based on the hydraulic diameter ( $Re_d$ ) and the local Grashof number  $Gr_x$  as proposed by Westinghouse (see Equations 1, 2 and 5 of the notes distributed by D. Spencer). No turbulent mixed (combined) heat transfer in an asymmetrically heated vertical channel could be identified in the published literature.

The experimental work of Kapoor and Jaluria [12] shows that the relevant heat transfer scaling parameter is the Richardson ( $Ri_D = Gr_D/Re_D^2$ ) number based on the width of the slot  $D$  and the horizontal distance  $L$  to width  $D$  ratio,  $L/D$ . Different correlations were obtained for the ceiling, wall and ceiling plus wall. This suggests to me that the correlation used by Westinghouse does not contain the relevant scaling parameters. The published results further show that the Nusselt number is not a monotonically decreasing function of the distance along ceiling and wall as measured from the slot. This indicates to me that the correlation used by Westinghouse would not capture the correct trends of the heat transfer coefficient variation along the dome and cylindrical part of the containment wall.

### Validity of Heat and Mass Transfer Analogy

Relatively little research attention has been focused on the heat and mass transfer analogy which is being used by Westinghouse (see Equation 7 in notes provided by D. Spencer) to relate the mass transfer coefficient to the heat transfer coefficient in the annular gap. Greiner and Winter [13] studied theoretically and experimentally the defects of heat and mass transfer analogy for laminar and turbulent forced convection along a horizontal flat plate and showed that significant defects in analogy exist when the normalized driving force of the evaporation process is relatively large. To eliminate the effect in the heat and mass transfer analogy a correction needs to be made in the film theory of Ackermann. This suggests that the heat, mass and momentum correction factors used by Westinghouse may not be appropriate.

### Technical Issues

A number of technical issues were raised at the meeting concerning Westinghouse's approach in modeling internal and external heat transfer in the AP600 containment. Here, I would like to repeat in writing some of the questions I raised at the meeting, provide relevant literature citations and elaborate on my technical concerns.

1. The correlation used by Westinghouse for external mixed convection heat transfer [Equations (1), (2), (5) and (6) in the notes of D.R. Spencer] are inconsistent in form with published correlations [1, 12] (see also Equation 5 above). The relevant scaling parameters are the local Reynolds ( $Re_x$ ) and the local Richardson ( $Ri_x$ ) numbers, and the location of the coordinate axis  $x$  needs to be clearly defined for the correlations to be applicable.
2. What are the relevant thermal-hydraulics scaling parameters for buoyancy (temperature and concentration difference) driven flow in the downcomer and the upcomer of the PCCS? Westinghouse has made no attempt to identify the relevant scaling (dimensionless) parameters for the physical system considered. For buoyancy driven flow the Reynolds number is not a relevant dimensionless parameter, because the velocity is not known and hence the Reynolds number can't be specified *a priori*.
3. For internal mixed convection in the channel formed by the containment wall and the air baffle, the combined (free and forced convection) Nusselt number used by Westinghouse [Equations (3), (4), (5) and (6) in the notes of D.R. Spencer] is inconsistent in form with the published results [2, 5] for internal mixed convection (see also Equation 2 given above). Equation (4) used by Westinghouse is for forced convection heat transfer along a vertical plate (i.e., when the effects of buoyancy are not important) and not for flow and heat transfer in a vertical, parallel-plate channel after the two boundary layers on the

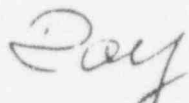


vertical walls have merged. I am afraid that Westinghouse is attempting to force their integral test data results to match correlations of highly questionable form that have not been used previously in the published mixed convection heat transfer literature [2, 5].

4. The heat and mass transfer analogy defined by Westinghouse [Equations (7) and (8) in notes of D.R. Spencer] and its modification to account for evaporation/condensation are based on a laminar film theory [14]. There is no evidence in the literature, at least that I could find, to suggest that these corrections are appropriate for physical situations relevant to AP600 PCCS. I feel uncomfortable with the equations used by Westinghouse, because the corrections are of theoretical nature, have not been developed for turbulent flow and have not been validated for the problems being considered. I am concerned that the analogy (as it now stands) is being misapplied, and I do not have much confidence in its use as it now stands. My question is how can Westinghouse address my concerns?

Please do not hesitate to call me if you or NRC have any questions or I can provide any additional information.

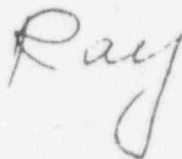
Sincerely,



R. Viskanta

RV/fb

P.S. I am enclosing with this letter some of the papers that I have cited in my remarks. Some references are just too long to be copied in full.



## References

1. T.S. Chen and B.F. Armaly, "Mixed Convection in External Flow, in *Handbook of Single-Phase Convection Heat Transfer*, edited by S. Kakac, R.K. Shah and W. Aung, John Wiley and Sons, New York, 1987, Section 14.
2. B.S. Pethukhov and A.F. Polyakov, *Heat Transfer in Turbulent Mixed Convection*, Hemisphere Publishing Corp., New York, 1988.
3. D.L. Siebers, R.J. Moffat and R.G. Schwind, "Experimental, Variable Properties Natural Convection from a Large, Vertical, Flat Surface," *J. Heat Transfer*, Vol. 107, pp. 124-132, 1985.
4. B.S. Pethukhov, A.F. Polyakov and O.G. Martynenko, "Buoyancy Effect on Heat Transfer in Forced Channel Flow," in *Heat Transfer — 1982*, Hemisphere Publishing Corp., Washington, 1982, Vol. 1, pp. 343-362.
5. W. Aung, "Mixed Convection in Internal Flows," in *Handbook of Single-Phase Convection Heat Transfer*, edited by S. Kakac, R.K. Shah and W. Aung, John Wiley and Sons, New York, 1987, Section 15.
6. B. Gebhart, Y. Jaluria, R.L. Mahajan and B. Sammakia, *Buoyancy-Induced Flows and Transport*, Hemisphere Publishing Corp., Washington, 1988, Chapter 10.
7. J.D. Jackson, M.A. Cotton and B.P. Axcell, "Studies of Mixed Convection in Vertical Tubes," *Int. J. Heat Fluid Flow*, Vol. 10, pp. 7-15, 1989.
8. M.A. Cotton and J.D. Jackson, "Vertical Tube Air Flows in the Turbulent Mixed-Convection Regime Calculated by a Low-Reynolds-Number  $k-\epsilon$  Model," *Int. J. Heat Mass Transfer*, Vol. 33, pp. 275-286, 1990.
9. P. Poskas and J. Vilemas, "Mixed Convection in Channels," in *Power Engineering*, "Academia," Vilnius (1993), Nr. 3, pp. 22-25 (in Russian).
10. M.A. Cotton and J.D. Jackson, "Comparison Between Theory and Experiment for Turbulent Flow of Air in a Vertical Tube with Interaction," in *Mixed Convection Heat Transfer — 1987*, edited by V. Prasad, I. Catton and P. Cheng, ASME, New York, 1987, HTD-Vol. 84, pp. 43-50.
11. B.J. Beak, M.B. Younger, B.F. Armaly, and T.S. Chen, "Mixed Convection in a Two-Dimensional Axisymmetrically Heated Vertical Duct," in *Mixed Convection Heat Transfer — 1991*, edited by D.W. Pepper, B.F. Armaly, M.A. Ebdian and P.H. Oosthuizen, ASME, New York (1991), HTD-Vol. 163, pp. 37-43.
12. K. Kapoor and Y. Jaluria, "Mixed Convective Heat Transfer Characteristics of a Downward Turning Buoyant Ceiling Jet," in *Mixed Convection Heat Transfer — 1991*, edited by D.W. Pepper, B.F. Armaly, M.A. Ebdian and P.H. Oosthuizen, ASME, New York (1991), HTD-Vol. 163, pp. 9-17.
13. M. Greiner and E.R.F. Winter, "Analogy Defects of Mass, Heat, and Momentum Transfer in Evaporation Boundary-Layer Flow," in *Studies in Heat Transfer: A Festschrift for E.R. G. Eckert*, edited by J.P. Hartnett, T.J. Irvine, Jr., E. Pfender and E.M. Sparrow, Hemisphere Publishing Corp., Washington, 1979, pp. 41-53.
14. R.R. Bird, W.E. Stewart and E.N. Lightfoot, *Transport Phenomena*, John Wiley and Sons, New York (1960), pp. 659-666.

# HANDBOOK OF SINGLE-PHASE CONVECTIVE HEAT TRANSFER

Edited by

**Sadik Kakaç**

Department of Mechanical Engineering  
University of Miami  
Coral Gables, Florida

**Ramesh K. Shah**

Harrison Radiator Division  
General Motors Corporation  
Lockport, New York

**Win Aung**

National Science Foundation  
Washington, D.C.

A Wiley-Interscience Publication

**JOHN WILEY & SONS**

New York · Chichester · Brisbane · Toronto · Singapore

# 15

---

## MIXED CONVECTION IN INTERNAL FLOW

*Win Aung*

*National Science Foundation  
Washington, D.C.*

- 15.1 Introduction
- 15.2 Governing Equations and Parameters
- 15.3 **Laminar Mixed Convection in Vertical Ducts**
  - 15.3.1 Hydrodynamically and Thermally Fully Developed Flow in Vertical Circular Tubes
  - 15.3.2 Thermally Developing Flow in Vertical Circular Tubes
  - 15.3.3 Hydrodynamically and Thermally Developing Flow in Vertical Circular Tubes
  - 15.3.4 Hydrodynamically and Thermally Fully Developed Flow in Vertical Annuli
  - 15.3.5 Thermally Developing Flow in Vertical Annuli
  - 15.3.6 Hydrodynamically and Thermally Fully Developed Flow between Vertical Parallel Plates
  - 15.3.7 Hydrodynamically and Thermally Developing Flow between Vertical Parallel Plates
- 15.4 **Laminar Mixed Convection in Horizontal Ducts**
  - 15.4.1 Thermally and Hydrodynamically Fully Developed Flow in Horizontal Circular Tubes
  - 15.4.2 Thermally Developing Flow in Horizontal Circular Tubes
  - 15.4.3 Flow in Circular, Concentric Horizontal Annuli
  - 15.4.4 Thermally Fully Developed Flow between Horizontal Parallel Plates
  - 15.4.5 Thermally Developing Flow between Horizontal Parallel Plates
  - 15.4.6 Flow in Rectangular Horizontal Channels
- 15.5 **Transition from Laminar to Turbulent Flow**
  - 15.5.1 Transitional Upward Flow in Vertical Circular Tubes
  - 15.5.2 Transitional Flow in Horizontal Circular Tubes
- 15.6 **Turbulent Mixed Convection in Ducts**
  - 15.6.1 Vertical Ducts
  - 15.6.2 Horizontal Tubes

Nomenclature

References

Indications are that for buoyancy-aided flow, the mechanism of transition is similar to that in boundary-layer flow over a flat plate. Here, transition consists of the appearance of regular oscillations which gradually grow in extent and amplitude until the disturbance breaks into fluctuating motion that is characteristic of turbulent flow. For buoyancy-opposed flow, transition consists of an asymmetric flow (resulting from an originally symmetric fully developed flow) which gives rise to reversed flow on one side of the tube. The extent of the reversed flow increases in size as  $Gr_s/Re$  increases, leading to an eddying flow. The transition to an eddying motion occurs suddenly.

The flow oscillations that accompany the transition process lead to fluctuations in wall temperatures, and these can in turn be used to indicate transition. Using this approach, Hallman [12] found that for buoyancy-assisted, hydrodynamically fully developed flow (at tube entrance) in a UHF vertical circular tube, the location of transition depends on the heating rate and the flow rate. At a constant flow rate, an increase in heating rate causes the point of transition to travel upstream (i.e., down the tube). If the heating rate is held fixed, increasing the flow rate moves the transition point downstream. Based on Hallman's data, the following correlation may be used to predict the location of transition:

$$Gr_s Pr = 2664 Gz^{1.83} \quad (15.70a)$$

### 15.5.2 Transitional Flow in Horizontal Circular Tubes

In a horizontal circular tube, the transition to turbulent flow is strongly affected by the presence of secondary flow. With a high initial turbulence level at the entrance to the tube, the onset of secondary flow tends to suppress the turbulence, while at a low initial turbulence level, secondary flow tends to increase the turbulence. Consequently, when the initial turbulence level is low, the experimental critical Reynolds number  $Re_c$ , defined as the value where an intermittency begins to appear in the flow [43], decreases with  $Re Ra^*$  but can be greater than 6000 at  $Re Ra^* = 1.5 \times 10^4$ . At a high level of initial turbulence such as that associated with a turbulence generator,  $Re_c$  increases with  $Re Ra^*$  but is only about 2500 at  $Re Ra^* = 1.5 \times 10^4$ . For  $Re Ra^* < 5 \times 10^5$  with UHF tubes, Mori et al. [43] recommend the following equation when the initial turbulence level is low:

$$Re_c = \frac{Re_{c0}}{1 + 0.14 \times 10^{-5} Re Ra^*} \quad (15.70b)$$

In the above,  $Re_{c0}$  is the critical Reynolds number without heating and can be more than 6 times larger than the high-initial-intensity critical Reynolds number of approximately 2000 [80]. Mori et al. [43] obtained a value of  $Re_{c0} = 7700$ . For high initial turbulence levels, Mori et al. [43] recommend, for UHF tubes,

$$Re_c = 128(Re Ra^*)^{1/4} \quad (15.70c)$$

## 15.6 TURBULENT MIXED CONVECTION IN DUCTS

For vertical upward flow in turbulent mixed convection in heated tubes, fairly well-established criteria for the onset of buoyancy-induced impairment of heat transfer are available. No satisfactory correlating equation, however, is available yet for the heat

transfer in downflow. In downflow, the experimental evidence shows that the onset of buoyancy-induced impairment of heat transfer occurs at a lower  $Gr_s/Re$  than in upflow.

### 15.6.1 Vertical Tubes

From the quantitative point of view, the onset of buoyancy-induced impairment of heat transfer in vertical tubes is characterized by the increased value of  $Gr_s/Re$  (since near-wall flow, where the transition to turbulence occurs, is where the natural convection is most intense).

The phenomenon is explained by a heated wall expansion which causes the direction of motion to be away from the wall. Consequently, laminarization occurs, and the onset of buoyancy-induced impairment of heat transfer is delayed.

where  $\overline{Gr} = g\beta\Delta T L^3 / \nu^2$

In tubes heated from the outside, sharp peaks in the heat transfer coefficient are reported [83], among others, for  $Gr_s/Re > 10^4$ . However, since the heat transfer coefficient starts to increase at a lower  $Gr_s/Re$  value at high  $Re$ , the reported onset of buoyancy-induced impairment of heat transfer in the UHF wall becomes maximum. The data show that the heat transfer coefficient is maximum at  $Gr_s/Re = 10^4$  (Herbert and Sieder [83]).

For turbulent flow, the heat transfer coefficient is semiempirical



transition is similar to that in laminar flow and consists of the onset of turbulence and amplitude until the onset of fully developed turbulent flow. The transition from laminar to turbulent flow (resulting from reversed flow on one side) occurs suddenly. As  $Gr_s/Re$  increases, the transition occurs suddenly. The transition is sensitive to fluctuations in inlet temperature. Using this criterion, the location of the transition for a constant flow rate, an inlet temperature, and a duct diameter may be used to

(15.70a)

is primarily affected by the inlet temperature at the entrance to the duct. At a low initial inlet temperature, the Reynolds number  $Re_s$  is high. Consequently, when the inlet temperature increases, the Reynolds number  $Re_s$  decreases. At a high level of inlet temperature,  $Re_s$  increases. For  $Re_s Ra^* < 5 \times 10^3$ , the transition occurs when the initial

(15.70b)

inlet temperature and can be more sensitive to the Reynolds number of approximately 7700. For high initial

(15.70c)

inlet tubes, fairly well-developed turbulent flow of heat transfer are observed. For high initial inlet temperatures, the heat transfer is generally enhanced over that for pure forced convection. A semiempirical equation for this situation has been developed by Jackson and Hall [82]:

transfer. In downflow, a satisfactory correlation now exists. For horizontal tubes, experimental evidence indicates that the effect of buoyancy is negligible in turbulent flow.

### 15.6.1 Vertical Ducts

From the quantitative information presented in Secs. 15.3 and 15.4, it is clear that in laminar mixed convection in a vertical duct, the heat transfer is improved (by virtue of the increased velocity near the wall) for aided flow but is worsened in opposed flow (since near-wall velocities are reduced). The situation is quite different in turbulent flow, where the heat transfer is sometimes less than the pure forced-convection value when natural convection aids forced convection, and where in opposed flow the heat transfer is generally larger than the corresponding forced convection value.

The phenomenon of heat transfer impairment in vertical heated upflow can be explained by a two-layer model [81]. In this concept, the fluid in the layer close to the heated wall experiences a buoyancy force owing to the reduced density. Acting in the direction of motion, this force tends to decrease the shear stress in the layer away from the wall. Consequently, turbulence production is reduced across the tube, resulting in laminarization. A simple approximate analysis [82] leads to the following criterion for the onset of buoyancy-induced impairment of heat transfer:

$$\frac{\overline{Gr}}{Re^{2.7}} \leq 10^{-3} \tag{15.71}$$

where  $\overline{Gr} = g(\rho_h - \bar{\rho})D_h^3/(\bar{\rho}\nu^2)$ . The integrated density  $\bar{\rho}$  is defined as

$$\bar{\rho} = \frac{1}{T_w - T_h} \int_{T_h}^{T_w} \rho \, dT \tag{15.71a}$$

In tubes heated at specified fluxes (UHF), the heat transfer impairment leads to sharp peaks in the local wall temperatures, which have been observed by Ackerman [83], among others. The thermal impairment does not persist at higher buoyancy, however, since the shear stress changes sign and energy inputs to the turbulent motion start to increase, as does the thermal performance of the tube. As a result, in buoyancy-aided flow, the heat transfer from the tube is impaired in the low ranges of the Grashof number, but recovers and may even exceed the pure forced-convection value at high Grashof numbers. Quantitative evidence of this behavior has been reported originally by Fewster [84] for upflow of carbon dioxide and water at supercritical pressures. Figure 15.22 shows the situation in which the temperatures of the UHF wall are below the pseudocritical temperature, the temperature at which  $c_p$  becomes maximum. It may be noted that the criterion of Eq. (15.71) is supported by the data shown in Fig. 15.22. Included in Fig. 15.22 are the UWT upflow data of Herbert and Sterns [3], of which more will be said later in this section.

For turbulent mixed convection in buoyancy-opposed flow in vertical UHF tubes, the heat transfer is generally enhanced over that for pure forced convection. A semiempirical equation for this situation has been developed by Jackson and Hall [82]:

$$\frac{Nu}{Nu_f} = \left[ 1 + 2750 \left( \frac{\overline{Gr}}{Re^{2.7}} \right)^{0.91} \right]^{1/2} \tag{15.72}$$

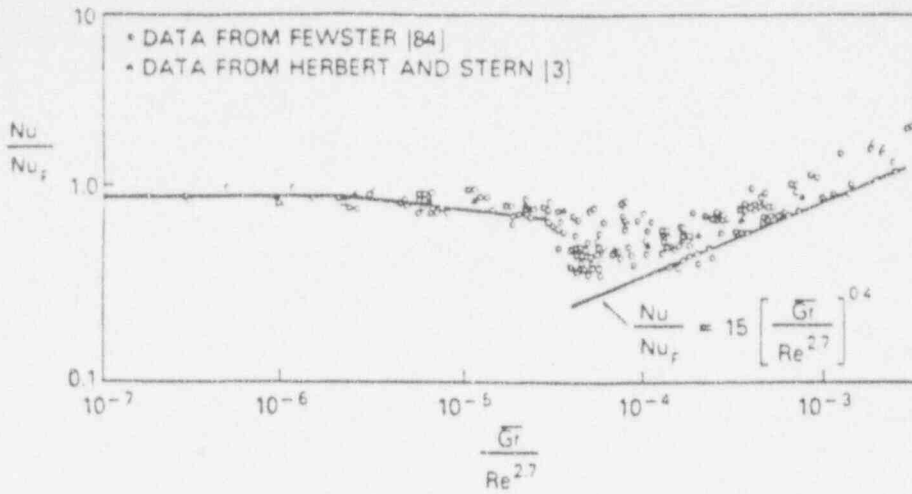


Figure 15.22. Average Nusselt number for buoyancy-assisted turbulent flow, normalized with Nusselt number for pure forced convection turbulent flow, in a vertical tube.

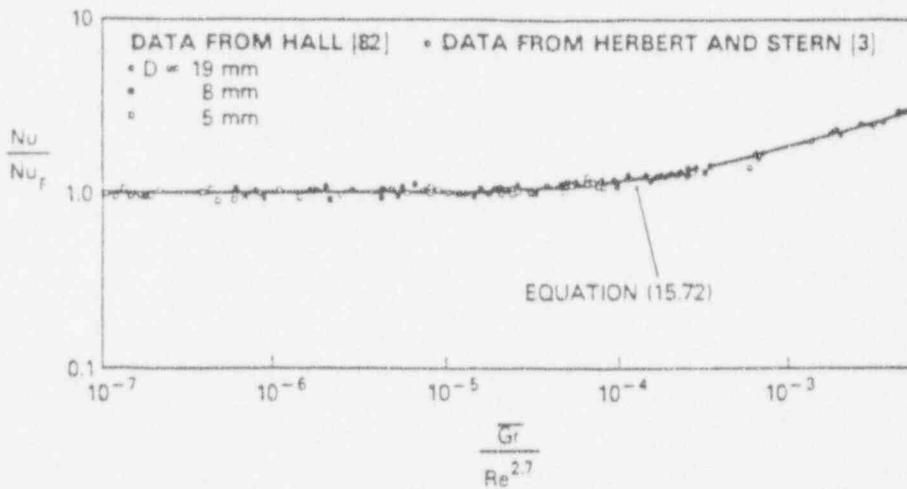


Figure 15.23. Average Nusselt number for buoyancy-opposed turbulent flow, normalized with Nusselt number for pure forced convection turbulent flow, in a vertical tube.

This equation is compared with experimental data for supercritical-pressure water in Fig. 15.23.

For vertical tubes at UWT, in the high Re range, Herbert and Sterns [3] have found that buoyancy effects on the heat transfer are negligible in aided turbulent mixed convection when Re exceeds a certain apparent critical value  $Re_{ac}$ . Their data were based on experiments with water, with Pr varying from 1.8 to 2.2 and  $Gr_4$  from  $2.0 \times 10^7$  to  $2.6 \times 10^7$ , approximately. The value of  $Re_{ac}$  may be calculated from the following equation:

$$Re_{ac} = 3000 + 0.00027 Gr_4 Pr \quad (15.73)$$

Thus, when Re is greater than  $Re_{ac}$ , the Nusselt number is given by the correlation for

pure forced convection correlation for b

This equation shows that  $L = 0.254$  is buoyancy-opposed that buoyancy effects are correlated by the

which gives values from Eqs. (15.73) to (15.74) are shown in Fig. 15.23 between  $Gr$  used in the correlation made:

In the above the outlet of the tube

For vertical tubes the Nusselt number is independent of the buoyancy parameter in the range  $Re = 10^4$  to  $10^5$  in the range of mixed convection [86].

For opposed flow

pure forced convection. When  $Re < Re_{sc}$ , Herbert and Sterns [3] suggest the following correlation for buoyancy-aided turbulent flow:

$$Nu = 8.5 \times 10^{-2} (Gr_4 Pr)^{1/3} \quad (15.74)$$

This equation should be used in the ranges  $Re = 4500$  to  $15,000$ ,  $D = 0.0127$  to  $0.0254$  m,  $L = 0.254$  to  $3.30$  m,  $Pr = 1.8$  to  $2.2$ ; and  $Gr_4 = 3 \times 10^6$  to  $30 \times 10^6$ . For buoyancy-opposed turbulent convection, the data of Herbert and Sterns [3] indicate that buoyancy effects may be neglected for  $Re > 15,000$ . For  $Re < 15,000$ , the data are correlated by the equation

$$Nu = 0.56 Re^{0.47} Pr^{0.4} \quad (15.75)$$

which gives values higher than those for pure forced convection for UWT tubes. In Eqs. (15.73) to (15.75), all properties are evaluated at the film temperature. Using the raw experimental data given in [3], comparisons may be made between the  $Nu/Nu_f$  results of [3] with those of Fewster [84] and Jackson and Hall [82]. These comparisons are shown in Figs. 15.22 and 15.23. The agreement is very good. To effect conversion between  $\overline{Gr}$  used in [82] and  $Gr_4$  used in [3], the following approximations have been made:

$$\bar{\rho} = \rho_f$$

$$\rho_h - \bar{\rho} = -\rho_h \beta (T_w - \bar{T}_f)$$

$$= \rho_h \beta \frac{T_w - \bar{T}_h}{2}$$

$$= \rho_h \beta \frac{T_w - T_m}{2}$$

$$\overline{Gr} = \frac{g(\rho_h - \bar{\rho}) D^3}{\bar{\rho} \nu^2}$$

$$= \frac{g \beta \rho^2 (T_w - T_m) D^3}{2 \mu^2}$$

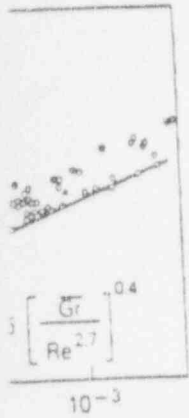
$$= \frac{Gr}{2}$$

In the above the overbar designates the arithmetic mean of the values at the inlet and outlet of the tube.

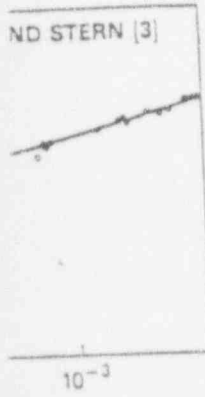
For vertical tubes at UWT in the low  $Re$  range, the turbulent mixed convection  $Nu$  is independent of  $Re$  in both aided and opposed flow. Testing with air in aided flow in the range  $Re = 385$  to  $4930$ , Brown and Gauvin [85] found that  $Nu$  may be predicted to  $\pm 7\%$  in the range  $Gr = 5 \times 10^6$  to  $1 \times 10^7$  by the following equation for pure free convection [86]:

$$Nu = 0.13 (Gr, Pr)^{1/3} \quad (15.76)$$

For opposed flow in the range  $Re = 378$  to  $6900$ , Brown and Gauvin [85] show that  $Nu$



\*, normalized with



flow, normalized with

al-pressure water in  
sterns [3] have found  
led turbulent mixed  
c. Their data were  
2.2 and  $Gr_4$  from  
calculated from the

$$(15.73)$$

by the correlation for

---

# HANDBOOK OF SINGLE-PHASE CONVECTIVE HEAT TRANSFER

Edited by

**Sadik Kakaç**

Department of Mechanical Engineering  
University of Miami  
Coral Gables, Florida

**Ramesh K. Shah**

Harrison Radiator Division  
General Motors Corporation  
Lockport, New York

**Win Aung**

National Science Foundation  
Washington, D.C.

A Wiley-Interscience Publication

**JOHN WILEY & SONS**

New York · Chichester · Brisbane · Toronto · Singapore

# 14

---

## MIXED CONVECTION IN EXTERNAL FLOW

*T. S. Chen and B. F. Armaly*

*University of Missouri — Rolla  
Rolla, Missouri*

- 14.1 Introduction
  - 14.2 Fundamentals of Mixed Convection
  - 14.3 Correlation Equations for Nusselt Numbers
  - 14.4 Correlations for Flat Plates
  - 14.5 Correlations for Continuous Moving Sheets
  - 14.6 Correlations for Vertical Cylinders in Longitudinal Flow
  - 14.7 Correlations for Horizontal Cylinders
  - 14.8 Correlations for Spheres
  - 14.9 Correlations for Vertical Flat Plates in Cross Flow
  - 14.10 Turbulent Heat Transfer Correlations for Flat Plates
  - 14.11 Instability and Transition
  - 14.12 Conclusions
- Acknowledgment  
Nomenclature  
References



The corresponding correlation for the average Nusselt number can be expressed by

$$\overline{Nu}_x Re_x^{-1/2} = 0.804 \left[ 1 + \left[ 0.752 \frac{L}{H} \left( \frac{Gr_{xH}}{Re_x^{1/2}} \right)^{1.75} \right]^{1/2} \right]^{1/2} \quad (14.39)$$

It should be emphasized here that the above correlations for vertical plates in cross flow are limited to fluids having  $Pr = 0.7$  and that fluid properties are evaluated at the free-stream temperature  $T_\infty$ . Correlation equations for fluids with Prandtl numbers other than 0.7 can be developed only when the results from analyses and experiments become available.

### 14.10 TURBULENT HEAT TRANSFER CORRELATIONS FOR FLAT PLATES

Reported studies on turbulent heat transfer in mixed convection are lacking in the literature. Turbulent mixed convection on vertical and horizontal flat plates under the UWT condition has been analyzed by Chen et al. [34,35] by employing a modified mixing-length model that accounts for the buoyancy-force effect. Their calculations for  $Pr = 0.7$  yield local Nusselt numbers that converge to the limit of pure forced convection, but underpredict by 20% the available results in the limit of pure free convection. The local Nusselt number for turbulent flow over a flat plate under UWT for  $0.5 \leq Pr \leq 1.0$  and  $5 \times 10^5 \leq Re_x \leq 5 \times 10^6$  is given by [36]

$$Nu_x Re_x^{-4/3} = 0.0287 Pr^{0.6} \quad (14.40)$$

The local Nusselt number for turbulent free convection along an isothermal vertical flat plate for all Prandtl numbers and for  $Gr_x$  to  $10^{12}$  is correlated by Churchill and Chu [37] as

$$Nu_x Gr_x^{-1/3} = 0.15 Pr^{1/3} \left[ 1 + \left( \frac{0.492}{Pr} \right)^{9/16} \right]^{-16/27} \quad (14.41)$$

For turbulent free convection over a heated horizontal flat plate facing upward, the local Nusselt number for  $Gr_x Pr > 5 \times 10^8$  is given by Fujii and Imura [38] as

$$Nu_x Gr_x^{-1/3} = 0.13 Pr^{1/3} \quad (14.42)$$

Equation (14.42), obtained under neither the UWT nor the UHF condition, was also verified later by Imura et al. for an isothermal horizontal flat plate [39].

If Eq. (14.12) is employed to propose a correlation for the local Nusselt number in mixed convection, the resulting form is

$$\frac{Nu_x Re_x^{-4/3}}{F(Pr)} = \left\{ 1 + c \left[ \frac{G(Pr)}{F(Pr)} \left( \frac{Gr_x}{Re_x^{1/2}} \right)^{1/3} \right]^n \right\}^{1/n} \quad (14.43)$$

where  $F(Pr) = 0.0287 Pr^{0.6}$  and  $G(Pr) = 0.15 Pr^{1/3} [1 + (0.492/Pr)^{9/16}]^{-16/27}$  for a vertical plate and  $0.13 Pr^{1/3}$  for a horizontal flat plate. The analytical local Nusselt numbers of Chen et al. [34,35] for  $Pr = 0.7$  agree fairly well with the proposed

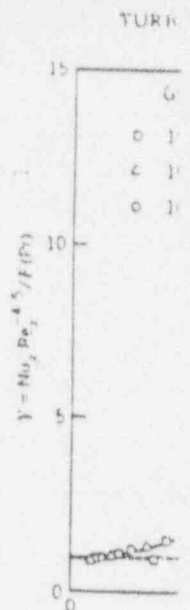


Figure 14.20. Correlation equation for vertical and horizontal plates.

correlation equation for vertical plates, corresponding average

with the same c. Turbulent mixed flow was analyzed number for a square and  $0 \leq Gr_{xH}/R$

Equation (14.45): Measurement along and  $H =$  et al. [33] have correlation equation form as

$$\frac{Nu_x}{0}$$

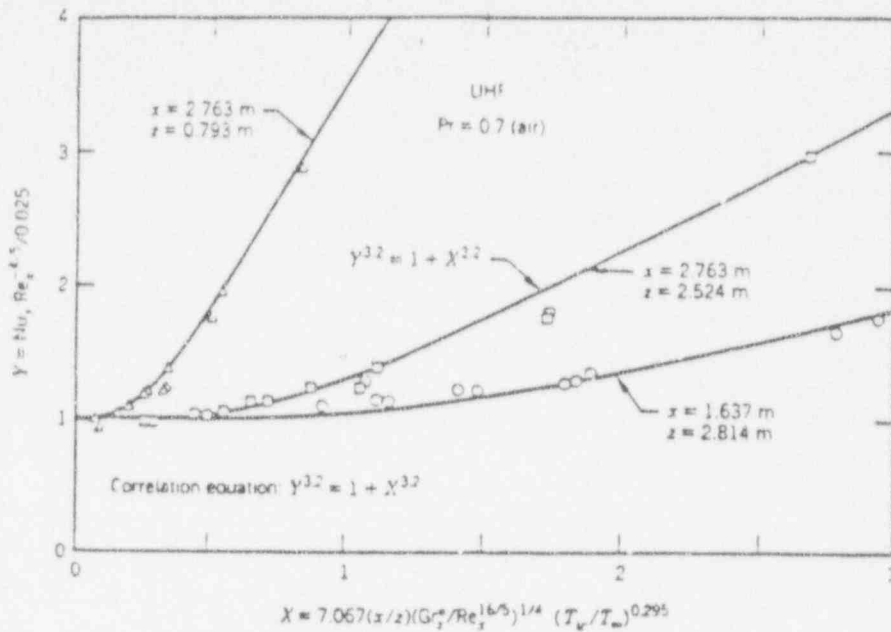


Figure 14.21. Comparison between measured and correlated local Nusselt numbers: turbulent air flow across a vertical flat plate. UHF [33]

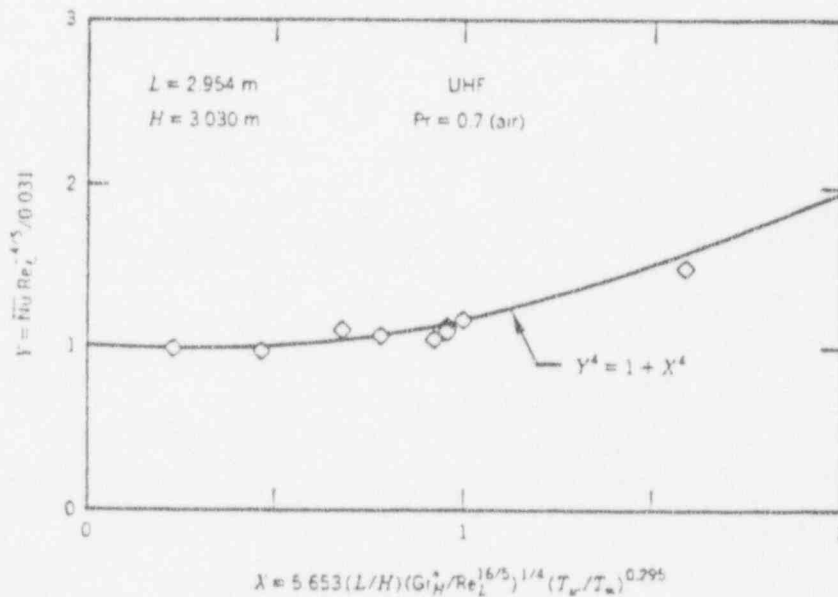


Figure 14.22. Comparison between measured and predicted average Nusselt numbers: turbulent air flow across a vertical flat plate. UHF [33]

in the range  $t \leq 600^\circ\text{C}$ .  
The correlation is expressed for

with  $n = 4$  for Figure 14.2 for a vertical flat plate at location  $(x, z)$  (14.46). A comparison of the two figures shows that the two figures agree. The properties are

### 14.11 INSTABILITY

Buoyancy forces in natural convection. They hence alter the nature of laminar mixing induced by the buoyancy modes. One of the modes in laminar mixing is the minimum number  $Re_{crit}$  becomes unstable.

From the analysis of a strong force stabilizing effect over a horizontal force opposes an inclined flat plate, destabilizing effect opposing buoyancy flow along a vertical plate opposing free convection.

The analysis shows that over a heated vertical plate, the critical  $Re_{crit}$  for  $Pr = 0.7$  is  $10^3 \leq Re_{crit} \leq 10^4$ . For a horizontal flat plate,  $Gr_{crit}/Re_{crit}^{3/2} = 78$ , for water or much lower for

in the range  $0 \leq Gr_{fl}/Re_l^2 \leq 30$ , with  $Re_l < 2 \times 10^6$ ,  $Gr_{fl}^* < 2 \times 10^{12}$ , and  $40 \leq T_w \leq 600^\circ\text{C}$ .

The corresponding expression for the average Nusselt number can be derived and expressed for  $Pr = 0.7$  as

$$\frac{\overline{Nu} Re_l^{-4/3}}{0.031} = \left( 1 + \left[ 5.653 \frac{L}{H} \left( \frac{Gr_{fl}^*}{Re_l^{6/5}} \right)^{1/4} \left( \frac{T_w}{T_\infty} \right)^{0.295} \right]^4 \right)^{1/4} \quad (14.47)$$

with  $n = 4$  providing a better fit than  $n = 3.2$ .

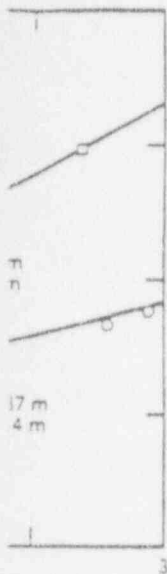
Figure 14.21 illustrates a comparison between the measured local Nusselt number for a vertical flat plate ( $L = 2.954$  m and  $H = 3.030$  m) in cross flow of air [33] at three  $(x, z)$  locations, as indicated in the figure, and the proposed correlation equation (14.46). A comparison between the measured average Nusselt number over the entire plate and the correlation equation (14.47) is shown in Fig. 14.22. As can be seen from the two figures, the proposed correlations for both the local and average Nusselt numbers agree well with the experimental results. In Eqs. (14.46) and (14.47) all fluid properties are evaluated at the free-stream temperature  $T_\infty$ .

## 14.11 INSTABILITY AND TRANSITION

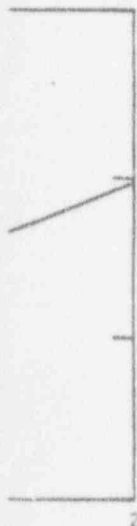
Buoyancy forces play a significant role in affecting the laminar flow regime in mixed convection. Their presence may enhance or diminish the stability of laminar flow and hence alter the transport characteristics of the mixed convection regime. The instability of laminar mixed convection flow and its subsequent transition to turbulent flow can be induced by the wave mode of instability, by the vortex mode of instability, or by both modes. One of the major criteria for use in determining the incipience of the instability in laminar mixed convection flows is the relationship between the critical Reynolds number  $Re_{c,c}$  and the critical Grashof number  $Gr_{c,c}$ , that is, the relationship between the minimum Reynolds and Grashof numbers that will cause the laminar flow to become unstable.

From the analyses of wave instability by the linear theory, it has been found that for a strong forced flow with weak buoyancy force, an aiding buoyancy force has a stabilizing effect on flow along a vertical plate [40], but a destabilizing effect on flow over a horizontal flat plate [41]. These trends are both reversed when the buoyancy force opposes the forced flow. For the laminar mixed convection flow adjacent to an inclined flat plate, an increase in the inclination angle from the vertical has a destabilizing effect for an aiding buoyancy force, but a stabilizing effect for an opposing buoyancy force [42]. For a strong free convection flow with very weak forced flow along a vertical flat plate, an aiding free stream has a stabilizing effect, whereas an opposing free stream tends to destabilize the flow [43].

The analysis of vortex instability by the linear theory for mixed convection flow over a heated, isothermal, horizontal flat plate has provided the relationships between the critical Reynolds number and the critical Grashof number as  $Gr_{c,c}/Re_{c,c}^2 = 0.447$  for  $Pr = 0.7$  and  $Gr_{c,c}/Re_{c,c}^2 = 0.434$  for  $Pr = 7$  in the Reynolds number range of  $10^3 \leq Re_{c,c} \leq 10^7$  [44]. On the other hand, experiments on isothermal, heated, horizontal flat plates provide relationships for the onset of vortex instability as  $Gr_{c,c}/Re_{c,c}^2 = 192$  for air [45] and  $Gr_{c,c}/Re_{c,c}^2 = 46$  to 100, with an average value of 78, for water [46]. Thus, for a given Reynolds number, the linear theory predicts a much lower critical Grashof number than that observed in experiments. In another



Numbers: turbulent



Numbers: turbulent

## BUOYANCY EFFECT ON HEAT TRANSFER IN FORCED CHANNEL FLOWS

E.S. Petukhov and A.F. Polyakov

Institute for High Temperatures, USSR Academy of Sciences,  
Moscow, USSR

O.G. Martynenko

Heat and Mass Transfer Institute, BSSR Academy of Sciences,  
Minsk, USSR

## ABSTRACT

The paper discusses the results of experimental and computational and theoretical studies of forced laminar and turbulent flows and heat transfer in channels under the condition of an essential buoyancy effect. The main attention is given to upward and downward turbulent motion of liquid in heated vertical tubes.

The boundaries and character of thermogravitational forces effect on velocity and temperature distribution, friction resistance and local heat transfer are determined. Relationships for calculation of boundaries of the gravity force field effect are generalized.

In the case of a turbulent flow, the buoyancy effect on the averaged flow and on fluctuating motion are analyzed.

## 1. INTRODUCTION

In the course of development of the convective heat transfer theory, the problems of forced and free convection were studied independently, while their combined effect was practically not studied at all. It was only recently that it became clear that the interaction of forced and free convection may be of essence. At the earlier stages of the problem investigation, the main emphasis was laid on laminar mixed convection, while in turbulent forced flows the buoyancy effect was considered irrelevant. In fact, only during the last fifteen years it became clear that in turbulent liquid flows in tubes the effect of free convection may be not only perceptible, but, under certain conditions, may govern the character of flow and heat transfer. The increased requirements imposed on the accuracy of determination of temperature fields and heat fluxes, particularly in such fields of technology as pipeline transport, rocket building, aerothermooptics and many others, gave an impetus to further development of such investigations.

In this review paper, the results of experimental as well as calculation and

theoretical studies on heat transfer and hydrodynamics in the case of both laminar and turbulent mixed convection in smooth channels are discussed. The main attention is given to the cases of flows in horizontal and vertical plane channels of a round cross-section (round tubes). These cases are the most interesting for practice and are the most comprehensively studied ones. The problems of flow stability are omitted from the discussion; studies pertaining to other channel configurations and considering additional effects on the flow, such as variability of physical properties, unsteady-state and others, are touched upon briefly. Among the information on the topic available to the authors, the main attention is given to the studies containing the most conclusive results and conducted during the last decade. The review also deals with the results obtained by the authors and reflects their scientific interests.

Further on, incompressible chemically homogeneous media will be considered, whose density variation is the function of temperature alone. The assumptions adopted give that isothermal compressibility of the medium with pressure variation is neglected, in contrast to thermal expansion due to the temperature variation of the medium. In other words, following Boussinesq, we shall assume that the following linear dependence of  $\rho$  on  $T$  is observed:

$$\rho = \rho_0 [1 - \beta(T - T_0)] \quad (1)$$

valid at relatively small differences  $(T - T_0)$ .

In the overwhelming majority of cases studied, mixed convection was described within the framework of Boussinesq approximation.

Since the density variation due to temperature variation alone is considered, we shall use along with the term "buoyancy forces" the terms "thermogravitational forces" and "thermogravitation", implying the process development in a homogeneous gravitational field.

## 2. LAMINAR FLOW

In Ref.1 the results are presented of investigations of laminar mixed convection in tubes, obtained before 1967. In subsequent years, a number of papers were published, dealing with heat transfer studies both in horizontal [ 2-10, 13, 19-24 ] and vertical tubes [ 11-18 ], and also in inclined tubes [ 25-28, 40 ]. These studies yielded experimental as well as calculation and theoretical data.

The problems of hydrodynamics and heat transfer in the case of mixed convection in vertical channels are relatively simple.

A theoretical solution of the problem of combined laminar forced and free convection in vertical tubes for the thermal stabilization region at  $q_w = \text{const}$  was obtained for the first time by Ostromov and Hallman [ 11 ]. These and some other similar solutions yielded analytical expressions for velocity and temperature distribution, friction resistance and heat transfer. In the case of coinciding directions of forced and free convection near the wall, i.e. of the ascending flow in heated tubes or the descending flow in cooled ones, the velocity in the vicinity of the wall is increased with an increase of Gr number (liquid flow rate being constant), and decreased in the core of the flow. At a certain value of the Grashof number, a concavity appears near the axis, which increases with the increasing Gr. In the opposite case, specifically, in a descending flow in heated tubes, the velocity near the wall is reduced and in the middle of the tube is increased with the increasing Gr number.

Along with the analytical solutions for stabilized heat transfer at  $q_w = \text{const}$ , approximate solutions were obtained for the starting length with the boundary conditions of the first and second kind, and also numerical solutions of the problem of heat transfer over the entire tube length. Numerical solutions on the basis of the finite-difference method were obtained using various simplified systems of differential equations of energy and motion. Differential equations in the boundary layer approximation for solution of the problem on viscous-gravitational flow (i.e. laminar liquid motion with an essential gravity field) in a tube were probably used for the first time in [ 11 ]. In this paper, ascending and descending air flows were studied at large temperature differences,  $T_w/T_{in} > 5$ , when the gas temperature assumed large values and the volumetric expansion coefficient was small. These studies yielded relatively small (within 20%) heat transfer variations at the starting length as compared to the case when the

mass force effect is absent.

This problem in a more complete statement was solved by Collins [ 12 ]. The calculations were conducted for a viscous-gravitational water flow in vertical tubes using complete two-dimensional equations of motion and energy with the boundary conditions  $t_w = \text{const}$  and  $q_w = \text{const}$ . In Fig.1, the heat transfer calculation results for the case  $q_w = \text{const}$  are shown. The calculations were conducted for the conditions realized in the experiments carried out by Schelle and Hanratty [ AIChE J., 1963, v.9, No.2 ] on studying the stability violation in an ascending flow in a heated tube. These data are denoted by dots in Fig.1, the calculations being made up to a corresponding value of X with the assigned  $Gr_Q/Re$ .

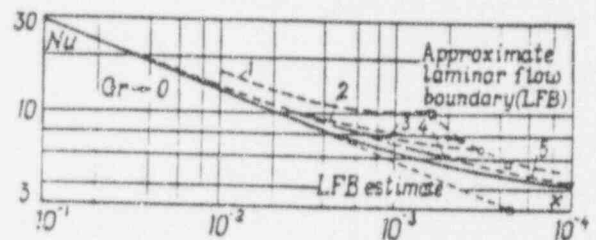


Fig.1. Calculation [ 12 ] of heat transfer in a viscous-gravitational flow in vertical tubes:

- ascending flow, heating;
- - - descending flow, heating;
- 1 -  $\nabla$  -  $Gr_Q/Re = 1904$ ;
- 2 -  $\circ$  - 1176;
- 3 -  $\circ$  - 800;
- 4 -  $\Delta$  - 400;
- 5 -  $\nabla$  - 240;
- 6 -  $\blacksquare$  - 504.

Results of experimental and calculation and theoretical investigation of heat transfer in an ascending flow in heated tubes at  $q_w = \text{const}$  show that the local Nu number depends on the reduced length  $Z = (1/Pe)(z/d)$  and the parameter  $(Gr/Re) = (g \gamma d^3 q_w / \lambda \nu \bar{u})$ , [or  $Ra_A = g \gamma d^4 \cdot (dT_b/dz) / 16 \nu a$ ]\*; the buoyancy effect on heat transfer near the heat source is essentially smaller than far from the inlet; with an increase of  $Gr_Q/Re$  the free convection effect on forced flow propagates closer and closer to the heat source; at a certain distance from the heat source, the local Nusselt number becomes stabilized. Stabilization is achieved at the values of Z which are the smaller the larger  $Gr_Q/Re$ . Many of

\* The values of  $Gr_Q/Re$  and  $Ra_A$  are unambiguously interconnected. For a uniformly heated round tube,  $(Gr_Q/Re) = 4Ra_A$ .



the enumerated specific features of heat transfer behaviour are illustrated in Fig.1.

Variation of the Nu number in vertical tubes in the case of coinciding forced and free convection near the wall is adequately described by the interpolation equation suggested in [13]:

$$Nu/Nu_0 = (1 + \frac{Gr}{ReB})^{0.27}, \quad (2)$$

where  $Nu_0$  is the Nusselt number in a laminar liquid flow not affected by mass forces with the corresponding values of the reduced length.

For the parameter  $B(Z)$ , the following relationships are chosen:

$$B = 5.4Z^{-1} + 312Z^{0.25} \quad \text{at } Z \leq 0.07$$

$$B = 240 \quad \text{at } Z \geq 0.07$$

The equation (2) describes with the accuracy of  $\pm 8\%$  experimental data on air and water over the entire tube length, including the thermal starting length. At  $Z \geq 0.07$ , neglecting the unity as compared to the second term in Eq.2, converts the latter into the interpolation Hallman equation for stabilized heat transfer.

Equation (2) is valid at  $Z < Z_{cr}$ . At  $Z = Z_{cr}$ , the laminar flow stability is violated. For  $Z_{cr} = \frac{1}{Re} \left( \frac{Z}{d} \right)_{cr}$ , the following equation was chosen in [13]:

$$Z_{cr} = 12.9(Gr_q/Re)^{-0.8} \quad (3)$$

The values of  $Z_{cr}$  calculated from (3) somewhat exceed those given in Fig.1 (dots), which is due to the different manner of their determination. In the first case (Fig.1) they were determined from the beginning of the current lines bending, in the second, Eq.3, from the beginning of deviation of the local heat transfer values from the relationships typical of a viscous-gravitational flow.

Usually, in the course of analysis of the calculation and theoretical investigation results, the boundary of stability violation for the case  $(\partial\varphi/\partial z) < 0$  is assigned to the parameters making the velocity value on the tube axis become zero, and for the case  $(\partial\varphi/\partial z) > 0$ , to those making the velocity gradient on the wall become zero. However, the experimental data given in Fig.1 and those given by the relationship (3) show that the stability violation occurs much earlier than the time when the calculated velocity values become the above-noted specific ones. Moreover, calculations using different approximations yield different results. Thus, in the case of a descen-

ding liquid motion in a heated tube, the velocity gradient on the wall, according to the data of [12] equals zero at  $Gr_q/Re=500$  independently of the coordinate  $z$ , while the analytical solutions for a stabilized flow give this value equal to 324.

The complex spatial flow character in the case of combined action of forced and free convection in horizontal channels makes impossible strict analytical solution of the problem. Calculation and theoretical studies of mixed convection in horizontal tubes was conducted using the method of small disturbances with respect to solution for purely forced convection [1,3,28] allowing for secondary flows in the boundary layer approximation [9,10], and the finite-difference method [4,5,22,23,25,27].

Thus, in Ref.28 an approximate solution of the problem on heat transfer in the tubes horizontally situated in space and a relatively small thermogravitation effect was obtained. The following dependence was derived for local heat transfer at  $q_w = \text{const.}$ :

$$Nu/Nu_0 = 1 + Nu_0 \left\{ 1.32 \cdot 10^{-4} (Gr_q/Re) [1 - \exp(-40Z)] \cdot \cos\psi - 9.1 \cdot 10^{-6} Ra_q [1 - \exp(-100Z)]^3 \cos\phi \sin\psi \right\}, \quad (4)$$

where  $\Phi$  is the angle over the tube circumference calculated from the upper generatrix;  $\psi$  the angle between the axis and vertical;  $Ra_q = PrGr_q$ .

Equation 4 satisfactorily describes the experimental data on both vertical and horizontal tubes at  $0.6 < (Nu/Nu_0) < 1.5$ . It is noteworthy that in the vertical tubes ( $\psi=0$ ) the Nu number depends on one buoyancy parameter, viz.  $Gr_q/Re$ , while in the horizontal tubes ( $\psi = \pi/2$ ), on another,  $Ra_q$ .

Interaction of free and forced convection in horizontal tubes leads to development of secondary flows in the plane normal to the tube axis. Secondary flows form a pair of vortices covering the entire cross-section of the tube. In the case of a heated wall, the liquid ascends along the lateral surfaces of the tube and descends in the central part of it; simultaneously, the liquid moves along the tube axis. Transverse circulation intensity increases with the increasing  $Ra$  number, while the vortices centres approach the wall and the ascending flow is concentrated near the surface. This fact was used in some studies for approximate calculation of heat transfer [9,10]. Results of these calculations adequately describe the experimental data on heat transfer far from the heat source at  $Ra_q > 10^6$ .

Development of secondary circulations leads to violation in the velocity and temperature distribution over the tube cross-section. Maximum velocity values and minimum temperature values (in the case of a heated wall) are displaced from the channel axis toward the lower generatrix. Then heat transfer near the lower generatrix is essentially increased, and near the upper one it is decreased. Just as with the vertical tubes, the buoyancy effect on heat transfer near the heat source is comparatively small and then increases, and at a certain distance the local Nusselt number becomes stabilized. This character of the process development was established as a result of numerous experimental and calculation and theoretical studies for homogeneous boundary conditions.

Figure 2 displays the calculation results of [6] on the circumference-average number  $Nu$  compared to the experimental data of [31]. The figure shows a good agreement of the calculation and experimental data. It is also clear that stabilization of the perimeter-average number  $Nu$  occurs at considerably smaller values of  $Z$  as compared to stabilization without the mass force effect. In this case, the constant value of  $Nu_{\infty}$  is established at the values of  $Z$  which are the smaller the larger  $Ra_q$ .

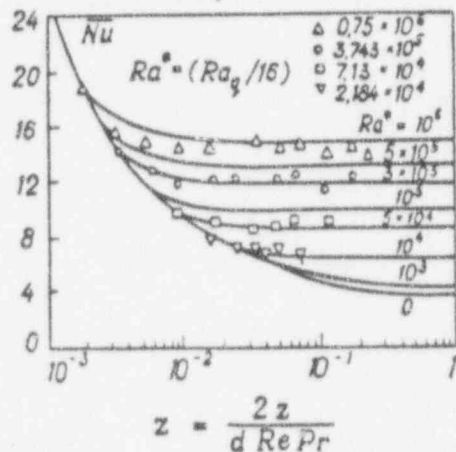


Fig. 2. Comparison of the calculation results of [6] with the experimental data of [31].

The data on perimeter-average heat transfer are generalized in [31] by means of the following equation:

$$\bar{Nu}/Nu_0 = [1 + (Ra_q/Ra_q^{(1)})^4]^{0.045}, \quad (5)$$

where  $Nu_0(Z)$  is the Nusselt number value in a viscous flow;  $Ra_q^{(1)}$  the limit value of  $Ra$  determined from the condition that  $Nu$  number in a viscous-gravitational flow differs from  $Nu_0$  no more than by 5%. For

$Ra_q^{(1)}$  the following equations are chosen:

$$Ra_q^{(1)} = 5 \cdot 10^3 Z^{-1} \quad \text{at } Z < 1.7 \cdot 10^{-3}$$

$$Ra_q^{(1)} = 1.8 \cdot 10^4 + 55 Z^{-1.7} \quad \text{at } Z > 1.7 \cdot 10^{-3}$$

The results of calculation of [8(1)] of the starting boundaries of free convection effect on the perimeter-average heat transfer are in a good agreement with the reduced dependences for  $Ra_q^{(1)}$ .

At  $Z \rightarrow \infty$ ,  $Ra_q^{(1)} = 1.8 \cdot 10^4$ , and  $Nu_0 = 4.36$ . In this case, on the basis of (5) we obtain:

$$\bar{Nu}_{\infty} = 4.36 [1 + (Ra_q / 1.8 \cdot 10^4)^4]^{0.045} \quad (5a)$$

For asymptotic values of  $\bar{Nu}_{\infty}$  at  $Ra_q > 6 \cdot 10^4$ , the following interpolation dependence is suggested in [6]:

$$\bar{Nu}_{\infty} = 1.287 \left( \frac{Ra_q}{16} \right)^{0.177}$$

which is quite close to the relationship (5a).

Correspondence between the numerical solution results and the experimental data on perimeter-average heat transfer prompts the possibility of calculating complex three-dimensional flows realized with mixed laminar convection in horizontal tubes. Unfortunately, calculation results on local heat transfer for the boundary conditions of the second kind are not presented in the published papers and the degree of their correspondence to the experimental results is not discussed.

The results considered above were obtained under the thermal boundary conditions homogeneous over the channel perimeter. In practice, the cases are encountered, when the condition of uniform temperature or heat flux distribution over circumference cannot be attained. For example, heat flux incident on the solar collector tube is distributed over its perimeter asymmetrically. These problems are close to the problems of temperature field control inside the channels. Such problems arise during laser radiation propagation in thermohydrodynamic light guides (gas lenses).

In Refs. 21, 22, the case was considered of a round horizontal tube with the heat flux on the wall dependent on the angular coordinate

$$q_w = q_{\phi=0} (1 + s \cos \phi + c \sin \phi),$$

and at the same time, independent of the

longitudinal coordinate. Such assignment of the boundary conditions makes it possible to determine the velocity and temperature profiles allowing for the mass force effect, which satisfy the pre-set conditions, e.g. which are close to the axisymmetric ones.

In [23], the problem on heat transfer with the following boundary conditions was considered: a) constant heat flux on the upper half of the tube, the lower one being thermoinsulated; b) constant heat flux on the lower part of the tube, the upper one being thermoinsulated.

For these cases, Figure 3 shows the dependence of the perimeter-average but invariable over the tube length Nu number on the Gr<sub>q</sub> number. In the case of heating from above, the relationship Nu/Nu<sub>0</sub> is considerably smaller than 1.5 over the entire studied range, while with the heating from below, the values of Nu/Nu<sub>0</sub> reach 6 and 12 for Pr = 0.7 and 5, respectively. For the case of heating from below, the data on heat transfer are described by the relationship Nu/Nu<sub>0</sub> = f(Ra<sub>q</sub>), while with heating from above such dependence is not observed.

The waviness of curves exhibited in Fig. 3 reflects the structure variation of the secondary flow. With small values of Gr<sub>q</sub>, the secondary flow is represented by a pair of vortices, while at larger Gr<sub>q</sub> values this simple flow pattern is transformed into a more complex one, composed of numerous vortices.

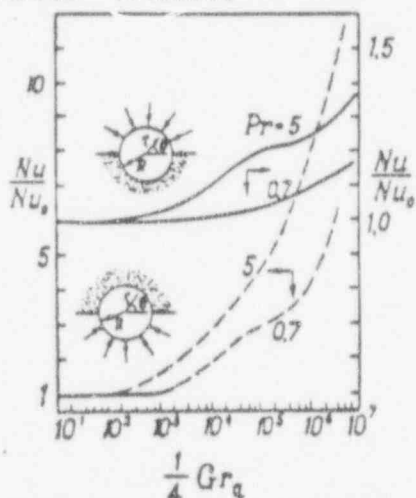


Fig. 3. Perimeter-average Nusselt number [23].

Unfortunately, the restricted length of this paper does not allow consideration of the studies dealing with mixed laminar convection in the conditions complicated by the effect of additional factors and non-Newtonian liquids [35,36].

In particular, works [32,33,37] consider the effect of unsteady-state, [41,42], the energy dissipation effect, [34], the effect of chemical conversi-

ons, [8,11,38,39], temperature dependences of physical properties. In [35,36], the data on Non-Newtonian liquids are obtained, in [29,40,44-50], on channels with different cross-section forms, and in [43], on channels with cross-sections variable over the length.

### 3. TURBULENT FLOW

It was assumed until recently that in a developed turbulent flow in tubes ( $Re > 10^4$ ), the buoyancy effect on hydrodynamics and heat transfer is inessential. Experimental data obtained in the recent years, however, demonstrate that under certain conditions the said effect can be not only essential but dominant. It was established experimentally and theoretically that under the action of thermogravitational forces variations are observed in the velocity and temperature fields of the averaged flow, turbulent transfer characteristics, heat transfer and resistance.

The system of equations of energy, momentum and mass conservation for a steady-state turbulent flow of an incompressible liquid with constant physical properties (except density in the equation for buoyancy forces) in the absence of internal heat sources and energy dissipation of an averaged flow is given by:

$$\rho c_p \langle u_k \rangle \frac{\partial \langle T \rangle}{\partial x_k} = \frac{\partial}{\partial x_k} \left( \lambda \frac{\partial \langle T \rangle}{\partial x_k} - \rho c_p \langle u'_k T'_k \rangle \right), \quad (6)$$

$$\rho \langle u_k \rangle \frac{\partial \langle u_i \rangle}{\partial x_k} = - \frac{\partial \langle P \rangle}{\partial x_i} + \rho \varepsilon_i + \frac{\partial}{\partial x_k} \left( \frac{\partial \langle u_i \rangle}{\partial x_k} - \rho \langle u'_i u'_k \rangle \right), \quad (7)$$

$$\frac{\partial \langle u_k \rangle}{\partial x_k} = 0, \quad (k=1,2,3; i=1,2,3). \quad (8)$$

This system takes into account the turbulent transfer of heat and momentum, respectively.

Let us also write down the energy balance equation of fluctuating motion:

$$\rho \langle u'_i u'_k \rangle \frac{\partial \langle u_i \rangle}{\partial x_k} - \langle \rho' u'_i \rangle \varepsilon_i + \rho D_T = 0 \quad (9)$$

Here, only generation of turbulent energy (first term), its dissipation (third term) and buoyancy force action (second term) are taken into account.

As can be seen from equations (6-9), the buoyancy forces affect not only the averaged, but also the fluctuating flow,



and, hence, the turbulent momentum and heat transfer. Thus, the effect of thermogravitation on the turbulent transfer is governed by two interconnected effects. On the one hand, thermogravitational forces change the fields of averaged velocity and temperature values, which entails variation of the turbulent transfer characteristics. On the other hand, thermogravitational forces directly affect the motion of turbulent elements of the liquid, enhancing or weakening the turbulent transfer intensity.

Buoyancy forces produce an effect, or rather, different effects on the turbulent transfer of momentum and heat, and, hence, on the turbulent Prandtl number (see the geophysical studies data of [51, 52]). Stratification of turbulent flows has been studied in the field of geophysics over several decades, and the results obtained predetermined to a large extent the approach to studying of the corresponding processes applied to engineering, which constitutes the subject of this review paper. The fundamental result of the theory of temperature-stratified turbulent flows consists in determination of the character of the gravitation field effect on turbulence. In the case of stable density distribution, the vertical motion of turbulent elements is accompanied by the energy consumed to counter the Archimedian forces, which leads to the decay of turbulent energy, and hence, of turbulent transfer. In the case of unstable density distribution, the Archimedian forces operate on the vertical motion of turbulent elements, causing an increase in the turbulent energy. Realization of these effects in nonisothermal channel flows may lead to essential qualitative changes in the character of heat transfer as compared to heat transfer in laminar flows under similar conditions. The first case occurs, for example, in horizontal channels with heated upper surface, and the second, with heated bottom surface, or, in other words, with upward and downward flows in vertical heated channels.

The results available on channel flows show that the effect of thermogravitational forces on turbulent transfer is not small as compared to that on the averaged flow. Depending on the conditions, both effects are commensurable or one of them is dominant. In order to establish the character and extent of each factor, it is expedient to consider such conditions which allow their separate analysis. This possibility is provided in the case of a plane horizontal channel flow, where the secondary free-convective flows are absent.

The parameter characterizing the effect of density inhomogeneity in the gravity field on turbulence is the Richardson

number,  $Ri = Pr_T Rf = \frac{g \gamma dT/dx}{(dw/dx)^2}$ , written

here in the gradient form. Represent it in the universal coordinates typical of turbulent flows near the wall:

$$Ri = \frac{Gr_q}{PrRe_*^4} \frac{dT^+/dx^+}{(dw^+/dx^+)^2} = \frac{Gr_q}{PrRe_*^4} \left(\frac{\delta}{\xi}\right)^2 \frac{dT^+/dx^+}{(dw^+/dx^+)^2}, \quad (1)$$

where

$$Gr_q = \frac{g \gamma q_w d_{eqv}^4}{\nu^2 \lambda}, \quad Re = \frac{\bar{w} d_{eqv}}{\nu},$$

$$Re_* = \frac{d_{eqv}}{\nu} \sqrt{\frac{\tau_w}{\rho}} = Re \sqrt{\frac{\xi}{\delta}},$$

$$w^+ = w / \sqrt{\tau_w / \rho}, \quad x^+ = \frac{x}{\nu} \sqrt{\frac{\tau_w}{\rho}}.$$

The Richardson number is a local parameter, and in the form of (10) it is convenient for analyzing the variation local hydrodynamic and thermal characteristics of the wall flow caused by the buoyancy effect on turbulence. In the homogeneous flows under study, the number  $Ri$  changes over the flow cross-section within a rather wide interval. The degree of thermogravitational force effect on turbulent wall flow is on the whole characterized by the  $Ri_w$  number determined from the heat flux density,  $q_w$ , and the friction stress on the wall,  $\tau_w$ , i.e. using derivative values of (10) on the wall:

$$\left\{ Ri_w = \frac{Gr_q}{Re_*^4} = \frac{Gr_q}{Re^4} \left(\frac{\delta}{\xi}\right)^2. \quad (11) \right.$$

Such determination of the global Richardson number is the most justifiable with the thermal boundary condition of the cond kind assigned on the surface.

### 3.1. Horizontal Plane Channel

It appears interesting to estimate first of all, the conditions which trigger the gravity force effect on the local heat transfer in the channel. This can be done on the basis of the problem solution under the assumption of a small effect of the Archimedian forces. From the solution carried out in [61] using the equation (9) for the relatively small buoyancy effect on the horizontal turbulent wall flow, the following equations for heat transfer and friction resistance in the plane channel at  $Pr > 0.5$  are obtained:

Work appears to be limited to turbulent air flow, in fd region.

$$Nu = Nu_0 \left[ 1 \pm \frac{Ri_w}{Pr} St_0 Re_* (4.5 \ln Re_* - 3.2 + B) \right]^{-1} \quad (12)$$

$$\xi = (\xi)_0 \left( 1 \pm 74 \frac{Gr_q}{Pr Re^{2.75}} \right) \quad (13)$$

in which the upper signs refer to the case of stable density distribution, and the lower signs, to the unstable ones;  $B=f(Pr)$  is the free term in the logarithmic law for the temperature profile (at  $Pr=0.7$ ,  $B=4$ ). From (12) it is clear that  $Ri_w$  does not completely define the heat transfer variation in the channel with a temperature-stratified turbulent liquid flow. The ratio  $Nu/Nu_0$  depends on the  $Pr$  and  $Re$  numbers.

On the basis of the solution obtained, the ratio  $Gr_q/Gr_q^{(1)}$  (see [54]) is introduced as a parameter characterizing the degree of buoyancy effect on heat transfer and channel liquid flow, where  $Gr_q^{(1)}$  determines the boundary of the 1% variation of heat transfer and is given by

$$Gr_q^{(1)} = 1.3 \cdot 10^{-4} Pr Re^{2.75} \frac{[Re^{1/8} + 2.4(Pr^{2/3} - 1)]}{\lg Re + 1.15 \lg \left( \frac{5Pr+1}{30} \right) + 0.5Pr} \quad (14)$$

derived from (12).

Experimental studies of thermal and hydrodynamic characteristics under the conditions of stable and unstable density stratification with stabilized, for mean values, heat transfer and flow ( $z/h > 30$ ,  $h$  being the channel height) were conducted in [53-56]. Earlier studies have been made of the boundary-layer flow structure [57-59] and the open tray [60].

Experimental investigations were made in [53-55] for electric heating of one of the channel surfaces ( $q_{w1} = \text{const}$ ), the other surface being adiabatic ( $q_{w2} = 0$ ). The results of velocity measurements in an air flow are presented in the universal coordinates  $(W^+ = W \sqrt{\frac{h}{\rho}}; x^+ = \frac{x}{h} \sqrt{\frac{h}{\rho}})$  in

Fig. 4 for different degrees of the stable and unstable density stratification effect. Temperature distribution is of a similar nature. It is noteworthy that the density stratification effect is noticeable as early as at relatively large values of  $Re$ ,  $Re = 3 \cdot 10^4$ , even with the channel of moderate dimensions ( $h=40\text{mm}$ ). This effect is developing beginning with the flow core and with the increasing  $Gr_q/Gr_q^{(1)}$ , i.e. buoyancy effect degree, spreads over the regions closer and closer to the wall. With the decreasing  $Re$  number, the buoyancy effect is essentially increased, which can be seen from Fig. 4 and the relationship (14). Under the unsteady stratification conditions, the curves are

displaced downwards from the distribution with indifferent density stratification, demonstrating an increase in the

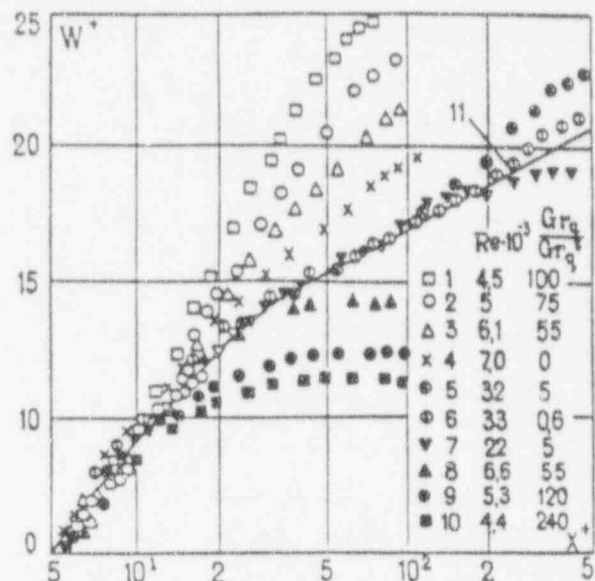


Fig. 4. Velocity distribution in the universal coordinates near the heated wall: 1-3, 5 - stable stratification; 7-10 - unstable stratification; 11 - calculation using the Reichardt formula.

momentum transfer. In the case of stable stratification, the curves  $W^+(x^+)$  are shifted upwards, demonstrating the momentum transfer decay and approaching the velocity distributions typical of laminar flows.

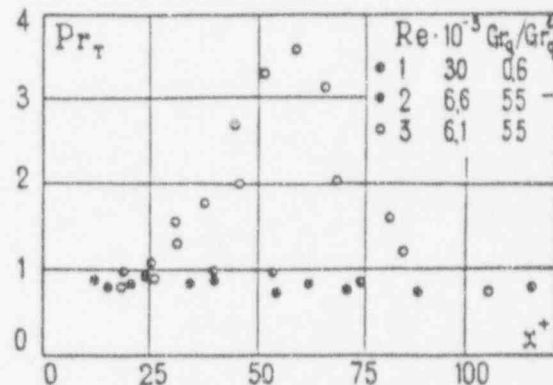


Fig. 5. Dependence of the turbulent Prandtl number on the dimensionless coordinate for the cases of neutral (1), unstable (2) and stable (3) density stratification.

Figure 5 displays the data obtained in [55] on the turbulent Prandtl number ( $Pr_T = \nu_m/\alpha_T$ ) distribution over the channel height from the heated wall up to the values  $2x/h=0.5$ . An essential difference in the character of this relationship behaviour is observed with diffe-



rent density stratifications. In the cases of neutral and unstable stratifications,  $Pr_T$  is slightly decreased from the value close to unity near the wall to the value of approximately 0.8 in the flow core, the difference in  $Pr_T$  in these cases being small. In the case of stable stratification, the relationship  $Pr_T(x^+)$  displays a pronounced maximum at  $(2x/h) \approx 0.2$ , reaching the value of 3.5. The value of  $Pr_T$  being larger than unity at stable stratification in the wall region, proves a stronger decay of heat transfer than of momentum transfer in these conditions.

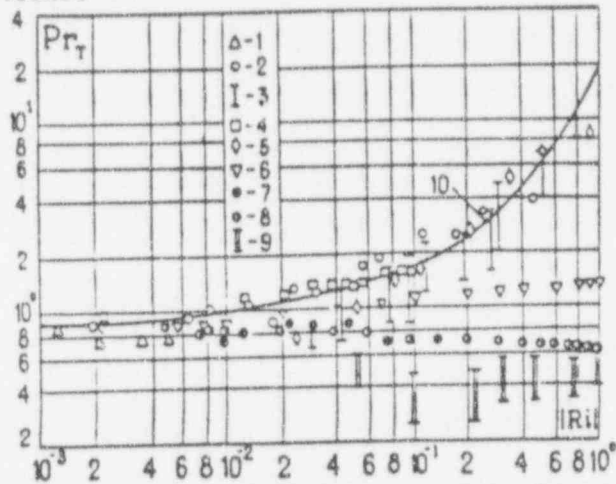


Fig.6. Dependence of the turbulent Prandtl number on the degree of buoyancy force effect with stable (1-6) and unstable (7-9) density stratification: 1-5, 7, 9 - laboratory studies; 6, 8 - atmospheric studies [62]; 10 - calculation using the Ellison relationship; 1, 2, 7 - [55]; 3, 9 - [60]; 4 - [63]; 5 - [64].

Experimental data on  $Pr_T$  obtained both in the laboratory and in natural atmospheric investigations are given in Fig.6 as a function of the local number  $|Ri|$ . The results of [55] are given for the wall region of the flow, corresponding to  $x^+ > 20$  and  $(2x/h) < 0.2$ . All the data at  $|Ri| < 0.01$  are grouped near the value  $Pr_T = 0.85$  with the accuracy  $\pm 10\%$  independently of the buoyancy effect conditions (stable or unstable stratification, laboratory or atmospheric studies). Evidently, the value  $|Ri| = 0.01$  can be considered as the initiation boundary of the buoyancy effect on the turbulent transfer processes. With the increasing effect of unstable stratification, the laboratory data [55] and atmospheric observations of W.Pruitt [62] exhibit a weak tendency toward the decrease of  $Pr_T$ . The data of [60] demonstrate a stronger decrease of  $Pr_T$  and yield the minimum value  $Pr_T = 0.3$  at  $Ri = -0.2$ . With stable density distribution,  $Pr_T$  increases with  $Ri$ . Experimental laboratory data of [55, 59,

63, 64] agree well with one another and with the Ellison relationship [65]:

$$Pr_T = (Pr_T)_0 \frac{(1-Ri)^2}{(1-Ri/Ri_{cr})}, \quad Ri_{cr} = \frac{Ri}{Pr_T} \quad (15)$$

The calculation curve plotted in Fig.6 corresponds to  $(Pr_T)_0 = 0.85$  and  $Ri_{cr} = 0.1$ . At the same time, the atmospheric studies data obtained by Pruitt [62] exhibit a considerably smaller increase of  $Pr_T$  with the increasing  $Ri$ .

The results presented in Figs.5,6 demonstrate the necessity of a more comprehensive studying of specific features of turbulent momentum and heat transfer in temperature-stratified wall flows, channels included.

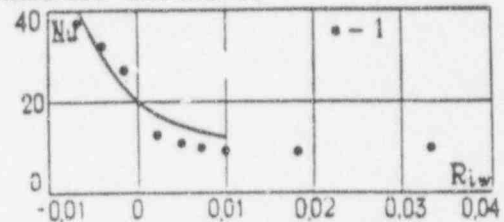


Fig.7. Heat transfer coefficient of the heated wall as a function of the density stratification conditions and the degree of buoyancy force effect: 1 - experimental data; 2 - calculation using [58].

Figure 7 presents the data [53-56] on heat transfer ( $Nu = q_w 2h / \lambda (T_w - T_b)$ ) for close values of  $Re = (6+8) \cdot 10^3$  depending on the global number  $Ri_w$ . Over the entire range of the conditions realized in the experiment, from the maximum instability ( $Ri_w = 0.008$ ) to the maximum stability ( $Ri_w = 0.035$ ) of density stratification, a monotonous variation of the  $Nu$  number is observed. Unstable stratification ( $Ri < 0$ ) leads to intensification of heat transfer, while stable one - to its deterioration and transfer to the laminated heat transfer regime, i.e. the flow with a constant value of  $Nu$ . Experimental data are compared with the calculation results obtained using the relationship of [12]. With unstable stratification, calculation and experimental results are in a good agreement, while in the case of stable stratification, the calculation data slightly exceed the experimental ones. The latter fact may be attributable to the calculation dependence of [12] being obtained without taking into account the considerable variation of  $Pr_T$ .

Thus, the data available demonstrate that the buoyancy forces may exert an essential influence directly on turbulence in the channels of limited dimensions, leading to changes in turbulent transfer of momentum and heat, and hence in heat release.

Figure 9 displays the experimental data obtained in [ 71 ] on turbulent energy distribution ( $b = 1/2 \sum_{i=1}^3 \langle u_i^2 \rangle$ ) in the horizontal and vertical diametral planes (the angle coordinate  $\Phi$  is calculated from the upper generatrix) at the relatively small ratio  $Gr_q/Gr_q^{(1)} = 12$  and with a

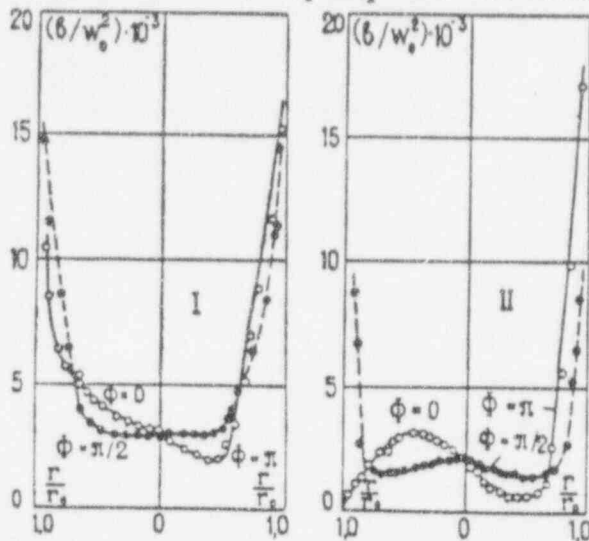


Fig. 9. Comparison of measurements results on turbulence energy with different degrees of the buoyancy effect:

- I -  $Re = 4.3 \cdot 10^4$ ,  $Gr_q/Gr_q^{(1)} = 12$ ;  
 II -  $Re = 1.2 \cdot 10^4$ ,  $Gr_q/Gr_q^{(1)} = 110$ .

strong influence of buoyancy forces ( $Gr_q/Gr_q^{(1)} = 110$ ). In the first case, although a certain asymmetry in the vertical distribution of  $b$  is observed, the differences in turbulent energy distributions in the vertical and horizontal planes are negligible; in the second case, i.e. at  $Gr_q/Gr_q^{(1)} = 110$ , the distribution of  $b$  is of a qualitatively different nature. In the vicinity of the upper generatrix,  $\Phi = 0$ , the turbulence decays under the action of stable density stratification, and the value of turbulent energy in the region near the wall ( $1-r/r_0 < 0.2$ ) here is much smaller, than in the same region in the vicinity of the middle generatrix,  $\Phi = \pi/2$ . In the vicinity of the lower generatrix,  $\Phi = \pi$ , the value of  $b$  near the wall is larger, than in the horizontal diametral plane, which reflects the turbulence intensification under the conditions of unstable density distribution in the lower portion of the tube.

It appears that exactly these specific features of turbulence variation over perimeter under the action of buoyancy entail changes in the secondary flows structure in a horizontal round tube. With the effect of thermogravitation being relatively small,  $Gr_q/Gr_q^{(1)} = 30$ , the radial velocity component in the vertical diametral plane is directed along the entire

diameter, while the tangential component in the horizontal diametral plane is directed upwards near the wall and downwards in the central part of the flow (Fig. 10, A). This pattern of distribution

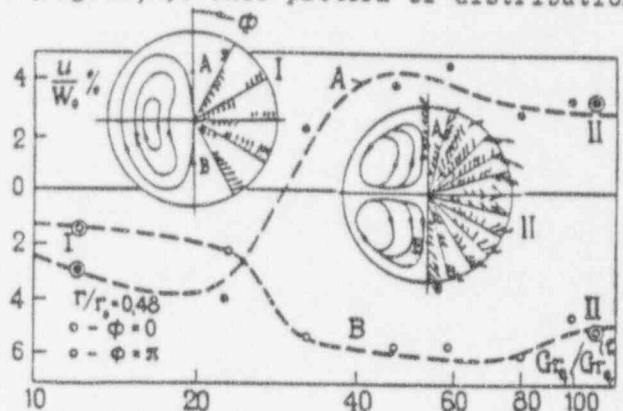


Fig. 10. Determination of the boundaries of existence of different forms of secondary flows [ 71 ]. Velocity vectors and provisional schemes of secondary flows:

- I -  $Re = 4.3 \cdot 10^4$ ,  $Gr_q = 2 \cdot 10^9$ ;  
 II -  $Re = 1.2 \cdot 10^4$ ,  $Gr_q = 5 \cdot 10^8$ .

of the velocity vector components corresponds to the two-vortex structure of secondary flows predicted in [ 72 ] and presented schematically in the same figure. It is similar to the secondary flow structure in the viscous-gravitational flow. Under a strong action of thermogravitation,  $Gr_q/Gr_q^{(1)} > 50$ , as can be seen from Fig. 10B, the radial velocity component in the vertical diametral plane in the upper part of the tube is directed upwards, and in the lower part, just as in the previous case, downwards. At the same time, the tangential velocity component in the horizontal diametral plane is absent, while the radial component in this plane is directed toward the centre. Variation of the secondary flows structure occurs at  $Gr_q/Gr_q^{(1)} = (30+35)$ , corresponding to  $Gr_q/Re = (1.5+2) \cdot 10^4$  (see the two curves displayed in Fig. 10). These curves demonstrate variation of the radial velocity component values at the two points of the vertical diameter ( $\Phi = 0, R = 0.48$ ) and ( $\Phi = \pi, R = 0.48$ ) as a function of the parameter  $Gr_q/Gr_q^{(1)}$ . The radial velocity component value on the plot is referred to the axial velocity component on the channel axis.

Specific features of the flow discussed above also determine the character of heat transfer. With the combined forced and free convection present in horizontal tubes, heat transfer changes over the tube perimeter the stronger, the larger the ratio  $Gr_q/Gr_q^{(1)}$ . On the upper generatrix, the Nu number has the minimum value, and is decreased with an

increase of  $Gr_q/Gr_q^{(1)}$ ; near the lower generatrix, it has the maximum value and increases with an increase of  $Gr_q/Gr_q^{(1)}$ .

Experimental investigation of local heat transfer over the length and perimeter during turbulent mixed convection in horizontal round tubes is discussed in [68,69,75]. The experiments were conducted with water and air and comprised the interval of values  $8 \cdot 10^3 \leq Re \leq 5 \cdot 10^4$ ;  $0.7 < Pr < 8$ ;  $0.2 \leq Gr_q/Gr_q^{(1)} \leq 300$ .

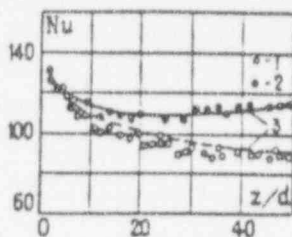


Fig.11. Distribution of the local Nu number along the horizontal tube. Experimental data [68]: 1 -  $\Phi=0$ ; 2 -  $\Phi=\pi$ ; 3 - calculation [77],  $Re=4.95 \cdot 10^4$ ,  $Gr_q = 1.9 \cdot 10^9$ .

Figure 11 shows the heat transfer variation along the upper and lower generatrices of the tube according to the data of [68] for the case of relatively small effect of thermogravitation forces. It can be seen in this figure, that the buoyancy effect increases with the increasing distance from the heat source, which is due to the thermal boundary layer formation. That is why in the initial thermal region the effect of thermogravitation forces appears at much larger values of Grashof number than in the region remote from the heat source. The local Gr number calculated using the parameters in the tube cross-section, where the relation

$$\frac{(T_w)_{\Phi=0} - (T_w)_{\Phi=\pi}}{2[(T_w)_{\Phi=\pi} - T_b]} = 0.05$$

is satisfied, is interpreted as the limit one at the given  $z/d$ , and is described by the following dependence:

$$Gr_q^{(1)} = 5Gr_q^{(1)} \left[ 1 + \frac{200}{z/d} \exp(-z/d) \right]. \quad (17)$$

The lines in Fig.11 represent the calculation results of [76,77] which are in fair agreement with the experimental data. The solution is carried out using the equations of motion and heat transfer in the boundary layer approximation and the equations for energy and turbulence dissipation (the  $k-\epsilon$  model). The equations describing turbulent heat transfer were not used. This, naturally, made it impossible to obtain the data on specific features of turbulent heat trans-

fer as compared to the momentum transfer. The absence of similarity between them at stable density stratification is demonstrated by the results given in Figs.5,6. The solution results satisfactorily describe the data of [67-71] on local heat transfer under the two-vortex secondary flow structure conditions, corresponding to  $Gr_q/Gr_q^{(1)} < 30$  (see Fig.10), and are presented, specifically, in Fig.11.

The experimental data obtained on local heat transfer near the upper and lower generatrix are generalized over the entire range of the determining parameters specified earlier, by the following empirical relationships:

$$Nu_x/Nu_0 = 1 + 0.035(Gr_q/Gr_q^{(1)})^{0.43} \quad (18)$$

$$Nu_\pi/Nu_0 = [1 + (Gr_q/Gr_q^{(1)})^3]^{0.048}, \quad (19)$$

in which  $Gr_q^{(1)}$  is determined using relationship (17). From equations (18),(19) it follows that at larger values of the thermogravitation effect parameter,  $Gr_q/Gr_q^{(1)} \approx 300$ , heat transfer on the lower generatrix of the tube is by 40% higher than in a forced turbulent flow, while on the lower generatrix, the  $Nu_{\Phi=0}$  number is smaller than  $Nu_0$  almost twice.

The effect of thermogravitation forces on the perimeter-averaged heat transfer is exhibited to a lesser extent than that on the local heat transfer, and appears at essentially larger values of  $Gr_q/Gr_q^{(1)}$ , which is proved by the calculation results of [76,77].

### 3.3. Vertical Tubes

In the first papers dealing with solution of the problem of turbulent flow and heat transfer in vertical tubes in the gravity force field [78,79], the thermogravitation effect only on the averaged flow was taken into account, while turbulent transfer characteristics were taken from the data on purely forced convection. This approach does not allow a correct description, not only quantitative, but also qualitative, of the character of dependence of the Nu number on the Gr number, which was established in later experimental investigations [80-88]. Thus, in the case of an ascending flow in a heated tube, the calculations showed that the Nu number increases monotonously with the increasing Gr, at  $Re=idem$ , and decreases in the case of a descending flow. This character of heat transfer variation qualitatively corresponds to that in a laminar flow. At the same time, the experimental data prove that in a turbulent ascending flow in heated tubes the Nu number first decreases with an increase of Gr number, and then increases; in the



case of a descending flow, it monotonously increases. The noted differences in the heat transfer behaviour during turbulent and laminar flow make it possible to expect a considerable variation of turbulent transfer characteristics in the gravity force field in the cases considered.

Theoretical analysis of the flow and heat transfer characteristics under a small gravity field effect on turbulent liquid flow in tubes conducted in [89, 90], made it possible to establish that the said differences in the heat transfer behaviour are due to the dominant effect of buoyancy directly on turbulence at the initial stage of the process (at  $Pr > 0.5$ ), as compared to its effect on the averaged flow. Under the assumption of heat transfer variation only under the effect of turbulent momentum transfer change due to buoyancy forces, the limit value of the  $Gr_q^{(1)}$  number has been established for a vertical round tube, which at  $Pr > 0.5$  coincides with the equation (14).

In the case of liquid motion in vertical tubes in the gravity force field, the ascending flow during liquid heating and the descending one during its cooling are practically equivalent; the ascending flow during cooling and the descending flow during heating are also equivalent. According to the experimental data available, we shall consider further on the ascending and descending flow during the liquid heating.

### 3.4. Ascending Flow With Liquid Heating

The data available on the thermogravitation effect on turbulent transfer in

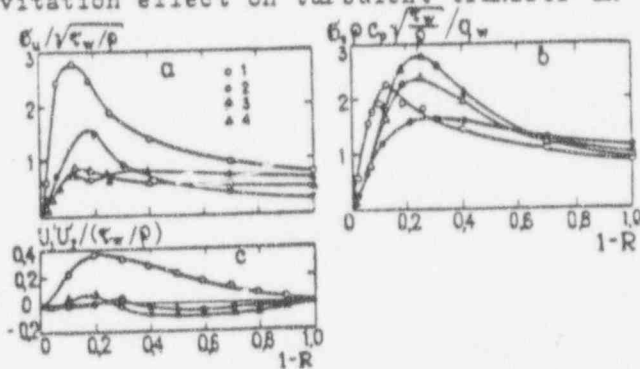


Fig.12. Distribution of turbulence characteristics over the tube cross-section at  $Re = 5300$  [85]:

- a - fluctuation intensity of the axial component; b - temperature fluctuation intensity; c - turbulent tangential stresses; 1 -  $Gr_q = 7 \cdot 10^6$ ; 2 -  $Gr_q = 1.5 \cdot 10^7$ ; 3 -  $Gr_q = 1.8 \cdot 10^7$ ; 4 -  $Gr_q = 2.2 \cdot 10^7$ .

vertical tubes are very scarce. In fact, this problem was never given a systematic

consideration. Some information on fluctuating characteristics in an air flow was obtained in [82,85,91,92]. Fig.12 displays the experimental investigation results on intensity of temperature fluctuation and axial velocity component, and also on turbulent tangential stress obtained in [85]. It can be seen in this figure that the intensity of the axial velocity component fluctuations (Fig.12a) is decreased with an increase of  $Gr_q$  at  $Re = const$ , provided that the temperature fluctuation intensity (Fig.12b) first decreases and then increases with simultaneous displacement of the maximum from the wall towards the tube axis. Similar results on temperature fluctuations were obtained in [82,91]. It is clear from Fig.12c that at  $Re = 5300$  the Reynolds stresses, decreasing with an increase of  $Gr_q$ , at  $Gr_q = 2.2 \cdot 10^7$  ( $Gr_q/Gr_q^{(1)} = 23$ ) approach zero over the entire flow cross-section.

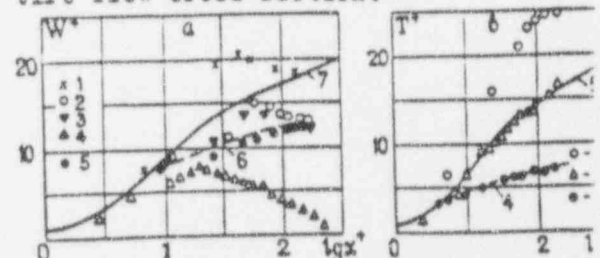


Fig.13. Velocity (a) and temperature (b) distribution in an ascending and descending air flow: a) ascending motion,  $Re = 5 \cdot 10^3$ ; 1 -  $Gr_q = 2.2 \cdot 10^7$ ,  $Gr_q/PrRe^4 = 5 \cdot 10^{-8}$ ,  $Gr_q/Gr_q^{(1)} = 23$  [82]; 2 -  $7.9 \cdot 10^7$ ,  $1.8 \cdot 10^{-7}$ , 120 [66]; 3 -  $8 \cdot 10^7$ ,  $1.8 \cdot 10^{-7}$ , 140 [82]; 4 - free-convective flow past a vertical plate,  $Gr_z = 2 \cdot 10^{12}$  [91]; b) descending flow, 5 -  $Re = 2.05 \cdot 10^3$ ,  $Gr_q = 1.2 \cdot 10^7$  [66],  $Gr_q/PrRe^4 = 1.6 \cdot 10^{-8}$ ; 6 - the "-1/3" law; 7 -  $Gr \rightarrow 0$ . Ascending motion, 1 -  $Re = 9.8 \cdot 10^3$ ,  $Gr_q = 1.2 \cdot 10^8$ ,  $Gr_q/PrRe^4 = 2 \cdot 10^{-7}$ ,  $Gr_q/Gr_q^{(1)} = 18$  [82]; 2 - free-convective flow past a vertical plate,  $Gr_z = 2 \cdot 10^{12}$  [98]. Descending motion, 3 -  $(Gr_q/PrRe^4) = 5.4 \cdot 10^{-6}$  [93]; 4 - the "-1" law; 5 -  $Gr \rightarrow 0$ .

An essential change in the character of heat transfer process in vertical tubes under the effect of thermogravitation, in particular, a decrease of turbulent transfer under certain conditions is demonstrated by the velocity and temperature distributions presented in universal coordinates in Fig.13. This figure displays the experimental data of [66,82,85,93] both for an ascending and descending air motion.

With the values of  $Gr_q$  number (or  $Gr_q/Gr_q^{(0)}$  parameter) being relatively small, the experimental data are situated above the curves denoting the purely forced flow ( $Gr_q \rightarrow 0$ ), which is due to a decrease in turbulent transfer. A qualitatively similar tendency of the velocity profile variation is exhibited by the data presented in Fig.4 for the case of stable density stratification leading to the decay of turbulence. While the  $Gr_q$  number increases under the action of thermogravitation forces on the averaged flow, the velocity and temperature profiles are gradually rearranged. The effect of buoyancy directly on the averaged flow is exhibited in the formation of a maximum on the velocity profile between the axis and the wall of the tube. Under these conditions, the flow is characterized by large-scale velocity and temperature fluctuations. With further increase of the  $Gr_q$  number, the effect of thermogravitation forces on the averaged flow becomes dominant, and finally, the "free convection" regime is developed in the forced flow. In the velocity distribution, the maximum point between the axis and the wall becomes more and more distinct, and the profile is situated below the velocity profile for a purely forced flow (see Fig.13a), approaching the one typical of turbulent free-convective flow along the vertical surface. It can be assumed, that in this case the temperature distribution also approaches that at free turbulent convection, coinciding with the distribution in a purely forced flow ( $Gr_q \rightarrow 0$ ), as can be seen in Fig.13b.

The few data available on the velocity and temperature fields reveal a number of specific features in transfer, exhibited in the character of heat transfer variation. Consider the experimental data on heat transfer in conjunction with the recently conducted calculation and theoretical studies [77,94,95] and also with the results of physical analysis and generalization [89,90,96].

In [94], an attempt was made to take into account the effect of thermogravitation forces on turbulent momentum transfer. However, it didn't help to solve the problem.

A more adequate approach was developed in [95]. The system of averaged equations of conservation, written in the boundary-layer approximation allowing for thermogravitation forces, was solved numerically. The relationships for the turbulent momentum transfer coefficient and the turbulent Prandtl number,  $Pr_T$ , were found from the analysis of approximate equations of turbulent energy balance and enthalpy fluctuations intensity, which has made it possible to account for the buoyancy effect on turbulent momentum and heat transfer. When the thermogravitation effect is absent ( $Gr=0$ ), the dependences for  $\psi_T$  and  $Pr_T$  are converted into the known dependen-

ces. Results of calculation of the Nu number for the case of an ascending flow ( $Pr=5+7$ ) in heated tubes with constant

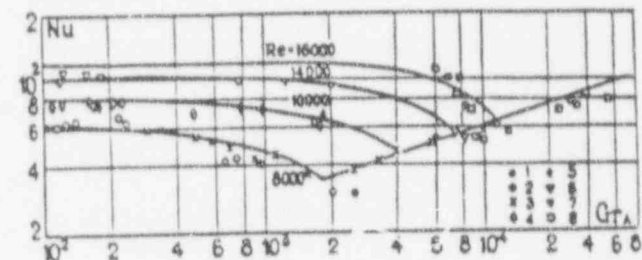


Fig.14 Theoretical calculation results of heat transfer in an ascending water flow in a vertical heated tube (curves) compared with the experimental data (dots).  $Re=8 \cdot 10^3$ : 1 - [80]; 2 - [83]; 3 - [87];  $Re=10^4$ : 4 - [80]; 5 - [83];  $Re = 1.4 \cdot 10^4$ : 6 - [80]; 7 - [83];  $Re = 1.6 \cdot 10^4$ : 8 - [87].

heat flux density on the wall are presented in Fig.14 as a function of the Grashof number determined from the mean-mass liquid temperature gradient:

$$Gr_A = \frac{8\gamma r_o^4 (dT_b/dz)}{\nu^2} = Gr_q/4 Pe.$$

The data refer to the region remote from the inlet ( $z/d=40$  and  $100$ ). At small  $Gr_A$  numbers, the Nu number is independent of  $Gr_A$  and is in a good agreement with the known dependences for purely forced convection. A further increase of  $Gr_A$  ( $Re$  being constant) leads to a decrease in the Nu number due to a decreasing turbulent transfer under the conditions of stable density stratification. Subsequent increase of  $Gr_A$  above a certain value (which is the larger the higher  $Re$ ) the dependence character is changed: the Nu number increases with  $Gr_A$  and is practically independent of  $Re$ . This portion of the curve corresponds to the dominant role of free convection in the flow formation. The calculation results satisfactorily describe the experimental data.

In a more comprehensive statement, the problem of turbulent flow and heat transfer in round tubes essentially affected by buoyancy was solved numerically in [77]. The case of an arbitrary tube position with respect to the free-fall acceleration vector was considered (see above).

A generalization of the experimental data on heat transfer in a water and air flow for  $(z/d) > 40$  is displayed in Fig.15. Experimental data over the entire range of the determining parameters variation, from the flow in the absence of mass forces effect to the flow with dominant mass forces effect ("free-convection" regime)

are described by a complex enough equation obtained in [96]. We shall consider a particular case only.

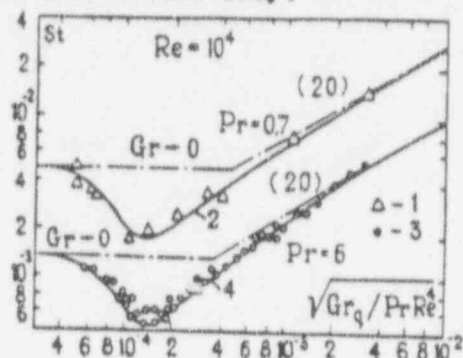


Fig.15. Dependence of the St number on the parameter  $Gr_0/PrRe^4$ . Air flow ( $Pr=0.7$ ): 1 - experimental data [66, 82], 2 - calculation using the formula of [96]. Water flow ( $Pr=6$ ): 3 - experimental data [83], 4 - calculation using the formula of [96].

At the values  $(Gr_0/PrRe^4) > 10^{-6}$  and  $Gr_0/Gr_c^{(1)} > 300$ , heat transfer is described by the following equation:

$$Nu_{\pm} = \frac{Pr^{3/4} Gr^{1/4}}{1.331g(Re/8) + 3.3(Pr^{2/3} - 0.7)} \quad (20)$$

The calculations using (20) are denoted in Fig.15 with dashed inclined lines. In this case, heat transfer considerably exceeds that in a forced flow in the absence of mass forces effect ( $Re$  values being the same).

Based on the analysis conducted in [96], a conclusion can be drawn that if it were not for the buoyancy effect on turbulence, the St number variation would practically follow the dependences denoted with dashed lines.

Previously, we considered the data on the buoyancy effect on turbulent flow and heat transfer of liquids with moderate Pr numbers. In [86, 90, 97] it is shown that for liquid metals ( $Pr \ll 1$ ) this effect is none the less important. The turbulent momentum and heat transfer coefficients, calculated in [86] from the measured velocity and temperature profiles in a mercury flow, depend both on Reynolds and Grashof numbers. The data obtained in the same paper on heat transfer demonstrate the character of the relationship  $Nu(Gr)$  at  $Re=const$ , similar to that given in Fig.14. A decrease in the Nu number is due, as shown earlier, to a decrease in turbulent transfer under the action of thermogravitation forces. Development of mixed convection in liquid metals, however, may obviously have its specific features. In particular, the analysis of [90] suggests that under certain condi-

tions (small Pr numbers and relatively small Re numbers), the ratio  $Nu(Gr)$  at  $Re=const$  may be a monotonously increasing one, having no point with the minimum value. Note that the discrepancy in the experimental data available on heat transfer to liquid metals, especially with small turbulent values of Pr, is probably due to different degrees of the free convection effect, which was not taken into account in the analysis.

### 3.5. Descending Flow With Liquid Heating

Experimental results of [66, 80, 83, 88] show that in this case heat transfer monotonously increases with the increasing buoyancy effect ( $Re=const$ ). In [89] it is shown that the heat transfer increase is caused by the turbulent transfer intensification under the unstable density distribution conditions. Numerical solutions of the problem conducted in [77, 95] proved this conclusion. The solution results are in fair agreement with the experimental data on heat transfer. Experimental data on the increase of velocity fluctuations intensity near the cooled surface with an increase of buoyancy effect in an ascending air flow in a vertical plane channel are obtained in [92].

An increase in turbulent transfer is demonstrated by the scarce experimental data on velocity and temperature distributions [66, 93], shown in Fig.13. Experimental data (black dots) are presented in the universal coordinates against the dependences (solid lines) characteristic of forced flow without the mass forces effect. The values of  $W^+$  and  $T^+$  with the buoyancy effect are displaced downwards from the corresponding values at  $Gr \rightarrow 0$ , which is similar to the results for horizontal flows under the unstable stratification conditions (see Fig.4).

Thus, in the case under study, which corresponds to unstable density distribution, the turbulent transfer is enhanced with an increase of Gr, leading to the increasing fullness of velocity and temperature profiles and a corresponding increase of resistance and heat transfer.

With strong effect of thermogravitation, a regime is developed, which can be defined as the regime of "thermogravitational initiation of turbulence". Then the flow and heat transfer characteristics are mainly governed by the intensive turbulent transfer caused by turbulence generation due to the Archimedian forces and not to the averaged flow. In equation (9), the second term is much larger than the first. The velocity and temperature profiles in the turbulent flow core are given by the relationship corresponding to the "-1/3" law, and denoted in Fig.13 with dashed lines. Heat transfer in this case is given by the following dependence



[ 99 ]:

$$Nu_{\xi} = \frac{0.5Pr^{0.5}Gr^{0.25}}{1 + Pr^{0.5}} \quad (21)$$

Figure 16 presents the experimental data on the local heat transfer ( $z/d > 40$ )

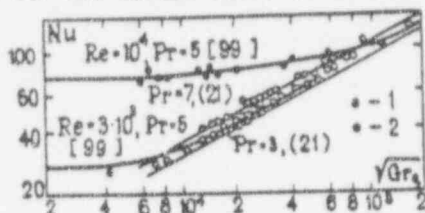


Fig. 16. Dependence of the Nu number on the Gr number in a descending water flow in vertical heated tubes: 1, 2 - experimental data of [ 80, 83, 88 ] at  $Pr = 5+6.4$ ,  $Re = (9.4+11.5) \cdot 10^3$  and  $Pr = 3+6$ ,  $Re = (2.2+4.6) \cdot 10^3$ , respectively.

obtained by several authors [ 80, 83, 88 ], who considered the water flow ( $Pr=3+7$ ) in comparison with the calculation results from the equation obtained in [ 99 ]. The relationship suggested in [ 99 ] generalizes the experimental data available on water and air over the entire range of the determining parameters variation, viz. from the conditions not affected by mass forces to the regime of thermogravitational initiation of turbulence at  $q_w = \text{const}$  and  $z/d > 40$ . In the latter case this relationship is transformed into the relationship (21), as shown in Fig. 16.

In the paper by Jackson and Fewster [ 88 ], another empirical dependence is suggested, derived on the basis of generalization of the experimental data obtained by the authors of [ 88 ].

Up till now, we have considered the data on tube cross-sections remote from the heat source ( $z/d > 40$ ). In [ 100 ], experiments were conducted on a relatively short tube of a large diameter ( $l/d=3$ ,  $d=200\text{mm}$ ), which revealed the presence, under certain conditions, of a reverse flow in the wall layer. With a relatively small height of the heat transfer length and small velocity, the forced flow may be "pushed off" from the wall by the opposite free-convective currents, converging beyond the heat transfer length of the channel. A pronounced inhomogeneity of the temperature field near the heat source also contributes to this. The presence of secondary flows directed opposite to the main forced flow in the long channels is hardly possible, and the thermal-hydrodynamic disturbances developed in the initial section and causing turbulence in this region of the flow are evidently "smeared" in the course of motion along

the tube length. The experimental data obtained in long tubes, demonstrating the appearance of heat transfer stabilization, speak in favour of it.

Modern calculation techniques and computers ensure solution of complete three-dimensional equations of energy and motion for laminar flows, thus providing a principle possibility of solution of various problems on mixed laminar convection. However, the region of mixed laminar convection existence is extremely limited owing to the intensive thermal-hydrodynamic flow disturbances realized in these conditions. This makes the necessity of systematic studying of stability violation of laminar channel flows essentially affected by buoyancy forces extremely important.

Further progress in studying of turbulent flow and heat transfer with combined forced and free convection, requires systematic experimental investigations of the flow structure and regularities of turbulent momentum and heat transfer. Apart from studying the structure, it is necessary to obtain more comprehensive experimental data on heat transfer and resistance over a wide range of Gr, Re and Pr numbers, with different orientations of the system in the gravity force field. On the basis of experimental data and modern methods of the turbulence theory, adequately general calculation techniques of heat transfer and resistance in the case of turbulent mixed convection in tubes can be developed.

#### REFERENCES

1. Petukhov, B.S., Heat Transfer and Resistance in Laminar Liquid Flow in Tubes, pp. 1-411, Energiya, Moscow, 1967.
2. Shannon, R.L., and Depew, C.A., Combined Free and Forced Laminar Convection in a Horizontal Tube With Uniform Heat Flux, Trans. ASME, vol. C90, pp. 78-83, 1968.
3. Paris, L.N., and Viskanta, R.A., An Analysis of Laminar Combined Forced and Free Convection Heat Transfer in a Horizontal Tube, Int. J. Heat Mass Transfer, vol. 12, pp. 1295-1310, 1969.
4. Siegwarth, D.P., and Hanratty, T.G., Computational and Experimental Study of Effect of Secondary Flow on the Temperature Field and Primary Flow in a Heated Horizontal Tube, Int. J. Heat Mass Transfer, vol. 13, pp. 27-42, 1970.
5. Newall, P.H., and Bergles, A.E., Analysis of Combined Free and Forced Convection for Fully Developed Laminar Flow in Horizontal Tubes, Trans. ASME, vol. C92, pp. 87-99, 1970.



6. Hong, S.W., Marcos, S.M., and Bergles, A.E., Analytical and Experimental Results for Combined Forced and Free Laminar Convection in Horizontal Tubes, Proc. 5th Int. Heat Transfer Conf., Tokyo, vol. 4, NC 4.6, pp. 154-158, 1974.
7. Marcos, S.M., and Bergles, A.E., Experimental Investigation of Combined Free and Forced Laminar Convection in Horizontal Tubes, Trans. ASME, vol. C97, pp. 54-62, 1975.
8. Cheng, K.C., and Jenn-Wuu Ou, Free Convection Effects on Graetz Problem for Large Prandtl Number Fluids in Horizontal Tubes With Uniform Heat Flux, Proc. 5th Int. Heat Transfer Conf., Tokyo, vol. 4, NC 4.7, pp. 159-163, 1974; Natural Convection Effects on Graetz Problem in Horizontal Isothermal Tubes, Int. J. Heat Mass Transfer, vol. 20, pp. 953-960, 1977; Maximum Density Effects on Forced Laminar Convection in Horizontal Water Pipes With Near Freezing Wall Temperature, Proc. 6th Int. Heat Transfer Conf., Toronto, vol. 1, NC 12, pp. 67-72, 1978.
9. Mori, Y., and Futagami, K., Forced Convective Heat Transfer in Uniformly Heated Horizontal Tubes, Int. J. Heat Mass Transfer, vol. 10, pp. 1801-1813, 1967.
10. Siegwarth, D.P., Mikesell, R.D., Redal, T.C., and Hanratty, T.Y., Effect of Secondary Flow on the Temperature Field and Primary Flow in a Heated Horizontal Tube, Int. J. Heat Mass Transfer, vol. 12, pp. 1535-1552, 1969.
11. Vilensky, V.D., Petukhov, B.S., and Kharin, B.E., Heat Transfer and Resistance in a Round Tube in Laminar Gas Flow With Variable Properties. 2. Calculation Results, Teplofiz. Vysok. Temp., vol. 9, pp. 563-570, 1971.
12. Collins, M.W., Heat Transfer by Laminar Combined Convection in a Vertical Tube - Prediction for Water, Proc. 6th Int. Heat Transfer Conf., Toronto, vol. 1, NC 5, pp. 25-30, 1978; Combined Convection in Vertical Tubes, Proc. Symp. Heat Mass Transfer by Combined Forced and Natural Convection, London, Inst. Mech. Eng., C 115/71, pp. 17-25, 1971.
13. Petukhov, B.S., Polyakov, A.F., and Strigin, B.K., Investigation of Heat Transfer in Viscogravitational Flow Through Tubes, in Heat and Mass Transfer, vol. 1, pp. 607-618, Energiya, Moscow, 1968.
14. Quintiere, J., and Mueller, W.K., An Analysis of Laminar Free and Forced Convection Between Finite Vertical Parallel Plates, Trans. ASME, vol. C95, pp. 53-59, 1973.
15. Kanev, S.N., and Ravs, V.V., Investigation of Heat Transfer and Resistance in Combined Convection Over the Starting Length of a Round Tube, Proc. 3rd All-Union Scientific and Engineering Conf. on Applied Aerodynamics, Kiev, 1973.
16. Nakajima, M., Fukui, K., Ueda, H., and Mizushima, T., Developing Combined Free and Forced Laminar Convection Between Vertical Parallel Plates With Constant Wall Temperature, J. Chem. Eng. Jap., vol. 2, pp. 24, 1978.
17. Guidice, S., Comini, G., and Mikhalov, M.D., Finite Element Analysis of Combined Free and Forced Convection, Int. J. Heat Mass Transfer, vol. 21, pp. 1619-1621, 1978.
18. Lerner, W.J., and McMillan, H.K., Theoretical Investigation of Laminar Mixed Convection With Vertical Opposed Flow, J. Heat Transfer, vol. 92, pp. 251-253, 1970.
19. Hieber, C.A., and Sreenivasan, S., Mixed Convection in an Isothermal Heated Horizontal Pipe, Int. J. Heat Mass Transfer, vol. 17, pp. 1337-1348, 1974.
20. Hussain, N.A., and McComas, S.T., Experimental Investigation of Combined Convection in a Horizontal Circular Tube With Uniform Heat Flux, Heat Transfer, vol. 4, NC 3.4, Elsevier Publ. Comp., Amsterdam, 1970.
21. Kolpashchikov, V.L., Martynenko, G., and Shnipp, A.I., A Mixed Free and Forced Laminar Convection in a Round Horizontal Tube With a Circumferentially Non-uniform Heat Flux, Proc. All-Union Conf. on Physicochemical Mechanics of Dispersed Media, Minsk, pp. 286-304, 1969.
22. Martynenko, G.G., Kolpashchikov, V., and Luikov, A.V., Peculiarities of Mixed Thermal Convection Under Non-uniform Boundary Conditions at Non-uniform Heat Generation, Preprint of Paper Presented at the 5th Int. Heat Transfer Conf., Tokyo, 1974.
23. Patankar, S.V., Ramadhyani, S., and Sparrow, E.L., Effect of Circumferentially Non-uniform Heating on Laminar Combined Convection in a Horizontal Tube, Trans. ASME, Heat Transfer, vol. 100, pp. 66-74, 1978.
24. Yao Lun-Shin, Entry Flow in a Heated Straight Tube, J. Fluid Mech., vol. 88, pp. 465-483, 1978.
25. Collins, M.W., Finite Difference Analysis for Developing Laminar Flow in Circular Tubes Applied and Combined Convection, Int. J. Numer. Methods in Eng., vol. 15, pp. 381-404, 1980.
26. Futagami Kozo and Abe Fumitaki, Heat Transfer in the Flow Inside an Inclined Cylindrical Pipe under mixed Convection Conditions, Trans. Jap. Soc. Mech. Eng., vol. 38, pp. 1795

- 1808, 1972.
27. Cheng, K.C., and Hong, S.W., Combined Free and Forced Laminar Convection in Inclined Tubes, Appl. Sci. Res., vol. 27, pp. 19-38, 1972.
  - .. Polyakov, A.P., Viscous-Gravitational Flow in Tubes Under Small Effect of Thermal Gravitation, Zh. Prikl. Mekh. Tekh. Fiz., No. 1, pp. 122-130, 1977.
  29. Ivanov, J.P., Polyakov, A.P., and Rinkevichyus, B.S., Investigation of Viscous-Gravitational Flow in a Circular Vertical Channel by Means of Laser Anemometer, Teplofiz. Vysok. Temp., vol. 16, pp. 217-219, 1978.
  30. Polyakov, A.P., Viscous-Gravitational Flow and Heat Transfer in Circular Vertical Channels Under Small Buoyancy Effect, in Problems of Convective and Radiative-Conductive Heat Transfer, pp. 67-76, Nauka, Moscow, 1980.
  31. Petukhov, B.S., and Polyakov, A.P., Experimental Investigation of Heat Transfer in Viscous-Gravitational Liquid Flow in a Horizontal Tube, Teplofiz. Vysok. Temp., vol. 5, pp. 122-130, 1967.
  32. Gupta, R.K., Unsteady Laminar Convection in Uniformly Heated Vertical Pipes, J. Fluid Mech., vol. 57, pp. 81-102, 1973.
  33. Shirkot, K.S., and Singh, S., Unsteady Combined Free and Forced Convection Effects on the Flow in a Horizontal Channel, Acta Phys. Acad. Sci. Hung., vol. 45, pp. 97-106, 1978.
  4. Santarrelli, P., and Foraboschi, F.P., Heat Transfer in Mixed Laminar Convection in a Reacting Fluid, Chem. Eng. J., vol. 6, pp. 59-68, 1973.
  35. Sastry, V.U.K., and Maiti, G., Numerical Solution of Combined Convective Heat Transfer of Micropolar Fluid in an Annulus of Two Vertical Pipes, Int. J. Heat Mass Transfer, vol. 19, pp. 207-213, 1976.
  36. Dash, G.C., and Behera, S.C., Combined Free and Forced Convection Flow of an Elastoviscous Liquid Through a Porous Channel, Wear, vol. 60, pp. 313-328, 1980.
  37. Antimirov, L.E., and Tabachnikov, E. B., Nonstationary Convection in a Plane Vertical Channel With the Prescribed Heat Flux on the Walls and Unique Specification of Steady-state Motions at the Stability Boundaries, Izv. Akad. Nauk Latv.SSR, Ser. Fiz. Tekh. Nauk, No. 3, pp. 49-57, 1975.
  38. Hong, S.W., and Bergles, A.E., Theoretical Solutions for Combined and Free Convection in Horizontal Tubes With Temperature-Dependent Viscosity, Trans. ASME, vol. C98, pp. 459-465, 1976.
  39. Szpiro, O., Allen, P.H.G., and Collins, L.W., The Influence of Temperature Dependence of Thermophysical Properties on the Prediction Accuracy in Laminar Mixed Convection Heat Transfer in Vertical Tubes, Proc. 6th Int. Heat Transfer Conf., Toronto, vol. 1, MC 6, pp. 31-36, 1978.
  40. Sabbagh, J.A., Aziz, A., El-Ariny, A.S., and Hamad, G., Combined Free and Forced Convection in Inclined Circular Tubes, Trans. ASME, No. 2, pp. 187-189, 1975.
  41. Rath, R.S., and Kabitanjali Satapathy, Combined Free and Forced Convection Flow Through Two Parallel Porous Walls, Indian J. Phys., vol. 48, pp. 432-438, 1974.
  42. Sastry, V.U.K., and Rama Mohan Rama, V., Numerical Study of the Effect of Viscous Dissipation of the Combined Convective Flow Through a Circular Pipe, Acta Mech., vol. 32, pp. 1-9, 1979.
  43. Lyubarsky, A.I., Skoropanov, Yu.S., and Popov, V.P., Heat Transfer in a Laminar Gas Flow Through a Circular Variable-Crosssection Channel, in Studies of Transport Phenomena in Complex Systems, pp. 52-63, Minsk, 1974.
  44. Makamura, H., Matsura, A., Kiwaki, J., Hirako, S., and Yamada, I., Combined Free and Forced Laminar Convection in Triangular Ducts, J. Chem. Eng. Jap., vol. 10, pp. 109-119, 1977.
  45. Lu Pau-Chang and Chen Tien-Hu, Jeffrey-Hamel Flow With Free Convection, Proc. 5th Int. Heat Transfer Conf., Tokyo, vol. 3, pp. 183-187, 1974.
  46. Maitra, D., and Subba Raju, K., Combined Free and Forced Convection Laminar Heat Transfer in a Vertical Annulus, Trans. ASME, vol. C97, pp. 135-137, 1975.
  47. Petrazhitzky, G.B., and Pisarevsky, A.E., Some Specific Features of Mixed Laminar Convection Flow in a Circular Cavity, in Trudy IVTU im. Baumana, No. 195, pp. 71-76, 1975.
  48. Gangal, M.K., and Aggarwala, B.D., Combined Free and Forced Laminar Convection in Internally Finned Square Ducts, Z. Angew. Math. und Phys., vol. 28, pp. 85-96, 1977.
  49. Kanev, S.P., Ris, V.V., and Marov, V.G., Laminar Flow Heat Transfer in a Vertical Annular Gap at Constant Temperature of the External Wall, J. Engng Phys., vol. 33, pp. 1-11, 1977.
  50. Abramov, M.N., Varapaev, V.P., and Perekalsky, V.M., Viscous Incompressible Gas Convection in Rectangular Regions With Supplying and Discharging Channels, Izv. Akad. Nauk SSSR, Mekh. Zhid. Gaza, No. 5, pp. 126-131, 1979.
  51. Monin, A.S., and Yaglom, A.M., Statistical Hydromechanics, pt. 1, Nauka, Moscow, 1965.
  52. Turner, J.S., Buoyancy Effects in

- Fluids, University Press, Cambridge, 1973.
53. Tsypulev, Yu.V., Petukhov, B.S., and Polyakov, A.F., Experimental Investigation of the Gravity Field Effect on Turbulent Air Flow in a Plane Horizontal Asymmetrically Heated Channel, Teplofiz. Vysok. Temp., vol. 17, pp. 366-371, 1979.
  54. Petukhov, B.S., Polyakov, A.F., and Tsypulev, Y.V., Peculiarities of Non-isothermal Turbulent Flow in Horizontal Flat Channels at Low Reynolds Number and Under Significant Influence of Buoyancy Forces, in Turbulent Shear Flows.2, pp. 158-167, Springer-Verlag, Berlin, 1980.
  55. Petukhov, B.S., Polyakov, A.F., and Tsypulev, Yu.V., Turbulent Momentum and Heat Transfer in a Temperature-Stratified Flow, in Heat and Mass Transfer - VI, vol. 1, pt. 1, pp.160-172, Minsk, 1980.
  56. Ustimenko, B.P., Zmeikov, V.N., and Dubilier, I.G., Investigation of Aerodynamics and Heat Transfer of a Turbulent Stratified Flow in a Horizontal Plane Channel, in Heat and Mass Transfer - VI, vol. 1, pt. 3, pp. 157-161, Minsk, 1980.
  57. Webster, C.A.G., An Experimental Study of Turbulence in a Density Stratified Shear Flow, J. Fluid Mech., vol. 19, pp. 221-245, 1964.
  58. Arya, S.P.S., Buoyancy Effects in a Horizontal Flat-Plate Boundary Layer, J. Fluid Mech., vol. 63, pt. 2, pp. 321-343, 1975.
  59. Nicholl, C.I.H., Some Dynamical Effects of Heat on a Turbulent Boundary Layer, J. Fluid Mech., vol. 40, pt. 2, pp. 361-384, 1970.
  60. Mizushina, T., Ogino, F., Ueda, H., and Komori, S., Buoyancy Effect on Eddy Diffusivities in Thermally Stratified Flow in an Open Channel, Proc. 6th Int. Heat Transfer Conf., Toronto, vol. 1, MC 16, pp. 91-96, 1978.
  61. Polyakov, A.F., Boundaries of the Archimedian Forces Effect on the Flow and Heat Transfer in Horizontal Turbulent Wall Flows, in Heat Transfer and Physical Hydrodynamics, pp. 23-33, Nauka, Moscow, 1974.
  62. Pruitt, W.O., Morgan, D.L., and Lawrence, F.I., Momentum and Mass Transfers in the Surface Boundary Layer, Quart. J. Roy. Met. Soc., vol. 99, pp. 370-386, 1973.
  63. Arya, S.P.S., and Plate, E.I., Modeling of the Stably Stratified Atmospheric Boundary Layer, J. Atmos.Sci., vol. 26, pp. 656-665, 1969.
  64. Ellison, T.H., and Turner, J.S., Mixing of Dense Fluid in a Turbulent Pipe Flow, J. Fluid Mech., No. 8, pp. 514-544, 1960.
  65. Ellison, T.H., Turbulent Transfer of Heat and Momentum From an Infinite Rough Plane, J. Fluid. Mech., vol. pp. 456-466, 1957.
  66. Mreiden, A., Etude de la Structure l'Ecoulement et du Transfert de Chaleur en Convection Mixte Dans un Tube de Section Circulaire, These de Docteur-Ingenieur, L'Universite de Paris, 1969.
  67. Polyakov, A.F., Kuleshov, V.A., and Shekhter, Yu.L., Velocity and Temperature Distribution in a Turbulent Air Flow Through a horizontal Tube Under the Effect of Thermogravitational Forces, J. Engng Phys., vol. 27, pp. 1422-1423, 1974.
  68. Petukhov, B.S., Polyakov, A.F., Kuleshov, V.A., and Shekhter, Yu.L., Turbulent Flow and Heat Transfer in Horizontal Tubes with Substantial Influence of Thermogravitational Forces, Proc. 5th Int. Heat Transfer Conf., Tokyo, vol. 3, NC 4.8, pp.16-168, 1974.
  69. Petukhov, B.S., Polyakov, A.F., Shekhter, Yu.L., and Kuleshov, V.A., Experimental Study of the Effects of Thermogravitation Upon Turbulent Flow and Heat Transfer in Horizontal Pipes, in Heat Transfer and Turbulent Buoyant Convection, vol. 2, pp. 719-727, Hemisphere Publ. Co., Washington, 1977.
  70. Petukhov, B.S., Polyakov, A.F., Troitsky, V.V., and Shekhter, Yu.L., Thermogravitational Field Effect on the Structure of a Turbulent Non-isothermal Flow in Horizontal Cylindrical Channels, Dokl. Akad. Nauk SSSR, vol. 236, pp. 280-283, 1977.
  71. Petukhov, B.S., Polyakov, A.F., Troitsky, V.V., and Shekhter, Yu.L., The Structure of Secondary Currents in Turbulent Flow in a Horizontal Tube With Substantial Thermogravitation, Proc. 6th Int. Heat Transfer Conf., Toronto, vol. 1, MC 14, pp. 79-83, 1978.
  72. Polyakov, A.F., Development of Secondary Free Convection Currents in Porced Turbulent Flow Through Horizontal Tubes, Zh. Prikl. Mekh. Tekh.Fiz No. 5, pp. 60-66, 1974.
  73. Metals, B., and Eckert, E.R.G., Forced, Mixed and Free Convection Regimes, Trans. ASME, Ser. C, Heat Transfer, vol. 86, pp. 196-198, 1964.
  74. Martynenko, O.G., Vatutin, I.A., and Skutova, I.V., Effect of Thermogravitational Convection on Distribution of Statistical Characteristics in Turbulent Non-isothermal Incompressible Liquid Flow in Tubes, in Heat Transfer and Turbulent Buoyant Convection, vol. 1, pp. 53-63, Hemisphere Publ. Co., Washington, 1977.
  75. Petukhov, B.S., and Polyakov, A.F., Flow and Heat Transfer in Horizontal Tubes, in Heat Transfer - 1970, vol. 8, NC 3.7, Elsevier Publ. Co., Am-



- sterdam, 1970.
76. Skiadaressis, D., and Spalding, D.B., Prediction of Combined Free and Forced Convection in Turbulent Flow Through Horizontal Pipes, Letts. Heat Mass Transfer, vol. 4, pp. 35-40, 1977.
  77. Abdelmeguid, A.M., and Spalding, D. B., Turbulent Flow and Heat Transfer in Pipes With Buoyancy Effects, J. Fluid Mech., vol. 94, pp. 383-400, 1979.
  78. Ber, L.E., Solution of the Problem on Superposition of Turbulent Forced and Free Heat Convection Through a Vertical Tube in the Presence of Internal Heat Sources in the Liquid, Izv. Akad. Nauk SSSR, Otd. Tekh. Nauk, No. 6, pp. 78-85, 1962.
  79. Ojalow, M.S., Anand, D.K., and Dunbar, R.P., Combined Forced and Free Turbulent Convection in a Vertical Circular Tube With Volume Heat Source and Constant Wall Heat Addition, Trans. ASME, Ser. C, J. Heat Transfer, vol. 89, pp. 54-62, 1967.
  80. Petukhov, B.S., and Sporygin, B.K., Experimental Study of Heat Transfer in a Viscous Inertial Gravitational Liquid Flow in Vertical Tubes, Teplofiz. Vysok. Temp., vol. 6, pp. 933-937, 1968.
  81. Alferov, N.S., Rybin, R.A., and Balunov, B.T., Heat Transfer in a Turbulent Water Flow Through a Vertical Tube Under the Conditions of Substantial Effect of Natural Convection, Teploenergetika, No. 12, pp. 66-70, 1969.
  82. Steiner, A., Etude de la Transition Inverse d'un Ecoulement Turbulent Sans l'Effet de la Pousse d'Archimede, J. Fluid Mech., vol. 47, pt. 3, pp. 503-512, 1971.
  83. Sarabi, A.R., Laminarisation Sans l'Influence de la Convection, These de Docteur-Ingenieur, l'Universite de Paris, 1971.
  84. Herbert, L.S., and Stern, V.J., Heat Transfer in Vertical Tubes - Interaction of Forced and Free Convection, Chem. Eng. J., vol. 4, pp. 46-52, 1972.
  85. Carr, A.R., Connor, M.A., and Buhr, H.O., Velocity, Temperature and Turbulence Measurements in Air for Pipe Flow With Combined Free and Forced Convection, Trans. ASME, Ser. C, J. Heat Transfer, vol. 95, pp. 15-22, 1973.
  86. Buhr, H.O., Horsten, E.A., and Carr, A.D., The Distortion of Turbulent Velocity and Temperature Profiles on Heating for Mercury in Vertical Pipe, Trans. ASME, Ser. C, J. Heat Transfer, vol. 96, pp. 38-45, 1974.
  87. Kenning, D.B.R., Shock, R.A.W., and Poon, J.Y.M., Local Reduction in Heat Transfer due to Buoyancy Effects in Upward Turbulent Flow, in Heat Transfer - 1974, Tokyo, vol. 3, NC 4.3, pp. 139-143, 1974.
  88. Jackson, J.D., and Fewster, J.J., Enhancement of Turbulent Heat Transfer due to Buoyancy for Downward Flow of Water in Vertical Tubes, Proc. Int. Seminar on Turbulent Buoyant Convection, Dubrovnik, 1976.
  89. Polyakov, A.F., The Boundary and Character of the Beginning of Thermogravitational Forces Effect on the Turbulent Flow and Heat Transfer in Vertical Tubes, Teplofiz. Vysok. Temp., vol. 11, pp. 106-116, 1973.
  90. Polyakov, A.F., Boundaries and Character of the Beginning of Thermogravitation Effect on the Turbulent Flow and Heat Transfer of Liquid Metals in Vertical Tubes, Teplofiz. Vysok. Temp., vol. 15, pp. 802-807, 1977.
  91. Byrne, J.K., and Eliogn, E., Combined Free and forced Convection Heat Transfer in a Vertical Pipe, Proc. Symp. Heat Mass Transfer by Combined Forced and Natural Convection, London, C 111/71, pp. 40-46, 1971.
  92. Takajima, M., Fukui, K., Ueda, H., and Mizushima, T., Buoyancy Effects on Turbulent Transport in Combined Free and Forced Convection Between Vertical Parallel Plates, Int. J. Heat Mass Transfer, vol. 23, pp. 1325-1336, 1980.
  93. Hall, B.W., and Price, P.H., Interaction Between Turbulent Free Convection Layer and a Downward Forced Flow, Proc. Conf. Heat and Mass Transfer by Combined Forced and Natural Convection, London, C 113/71, pp. 7-12, 1971.
  94. Ber, L.E., On Combined (Forced and Free) Turbulent Convection in a Channel Between Vertical Parallel Plates, Izv. Akad. Nauk SSSR, Mekh. Zhid. Gaza, No. 3, pp. 126-133, 1974.
  95. Petukhov, B.S., and Ledvetskaya, K.V., Turbulent Flow and Heat Transfer in Vertical Tubes With Strong Buoyancy Effect, Teplofiz. Vysok. Temp., vol. 16, pp. 778-786, 1978.
  96. Polyakov, A.F., Turbulent Forced Flow in Vertical Channels Under Free Convection Conditions, J. Engng Phys., vol. 35, pp. 801-811, 1978.
  97. Jacoby, J.K., and Sesonke, A., Free Convection Distortion and Eddy Diffusivity Effects in Turbulent Mercury Heat Transfer, Trans. Amer. Nucl. Soc., vol. 15, pp. 403-409, 1972.
  98. Contanceau, J., Convection Natural Turbulence Sur Une Plaque Verticale Isotherme, Int. J. Heat Mass Transfer, vol. 12, pp. 753-769, 1969.
  99. Polyakov, A.F., Flow and Heat Transfer in the Thermogravitation Generation Regime, Proc. 5th Int. Heat Transfer Conf., Tokyo, vol. 3, NC 4.4, pp. 144-148, 1974.

### 3.2. Horizontal Round Tubes

The buoyancy effect on the averaged flow in horizontal tubes exhibits itself in the formation of secondary flows in the plane normal to the tube axis. A complex character of the averaged flow is demonstrated by the results of experimental studies of a turbulent nonisothermal air flow structure in horizontal tubes 88 mm [66] and 144 mm [67-81.7 in diameter, at  $q_w = \text{const}$ .

In order to determine the boundaries of initiation of the possible development of secondary free-convective flows and their character, equations (6)-(8) were solved in [72] for the stabilized motion and heat transfer under the assumption of a relatively small thermogravitation effect. In this case, the gravity force field effect on turbulent transfer is neglected. Combined analysis of the solutions of [61,72] shows that in horizontal tubes with small Gr number values, thermogravitation forces affect primarily the averaged flow. The buoyancy effect on turbulent transfer becomes noticeable at somewhat larger Gr number values. The approximate solution of [72] made it possible to obtain an equation defining the boundary of a 1% deviation of the local heat transfer (Nu numbers on the upper or lower generatrix) from its value during "purely" forced convection:

$$Gr_q^{(1)} = 3 \cdot 10^{-5} Pr^{0.5} Re^{2.6} [Re^{0.125} + 2.4(Pr - 1)] \quad (16)$$

Equation (16) is valid for the region far from the heat source at  $q_w = \text{const}$  and  $Pr > 0.5$ . Using the ratio  $Gr_q/Gr_q^{(1)}$  as an argument, it is convenient to analyze the buoyancy effect on turbulent flow and heat transfer in horizontal round channels.

The attempts to determine the initiation boundaries of the buoyancy effect on heat transfer were made in earlier studies. In [73], diagrams are given for horizontal and vertical tubes, defining the boundaries between forced and mixed turbulent convection. In this paper, the said boundaries are obtained on the basis of analysis of the data on the length-average heat transfer, that is why the boundary of initiation of the buoyancy effect on heat transfer corresponds to larger values of Gr number, than those following from relationship (16).

The measurement results on velocity and temperature profiles obtained in [67] are shown in Fig.8. An essential asymmetry of velocity and temperature distributions in the vertical diametric plane is noticeable. It should be stressed that the profile deformation is seen even at  $Re = 5 \cdot 10^4$ . Velocity maxima and temperature

minima are shifted downwards. The deviations of velocity and temperature fields

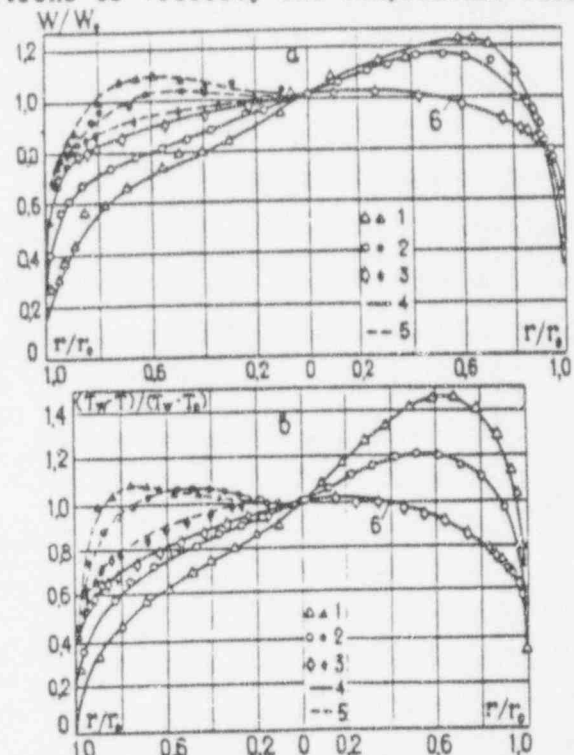


Fig.8. Velocity (a) and temperature (b) profiles in a horizontal tube [67]: 1 -  $Re = 1.3 \cdot 10^4$ ,  $Gr_q = 4.2 \cdot 10^8$ ,  $Gr_q/Gr_q^{(1)} = 100$ ; 2 -  $Re = 2.6 \cdot 10^4$ ,  $Gr_q = 7.7 \cdot 10^8$ ,  $Gr_q/Gr_q^{(1)} = 24$ ; 3 -  $Re = 5.2 \cdot 10^4$ ,  $Gr_q = 1.03 \cdot 10^9$ ,  $Gr_q/Gr_q^{(1)} = 5$ ; 4 - measurements in a vertical diametral plane; 5 - measurements in a horizontal diametral plane; 6 - calculations of [72,74,76,77].

from those typical of purely forced flow are the larger the higher the Gr number and the smaller the Re number, i.e. they increase with the increasing  $Gr_q/Gr_q^{(1)}$ . This statement is also justified by the data obtained in [66]. At  $Gr_q/Gr_q^{(1)} = 5$ , temperature and velocity distributions are in fair agreement with the solutions of [72,74,76,77]. As shown in the first part of the paper, a qualitatively similar character of velocity and temperature fields deformation under the effect of buoyancy is observed also in a laminar flow in the case of homogeneous thermal boundary conditions. However, the quantitative results and functional connections between the parameters determining the value of thermogravitation forces effect are, naturally, different. Besides, the data cited in the previous section allow us to expect, in the case of turbulent liquid flow in a horizontal tube in the presence of heat exchange with the wall, the effect of gravity force field directly on turbulence.

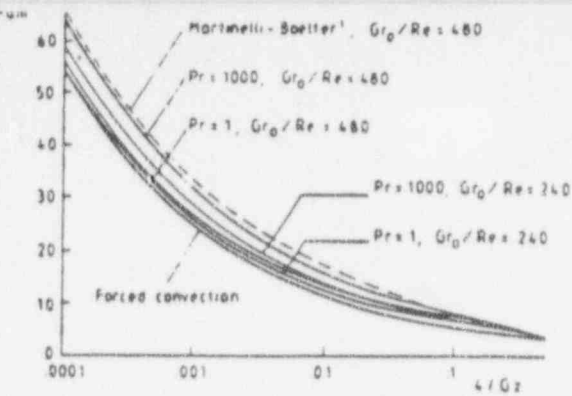


Figure 1 Comparison of arithmetic mean Nusselt numbers with the results of Martinelli and Boelter (adapted from Marner and McMillan<sup>16</sup>, with permission of the American Society of Mechanical Engineers)

Lawrence and Chato<sup>11</sup> and Collins<sup>12,13</sup> have developed numerical models for predicting developing mixed convection taking account of viscosity and density variations and using marching solution procedures. Zeldin and Schmidt<sup>14</sup> solved the full elliptic equations governing the problem using an iterative method in order to avoid the use of marching procedures, which had been questioned for conditions of strong

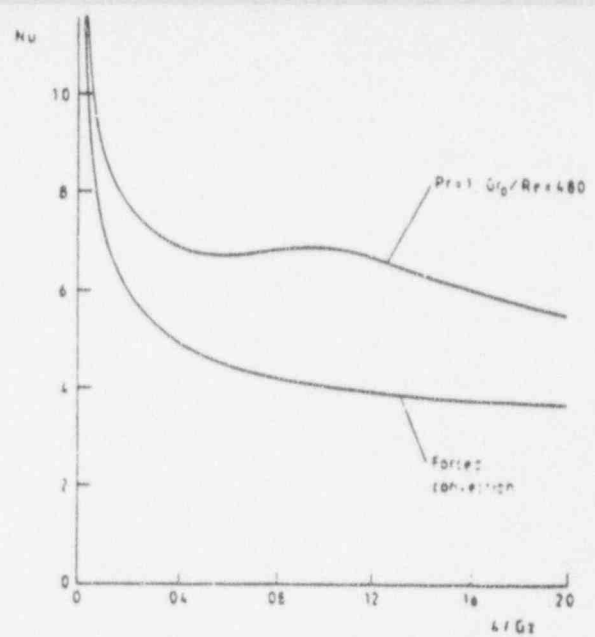


Figure 2 Typical behavior of local Nusselt number near the point of maximum velocity profile distortion (adapted from Marner and McMillan<sup>16</sup>, with permission of the American Society of Mechanical Engineers)

### Notation

$a$	Radius of tube, $d/2$ (m)
$C_p$	Specific heat at constant pressure (J/kgK)
$\bar{C}_p$	Integrated specific heat, $\frac{1}{(T_w - T_b)} \int_{T_b}^{T_w} C_p dT$ (J/kgK)
$C_n$	Coefficient in 2 equation turbulence model
$d$	Tube diameter (m)
$g$	Acceleration due to gravity (m/s <sup>2</sup> )
$G$	Mass velocity, $4M/\pi d^2$ (kg/m <sup>2</sup> s)
$Gr$	Grashof number, $(\rho_b - \rho_w) d^3 g / \rho_w^2$
$\bar{Gr}$	Grashof number based on $\bar{\rho}$ , $(\rho_b - \bar{\rho}) d^3 g / \rho_w^2$
$Gr^*$	Grashof number based on heat flux, $g \beta d^4 q_w / \nu^2$
$Gz$	Graetz number, $Re Pr d/z$ ( $= 1/z^*$ )
$h$	Heat transfer coefficient, $q_w / (T_w - T_b)$ (W/m <sup>2</sup> K)
$i$	Specific enthalpy (J/kg)
$k$	Turbulent kinetic energy (m <sup>2</sup> /s <sup>2</sup> )
$l$	Length scale (m)
$L$	Tube length (m)
$M$	Mass flow rate (kg/s)
$Nu$	Nusselt number, $hd/\lambda$
$Nu_{am}$	Arithmetic mean Nusselt number $\frac{\left\{ \frac{1}{z} \int_0^z q_w dz \right\} D}{\lambda(T_w - \frac{1}{2}(T_w + T_b))}$
$p$	Pressure (N/m <sup>2</sup> )
$Pe$	Peclet number, $Re Pr$
$Pr$	Prandtl number, $\mu C_p / \lambda$
$\bar{Pr}$	Prandtl number based on $\bar{C}_p$ , $\mu \bar{C}_p / \lambda$
$q_w$	Heat flux at the wall (W/m <sup>2</sup> )
$r$	Radial coordinate (m)
$Ra$	Rayleigh number, $Gr Pr$
$Ra^*$	Rayleigh number based on heat flux, $Gr^* Pr$
$Re$	Reynolds number, $Gd/\mu$
$T$	Temperature (°C or K)
$T'$	Temperature fluctuation (K)

$v$	Radial velocity fluctuation (m/s)
$V$	Radial velocity (m/s)
$w$	Axial velocity fluctuation (m/s)
$W$	Axial velocity (m/s)
$y$	Transverse coordinate measured from wall, $a - r$ (m)
$y^*$	$y \sqrt{\tau_w / \rho \nu}$
$z$	Axial coordinate (m)
$z^*$	Dimensionless axial coordinate, $\frac{z}{d Re Pr}$
$\beta$	Coefficient of volume expansion (K <sup>-1</sup> )
$\Delta T$	Wall to bulk temperature difference, $T_w - T_b$ (K)
$\epsilon$	Rate of dissipation of $k$ (m <sup>2</sup> /s <sup>3</sup> )
$\kappa$	Von Karman constant
$\lambda$	Thermal conductivity (W/mK)
$\mu$	Dynamic viscosity (kg/ms)
$\nu$	Kinematic viscosity, $\mu/\rho$ (m <sup>2</sup> /s)
$\rho$	Density (kg/m <sup>3</sup> )
$\bar{\rho}$	Integrated density, $\frac{1}{(T_w - T_b)} \int_{T_b}^{T_w} \rho dT$ (kg/m <sup>3</sup> )
$\sigma_t$	Turbulent Prandtl number
$\tau$	Shear stress, N/m <sup>2</sup>

### Subscripts

$b$	Refers to fluid bulk conditions
$c$	Refers to thermodynamic critical pressure
$F$	Forced convection
$m$	Mean or mixing length
$min$	Minimum
$pc$	Refers to pseudocritical value
$ref$	Reference value
$t$	Turbulent
$w$	Refers to conditions at the tube wall
$z$	Based on axial length
$0$	Refers to inlet conditions
$\infty$	Refers to the fully developed condition

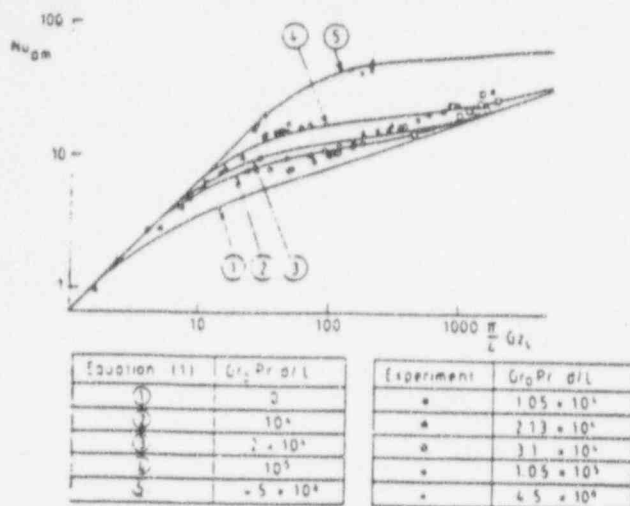


Figure 3 Experimental and predicted magnitudes of  $Nu_m$  as a function of  $Gz_1$  (adapted from Martinelli et al.<sup>18</sup>; with permission of the American Institute of Chemical Engineers)

buoyant influences. Nevertheless, difficulties in obtaining a solution were still encountered beyond a certain value of  $Gr/Re$  corresponding to a reversed flow in the central region of the pipe.

In the case of buoyancy-aided convection, i.e. upward flow in a heated pipe or downward flow in a cooled one, the velocity in the vicinity of the wall increases with wall-to-fluid temperature difference (at constant flow rate) and decreases in the core. Eventually a concavity develops in the velocity profile in the core flow. Associated with these changes there is an enhancement of heat transfer coefficient. In practice, with sufficiently strong heating or cooling, the velocity profile gradually becomes unstable at the point of inflexion and flow unsteadiness results (see below).

In the opposite case, i.e. downward heated flow or upward cooled flow, the velocity near the wall is reduced and there is an impairment of heat transfer. With strong enough heating (or cooling), the velocity gradient at the wall approaches zero and an instability develops there suddenly.

The numerical solutions of Collins<sup>13</sup> illustrate the above behavior. These calculations were carried out for conditions covered in the experimental work of Scheele and other workers on the influence of heat transfer on stability of laminar flow in vertical tubes.<sup>11,15-17</sup> It was observed that as Reynolds number decreased, the critical value of  $Gr^*/Re$  for onset of gradual instability decreased asymptotically to approximately 42.5 for the case of upward flow with uniform heat flux. An increase in the critical value of  $Gr^*/Re$  with decrease in Reynolds number was observed for the case of downward flow with uniform heat flux. The highest critical value of  $Gr^*/Re$  encountered was approximately 75 and this was for Reynolds numbers approaching zero.

#### Experimental studies of laminar mixed convection in vertical tubes

The early experimental work involving mixed convection in vertical tubes was carried out using test sections in the form of double tube heat exchangers. Watzinger and Johnson<sup>18</sup> in 1939 reported experiments in which water flowing downward in a tube was cooled by an external flow. For that arrangement free convection aided forced convection. Martinelli et al.<sup>18</sup> shortly afterwards reported experiments with upward flow of water and oil in tubes having uniform wall temperatures, heated by means of steam. Overall heat transfer rates considerably in excess of

those predicted for forced convection were observed (Figure 3). The approximate theoretical model of Martinelli and Boelter<sup>1</sup> was used with remarkable success as a basis for correlating the data. The following equation, which is identical with the theoretical result, apart from the slight adjustment of an index from 0.75 to 0.84, correlates all their data and that of Watzinger and Johnson to within  $\pm 20\%$ .

$$Nu_{am} = 1.75 F_1 \left\{ Gz_m + 0.0722 F_2 \left( \frac{Gr Pr d}{L} \right)^{0.84} \right\}^{1/3} \quad (1)$$

$F_1$  and  $F_2$  are functions which are derived from theory and tabulated in Ref. 1. No data were produced by Martinelli et al. for the case where free convection opposed forced convection (heated downward flow).

Subsequent work on laminar vertical mixed convection has been carried out using uniformly heated tubes. Clark and Rosenhow,<sup>20</sup> in experiments on water at high subcritical pressure flowing upwards in an electrically heated tube, produced data which were used by Hallman<sup>3</sup> for comparison with his analytical predictions for the fully developed case. Further experimental investigations were reported later by Hallman<sup>21</sup> and Brown.<sup>3</sup> These data are in good agreement with Hallman's analysis, which is fitted well for  $100 < Gr^*/Re < 10,000$  by the equation:

$$Nu = 0.95 \left( \frac{Gr^*}{Re} \right)^{0.28} \quad (2)$$

Experimental results obtained by Kemeny and Somers<sup>22</sup> using water and oil are shown in Figure 4. However, direct comparison of these results with earlier work cannot be made because the Nusselt numbers used by Kemeny and Somers were based on the inlet fluid temperature. More recent experiments by Barozzi et al.<sup>23</sup> have been compared with numerical solutions by Collins and good agreement is reported. Evidence of transition to turbulent flow near the end of the heated section was observed for Reynolds numbers of less than 1000.

Further data can be found in the papers by Scheele and Hanratty<sup>24</sup> and Brown and Gauvin.<sup>25</sup> However, these experiments were concerned primarily with transitional flow.

The above discussion of experimental studies of laminar

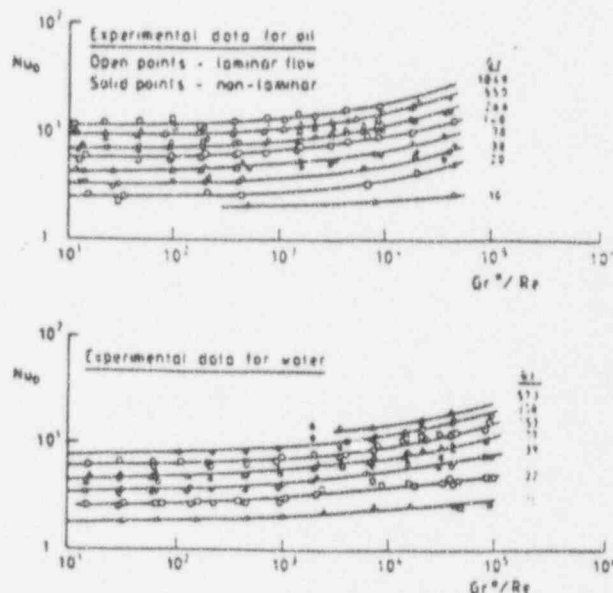


Figure 4 Plots of  $Nu_0$  versus  $Gr^*/Re$  for different values of  $Gz$  (adapted from Kemeny and Somers<sup>22</sup>; with permission of the American Society of Mechanical Engineers)



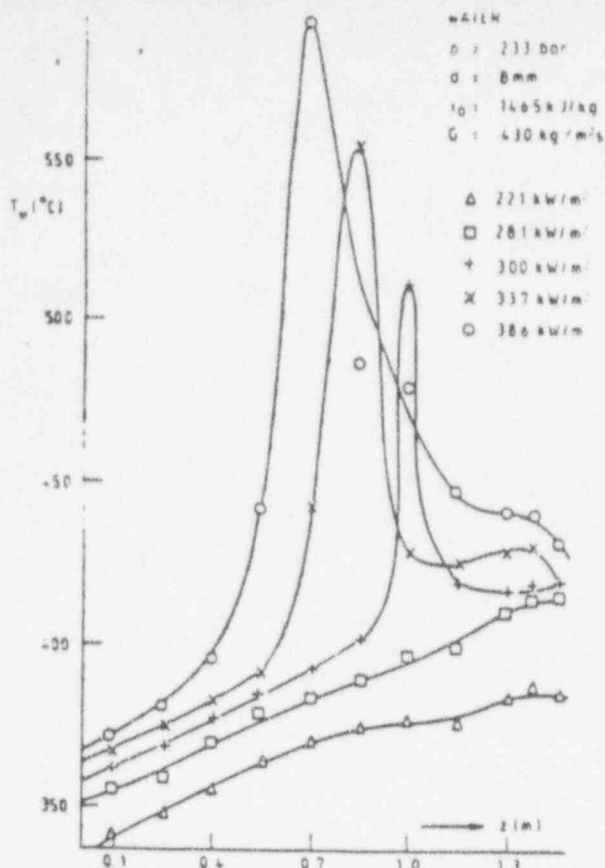


Figure 5 Localized impairment of heat transfer due to buoyancy (adapted from Shitsman<sup>37</sup>; with permission of Plenum Publishing Corp.)

mixed convection in vertical tubes has been restricted to the case where free convection aids forced convection. An interesting conclusion which has emerged from the present review is that virtually no laminar flow heat transfer measurements have been reported for conditions where free convection opposes forced convection (heated downward flow or cooled upward flow). For such flows the influence of buoyancy should be to impair heat transfer relative to that for conditions of pure forced convection, provided the flow remains steady and laminar. However, as a result of the work of Scheele *et al.* on buoyancy-induced instability in laminar flow, it is clear that the range of conditions available for such experiments is likely to be rather limited.

### Turbulent flow mixed convection

Whereas the effects of buoyancy on heat transfer can be predicted readily for the laminar case, the situation is very different with turbulent flows: the data for such conditions show some unexpected trends (see reviews<sup>26-28</sup>). In configurations with forced and free convection aligned, local heat transfer coefficients significantly lower than those for forced flow alone can result. In contrast, for downward flow in heated tubes buoyancy forces cause a general enhancement of the turbulent diffusion properties of the flow, with the result that wall temperature distributions are well-behaved and heat transfer coefficients are higher than those for forced flow alone. Eventually, as the free convection component becomes more and more dominant, heat transfer for upward flow also becomes

two cases are the same.

### Examples of buoyancy-induced impairment of heat transfer

In the earliest studies of turbulent mixed convection with atmospheric pressure water and air,<sup>18,29-34</sup> there was little indication of the dramatic influences of buoyancy on heat transfer that were later to become evident in the work on fluids near the critical point<sup>35,36</sup> and which have provided the incentive for considerable research work in recent years.

During early development work on supercritical pressure steam generators, Shitsman<sup>37</sup> and Ackerman<sup>38</sup> found severe localized impairment of heat transfer for upward flow in heated tubes at near-critical conditions (Figure 5). The effect was initially thought to be similar to film-boiling and was, in fact, given the name "pseudoboiling." There were, however, some surprising conditions where the wall temperatures were well below the pseudocritical value.<sup>39,40</sup> Under such conditions the fluid must have been in a liquid-like state even in the wall-layer region.

It became apparent that the effect was due to buoyancy and not a form of film boiling when experiments with upflow were compared with those for downflow at otherwise identical conditions. Investigations of this type were first reported by Shitsman<sup>41,42</sup> and Jackson and Evans-Lutterodi<sup>43</sup> (Figure 6). Similar comparisons have since been made by a number of researchers, notably Bourke *et al.*,<sup>44</sup> Fewster,<sup>45</sup> Alferov *et al.*,<sup>40,46,47</sup> Watts and Chou,<sup>48</sup> and Bogachev *et al.*<sup>49</sup>

The fact that the phenomenon of localized impairment due to buoyancy is not restricted to fluids at high pressure, but can occur in liquids and gases at normal pressure, has subsequently become clear as a result of experiments by Steiner,<sup>50</sup> Kenning *et al.*,<sup>51</sup> Hall and Price,<sup>52,53</sup> and Fewster.<sup>45</sup> Kenning *et al.* found wall temperature peaks for upward flow of water at 5 bar (Figure 7) and Fewster made comparisons between upward and downward flow of atmospheric pressure water (Figures 8 and 9). The case shown in Figure 9 is of special interest because the Reynolds number is below that normally associated with turbulent flow. The measurements suggest that buoyancy-induced turbulence is present, the sudden fall in wall temperature for upward flow being due to transition.

Mixed convection at low Reynolds number has also been studied by Rouai.<sup>54</sup> Buoyancy-induced transition to turbulent

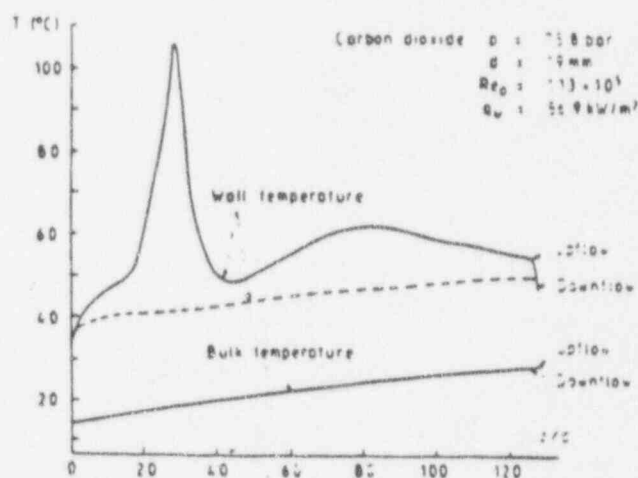


Figure 6 Comparison of upward and downward flow cases at near critical conditions (from Jackson and Evans-Lutterodi<sup>44</sup>)

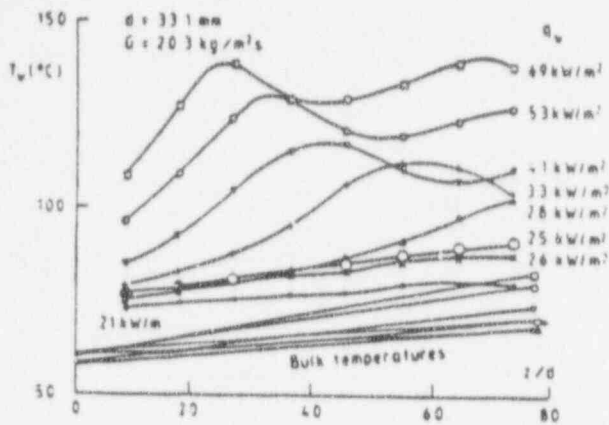


Figure 7 Buoyancy-induced impairment with water at a pressure of 5 bar (adapted from Kenning *et al.*<sup>31</sup>, with permission of Harper and Row)

flow was clearly observed in upward flow (Figure 10a) whereas for downward flow turbulence existed throughout the heated section (Figure 10b). In downward flow a periodic Nusselt number variation (Figure 11) suggested that small, buoyancy-induced recirculation cells might have been present. Wilkinson *et al.*<sup>33</sup> examined the conditions for flow reversal at the pipe wall in a buoyancy-opposed flow; otherwise the problem has received little attention.

The examples quoted above illustrate the importance of interactions between forced and free convection for flow in vertical pipes. An explanation of the mechanism involved has been given by Hall and Jackson.<sup>36</sup> They suggested that the dominant factor was the modification of the shear stress distribution across the pipe, with consequential change in turbulence production. The analysis of Hall and Jackson<sup>36</sup> has been extended by Jackson and Hall<sup>28</sup> to provide a general criterion for the onset of buoyancy effects applicable both for supercritical and normal pressure fluids. For influences of buoyancy on heat transfer coefficient to be less than 5% of the forced convection value, the analysis yields a limit:

$$\frac{\overline{Gr}_b}{Re_b^{2.7}} < 10^{-5} \quad (3)$$

#### Comparison of predicted criterion with experiment

In order to test the validity of the criterion, experimental data from the authors' programme of research on heat transfer to supercritical pressure carbon dioxide have been presented in terms of the parameter  $\overline{Gr}_w/Re_b^{2.7}$ . Figures 12(a) and (b) show experimental data that are consistent with the criterion (the ordinate is the ratio of the observed Nusselt number to that for forced flow in the absence of buoyancy effects but under conditions that are otherwise identical).

Alferov *et al.*<sup>37</sup> presented data for supercritical pressure water in terms of the ratio of calculated heat transfer coefficients for forced and free convection (Figure 13). It can be demonstrated with the aid of established correlation equations for free and forced convection that  $h_{free}/h_{forced}$  is proportional to  $Gr/Re^{2.46} Pr^{0.5}$  raised to the power one third. Thus the criterion for negligible buoyancy suggested by the data of Alferov *et al.*<sup>37</sup> (Figures 13 and 14), namely  $h_{forced}/h_{free} > 3$ , can be re-expressed as:

$$\frac{Gr}{Re^{2.46} Pr^{0.5}} < 2.4 \cdot 10^{-5} \quad (4)$$

For  $10^4 < Re < 10^5$ , this criterion gives effectively the same classification of data as that of Jackson and Hall.

Some further data which can be used for testing the validity of the criterion have been produced by Brassington and Cairns<sup>38</sup> for supercritical pressure helium. Buoyancy-induced wall temperature peaks occurred over a wide range of reduced pressure but it was found that such effects were not present

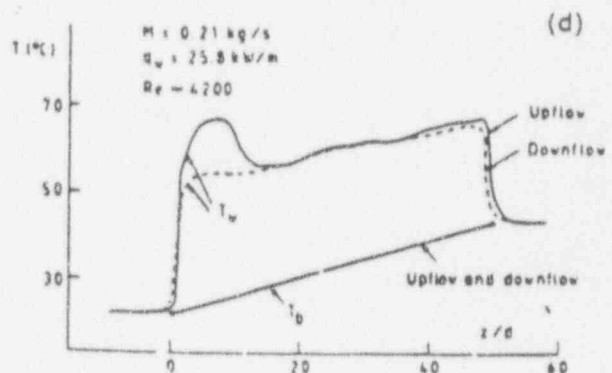
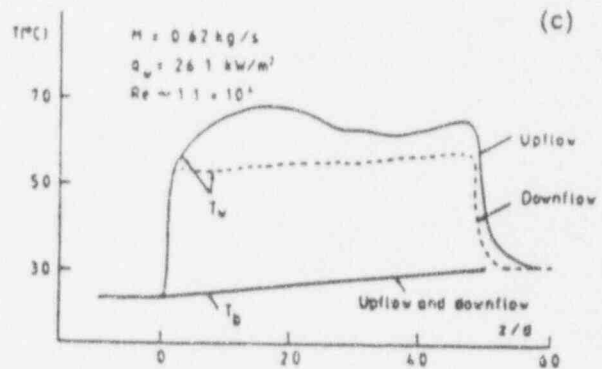
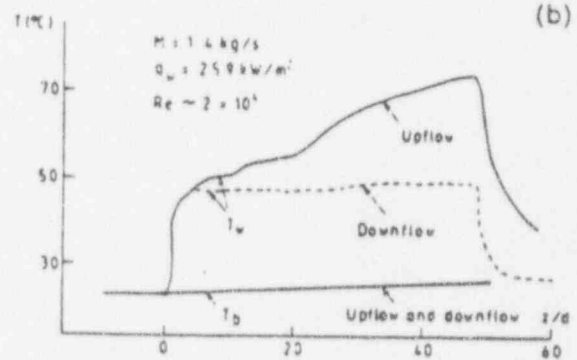
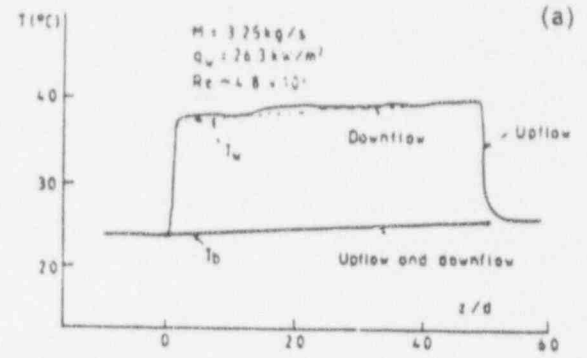


Figure 8(a-d) Comparison of heat transfer for upward and downward flow of water at atmospheric pressure in a tube of diameter 100 mm (adapted from Fewster<sup>38</sup>)

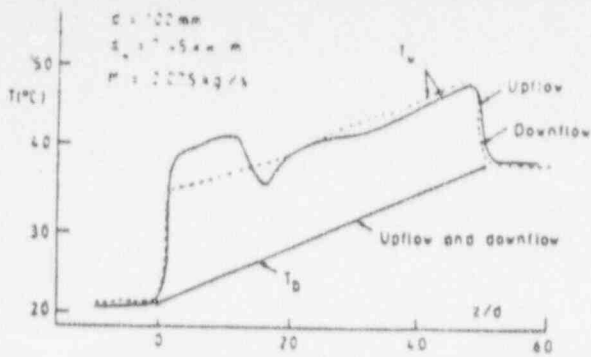


Figure 9 Buoyancy-induced transition to turbulent flow in water at atmospheric pressure at a Reynolds number of 1500 (adapted from Fewster<sup>18</sup>)

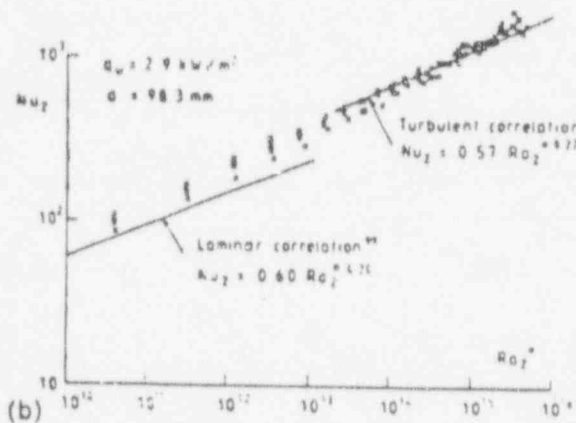
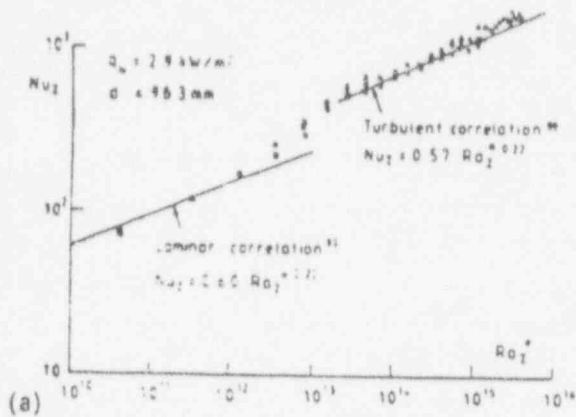


Figure 10 Correlation of low flow data for water (adapted from Rouai<sup>16</sup>): (a) upflow and (b) downflow

under conditions where:

$$\frac{Gr_b}{Re_b^{1.7}} < 2.4 \cdot 10^{-3} \quad (5)$$

Bearing in mind that  $\overline{Gr}_b$  is somewhat less than  $Gr_b$ , the agreement with the criterion is extremely good.

Although the main sources of data concerning the onset of buoyancy effects have been investigations with supercritical pressure fluids, some work has also been done using water at pressures near to atmospheric<sup>43,51</sup> and with atmospheric pressure air.<sup>52</sup> These studies have further substantiated inequality (3) as

which buoyancy effects can be neglected.

### A simple equation describing mixed convection heat transfer in vertical tubes

Although the theory of Hall and Jackson was developed in order to obtain a criterion for the onset of heat transfer impairment for the case of upward flow in a heated pipe, it is also applicable to downward flow where there is heat transfer enhancement. It has been generalized<sup>28</sup> to provide the following simple description of the manner in which the ratio of buoyancy-influenced to buoyancy-free Nusselt numbers varies with the buoyancy parameter  $\overline{Gr}_b/Re_b^{1.7} Pr_b^{0.5}$

$$\frac{Nu}{Nu_f} = \left| 1 \pm \frac{10^4 \overline{Gr}_b}{Re_b^{1.7} Pr_b^{0.5}} \right|^{0.25} \quad (6)$$

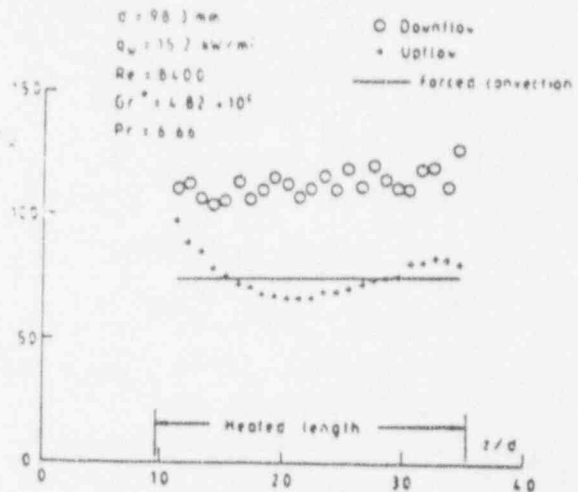


Figure 11 Nusselt number variation in mixed convection heat transfer to water (adapted from Rouai<sup>16</sup>)

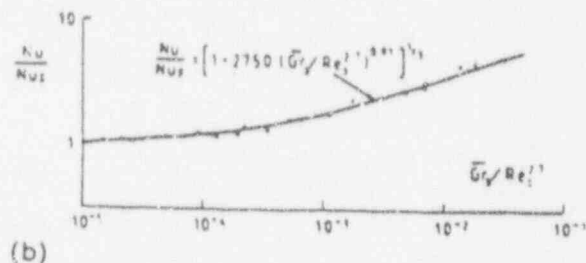
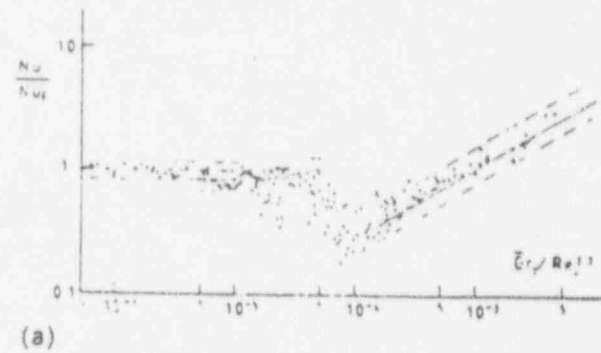


Figure 12(a-b) Mixed convection data for supercritical carbon dioxide (adapted from Fewster<sup>18</sup>): (a) upward flow and (b) downward flow

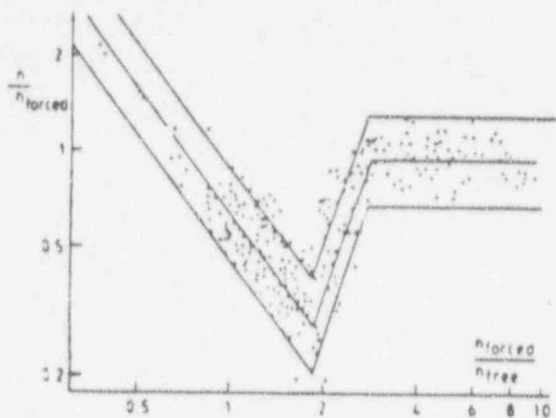


Figure 13 Correlation of data for upward flow of supercritical pressure fluids (adapted from Alferov et al.<sup>11</sup>; with permission of Scripta Technica Inc.)

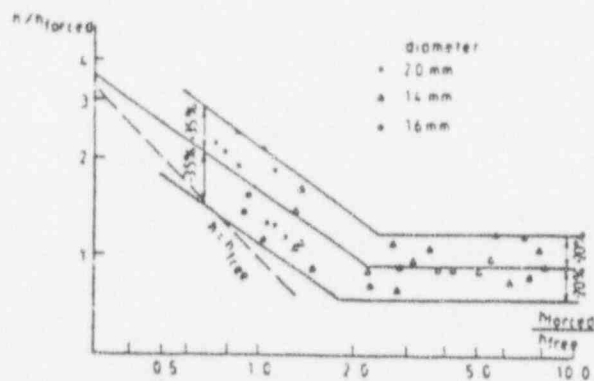


Figure 14 Correlation of downward flow mixed convection data for supercritical pressure water (adapted from Alferov et al.<sup>11</sup>; with permission of Scripta Technica Inc.)

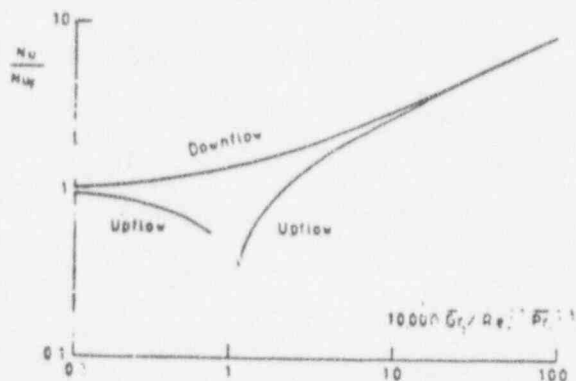


Figure 15 Theoretical prediction of general features of mixed convection heat transfer in vertical tubes (adapted from Jackson<sup>10</sup>)

The negative sign refers to the buoyancy-aided case and the positive sign to the opposed case. It should be borne in mind that this expression was obtained using simple physical theory and empirical relationships for buoyancy-free heat transfer (for details see Ref. 28). In consequence it merely represents an attempt to predict gross trends as buoyancy effects begin to modify the forced flow significantly, however it is surprisingly consistent with observed behavior (see below).

With increase in the buoyancy parameter, an impairment of heat transfer is indicated for upward flow and an enhancement for downflow. The curves representing Equation 6 for the two cases are shown in Figure 15. It is of interest to note that for

upward flow with strong enough buoyancy influence a recovery in heat transfer is indicated, leading eventually to enhancement at high values of the buoyancy parameter. Data for upward flow of air<sup>39</sup> and mercury<sup>61</sup> and for downward flow of water<sup>62</sup> are shown in Figures 16, 17, and 18, respectively. These show behavior consistent with that indicated by Equation 6.

Correlation of data for mixed convection

The theory referred to in the previous sections has proved to be useful for correlating data and has been employed when presenting data from the authors' program of research into heat transfer to fluids at supercritical pressure—see Figures 12(a) and (b) (earlier). It is clear that for upward flow (Figure 12a) the data do not correlate in the region where heat transfer is impaired in terms of the parameters  $Nu/Nu_f$  and  $\overline{Gr}_b/Re_b^{2.7}$ . However, for downward flow (Figure 12b) an excellent correlation is achieved throughout the mixed convection regime by the equation

$$\frac{Nu}{Nu_f} = \left[ 1 + 2750 \left( \frac{\overline{Gr}_b}{Re_b^{2.7}} \right)^{0.91} \right]^{1/3} \quad (7)$$

The form of the above equation was chosen such that  $Nu$  becomes independent of  $Re_b$  for conditions where buoyancy is dominant (i.e. tending towards pure free convection).

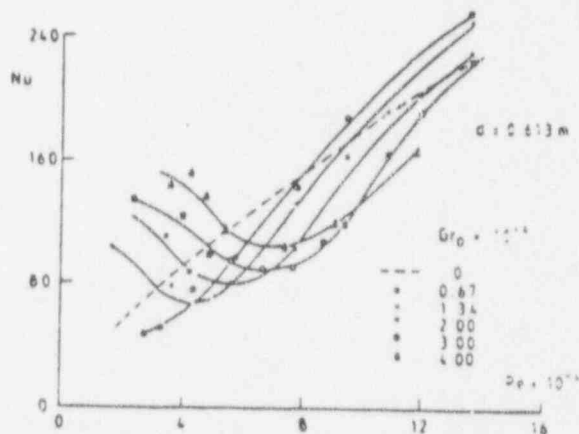


Figure 16 Effect of buoyancy on heat transfer to air at atmospheric pressure for upward flow (adapted from Byrne and Ejiogu<sup>39</sup>; with permission from the Council of the Institute of Mechanical Engineers)

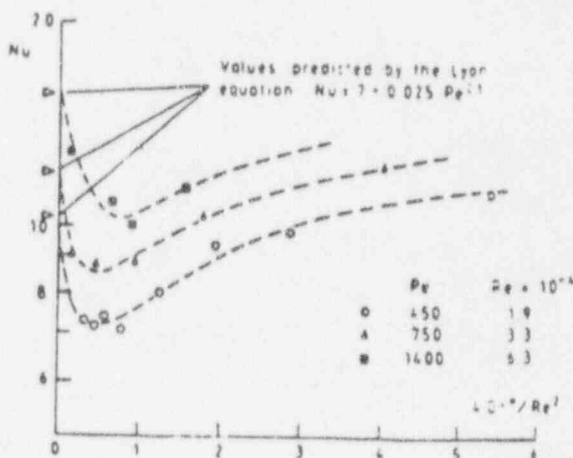


Figure 17 Heat transfer with an ascending mercury flow in a heated vertical pipe (adapted from Buhr et al.<sup>61</sup>; with permission of the American Society of Mechanical Engineers)

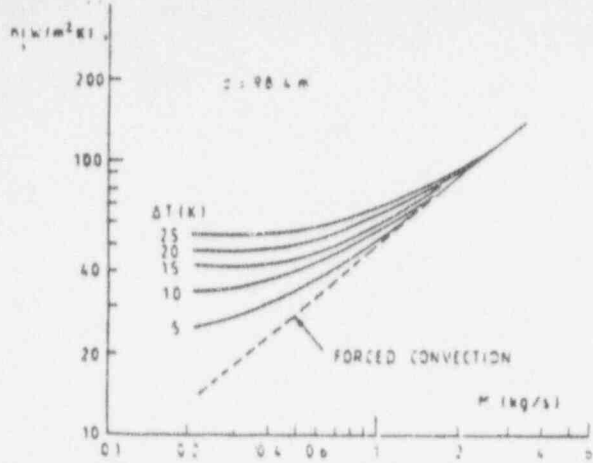


Figure 18 Effect of buoyancy on heat transfer to water at atmospheric pressure for downward flow (adapted from Jackson and Fewster<sup>62</sup>; with permission of Harper and Row)

The contrast between the upward and downward flow cases is interesting: for the former, buoyancy forces lead to localized effects (wall temperature peaks), whereas for the latter they do not. For upward flow impairment or enhancement of heat transfer can occur depending on the magnitude of the buoyancy force, whereas for downward flow only enhancement is found. Although the effects might seem to be anomalous when viewed without the aid of the model of Jackson and Hall, they can be seen to follow a meaningful pattern when considered in the light of the model. The general picture of mixed convection in vertical tubes embodied in Equation 6 and illustrated in Figure 15 thus proves to be surprisingly accurate.

In parallel with work on supercritical pressure fluids, the present authors and co-workers have also studied mixed convection to water and to air, both at atmospheric pressure (Jackson and Fewster<sup>62</sup> and Axcell and Hall<sup>64</sup>). Again the theoretical guidelines have proved to be useful. Jackson and Fewster used as their correlating parameter the group  $\overline{Gr}_w/Re^{2.625}Pr^{0.5}$ . The data of Jackson and Fewster for downward flow of water in a heated tube are shown in Figure 19 and can be seen to be satisfactorily correlated. A correlation equation which fitted the data over the entire range of conditions was arrived at by adjusting the index in order to make Nusselt number independent of Reynolds number when buoyancy influences become dominant. This equation is:

$$\frac{Nu}{Nu_F} = \left[ 1 + \frac{4500 \overline{Gr}_w}{Re^{2.625} Pr^{0.5}} \right]^{0.21} \quad (8)$$

Figure 19 also includes some early data for atmospheric pressure water.<sup>18,32</sup> The agreement between the equation and the data is quite reasonable when account is taken of the uncertainties involved, particularly in the values of  $Nu_F$  used for normalizing the data.

Figure 20 shows the data of Axcell and Hall<sup>64</sup> for downward flow of air in a heated pipe plotted on the same basis. Some measurements by Easby<sup>63</sup> of downward flow mixed convection to nitrogen at about 4 bar are also of interest. When compared with Equation 7 (the correlation equation developed for the supercritical pressure carbon dioxide data) they are found to be in fair agreement. This is also the case for the data of Brown and Gauvin,<sup>25</sup> who found enhancement of heat transfer by up to 70% in downward flow experiments on air. Further sources of data on downward flow mixed convection are Krasyakova *et al.*,<sup>66</sup> Ikryannikov *et al.*,<sup>67,68</sup> and Alferov *et al.*<sup>37</sup> Thus it can be seen that there is a significant body of information

available concerning the enhancement of heat transfer due to buoyancy effects for downward flow in heated tubes. The observed trends are in all cases consistent with the simple model of mixed convection in vertical tubes of Jackson and Hall and can be adequately described by expressions such as Equations 7 or 8. For upward flow in heated tubes a significant amount of experimental data is also available. Whilst the trends are broadly consistent with the model, the problem of correlating data is more complicated, particularly because of complex flow development behavior.

The difficulty of correlating upward flow data in terms of purely local parameters (Figure 21) led Rouai<sup>54</sup> to examine conditions at wall temperature peaks. Minimum heat transfer was correlated by:

$$\frac{Nu_{\min}}{Nu_F} = 14.91 \left[ \frac{\overline{Gr}^*}{Re^{1.425} Pr^{0.8}} \right]^{0.28} \quad (9)$$

and the distance to the first wall temperature peak by:

$$\frac{z}{d} = 0.051 \left[ \frac{\overline{Gr}^*}{Re^{1.425} Pr^{0.8}} \right]^{-0.18} \quad (10)$$

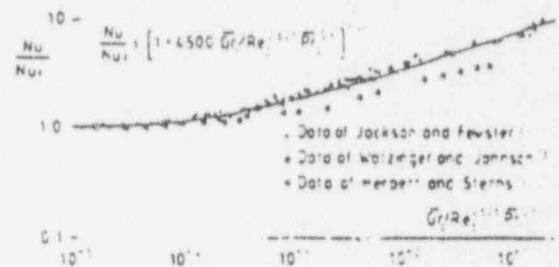


Figure 19 Correlation of mixed convection data for downward flow of water (adapted from Jackson and Fewster<sup>62</sup>; with permission of Harper and Row)

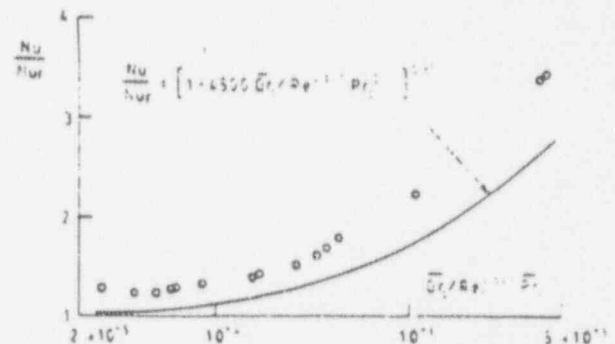


Figure 20 Comparison of downward flow correlation with data for air (adapted from Axcell and Hall<sup>64</sup>; with permission of Harper and Row)

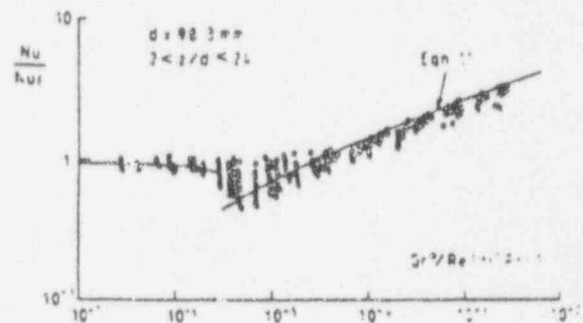


Figure 21 Upward flow data for water at atmospheric pressure (from Rouai<sup>54</sup>)



Rouai also compared his data with a refinement of Hall and Jackson's model which accounts for the influence of heat transfer on the buoyant layer.<sup>34,39</sup> An implicit expression for  $Nu/Nu_F$  results:

$$\frac{Nu}{Nu_F} = \left[ 1 \pm 8 \times 10^4 \frac{Gr^*}{Re^{3.425} Pr^{0.8}} \left( \frac{Nu}{Nu_F} \right)^{-2} \right]^{0.46} \quad (11)$$

It should be noted that this correlation gives a discontinuity in Nusselt number for heated upward flow when  $Gr^*, Re^{3.425} Pr^{0.8} \sim 3 \times 10^{-6}$ .

### Numerical studies of turbulent mixed convection in vertical tubes

The various applications of turbulence closures to mixed convection are considered under the following headings:

- (i) Prescribed eddy diffusivity models
- (ii) Mixing length models
- (iii) One-equation transport models
- (iv) Two-equation transport models
- (v) Higher order models

The categorization above does not convey the complete picture because of the absence of any reference to the flow formulations adopted (whether fully developed or developing thermal-hydraulic conditions are assumed to prevail). It is well established that very long flow development lengths occur in regions of the ascending mixed convection regime and therefore the validity of studies using even the most refined turbulence models cast in a fully developed formulation can be seriously compromised.

The most general form of the mean flow governing equations used in the works reviewed below are the time-averaged momentum and energy equations written in the "thin shear" (or "boundary layer") formulations. Thus, in cylindrical polar coordinates:

#### Momentum

$$\frac{1}{r} \frac{\partial}{\partial r} (rVW) + \frac{\partial}{\partial z} (W^2) = -\frac{1}{\rho} \frac{dp}{dz} + \frac{1}{r} \frac{\partial}{\partial r} \left[ r \left( \nu \frac{\partial W}{\partial r} - \overline{vw} \right) \right] + [1 - \beta(T - T_{ref})] g_z \quad (12)$$

where

$$g_z = \begin{cases} -g & \text{for ascending flow} \\ +g & \text{for descending flow} \end{cases}$$

#### Energy:

$$\frac{1}{r} \frac{\partial}{\partial r} (rVT) + \frac{\partial}{\partial z} (WT) = \frac{1}{r} \frac{\partial}{\partial r} \left[ r \left( \frac{\nu}{Pr} \frac{\partial T}{\partial r} - \overline{vT} \right) \right] \quad (13)$$

The equations are written in the Boussinesq approximation: density variations are neglected except in the body force term of the momentum equation where a linearized function of temperature is employed. The models in categories (i) to (iv) above make recourse to the concept of turbulent viscosity by which Reynolds stress appearing in the momentum equation is related to the mean velocity gradient:

$$-\overline{vw} = \nu_t \frac{\partial W}{\partial r} \quad (14)$$

Similarly, the turbulent heat flux in the energy equation is related to the mean temperature gradient:

$$-\overline{vT} = \frac{\nu_t}{\sigma_t} \frac{\partial T}{\partial r} \quad (15)$$

The usual practice is to set the turbulent Prandtl number to a constant value,  $\sigma_t = 0.9$ . The different strategies adopted to determine turbulent viscosity,  $\nu_t$ , are vital to the success (or lack of it) experienced in the application of turbulence models to turbulent mixed convection: it will be seen below that the simpler models fail to capture even the general trends of heat transfer impairment and enhancement.

#### (i) Prescribed eddy diffusivity models

The "eddy diffusivity" approach prescribes turbulent viscosity as a function of position in the flow without any direct reference to local features of either the mean field or time-averaged turbulence field. Tanaka *et al.*<sup>20</sup> examined turbulent mixed convection tube flows using a modification of Reichardt's<sup>21</sup> eddy diffusivity model. The wall temperature distributions for a vertical heated tube computed by Tanaka *et al.* were opposite to observed behavior, showing heat transfer enhancement for ascending flow and impairment for descending flow. It was concluded that "the theory is not sufficient to estimate heat transfer coefficients." The work of Tanaka *et al.* is the first of a number of numerical studies to be reviewed in which the developing flow formulation of Equations 12 and 13 is not employed.

#### (ii) Mixing length models

In the Prandtl-Taylor mixing length hypothesis (MLH) it is postulated that  $\nu_t$  may be expressed in terms of a mixing length,  $l_m$ , and the mean velocity gradient:

$$\nu_t = l_m^2 \left| \frac{\partial W}{\partial r} \right| \quad (16)$$

Numerous modifications to the original prescription of  $l_m$  ( $l_m = \kappa y$ ) have been proposed (see the discussion of Launder and Spalding,<sup>72</sup> for example). A modification that has found widespread application is due to van Driest<sup>73</sup> in which allowance is made for the damping effect of a solid boundary upon turbulence in the vicinity of the boundary:

$$l_m = \kappa y [1 - \exp(-y^+/A^*)] \quad (\kappa = 0.4; A^* = 26.0) \quad (17)$$

Malhotra and Hauptmann<sup>74</sup> implemented the van Driest mixing length model in a fully developed mean flow equation set. Computed wall temperature distributions for heated ascending and descending flow demonstrated the correct trends, indicating heat transfer impairment for upflow and enhancement for downflow. Comparison with the wall temperature data of Jackson and Evans-Lutterodi<sup>43</sup> for carbon dioxide at near-critical conditions showed good agreement for descending flow but poor quantitative agreement for ascending flow (Figure 22), although the highly variable fluid properties of the experiment represent a considerable added complication.

Walklate<sup>75</sup> tested four mixing length models against the data for heated upflow of air with uniform wall flux obtained by Carr *et al.*<sup>44</sup> The data show significant influences of buoyancy, demonstrating velocity profile inversion in three of the four test cases and a marked reduction in the level of Reynolds stress. The four mixing length models used by Walklate represent various modifications of the van Driest formulation. Walklate used the developing flow equations of the form given above, thus eliminating an uncertainty present in the work of Tanaka *et al.*<sup>20</sup> and Malhotra and Hauptmann.<sup>74</sup> Comparison was made with the bulk parameter data (Stanton number and local friction coefficient) and profile measurements of Carr *et al.* Discrepancies between calculated and measured bulk parameters were large, and computed velocity, temperature and Reynolds stress profiles were in poor agreement with the experimental data.



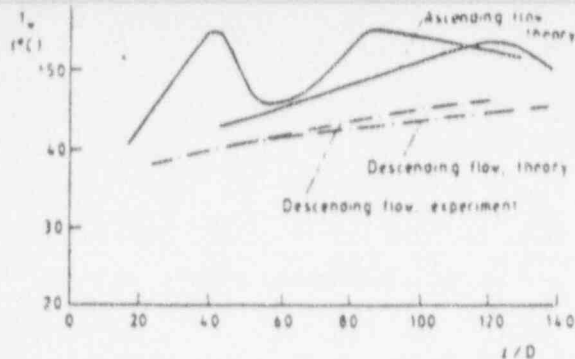


Figure 22 Comparison between calculations of Malhotra and Hauptmann<sup>10</sup> and data of Jackson and Evans-Lutterodt<sup>11</sup> for supercritical pressure carbon dioxide (adapted from Malhotra and Hauptmann<sup>10</sup>; with permission of Harper and Row)

An early hybrid work by Hsu and Smith<sup>17</sup> combined an expression for near-wall turbulent viscosity due to Deissler<sup>17</sup> with the mixing length model for the outer region. The calculations indicated only enhancement of heat transfer for heated ascending flow, a result that is again contrary to observed behavior. The likely cause of this result is the Deissler near-wall formulation which, although strictly not a prescribed eddy diffusivity model as defined earlier, nonetheless does not correctly reflect turbulence production. It should be added that fully developed flow was assumed in this early attempt to calculate turbulent mixed convection.

### (iii) One-equation transport models

Studies of turbulent mixed convection in vertical tubes have been performed using turbulence models that employ the turbulent viscosity concept but which form  $\nu_t$  from turbulence quantities and include transport effects. The basis for introduction of turbulence quantities into an equation for  $\nu_t$  is the Prandtl-Kolmogorov formula in which the square root of turbulent kinetic energy,  $k$ , forms the velocity scale in the constitutive equation. Thus,

$$\nu_t = k^{1/2} l_t \quad (18)$$

Models in which a transport equation for one of the scales (in practice the velocity scale via  $k$ -transport) is employed are known as "one-equation" models. Axcell and Hall<sup>64</sup> applied a variation of Wolfshtein's<sup>78</sup> one-equation model to their experimental data for heated descending air flows. An important feature of the Wolfshtein model is that it is applicable over the entire flow domain, including the viscosity-affected near-wall region and thus does not require the specification of "wall functions" to bridge that region. Axcell and Hall's calculations were qualitatively correct, showing enhancement of heat transfer with respect to forced convection. The predicted enhancement was, however, considerably less than that found experimentally (Figure 23). It was concluded that the one-equation model does not offer any advantage over a mixing length model in mixed convection calculations. Again there are discrepancies between the thermal-hydraulic conditions of the experiment and the modeled problem and a fully developed condition was assumed in the analysis (although rapid thermal-hydraulic development in descending mixed convection flows makes the assumption far less limiting than in ascending flows where in many cases it is wholly inappropriate).

### (iv) Two-equation transport models

"Two-equation" models have been applied with some success to turbulent mixed convection. These incorporate transport

constitutive equation for  $\nu_t$ . The turbulence quantities most often selected to form the scales are the turbulent kinetic energy,  $k$ , and its rate of dissipation,  $\epsilon$ , as evidenced by Shih's literature surveys.<sup>79,80</sup> The length scale is obtained as  $k^{3/2}/\epsilon$ , and the Prandtl-Kolmogorov formula takes the following form:

$$\nu_t = C_\mu k^2/\epsilon \quad (19)$$

Walklate<sup>73</sup> tested three versions of the  $k-\epsilon$  model with developing flow formulations against data of Carr *et al.*,<sup>76</sup> the first model examined was a standard "high-Reynolds-number" model (Launder and Spalding<sup>81</sup>) in which the  $k$  and  $\epsilon$  transport equations were solved for the region  $y^+ \geq 30$ , analytical wall functions being employed to bridge the near-wall region. The other two models were variants of a partial low-Reynolds-number treatment in which a damping term was applied to the expression for  $\nu_t$  (Equation 19) following Jones and Launder.<sup>82,83</sup> The forms of the  $k$  and  $\epsilon$  equations were unaltered from the high-Reynolds-number version (although  $k$ -transport was solved over the entire flow). Walklate found that, as a group, the  $k-\epsilon$  models performed better than the mixing length models in computing turbulent mixed convection. Heat transfer calculated using the partial low-Reynolds-number models showed relatively good agreement with the data of Carr *et al.*; poorer agreement was evident when the high-Reynolds-number model was applied. These results were supported by comparisons with the flow profile measurements of Carr *et al.*; the general picture to emerge was that improvement could be gained by the use of partial low-Reynolds-number modifications. However, no model yielded high quantitative accuracy. Walklate made a single test of a partial low-Reynolds-number model against one of the velocity profiles measured by Axcell and Hall<sup>64</sup> for descending flow but found that agreement with data was poorer than that found in the comparisons made with the ascending flow profile data of Carr *et al.*

Abdelmeguid and Spalding<sup>84</sup> combined a standard  $k-\epsilon$  model with (unspecified) wall functions in a developing flow solution scheme. Computed results demonstrated the correct trends in mixed convection heat transfer, i.e. for heated upflow, impairment at low Grashof number was succeeded by enhancement at high Grashof number and, for heated downflow, enhancement was found for all values of Grashof number (Figure 24). There was no comparison with experimental data for bulk parameters; however, reasonable agreement was obtained with the velocity and temperature profile measurements of Buhr *et al.*<sup>61</sup> for heated ascending flow of mercury.

Thus, from the results of Walklate<sup>73</sup> and Abdelmeguid and Spalding,<sup>84</sup> it would appear that the  $k-\epsilon$  model offers an improvement over simpler models in the calculation of turbulent mixed convection, although there are significant discrepancies

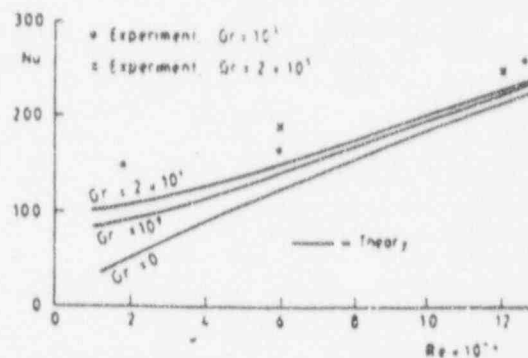


Figure 23 Comparison between experimental data and theory for downward flow turbulent mixed convection (adapted from Axcell and Hall<sup>64</sup>; with permission of Harper and Row)

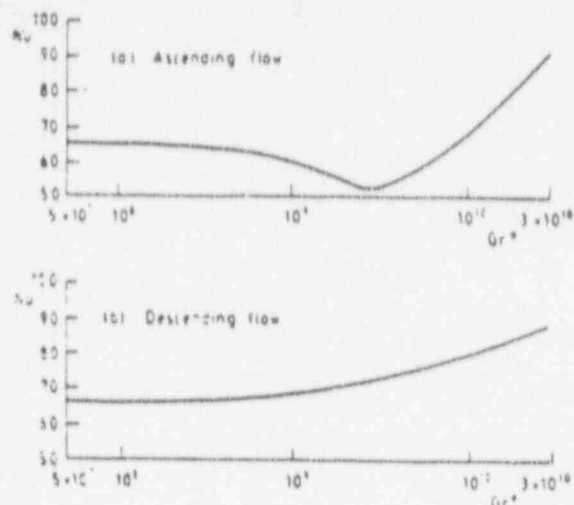


Figure 24 Calculated variation of  $Nu$  with  $Gr^*$  for  $Re = 25,000$  (adapted from Abdelmeguid and Spalding<sup>68</sup>; with permission of Cambridge University Press)

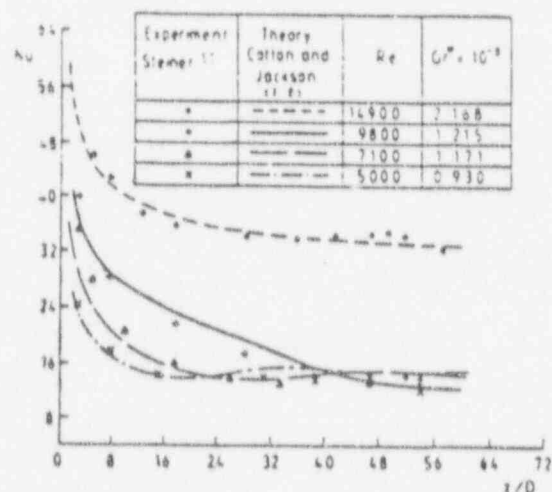


Figure 25 Comparison between calculations of Cotton and Jackson<sup>68,69</sup> and data of Steiner<sup>66</sup> for ascending air flow (adapted from Cotton and Jackson<sup>68,69</sup>; with permission of the American Society of Mechanical Engineers)

between computational results and experimental data. The likely cause of these discrepancies lies in the treatment of the near-wall region: Hall and Jackson<sup>36</sup> identified the importance of deviations from "universal" behavior in this region in determining levels of mixed convection heat transfer and Walklate found that agreement with experimental data was improved by the adoption of a partial low-Reynolds-number treatment.

Cotton and Jackson<sup>68,69</sup> examined the performance of a low-Reynolds-number  $k \sim \epsilon$  model due to Launder and Sharma<sup>66</sup> (a minor re-optimization of the Jones and Launder<sup>82,83</sup> model) against a wide range of mixed convection data for air flows. It was found that the full low-Reynolds-number treatment cast in the developing flow formulation reproduced to good accuracy both the experimental heat transfer and (where available) velocity, Reynolds stress and temperature profile measurements of Carr *et al.*,<sup>76</sup> Byrne and Ejiogu<sup>39</sup> and Steiner<sup>30</sup> (all ascending flow) and of Easby<sup>63</sup> (descending flow with moderate buoyancy influence). Figure 25 shows an example of the results obtained by Cotton and Jackson: the heat transfer data of Steiner are

computed accurately over a development length of approximately sixty tube diameters. Good agreement was also obtained with the velocity profiles of Axcell and Hall<sup>64</sup> for descending flow at high levels of buoyancy, but predictions were in less than complete accord with heat transfer data, a feature that is examined further below. Polyakov and Shindin<sup>87</sup> have recently published experimental data showing heat transfer, velocity, temperature and turbulence parameters in heated upward flow, and the present authors intend to make comparisons with theoretical predictions as part of their continuing programme of research.

It was noted above that the data of Axcell and Hall were not computed satisfactorily by Cotton and Jackson using the Launder and Sharma model; results presented in Refs. 69 and 85 show that the calculations return considerably higher levels of heat transfer than those measured experimentally (Figure 26). Recent work by the authors<sup>88</sup> indicates that improved agreement with data is obtained by the inclusion of an additional source term in the  $\epsilon$ -equation proposed by Yap.<sup>89</sup> Further work is in progress to investigate buoyancy-induced recirculation using an elliptic solver developed by Huang and Leschziner.<sup>90</sup>

Two further low-Reynolds-number  $k \sim \epsilon$  studies are reviewed. Renz and Bellinghausen<sup>91</sup> used the Jones and Launder model to compute heat transfer to an ascending flow of a refrigerant under the conditions of an experiment by Scheidt<sup>92</sup> carried out near the thermodynamic critical point (and therefore with highly variable fluid properties). The correct qualitative trends of wall temperature development were found, although there were some significant quantitative discrepancies as shown in Figure 27. Tanaka *et al.*<sup>93</sup> compared a slight variant of the Jones and Launder model against their data for heated upflow of nitrogen and found generally good agreement between measured and calculated Nusselt numbers. Comparison with data was limited, however, and does not appear to include points in the vicinity of maximum heat transfer impairment. Tanaka *et al.* used the fully developed formulation for their calculations which is unsuitable for application to flows with high heat transfer impairment where long development lengths occur.

(v) Higher order models

"Reynolds stress" or "second moment" turbulence models do not rely upon the turbulent viscosity concept, but instead incorporate transport equations for second order velocity and temperature correlations. Launder<sup>94</sup> provides a comprehensive discussion of these models. The complexity of Reynolds stress models led to the development of truncated forms known as

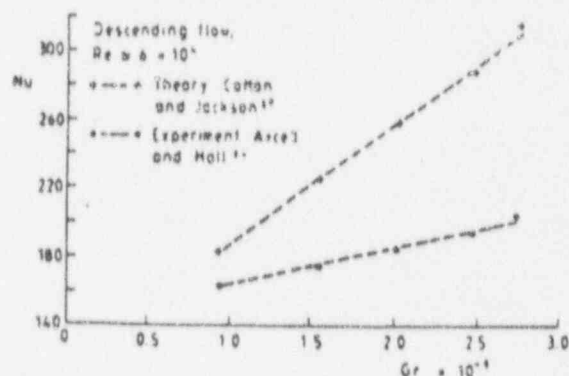


Figure 26 Comparison between calculations of Cotton and Jackson<sup>68</sup> and data of Axcell and Hall<sup>64</sup> for descending air flow (re-drawn from Cotton and Jackson<sup>68</sup>; with permission of the American Society of Mechanical Engineers)

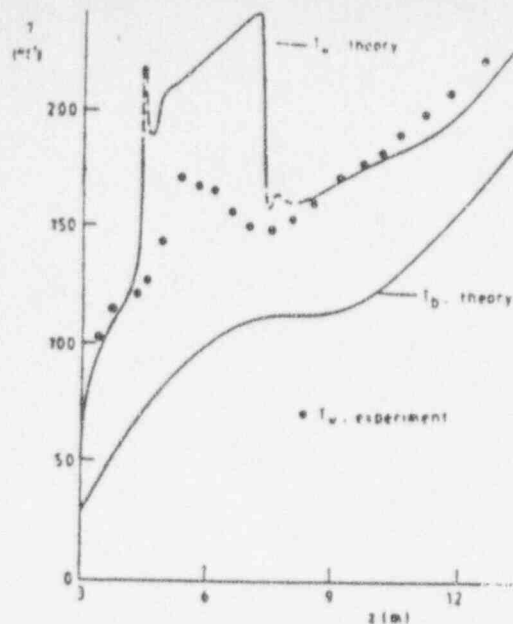


Figure 27 Comparison between calculations of Renz and Bellinghausen<sup>91</sup> and data of Scheidt<sup>92</sup> for ascending refrigerant flow (adapted from Renz and Bellinghausen<sup>91</sup>, with permission of Harper and Row)

"algebraic stress models" (ASMs). Reynolds stress models and ASMs have found application in complex flows; however, as shown by Launder,<sup>95</sup> the ASM formulation reduces to  $k \sim z$  form in thin shear flows. To and Humphrey<sup>96</sup> applied low-Reynolds-number  $k \sim z$  and ASM formulations to free convection along a heated vertical plate but found only slight differences between the performance of the two models. De Lemos and Sesonske<sup>97</sup> applied an ASM to mercury mixed convection tube flow and found qualitative agreement with data.

Finally, the direct interaction of buoyancy and turbulence via the fluctuating density-velocity correlation is considered. Abdelmeguid and Spalding<sup>94</sup> presented results neglecting buoyant production and reported that tests indicated that inclusion of such terms in the  $k$  and  $\epsilon$  equations had no significant effect upon their results. The results of Cotton and Jackson<sup>95</sup> confirm this finding, at least to the extent that the buoyant production terms were found to exert at most a second order influence. Petukhov and Medvetskaya<sup>98</sup> adopted a somewhat unusual two-equation turbulence model in which equations were formulated for turbulent kinetic energy and mean square enthalpy fluctuations with buoyant production terms included but convection and diffusion neglected. Bulk parameter calculations were consistent with experimental data but no comparison with profile measurements were made. Further work is necessary in order to clarify the importance of direct interaction terms.

## Conclusions

In laminar mixed convection heat transfer is enhanced in heated upward flow and impaired in heated downward flow. The problem is amenable to calculation, although transition to turbulent flow may occur earlier than for forced convection or free convection alone.

Turbulent mixed convection heat transfer to moderate Prandtl number fluids is dictated by changes in turbulent diffusion. In heated upward flow heat transfer is impaired with modest buoyancy and enhanced with high buoyancy. It is not possible

impairment using local parameters. In contrast heat transfer levels in heated downflow increase monotonically with increasing buoyancy and have been correlated successfully in terms of local variables.

Turbulent mixed convection may often be calculated accurately using turbulence modeling techniques provided that a developing flow solution is used and that the turbulence model allows for changes in both turbulence velocity and length scale. "Low-Reynolds-number" models should be used, permitting solution up to the heated surface; the shear stress may vary significantly close to the wall and wall functions based on uniform shear are not applicable.

## References

- 1 Martinelli, R. C. and Boelter L. M. K. Analytical prediction of superimposed free and forced convection in a vertical pipe. *University of California, Publications in Engineering*, 1942, 5, 23-58
- 2 Ostroumov, G. A. The mathematical theory of heat transfer in circular, vertical tubes with combined forced and free convection (in Russian). *Zhurnal Tekhnicheskoi Fiziki*, 1950, 20, 750-757
- 3 Hallman, T. M. Combined forced and free laminar heat transfer in vertical tubes with uniform internal heat generation. *Trans. ASME*, 1956, 78, 1831-1841
- 4 Hanratty, T. J., Rosen, E. M., and Kabel, R. L. Effect of heat transfer on flow field at low Reynolds numbers in vertical tubes. *Industrial and Engineering Chemistry*, 1958, 50, 815-820
- 5 Brown, W. G. The superposition of natural and forced convection at low flow rates in a vertical tube. *Forschung auf dem Gebiete des Ingenieurwesens*, 1960, 26, VDI-Forschungsheft 480
- 6 Morton, B. R. Laminar convection in uniformly heated vertical pipes. *J. Fluid Mech.*, 1960, 8, 227-240
- 7 Rosen, E. M. and Hanratty, T. J. Use of boundary layer theory to predict the effect of heat transfer on the laminar flow field in a vertical tube with a constant temperature wall. *A.I.Ch.E. Journal*, 1961, 7, 112-123
- 8 Pigford, R. F. Nonisothermal flow and heat transfer inside vertical tubes. *Chemical Engineering Progress Symposium Series*, 1955, 51, 79-92
- 9 Bradley, D. and Entwistle, A. G. Developed laminar flow heat transfer from air for variable physical properties. *Int. J. Heat Mass Transfer*, 1965, 8, 621-638
- 10 Marner, W. J. and McMillan, H. K. Combined free and forced laminar convection in a vertical tube with constant wall temperature. *Trans. ASME C, J. Heat Transfer*, 1970, 92, 559-562
- 11 Lawrence, W. T. and Chao, J. C. Heat transfer effects on the developing laminar flow inside vertical tubes. *Trans. ASME C, J. Heat Transfer*, 1966, 88, 214-222
- 12 Collins, M. W. Combined convection in vertical tubes. Symposium on Heat and Mass Transfer by Combined Forced and Natural Convection. Inst. Mech. Engrs., Manchester, 1971, Paper C115/71
- 13 Collins, M. W. Heat transfer by laminar combined convection in a vertical tube—predictions for water. Proc. 6th Int. Heat Transfer Conf., Toronto, 1978, 25-30, Paper MC-5
- 14 Zeldin, B. and Schmidt, F. W. Developing flow with combined forced-free convection in an isothermal vertical tube. *Trans. ASME C, J. Heat Transfer*, 1971, 94, 211-223
- 15 Scheele, G. F., Rosen, E. M., and Hanratty, T. J. Effect of natural convection on transition to turbulent flow in vertical pipes. *Canadian Journal of Chemical Engineering*, 1960, 38, 67-73
- 16 Scheele, G. F. and Hanratty, T. J. Effect of natural convection on stability of flow in a vertical pipe. *J. Fluid Mech.*, 1962, 14, 244-256
- 17 Scheele, G. F. and Greene, H. L. Laminar-turbulent transition for nonisothermal pipe flow. *A.I.Ch.E. Journal*, 1966, 12, 737-740
- 18 Watzinger, A. and Johnson, D. G. Wärmeübertragung von Wasser an Rohrwand bei senkrechter Strömung im Übergangs-

100. Khosla, J., Hoffman, T.W., and Pollock, E.G.; Combined Forced and Natural Convection Heat Transfer to Air in a Vertical Tube, Proc. 5th Int. Heat Transfer Conf., Tokyo, vol. 3, NC 4.4, pp. 144-148, 1974.



## REVIEW

# Studies of mixed convection in vertical tubes

J. D. Jackson, M. A. Cotton, and B. P. Axcell

Department of Engineering, University of Manchester, Manchester, UK

Received 3 August 1988 and accepted for publication 6 December 1988

The early study of convective heat transfer considered the branches of forced and free convection independently with only passing reference to their possible interaction. In fact the two are extreme cases of the general condition of "mixed" or "combined" forced and free convection where both mechanisms operate simultaneously. The present contribution aims to provide an up-to-date review of those works concerned with mixed convection heat transfer in vertical tubes. The review is divided into two sections, the first dealing with laminar flow, and the second with turbulent flow; further subdivisions are made according to whether the work is theoretical or experimental. Comparisons between theory and experiment are made where possible, expressions defining the conditions for onset of buoyancy effects are presented and equations for determining heat transfer are given. The paper ends with some general comments and recommendations. The survey is restricted to fluids of moderate Prandtl number; mixed convection in liquid metals can display very different characteristics which will be discussed in a future paper.

**Keywords:** mixed convection; combined convection; buoyancy-influenced flow; interaction between forced and free convection; laminarization; thermogravitation

## Introduction

The term "mixed convection" is used to describe the process of heat transfer in fluids where, due to variations of gravitational body force associated with non-uniformity of density within the system, the flow field is significantly modified from that which would prevail under conditions of uniform density. The processes involved are usually thought of in terms of the concept of fluid buoyancy and the effects are frequently referred to as effects of buoyancy on heat transfer.

In the early development of the subject of convective heat transfer, free and forced convection were studied separately and any interaction between the two was ignored. When the possibility of such interactions began to be investigated, attention was at first restricted to laminar and transitional flow conditions. More recently it has become clear not only that measurable influences of buoyancy can exist in fully turbulent flow, but that under certain conditions buoyancy effects can in fact be the dominant factor in determining heat transfer.

In this paper attention is focussed on mixed convection in vertical tubes. Two thermal boundary conditions are of particular interest, namely uniform wall temperature and uniform wall heat flux. The early experimental work on mixed convection was carried out using test sections heated by means of saturated steam, resulting in approximately uniform wall temperature. Later workers have in the main utilized electrical heating leading to approximately uniform wall heat flux.

The effects of buoyancy on heat transfer rates can be either to enhance the process or to impair it depending on the flow orientation (ascending or descending), the flow conditions and on heated length. A sound understanding of the processes involved is needed in order to take proper account of the effects of buoyancy on heat transfer in the design of thermal systems.

## Laminar flow mixed convection

The effect of simultaneous buoyancy forces and externally-applied pressure forces on steady laminar flow in a vertical pipe is amenable to calculation. The general result is that when the flow is in the upward direction past a heated surface (or downwards past a cooled surface) heat transfer is enhanced, whereas in the opposite cases heat transfer is impaired. These influences are not the result of any change in thermal diffusivity but are instead a consequence of the distortion of the velocity field and pattern of convection in the fluid.

### *Theoretical studies of laminar mixed convection*

Work on the subject dates from 1942, when Martinelli and Boelter<sup>1</sup> analysed a very simple fully developed flow model. Other fully developed solutions were subsequently reported by Ostroumov,<sup>2</sup> Hallman,<sup>3</sup> Hanratty *et al.*,<sup>4</sup> Brown,<sup>5</sup> and Morton.<sup>6</sup>

With time and the advent of digital computers the number of the simplifying assumptions decreased and, in particular, attempts were made to obtain developing flow solutions. Rosen and Hanratty,<sup>7</sup> following earlier work by Pigford,<sup>8</sup> used the boundary layer integral method with power series for the velocity and temperature profiles. Thus they reduced the problem to one of integrating a number of simultaneous non-linear differential equations. Numerical solutions, taking account of the variations of all the physical properties, were obtained for upward flow of air with uniform temperature by Bradley and Entwistle.<sup>9</sup> Marner and McMillan<sup>10</sup> also obtained numerical solutions for this boundary condition taking account of flow development. Their predictions of arithmetic mean Nusselt number are shown in Figure 1. Figure 2 shows an interesting calculation of local Nusselt number for which the influence of buoyancy increases following the thermal entry development and then reduces further downstream as the fluid temperature approaches the wall temperature.

Address reprint requests to Professor Jackson, at the Department of Engineering, University of Manchester, Manchester M13 9PL, UK.



- gebiet zwischen laminarer und turbulenter Strömung. *Forschung auf dem Gebiete des Ingenieurwesens*, 1939, 10, 182-196
- 19 Martinelli, R. C., Southwell, C. J., Alves, G., Craig, H. L., Weinberg, E. B., Lansing, N. F., and Boelter, L. M. K. Heat transfer and pressure drop for a liquid flowing in the viscous region through a vertical pipe. *Trans. Amer. Inst. Chem. Engrs.*, 1943, 7, 493-530
- 20 Clark, J. A. and Rohsenow, W. M. Local boiling heat transfer to water at low Reynolds numbers and high pressure. Technical Report No. 4, 1952, Division of Industrial Cooperation, Massachusetts Institute of Technology, Cambridge, Mass., D.I.C. Project No. 6627
- 21 Hallman, T. M. Experimental study of combined forced and free laminar convection in a vertical tube. *N.A.S.A. T.N. D-1104*, 1961
- 22 Kemeny, G. A. and Somers, E. V. Combined free and forced-convective flow in vertical circular tubes—experiments with water and oil. *Trans. ASME C, J. Heat Transfer*, 1962, 84, 339-346
- 23 Barozzi, G. S., Dumas, A., and Collins, M. W. Sharp entry and transition effects for laminar combined convection of water in vertical tubes. *Int. J. Heat and Fluid Flow*, 1984, 5, 235-241
- 24 Scheele, G. F. and Hanratty, T. J. Effect of natural convection instabilities on rates of heat transfer at low Reynolds numbers. *A.I.Ch.E. Journal*, 1963, 9, 183-185
- 25 Brown, C. K. and Gauvin, W. H. Temperature profiles and fluctuations in combined free and forced convection flows. *Chem. Eng. Sci.* 1966, 21, 961-970
- 26 Petukhov, B. S. Turbulent flow and heat transfer in pipes under considerable effect of thermogravitational forces. *Heat Transfer and Turbulent Buoyant Convection, Seminar of International Centre for Heat and Mass Transfer, Dubrovnik, Yugoslavia*, 1976 (eds. Spalding, D. B. and Afgan, N.), Hemisphere Publishing Corporation, Washington D.C., 1977, 701-717
- 27 Hsu, Y. Y. and Smith, J. M. The effect of density variation on heat transfer in the critical region. *Trans. ASME C, J. Heat Transfer*, 1961, 83, 176-182
- 28 Jackson, J. D. and Hall, W. B. Influences of buoyancy on heat transfer to fluids flowing in vertical tubes under turbulent conditions. *Turbulent Forced Convection in Channels and Bundles Theory and Applications to Heat Exchangers and Nuclear Reactors*, 2. *Advanced Study Institute Book* (eds. Kakac, S. and Spalding, D. B.), 1979, 613-640
- 29 Petukhov, B. S. and Noldé, L. D. Heat transfer to water flowing in a vertical tube. *Teplotenergetika*, 1959, 6, 72-80
- 30 Petukhov, B. S. and Strigin, B. K. Experimental investigation of heat transfer with viscous inertial-gravitational flow of a liquid in vertical tubes. *Teplotfizika Vysokikh Temperatur*, 1968, 6, 933-937
- 31 Herbert, L. S. and Sierns, U. J. An experimental investigation of heat transfer to water in film flow. *Canadian Journal of Chemical Engineering*, 1968, 46, 401-412
- 32 Herbert, L. S. and Sierns, U. J. Heat transfer in vertical tubes—interactions of forced and free convection. *Chemical Engineering Journal*, 1972, 4, 46-52
- 33 Eckert, E. R. G., Diaguila, A. J., and Curren, A. N. Experiments on mixed free and forced convective heat transfer connected with turbulent flow through a short tube. *NACA TN 2974*, 1953
- 34 Eckert, E. R. G. and Diaguila, A. J. Convective heat transfer for mixed free and forced flow through tubes. *Trans. ASME*, 1954, 76, 497-504
- 35 Hall, W. B. and Jackson, J. D. Heat transfer near the critical point. Keynote Lecture, Proc. 6th International Heat Transfer Conference, Toronto, Canada, 1978
- 36 Jackson, J. D., Hall, W. B., Fewster, J., Watson, A., and Watts, M. J. Heat transfer to supercritical pressure fluids. UKAEA, Harwell, Report No. AERE R 8158, 1975
- 37 Shitsman, M. E. Impairment of the heat transmission at supercritical pressures. *High Temperature*, 1963, 1, 237-243
- 38 Ackerman, J. W. Pseudoboiling heat transfer to supercritical pressure water in smooth and ribbed tubes. *Trans. ASME C, J. Heat Transfer*, 1970, 92, 490-498
- 39 Vikhrev, V., Barulin, D., and Kon'kov, A. S. A study of heat transfer in vertical tubes at supercritical pressures. *Teplotenergetika*, 1967, 14, 116-119
- 40 Alferov, N. S., Balunov, V. F., Zhukowski, A. V., Rybin, R. A., and Fokin, B. S. Features of heat transfer due to combined free and forced convection with turbulent flow. *Heat Transfer Soviet Research*, 1973, 5, 57-59
- 41 Shitsman, M. E. Temperature conditions in tubes at supercritical pressures. *Teplotenergetika*, 1968, 15, 57-61
- 42 Shitsman, M. E. Natural convection effect on heat transfer to turbulent water flow in intensively heated tubes at supercritical pressures. *Heat Transfer and Fluid Dynamics of Near Critical Fluids, Proc. I. Mech. E.*, 1967-68, 182, Paper 6, 36-41
- 43 Jackson, J. D. and Evans-Lutterodi, K. O. J. Impairment of turbulent forced convection heat transfer to supercritical pressure CO<sub>2</sub> caused by buoyancy forces. Report N.E.2. University of Manchester, 1968
- 44 Bourke, P. J., Pulling, D. J., Gill, L. E., and Denton, W. H. Forced convective heat transfer to turbulent carbon dioxide in the supercritical region. *Int. J. Heat Mass Transfer*, 1970, 13, 1339-1348
- 45 Fewster, J. Mixed forced and free convective heat transfer to supercritical pressure fluids flowing in vertical pipes. Ph.D. Thesis, University of Manchester, 1976
- 46 Alferov, N. S., Balunov, B. F., and Rybin, R. A. The effect of natural convection on the heat transfer of a single-phase flow with sub-critical and supercritical pressures. *Teplotfizika Vysokikh Temperatur*, 1976, 14, 1215-1221
- 47 Alferov, N. S., Rybin, R. A., and Balunov, B. F. Heat transfer with turbulent water flow in a vertical tube under conditions of appreciable influence of free convection. *Teplotenergetika*, 1969, 16, 66-70
- 48 Watts, M. J. and Chou, C. T. Mixed convection heat transfer to supercritical pressure water. Proc. 7th International Heat Transfer Conference, Munich, 1982, Paper MC16
- 49 Bogachev, V. A., Yeroshenko, V. M., Snyitina, O. F., and Yashkin, L. A. Measurement of heat transfer to supercritical helium in vertical tubes under forced and mixed convection conditions. *Cryogenics*, 1985, 25, 198-201
- 50 Steiner, A. A. On the reverse transition of a turbulent flow under the action of buoyancy forces. *J. Fluid Mech.*, 1971, 47, 503-512
- 51 Kenning, D. B. R., Shock, R. A. W., and Poon, J. Y. M. Local reduction in heat transfer due to buoyancy effects in upward turbulent flow. Proc. 5th Int. Heat Transfer Conference, Tokyo, 1974, Paper NC 4.3
- 52 Hall, W. B. and Price, P. H. Mixed forced and free convection from a vertical plate to air. Proc. 4th Int. Heat Transfer Conference, Paris, 1970, Paper NC 3.3
- 53 Hall, W. B. and Price, P. H. Interaction between a turbulent free convection layer and a downward forced flow. Symposium Heat and Mass Transfer by Combined Forced and Natural Convection. Inst. Mech. Engrs., Manchester, 1971, Paper C113,71
- 54 Rouxi, N. M. Influences of buoyancy and imposed flow transients on turbulent convective heat transfer in a tube. Ph.D. Thesis, University of Manchester, 1987
- 55 Wilkinson, G. T., Tsang, B. K.-H., and Hoffman, T. W. Flow reversal in turbulent mixed convection. Proc. 7th International Heat Transfer, Munich, 1982, Paper MC17
- 56 Hall, W. B. and Jackson, J. D. Laminarisation of a turbulent pipe flow by buoyancy forces. ASME, Paper No. 69-HT-55, 1969
- 57 Alferov, N. S., Balunov, B. F., and Rybin, R. A. Reduction in heat transfer in the region of supercritical state variables of a liquid. *Heat Transfer—Soviet Research*, 1973, 5, 49-52
- 58 Brassington, D. J. and Cairns, D. N. H. Measurements of forced convective heat transfer to supercritical pressure helium. CEGB, CERL, Report RD/L/N/1975
- 59 Byrne, J. E. and Ejiogu, E. Combined free and forced convection heat transfer in a vertical pipe. Symposium Heat and Mass Transfer by Combined Forced and Natural Convection. Inst. Mech. Engrs., Manchester, 1971, Paper C118 71
- 60 Jackson, J. D. Mixed forced and free convection—the influence of buoyancy on heat transfer in vertical pipes. Paper presented at Session V, Euromech—72 Conference, Salford University, March 1976
- 61 Buhr, H. O., Horstien, E. A., and Carr, A. D. The distortion of turbulent velocity and temperature profiles on heating of mercury in a vertical pipe. *Trans. ASME C, J. Heat Transfer*, 1974, 96, 152-158

- Heat Transfer and Turbulent Buoyant Convection, Seminar of International Centre for Heat and Mass Transfer, Dubrovnik, Yugoslavia, 1976* (eds. Spalding, D. B. and Afgan, N.), Hemisphere Publishing Corporation, Washington D.C., 1977, 759-775
- 63 Alferov, N. S., Balunov, B. F., and Rybin, R. A. Calculating heat transfer with mixed convection. *Teplotenergetika*, 1975, 22, 71-75
- 64 Acceli, B. P. and Hall, W. B. Mixed convection to air in a vertical pipe. Proc. 6th Int. Heat Transfer Conference, Toronto, Canada, 1978, Paper MC-7
- 65 Easby, J. P. The effect of buoyancy on flow and heat transfer for a gas passing down a vertical pipe at low Reynolds numbers. *Int. J. Heat Mass Transfer*, 1978, 21, 791-801
- 66 Krasnyakova, L. Y., Belyakov, I. I., and Fedelova, N. D. Heat transfer with a downward flow of water at supercritical pressure. *Teplotenergetika*, 1977, 24, 8-13
- 67 Ikryannikov, N. P., Petukhov, B. S., and Protodopov, V. S. An experimental investigation of heat transfer in the single-phase near-critical region with combined forced and free convection. *Teplotizika Vysokikh Temperatur*, 1972, 10, 96-100
- 68 Ikryannikov, N. D., Petukhov, B. S., and Protodopov, V. S. Calculation of heat transfer in the single-phase, near-critical region in the case of a viscosity-inertia-gravity flow. *Teplotizika Vysokikh Temperatur*, 1973, 11, 1068-1075
- 69 Cotton, M. A. and Jackson, J. D. Comparison between theory and experiment for turbulent flow of air in a vertical tube with interaction between free and forced convection. *Mixed Convection Heat Transfer—1987* (eds. V. Prasad, I. Catton, and P. Cheng), ASME publication HTD-84, 1987, 43-50
- 70 Tanaka, H., Tsuge, A., Hirata, M., and Nishiwaki, N. Effects of buoyancy and of acceleration owing to thermal expansion on forced turbulent convection in vertical circular tubes—criteria of the effects, velocity and temperature profiles, and reverse transition from turbulent to laminar flow. *Int. J. Heat Mass Transfer*, 1973, 16, 1267-1288
- 71 Reichardt, H. The principles of turbulent heat transfer. *Recent Advances in Heat and Mass Transfer* (ed. J. P. Hartnett), McGraw-Hill, New York, 1961, 223-252
- 72 Launder, B. E. and Spalding, D. B. *Lectures in mathematical models of turbulence*. Academic Press, London, 1972
- 73 Van Driest, E. R. On turbulent flow near a wall. *J. Aero. Sci.*, 1956, 23, 1007-1011, 1036
- 74 Malhotra, A. and Hauptmann, E. G. Heat transfer to a supercritical fluid during turbulent vertical flow in a circular duct. *Heat Transfer and Turbulent Buoyant Convection, Seminar of International Centre for Heat and Mass Transfer, Dubrovnik, Yugoslavia, 1976* (eds. Spalding, D. B. and Afgan, N.), Hemisphere Publishing Corporation, Washington D.C., 1977, 414
- Walklate, P. J. A comparative study of theoretical models of turbulence for the numerical prediction of boundary layer flows. Ph.D. Thesis, University of Manchester Institute of Science and Technology, 1976
- 76 Carr, A. D., Connor, M. A., and Buhr, H. O. Velocity, temperature and turbulence measurements in air for pipe flow with combined free and forced convection. *Trans. ASME C, J. Heat Transfer*, 1973, 95, 445-452
- 77 Dessler, R. G. Analysis of turbulent heat transfer, mass transfer and friction in smooth tubes at high Prandtl and Schmidt numbers. NACA TN 3145, 1954
- 78 Wolfshtein, M. The velocity and temperature distribution in one-dimensional flow with turbulence augmentation and pressure gradient. *Int. J. Heat Mass Transfer*, 1969, 12, 301-318
- 80 Shih, T. M. A literature survey on numerical heat transfer (1982-1983). *Numerical Heat Transfer*, 1985, 8, 1-24
- 81 Launder, B. E. and Spalding, D. B. The numerical computation of turbulent flows. *Comp. Meth. Appl. Mech. and Eng.*, 1974, 3, 269-289
- 82 Jones, W. P. and Launder, B. E. The prediction of laminarization with a two-equation model of turbulence. *Int. J. Heat Mass Transfer*, 1972, 15, 301-314
- 83 Jones, W. P. and Launder, B. E. The calculation of low-Reynolds-number phenomena with a two-equation model of turbulence. *Int. J. Heat Mass Transfer*, 1973, 16, 1119-1130
- 84 Abdelmequid, A. M. and Spalding, D. B. Turbulent flow and heat transfer in pipes with buoyancy effects. *J. Fluid Mech.*, 1979, 94, 383-400
- 85 Cotton, M. A. and Jackson, J. D. Calculation of turbulent mixed convection in a vertical tube using a low-Reynolds-number  $k-\epsilon$  turbulence model. Proc. 6th Symposium on Turbulent Shear Flows, Toulouse, 1987, Paper 6-9
- 86 Launder, B. E. and Sharma, B. I. Application of the energy-dissipation model of turbulence to the calculation of flow near a spinning disc. *Lett. Heat Mass Transfer*, 1974, 1, 131-138
- 87 Polyakov, A. F. and Shindin, S. A. Development of turbulent heat transfer over the length of vertical tubes in the presence of mixed air convection. *Int. J. Heat Mass Transfer*, 1988, 31, 987-992
- 88 Cotton, M. A., Jackson, J. D., and Yu, L. Application of the low-Reynolds-number  $k-\epsilon$  model to mixed convection in vertical tubes. Proc. 3rd UMIST Computational Fluid Dynamics Colloquium, 1988, Paper 2.3
- 89 Yap, C. R. Turbulent heat and momentum transfer in recirculating and impinging flows. Ph.D. Thesis, University of Manchester Institute of Science and Technology, 1987
- 90 Huang, P. G. and Leschziner, M. A. An introduction and guide to the computer mode TEAM. Report, University of Manchester Institute of Science and Technology, 1983
- 91 Renz, U. and Bellinghausen, R. Heat transfer in a vertical pipe at supercritical pressure. Proc. 8th International Heat Transfer Conference, San Francisco, 1986, Paper IF-15
- 92 Scheidt, M. Dissertation, University of Hannover, 1983
- 93 Tanaka, H., Maruyama, S. and Hatano, S. Combined forced and natural convection heat transfer for upward flow in a uniformly heated vertical pipe. *Int. J. Heat Mass Transfer*, 1987, 30, 165-174
- 94 Launder, B. E. Second-moment closure: methodology and practice. *Turbulence models and their applications, Vol. 2* (eds. Launder, B. E., Reynolds, W. C. and Rodi, W.), Editions Eyrolles, Paris, 1984
- 95 Launder, B. E. A generalized algebraic stress transport hypothesis. *AIAA J.*, 1982, 20, 436-437
- 96 To, W. M. and Humphrey, J. A. C. Numerical simulation of buoyant turbulent flow—I. Free convection along a heated, vertical, flat plate. *Int. J. Heat Mass Transfer*, 1986, 29, 573-592
- 97 De Lemos, M. J. S. and Sesonske, A. Turbulence modelling in combined convection in mercury pipe flow. *Int. J. Heat Mass Transfer*, 1985, 28, 1067-1088
- 98 Petukhov, B. S. and Medvedskaya, N. V. Turbulent flow and heat exchange in vertical pipes under conditions of strong influence of upward forces. *Teplotizika Vysokikh Temperatur*, 1973, 16, 778-786
- 99 Vliet, G. C. and Liu, C. K. An experimental study of turbulent natural convection boundary layers. *Trans. ASME C, J. Heat Transfer*, 1969, 91, 517-531

# Experimental, Variable Properties Natural Convection From a Large, Vertical, Flat Surface

D. L. Siebers

Sandia National Laboratories,  
Livermore, Calif.  
Assoc. Mem. ASME

R. F. Moffatt

Dept. of Mech. Engineering,  
Stanford University,  
Stanford, Calif.  
Mem. ASME

R. G. Schwind

Nielsen Engineering and Research Inc.,  
Mountain View, Calif.  
Mem. ASME

*Natural convection heat transfer from a vertical, 3.02 m high by 2.95 m long, electrically heat surface in air was studied. The air was at the ambient temperature and the atmospheric pressure, and the surface temperature was varied from 60 C to 520 C. These conditions resulted in Grashof numbers up to  $2 \times 10^{12}$  and surface-to-ambient temperature ratios up to 2.7. Convective heat transfer coefficients were measured at 105 locations on the surface by an energy balance. Boundary layer mean temperature profiles were measured with a thermocouple. Results show that: (1) the turbulent natural convection heat transfer data are correlated by the expression*

$$Nu_s = 0.098 Gr_s^{1/3} \left( \frac{T_s}{T_\infty} \right)^{-0.14}$$

*when all properties are evaluated at  $T_\infty$ ; (2) variable properties do not have a significant effect on laminar natural convection heat transfer; (3) the transition Grashof number decreases with increasing temperature; and (4) the boundary layer mean temperature profiles for turbulent natural convection can be represented by a "universal" temperature profile.*

## Introduction

An experimental study of the effects of variable properties on natural convection from a large, vertical, flat, electrically heated surface has been conducted. The vertical surface was placed in air at the ambient temperature and atmospheric pressure and heated to temperatures between 60 and 520°C. These conditions resulted in  $Gr_s$  up to  $2 \times 10^{12}$ , and  $T_s/T_\infty$  ranging from 1.1 to 2.7. The objective of this paper is to present the effects of variable properties noted in the experiment on the natural convection heat transfer from the surface, on the location of transition from laminar to turbulent flow in the natural convection boundary layer, and on the natural convection turbulent boundary layer temperature profile. In addition, comparison of the turbulent boundary layer temperature profiles to others in the literature indicate the existence of a "universal" temperature profile for turbulent natural convection. This work was part of a larger effort to examine a range of heat transfer conditions, varying from natural convection, to mixed convection driven by orthogonal buoyant and inertia forces, to forced convection, all from the same vertical surface [1].

Interest in variable properties effects on natural convection stems from the desire to predict more accurately the heat loss by convection heat transfer from the external-type receivers used in large-scale solar central receiver power plants. Convective heat loss from receivers can occur in a natural, mixed, or forced convection mode. In the natural convection mode, the convective heat transfer from an external-type receiver, essentially a large vertical, high-temperature surface, is complicated by variable properties effects as a result of the high operating temperatures. There is little information in the literature concerning variable properties effects on natural convection, particularly in the turbulent flow regime.

## Literature Review

The effects of variable properties on laminar natural convection in liquids have been reviewed in two recent articles [2, 3]. Variable properties effects on laminar natural con-

vection in gases have been examined experimentally and analytically by several authors [4-7]. The general consensus is that the effects of property variations on laminar natural convection are small in gases for the  $T_s/T_\infty$  range studied to date (0.25-4.0). Reference temperature methods are recommended by most authors to account for the small variable properties effects. One author, Hara [4], demonstrated analytically that when all properties were evaluated at  $T_\infty$ , the following relationship would account for variable properties effects in air

$$Nu = Nu_{cp} \left[ 1 - 0.055 \left( \frac{T_s - T_\infty}{T_\infty} \right) \right] \quad (1)$$

For those authors recommending a reference temperature method, definitions of  $T_{ref}$  ranged from a film temperature [6, 7] to that given in [5]

$$T_{ref} = T_\infty - 0.38(T_s - T_\infty) \quad (2)$$

In most reference temperature methods,  $\beta$  is evaluated at  $T_\infty$ . One exception is Clausing [7], who recommends that  $\beta$  be evaluated at  $T_f$ . This recommendation was based on experimental laminar heat transfer data taken at cryogenic temperatures, where  $T_s/T_\infty$  ranged from 1.0 to 2.6.

Variable properties effects on turbulent natural convection in gases have also been examined by several authors [6-8]. The numerical predictions of Siebers [8] for natural convection from a vertical surface in the  $T_s/T_\infty$  range of 1.0 to 3.0 with  $T_\infty$  at 20°C showed that evaluating the properties, including  $\beta$ , at  $T_f$  did not correlate the turbulent natural convection heat transfer predictions in terms of  $Nu$  and  $Gr$ . Pirovano et al. [6] correlated their turbulent natural convection experimental results in air in the  $T_s/T_\infty$  range of 1.0 to 1.5, with a  $T_{ref}$  heavily weighted toward  $T_\infty$  and with  $\beta$  evaluated at  $T_\infty$ . Pirovano et al. defined  $T_{ref}$  as

$$T_{ref} = T_\infty + 0.2(T_s - T_\infty) \quad (3)$$

If Siebers [8] had used the recommendations of Pirovano et al. to correlate his numerical predictions of turbulent natural convection heat transfer, the results, when expressed in terms of  $Nu$  and  $Gr$ , would have agreed closely with the experimental results of Pirovano et al. Clausing [7] used  $T_f$  with

Contributed by the HEAT TRANSFER DIVISION for publication in the JOURNAL OF HEAT TRANSFER. Manuscript received by the Heat Transfer Division May 23, 1983.



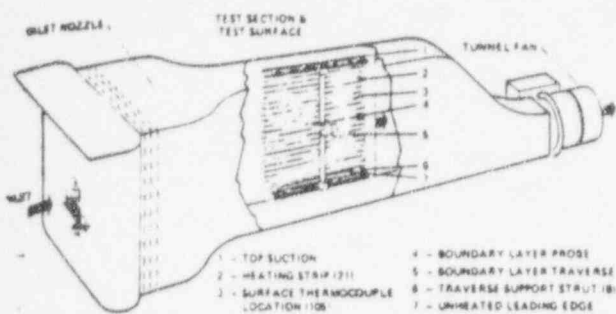


Fig. 1 Schematic of the apparatus, including the wind tunnel, the test surface, and the boundary layer traverse (+'s represent heat transfer coefficient measurement locations)

an additional large temperature-dependent correction to correlate the turbulent natural convection data obtained at cryogenic temperatures. He did note, however, that using  $T_m$  as the reference temperature for evaluating the properties significantly reduced the size of the temperature-dependent correction needed to correlate the data. Most basic heat transfer textbooks generally recommend a  $T_{ref}$  given by equation (2) or  $T_f$  with  $\beta$  evaluated either at  $T_m$  or at  $T_{ref}$  to account for variable properties effects in both laminar and turbulent flow.

The review of the literature shows that here are conflicting recommendations on how to account for variable properties effects on turbulent natural convection heat transfer in gases. These recommendations range from using a  $T_{ref}$  weighted toward  $T_w$ , given by equation (2), to a  $T_{ref}$  weighted toward  $T_m$ , given by equation (3). Basic heat transfer textbooks generally recommended a  $T_{ref}$  given by equation (2) or  $T_f$  to account for variable properties effects on turbulent natural convection heat transfer in gases, but recent experimental and numerical works [6-8] point to a  $T_{ref}$  weighted toward  $T_m$  with  $\beta$  evaluated at  $T_m$ . The differences in these various recommendations are significant when there are large temperature differences across the boundary layer.

#### Apparatus and Instrumentation

The following is a brief discussion of the apparatus and instrumentation. Further details can be found in [1]. Much of the apparatus was designed for the mixed- and forced-convection experiments and is described here only to completely describe the environment for the natural convection experiments.

An open-return, draw-through wind tunnel, 18 m long with a 4.8 m wide by 4.3 m high inlet, was built for these experiments (Fig. 1). The inlet nozzle to the test section has a two-dimensional 3:1 contraction. The heat transfer test surface, 3.02 m high by 2.95 m long, is mounted in a sidewall of the test section. The test section is 4.3 m high, 1.2 m wide, and 4.3 m long. The walls of the test section facing the heat transfer surface are water cooled to the ambient temperature. A small amount of boundary layer suction along the top of the test surface is used to ingest most of the hot, inner region of the boundary layer that leaves the top of the test surface, thereby preventing stratification in the tunnel. The suction rate was adjusted using velocity measurements and smoke flow visualization. The bottom leading edge is defined as the horizontal line where heating starts. Below this line are another 6 cm of smooth unheated surface; the struts that support the boundary layer traverse 30 cm off of the test surface extend through this unheated surface. Figure 1 shows the boundary layer traverse centrally located over the test surface. The traverse was used in some tests to take boundary layer mean velocity, temperature, and flow angle profiles. The traverse could move a boundary layer probe vertically or horizontally over the test surface, rotate a probe about an axis normal to the test surface, or move a probe normal to the test surface. The struts supporting the traverse had no effect on the vertical boundary layer flow in the natural convection mode.

The test surface consisted of 21 horizontal strips of 304 stainless steel foil stretched tightly over a slightly crowned surface of high-temperature insulating material 5.38 cm thick (Fig. 1). The strips were heated electrically using a-c current. Each strip was made from a 14.43-cm-wide by 0.13-mm-thick piece stainless steel foil. Along the entire length of both edges of each strip, 0.32 cm of the 14.43 cm width was tightly folded under, creating a strip with a net width of 13.79 cm. The 21 strips were mounted horizontally with a 0.64 cm wide gap between them to assure electric isolation of the strips from one another even with thermal expansion of the strips when heated. Folding the edges of the strips under was done for two reasons: first, it helped keep the strips flat on the surface [1] and, second, it provided additional electric power dissipation (4 percent of the total strip power dissipation) along the gaps between strips to exactly compensate for the unheated gap area (4 percent of the total area).

Surface temperatures on the test surface were measured at 105 locations, each equipped with a rosette of three ther-

#### Nomenclature

$g$ = gravitational constant, $m/s^2$	$y$ = vertical direction, m	$\eta_i$ = length scalar for the inner region of the boundary layer (24), $(\alpha^2/g\beta(T_w - T_m))^{1/3}$
$Gr_y$ = Grashof number, $g\beta(T_w - T_m)y^3/\nu^2$	$z$ = distance normal to the wall, cm	$\eta'_i$ = modified length scalar for the inner region of the boundary layer,
$\dot{q}$ = convective heat transfer coefficient, $W/m^2C$	<b>Greek</b>	$\eta_i \left( \frac{k_w}{k_m} \right) \left( \frac{T_w}{T_m} \right)^{0.14}$
$ID$ = test identification number	$\alpha$ = thermal diffusivity, $m^2/s$	<b>Subscripts</b>
$k$ = thermal conductivity, $W/mC$	$\beta$ = coefficient of volumetric expansion, $K^{-1}$	$c$ = conduction heat transfer
$n$ = exponent on the variable properties correction	$\theta$ = dimensionless temperature,	$cp$ = constant properties solution
$Nu_y$ = Nusselt number, $hy/k$	$\left( \frac{T_w - T}{T_w - T_m} \right)$	$e$ = electric power
$Nu'_y$ = $Nu_y (T_w/T_m)^n$ , $n = 0.14$ for turbulent flow, $n = 0.04$ for laminar flow	$\delta$ = Length scalar for the outer region of the boundary layer	$f$ = film temperature
$Pr$ = Prandtl number, $\nu/\alpha$	$\delta_i$ = thermal boundary layer thickness,	$r$ = radiation heat transfer
$q$ = heat flux, $W/m^2$	$\int_0^\infty \left( \frac{T - T_m}{T_w - T_m} \right) dz$	$ref$ = reference temperature
$T$ = temperature, $^{\circ}C$		$w$ = wall or surface temperature
$T_0$ = temperature scalar for the outer region of the boundary		$\infty$ = ambient condition

thermocouple junctions arranged equally spaced on the circumference of a 7.5-cm-dia circle. The three thermocouple junctions of a rosette were connected electrically in parallel so that the average temperature at the three junction locations was sensed. The thermocouple rosettes were located underneath the stainless steel heating strips, electrically insulated from the strips by a thin layer of mica. The 105 thermocouple rosettes on the test surface formed a staggered array with a 10 vertical columns, as shown by the "+"s in Fig. 1. Columns 1, 3, 5, etc., had 11 measuring stations, open on each of heating strips 1, 3, 5, etc.; Columns 2, 4, 6, etc., had 10 measuring stations, located on heating strips 2, 4, 6, etc.

An extensive program of analysis and bench testing was conducted on prototypes of the electrically heated test surface. The analysis and tests verified that the surface thermocouples installation would measure  $T_w$  (in °C) within  $\pm 1$  percent, even though the thermocouples were not welded to the strips [1].

The natural convection data were taken only on calm nights since the tunnel was outside. A hatch in the roof of the tunnel was open and the top-edge suction was operated to minimize stratification in the test section. Flow visualization with smoke showed that the air in the test section was essentially at rest. Except for the boundary layer on the heated test surface, there was no discernible flow. The stratification in the test section for the natural convection tests was small, ranging from less than 1 °C from top to bottom of the test surface for low-temperature tests to 10 °C over the top half of the test surface at a  $T_w$  of 520 °C. (The bottom half showed no stratification for any tests.) For tests where stratification occurred over the top half of the test surface, the local  $T_w$  at a given elevation was used in the data reduction.

Heat transfer coefficients were calculated at each of the 105 surface temperature measurement locations on the test surface on the basis of an energy balance

$$h = \frac{q_r - q_f - q_c}{(T_w - T_\infty)} \quad (4)$$

where

- $q_r$  = electrical power dissipated
- $q_f$  = net radiation heat transfer from the front of the test surface
- $q_c$  = conduction heat transfer through the back of the test surface

The data reduction was done on a minicomputer system which acquired and then reduced the data on-line. For natural convection tests,  $q_r$  ranged from 14 percent for the lowest  $T_w$  cases to 44 percent of the electrical power dissipated for the highest  $T_w$  cases, while  $q_c$  was typically 8 to 14 percent of the electrical power dissipated.

The electric power dissipated per unit area at a temperature measurement point on a given heating strip,  $q_r$ , was equal to the average electric power dissipated per unit area for that strip. This resulted from the uniformity of the electric power dissipation by each heating strip, which in turn resulted from the uniformity of temperature (i.e., uniformity of resistivity) on each horizontal heating strip for the natural convection mode of heat transfer and the uniformity of the heating strip thickness,  $\pm 1$  percent. The average electric power dissipated per unit area on a heating strip was determined from the product of the measured RMS voltage drop across the length of a heating strip and the measured RMS current through a heating strip, divided by the surface area of the strip (including the folded under edges) between the voltage measurement points. The small effect of thermal expansion on the surface area of a heating strip, which caused a 1 percent increase in surface area for the highest temperature case, was taken into account. The uniformity of electric power dissipation for all the 105 surface temperature measurement points was  $\pm 2.5$  percent.

Several checks were made on the uniformity of and the measurement of the electric power dissipated [1]. One important check confirmed the accuracy of the voltage and the current measurements used to determine  $q_r$ . In this check, the resistivity of the stainless steel as a function of temperature determined from the strip dimensions and from the strip voltage and current measurements made during actual heat transfer tests was compared with direct measurements of the resistivity of a sample of the 304 stainless steel heated in an oven and with resistivities reported in the literature for 304 stainless steel. The independently measured resistivities agreed within 1 percent over the temperature range of the experiment. There was also similar good agreement between the measured resistivities and those reported in the literature.

The radiation heat transfer from the surface to the tunnel walls  $q_r$ , was determined from a three zone, diffuse, gray body radiation heat transfer model. The zones in the model were (i) the tunnel walls surrounding the test surface (which were water cooled), (ii) the local spot on the surface where  $h$  was being measured, and (iii) the remainder of the test surface. Shape factors between the zones were: 0, 1, or an area ratio in the case of the tunnel wall to test surface shape factor. The temperature boundary conditions for the three zones were respectively (i) the average tunnel wall temperature determined from the measurement of the tunnel wall temperature at 35 locations with thermocouples, (ii) the local surface temperature measurement on the test surface where  $h$  was being measured, and (iii) the average test surface temperature measurement calculated from all 105 surface temperature measurements. The tunnel wall temperature rarely exceeded 40 °C at any spot, since it was water cooled. As a result, the average tunnel wall temperature was always near ambient and not an important factor in determining  $q_r$  in equation (4).

The emittance of the stainless steel test surface was determined from measurements of the normal, spectral reflectance of the 304 stainless steel in the 2.0 to 25.0 micron wavelength range at up to 70 wavelengths with a paraboloid reflectometer. These measurements were integrated over the appropriate Planckian blackbody distribution for each temperature considered and subtracted from one to give the normal, total emittance. The hemispherical, total emittance was then obtained from the relationship that exists between the hemispherical, total and normal, total emittances of smooth metal surfaces found in [9]. These measurements of hemispherical, total emittance agreed very well with previous measurements of emittance for the same material by other researchers [10, 11] and with the theory for smooth metal surfaces found in [9]. Also, the measured temperature dependence agreed with the temperature dependence given by the smooth metal surface theory. The measurements show the emissivity is  $0.13 \pm 0.01$  at ambient temperatures and  $0.22 \pm 0.01$  at the peak temperatures of the experiment. No detectable effect of material aging during testing was recorded for test conditions reported in this paper. Measurements of the emissivity over the temperature range of the experiment were made on samples of the stainless steel from before, during, and after testing.

The conduction through the insulation on the back of the test surface  $q_c$  was determined at each of the 105 surface temperature measurement points by applying a one-dimensional conduction model between two locations through the 5.38 cm depth on the insulation. The two locations were (i) the surface temperature measurement point and (ii) a point directly behind the surface temperature measurement point where a thermocouple was located between the two layers of insulation that made up the insulated back of the test surface. Variation of the thermal conductivity of the insulation with temperature was accounted for in the one-dimensional model. A numerical, three-dimensional conduction analysis of the insulation showed that the one-dimensional conduction model



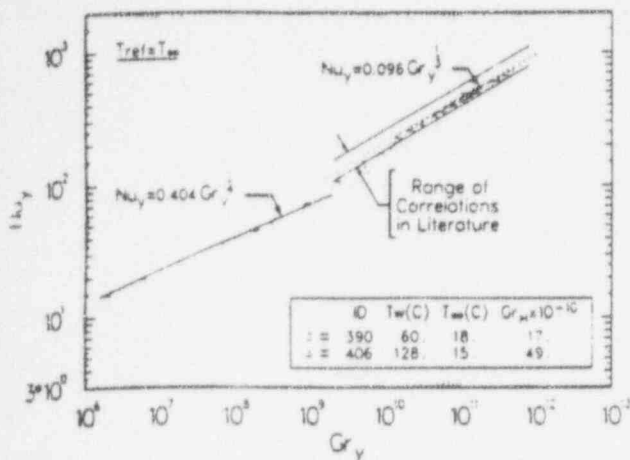


Fig. 2 Natural convection baseline results—Nusselt number versus Grashof number

was accurate to within 1 percent for areas of the 3 m by 3 m test surface 8 cm away from its edges. The calculated one-dimensional conduction loss through the insulation for the thermocouple locations on the top and the bottom heating strips, which were within 8 cm of an edge of the test surface (10 of the 105 locations), was increased by 5 percent, based on the results of the numerical, three-dimensional conduction analysis.

The values of  $h$  obtained by equation (4) are reliable within  $\pm 6$  percent for the baseline cases and the low- $T_w$  cases and within  $\pm 10$  percent for the high- $T_w$  cases. The uncertainties were calculated following the method of Kline and McClintock [12], using observed values for the individual uncertainties in the input terms. The uncertainty analysis was an important part of the experimental planning process and served as the principal criterion for choosing among alternative measurement techniques and for setting the standards for acceptable accuracy on the individual measurements.

Boundary layer mean temperature profiles were taken with a 0.052 mm type-K thermocouple probe [1]. Natural convection velocity profiles, taken with a pressure probe, were used in making a correction to the thermocouple readings. The correction accounted for errors caused by radiation between the thermocouple, the hot test surface, and the cold tunnel walls, as well as conduction heat transfer down the thermocouple stem. The model used for the radiation correction is similar to the three-zone model used for the radiation correction in equation (4), except that a fourth zone has been added to the model to represent the thermocouple. The corrections made were small. The boundary layer mean temperature data are reliable within the larger of  $\pm 2^\circ\text{C}$  or  $\pm 4$  percent based on the same method of uncertainty analysis that was used to determine the uncertainty of  $h$ . The measurement of distance normal to the test surface for the boundary layer profiles was accurate to within  $\pm 0.12$  mm.

#### Apparatus and Instrumentation Qualification

To qualify the apparatus and instrumentation, baseline (i.e., low wall-to-ambient temperature difference) heat transfer tests were taken in both the forced and natural convection modes and compared with accepted flat-plate, uniform heat flux, constant properties correlations appearing in the literature. Also, baseline boundary layer profiles of temperature and velocity were taken for forced convection and compared with accepted profiles appearing in the literature for flow on a flat, uniform heat flux surface. The forced convection baseline results are presented in [1]. The forced convection heat transfer results show excellent agreement with the accepted forced-convection heat transfer correlations for both laminar and turbulent flow on a flat,

uniform heat flux surface. The transition from laminar to turbulent flow occurs at Reynolds numbers noted by the others in the literature. The forced convection baseline boundary layer velocity and temperature profiles show similar good agreement with accepted forced convection profiles for both laminar and turbulent flow on a flat, uniform heat flux surface.

The natural convection baseline heat transfer results are shown in Fig. 2. Two natural convection baseline heat transfer tests were taken with  $T_w$  equal to  $60^\circ\text{C}$  and  $128^\circ\text{C}$  and  $T_\infty$  equal to  $15^\circ\text{C}$  and  $18^\circ\text{C}$ , respectively. The baseline results are plotted in  $Nu_y$  versus  $Gr_y$  coordinates in Fig. 2 with fluid properties evaluated at a  $T_{ref}$  equal to  $T_w$ . (The choice of  $T_{ref}$  for these low-temperature difference tests has very little effect on the data in Fig. 2). The 21 points shown for each test are each the average of the five data points along a horizontal heating strip (see Fig. 1). The RMS variation of the five data points along a heating strip was 4 percent or less.

The solid line in the laminar flow region in Fig. 2 ( $Gr_y < 10^9$ ) represents accepted constant properties natural convection correlation for laminar flow on a vertical, uniform heat flux surface in air [13]

$$Nu_y = 0.404 Gr_y^{1/4} \quad (5)$$

In the turbulent flow region ( $Gr_y > 10^{10}$ ), three lines are shown. The two solid lines represent the range of correlations in the literature for turbulent natural convection from a vertical surface. The dashed line is a "best-fit" line through the data in the literature, represented by

$$Nu_y = 0.096 Gr_y^{1/3} \quad (6)$$

Equation (6) is the correlation recommended by Churchill and Chu [14] for turbulent natural convection from a vertical surface with the coefficient 0.096 evaluated for a  $Pr$  of 0.71. The equation is based on their survey of the then current data (1975). The data at that time included only low-temperature difference data with minor variable properties effects.

Figure 2 shows three main points. First, the agreement between baseline laminar data and the accepted constant properties correlation is good. Second, the baseline turbulent data lie within the range of correlations appearing in the literature and agree very well with the "best-fit" correlation of Churchill and Chu. Third, the transition location for the baseline data agrees with other data in the literature that show transition between a  $Gr_y$  of  $10^9$  and  $10^{10}$ . This close agreement between baseline data and the data in the literature qualifies the apparatus and instrumentation. In addition, the close agreement shows that the small horizontal gaps between the 21 heating strips have little, if any, effect on the results. The lack of effect was expected, since the total area of the gaps was small compared to the heated area of the test surface, a small amount of additional heating to make up for the unheated gaps was provided along the gap edges by the folded under strip edges, and the depth of the step created by the gap ( $\approx 0.13$  mm) was small compared to the boundary layer thickness, which was as large as 15 cm.

In addition to the baseline tests, a comparison was made between the heat transfer coefficient as determined by equation (4) at a given location on the surface and one which could be determined from a boundary layer temperature profile measured at that same location by the following relationship

$$h = \frac{d\theta}{dz} \quad (7)$$

This comparison was possible for 43 cases. These were cases which had boundary layer temperature profiles with temperature measurements well into the viscous sublayer of the turbulent boundary layer or the inner region of the laminar boundary layer ( $\theta < 0.2$ ), where equation (7) is valid. Two of the cases were natural convection profiles, and 41 were forced

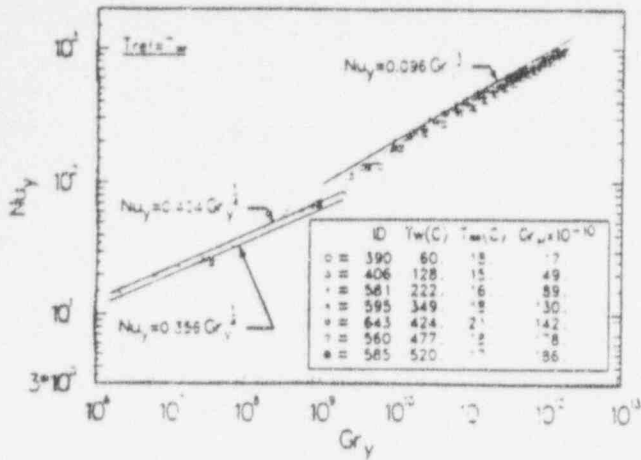


Fig. 3 Effect of variable properties on natural convection from a vertical surface in air

or mixed convection profiles taken as part of the forced and mixed convection experiments also conducted with this apparatus. The profiles were for the  $T_w$  in the 200°C to 580°C range. The average ratio of the measurement of  $h$  from equation (4) to the measurement of  $h$  from equation (7) for the 43 cases was 1.008 with a standard deviation of 14 percent. The closeness of this ratio to 1.0 is a check on the consistency of the independently measured surface heat transfer data and boundary layer temperature profiles over the entire temperature range of the experiment. Other consistency checks are presented in [1].

## Results and Discussion

**Heat Transfer.** Variable properties effects on natural convection heat transfer from an electrically heated, vertical, 3.02-m-high by 2.95-m-long surface were studied. The ambient temperature was approximately 20°C. Average values of  $T_w$  that were considered were 60, 128, 222, 349, 424, 477, and 520°C. These temperatures resulted in  $T_w/T_\infty$  ratios from 1.1 to 2.7. Figure 3 shows the heat transfer results in terms of  $Nu_y$  and  $Gr_y$  with all properties, including  $\beta$ , evaluated at  $T_w$  for each test. The 21 data points shown in Fig. 3 for each surface temperature were obtained in the same manner as those for the baseline cases shown in Fig. 2. For all tests except test ID 585, the test surface was at steady-state conditions. Test 585, which had to be stopped before steady state was reached, has a transient energy storage correction equal to -5 percent of electric power dissipated. This correction accounted for energy being stored in the insulation. The correction was based on measurements of the insulation temperature taken over a 10-min interval and was made along with the radiation and conduction corrections in equation (4).

In the turbulent region ( $Gr_y > 10^{10}$ ) in Fig. 3, the data shows two important points. First, there is a small decrease in  $Nu_y$  for a given  $Gr_y$  as  $T_w$  increases, when properties are evaluated at  $T_w$ . Second, each data set for each temperature remains parallel to the low-temperature difference correlation given by equation (6) from Churchill and Chu; the second point is most visible for test 585. This latter point means that  $Nu_y$  remains dependent on  $Gr_y^{1/3}$  in the turbulent flow region with increasing temperature difference across the boundary layer, or in other words, the heat transfer coefficient remains uniform in the turbulent region. Only the coefficient in equation (6) is changing with increasing temperature. It decreases from the 0.096 value for a small temperature difference across the boundary layer to a value of 0.08 for the 520 C test, a decrease of 15 percent. This decrease does not imply that the turbulent natural convective heat transfer coefficient at a fixed location is lower for higher  $T_w$ . It only indicates that, as a result of property variations across the

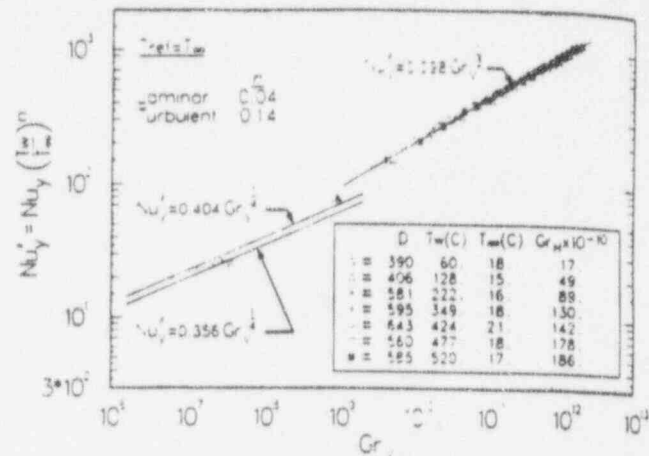


Fig. 4 Correlation of variable properties effects on natural convection from a vertical surface in air

boundary layer, the heat transfer coefficient is less than would be predicted by the low-temperature difference constant-properties correlation with all properties evaluated at  $T_\infty$ .

In the laminar region ( $Gr_y < 5 \times 10^8$ ) in Fig. 3, there is a small decrease in  $Nu_y$  for a given  $Gr_y$  as  $T_w$  increases. The decrease in  $Nu_y$  with increasing  $T_w$  is most clearly shown by the lower  $Gr_y$  data point for each  $T_w$ . As  $T_w$  increases, the lowest  $Gr_y$  data point for each  $T_w$  lies progressively farther below the uniform heat flux correlation given by equation (5), the upper line in the laminar region.

The decrease in  $Nu_y$  with increasing  $T_w$  in the laminar region is not totally due to variable properties effects as was the case in turbulent flow. The decrease in  $Nu_y$  is partly due to a change in the heat transfer boundary condition on the test surface as  $T_w$  increases. At low temperatures, the surface has a uniform heat flux, as described earlier. At high temperatures, the surface approaches a uniform temperature as a result of the radiation heat transfer from the surface. For the highest temperature case, 520°C, the test surface is within 2 percent of a uniform temperature surface in the laminar and transition regions. The correlation for uniform surface temperature is the lower line in the laminar region in Fig. 3 [15]. A combination of variable properties effects and a change in boundary condition are indicated by the fact that the highest temperature laminar data point lies about 8 percent below the uniform surface temperature relationship.

Unlike the situation in the laminar region, a change in boundary condition does not occur in the turbulent region. A vertical surface with a turbulent natural convection flow over it is simultaneously a uniform temperature and a uniform heat flux surface (i.e.,  $h$  is spatially uniform for a given  $T_w$ ). Churchill and Chu's uniform temperature and uniform heat flux correlations based on "best fits" of data in the literature are only different by 2 percent for a  $Pr$  of 0.71. The difference is well within the uncertainty of the data available.

When all the properties are evaluated at  $T_w$ , the variable properties effects noted in Fig. 3 for turbulent natural convection in air are accounted for by the following relationship

$$Nu_y = 0.098 Gr_y^{1/3} \left( \frac{T_w}{T_\infty} \right)^{-0.14} \quad (8)$$

This equation is based on a "best fit" of the natural convection data in Fig. 3, where the  $1/3$  power on  $Gr$  was assumed as a result of the lack of dependence of  $h$  on  $y$  (shown by each set of the heat transfer coefficient data for each  $T_w$ ). The coefficient in equation (8) is 2 percent higher than that in the baseline equation, equation (6), and a temperature ratio correction has been added to account for the effects of variable properties. Figure 4 (where the Nusselt number,  $Nu_y$ , is defined so that it includes the temperature ratio correction

Table 1  
variable  
( $T_w = 2$ )  
Ref.  
 $T_w$   
 $\beta$   
 $T_w$  (°C)

term in  
(8) acco  
increasi  
bulent c  
given b  
constant  
The  
vection  
the prop  
is

The tem  
The  
transfe

is

The ter

0.356 f  
in the  
predict  
more c  
perime  
[1-5].

ffects

The di

withou  
be 4 p

The  
convec  
by eve

Sparr  
still b

The  
are ne

tempe  
differ

perati

Pirov

1.5. T

acros  
perat

differ

as Ta

Prop

Keyer

meth  
predi  
6.7,  
the  
acor  
prop  
wall-  
show  
Fo  
gives  
para

**Table 1** A comparison of recommendations for evaluating variable properties effects on turbulent natural convection ( $T_w = 20^\circ\text{C}$ ).

Ref.	[6]	[7]	[16]	[17]	[18]
$T_{ref}$	Eq. (3)	$T_f$	$T_f$	$T_f$	Eq. (2)
$\beta$	$1/T_w$	$1/T_f$	$1/T_w$	$1/T_f$	$1/T_w$
$T_w$ ( $^\circ\text{C}$ )	$h/h$ predicted by Eq. (8)				
300	1.03	1.30	0.95	0.82	0.90
600	1.04	1.17	0.90	0.71	0.87
900	1.06	1.10	0.88	0.65	0.82

term in the definition of Nusselt number) shows that equation (8) accounts for the small systematic decreases in  $Nu$ , with increasing temperature, which appeared in Fig. 3. The turbulent data collapse to within  $\pm 6$  percent of the correlation given by equation (8). This percentage is within the uncertainty band on the heat transfer data.

The variable properties effects on turbulent natural convection could also have been accounted for by evaluating all the properties, except  $\beta$  in  $Gr$ , at a  $T_{ref}$  defined as:

$$T_{ref} = 0.3T_w + 0.7T_w \quad (9)$$

The term  $\beta$  should still be evaluated at  $T_w$ .

The correlation for the laminar natural convection heat transfer data, with all properties for air evaluated at  $T_w$ , is

$$Nu_f = aGr_f^{1/4} \left( \frac{T_w}{T_w} \right)^{-0.04} \quad (10)$$

The term  $a$  equals 0.404 for a uniform heat flux surface and 0.56 for a uniform temperature surface, the values reported in the literature. Equation (10) agrees with numerical predictions made by Siebers [8] for  $T_w/T_w < 3.0$ , with the more detailed laminar data for  $T_w/T_w < 1.5$  from the experiments of Pirovano et al. and with various analyses for air [5]. Equation (10) demonstrates that variable properties effects on laminar natural convection heat transfer are small. The difference in  $h$  calculated from equation (10) with and without the  $T_w/T_w$  corrections at a  $T_w/T_w$  of 3.0 would only be 4 percent.

The effects of variable properties on laminar natural convection heat transfer can also be accurately accounted for by evaluating all properties except  $\beta$  in  $Gr$ , at  $T_f$ , as noted by Sparrow and Gregg [5] and Pirovano et al. The term  $\beta$  should still be evaluated at  $T_w$ , as in turbulent flow.

The trends noted in the turbulent natural convection region are new. No experiments were found in the literature for high-temperature flows on a vertical surface with large temperature differences across the boundary layer. The highest temperature experiment with turbulent flow in gases was by Pirovano et al. with temperatures up to  $150^\circ\text{C}$  and  $T_w/T_w < 1.5$ . The one experiment that had large temperature variations across a turbulent boundary layer was at cryogenic temperatures. Clausing, who conducted this experiment, noted different trends.

Table 1 shows a comparison of the effects of variable properties on turbulent natural convection heat transfer from a vertical surface in air predicted by various recommended methods to account for those effects. In the table, the effects predicted by five recommendations appearing in the literature [6, 7, 16, 17, 18] are compared with the effects predicted by the method proposed in this paper. The present work recommends evaluating all properties in the constant properties heat transfer relationship at  $T_w$  and making the wall-to-ambient temperature ratio correction,  $(T_w/T_w)^{-0.14}$ , shown in equation (8).

For each of the five methods from the literature, the table gives the  $T_{ref}$  at which properties are evaluated, the temperature used to determine  $\beta$ , and the ratio of  $h$  predicted by

that method to  $h$  predicted by equation (8) for three different values of  $T_w$  (300, 600, and  $900^\circ\text{C}$ ) and a  $T_w$  of  $20^\circ\text{C}$ . The first two methods listed [6, 7] are recent recommendations reported in the literature based on experimental data. The next three [16, 17, 18] are recommendations reported in most basic heat transfer textbooks. All of the methods except Clausing's, the second method, are reference temperature methods. Clausing evaluates all properties, including  $\beta$ , at  $T_f$  and makes a large correction based on  $T_w/T_w$  to account for variable properties effects. The correction is given in Fig. 1 of [7].

The constant properties Nusselt-Grashof number correlation to which all the recommended methods presented in Table 1 are applied is given by equation (8) without the  $(T_w/T_w)^{-0.14}$  term. The correlation represented by equation (8) without the temperature ratio term is not significantly different than the constant properties correlations used in each of the references in Table 1. The only difference is in the coefficient (0.098 in equation (8)) in each correlation. Applying all methods to one constant properties correlation allows the different methods of handling variable properties to be compared, without introducing the small differences in the coefficient of the constant properties relationship that is recommended in each work. Effectively, this means that Table 1 compares with relative trend in the variable properties effects predicted by each method for increasing  $T_w$  with that predicted by equation (8).

Table 1 shows that the first method, from Pirovano et al. (the most closely related experiment to the work described in this paper), predicts substantially the same variable properties effect as equation (8) for all temperatures. This reference temperature method uses a  $T_{ref}$  heavily weighted toward  $T_w$ , given by equation (3), with  $\beta$  evaluated at  $T_w$ . It is based on an experiment with values of  $T_w$  up to  $150^\circ\text{C}$ . The second method in the table, the method recommended by Clausing based on data taken at cryogenic temperatures, predicts 30 percent higher heat transfer at  $300^\circ\text{C}$ , but only 10 percent higher at  $900^\circ\text{C}$ . This trend indicates that his method predicts a different variable properties effect on turbulent natural convection with increasing  $T_w$  than equation (8) does. The last three methods in Table 1—the textbook methods—predict progressively lower heat transfer coefficients with increasing  $T_w$ . This trend is particularly true for the fourth method, where  $\beta$  is evaluated at  $T_f$  along with the rest of the properties.

The disagreement between the methods recommended in this work and the last three methods is most likely explained by the fact that these recommendations are based on forced convection experience or on a laminar flow natural convection analysis by Sparrow and Gregg [5]. No turbulent natural convection data with significant variable properties effects are available. Recommendations based on forced convection experience should not be expected to work a priori for turbulent natural convection. Similarly, recommendations based on Sparrow and Gregg's laminar flow analysis should not be expected to work a priori for turbulent natural convection since, first, the analysis was for laminar natural convection heat transfer and, second, the variable properties effects on which they based their conclusions in that analysis were only a few percent for the realistic gas models and temperature ranges studied ( $330\text{ K} < T < 1000\text{ K}$ ,  $T_w/T_w < 3.0$ ). For example, if an  $h$  for air predicted using  $T_f$  as the reference temperature in the laminar heat transfer relationship, equation (5), is compared to an  $h$  predicted with the same relationship using Sparrow and Gregg's recommended reference temperature, given by equation (2), there would be less than a 1 percent difference for  $T_w$  at  $600^\circ\text{C}$  and  $T_w$  at  $20^\circ\text{C}$  ( $T_w/T_w = 3.0$ ). The reasons for the disagreement with the results of Clausing are not clear at this point. One possibility is that variable properties effects on



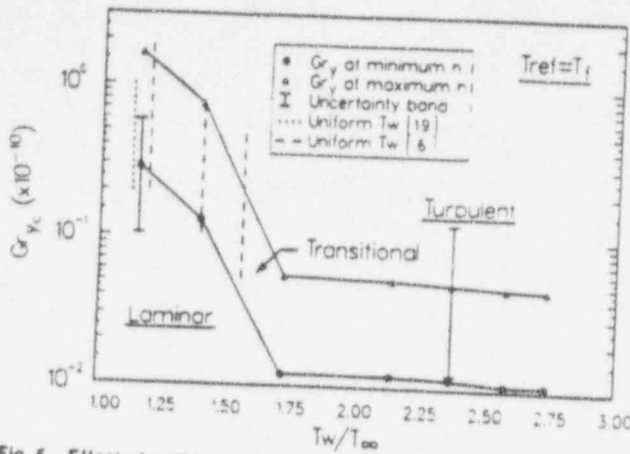


Fig. 5 Effect of wall temperature on the transition Grashof number in natural convection from a vertical surface in air

turbulent natural convection are different for different fluids in significantly different temperature ranges.

**Transition.** Figure 5 shows the effect of  $T_w$  on the natural convection transition from laminar to turbulent flow for fixed  $T_\infty$ . The figure is a plot of the  $\log_{10}$  of the Grashof number based on  $y_c$  versus  $T_w/T_\infty$ . The length  $y_c$  is the location of either the minimum  $h$  or the maximum  $h$ . The location of the minimum  $h$  is the point where  $h$  begins to deviate from the laminar  $h$  value. The location of the maximum  $h$  is the first point at which  $h$  equals its fully turbulent value, which is a constant. The resolution in determining these locations is plus or minus the width of one heating strip. Uncertainty bands based on this resolution are shown in Fig. 5. The upper value for  $Gr_{y_c}$  at each  $T_w/T_\infty$  corresponds to the location of maximum  $h$ ; the lower value corresponds to the minimum  $h$  location. The zone between the minimum and maximum  $h$  is defined here as the "transition zone" (the crosshatched area). All properties in this figure are evaluated at  $T_f$  with the exception of  $\beta$ , which is evaluated at  $T_\infty$ . Film temperature was used largely because transition starts in the laminar boundary layer where one way to correlate heat transfer data is to evaluate properties at  $T_f$ , as discussed earlier. The solid lines connecting the data points from this experiment are for visual reference only.

Figure 5 shows that  $T_w$  has a significant effect on the stability of the boundary layer for a fixed  $T_\infty$ . As  $T_w/T_\infty$  increases, the Grashof number at which transition occurs,  $Gr_{y_c}$ , decreases significantly up to a  $T_w/T_\infty$  of 1.75. Furthermore, the size of the transition zone, in terms of the difference between  $Gr_{y_c}$  at the minimum and maximum  $h$  locations, decreases up to a  $T_w/T_\infty$  of 1.75. This decrease in size is also true in terms of vertical distance. However, the ratio of Grashof numbers at the minimum and maximum  $h$  locations remains fixed at approximately 5.0. These results agree closely with the results of Pirovano et al. for  $T_w/T_\infty$  up to 1.5. The very low-temperature ratio case agrees with the results of Cheesewright [19].

Beyond a  $T_w/T_\infty$  of 1.75, transition zone size and location in terms of  $Gr_{y_c}$  appear fixed. This apparent trend is believed due to a loss of resolution in locating the transition zone. By  $T_w/T_\infty = 1.75$ , the transition zone has moved down to the first three heating strips on the test surface (see Fig. 1) and is occurring over a very short distance ( $\approx 1$  strip). On the basis of the resolution of the transition zone location, accurate location of the transition zone is impossible when  $T_w/T_\infty$  exceeds 1.75. It is only clear that the transition zone does not move upward on the surface for  $T_w/T_\infty > 1.75$ .

**Temperature Profiles.** Boundary layer mean temperature profiles were taken for turbulent natural convection for a  $T_w$

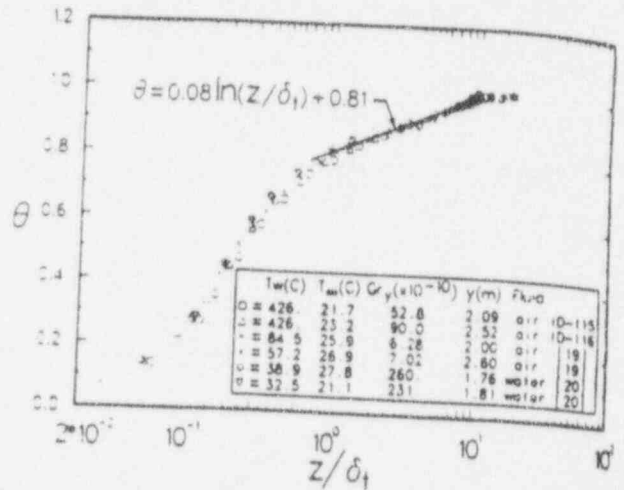


Fig. 6 Temperature profiles in a turbulent natural convection boundary layer on a vertical surface

equal to  $420^\circ\text{C}$ . The corrections to the temperature measurements accounting for errors caused by radiation heat transfer and conduction heat transfer (discussed earlier) were small, ranging from  $+10^\circ\text{C}$  near the wall to  $-2^\circ\text{C}$  at the outer edge of the boundary layer. In the following figures, the uncertainty in  $z$ ,  $\pm 0.12$  mm, results in a  $\pm 15$  percent uncertainty in the nondimensional distances used in the figures for the point closest to the wall for each profile from this experiment. This uncertainty is inversely proportional to the distance from the wall.

The temperature profiles are shown in Fig. 6, which is a plot of dimensionless temperature  $\theta$  versus distance normal to the wall  $z$  divided by  $\delta$ . Also shown are turbulent boundary layer temperature profiles from other works for which tabular data were available to plot. Two of the profiles shown were taken in air by Cheesewright and two were taken in water by Chokouhmand [20]. For Cheesewright's profiles,  $T_w$  equals  $84.5$  and  $57.2^\circ\text{C}$ . For Chokouhmand's profiles,  $T_w$  equals  $38.9$  and  $32.5^\circ\text{C}$ . The high-temperature profiles from this experiment compare well with the profiles for air and water at lower temperatures taken by Cheesewright and Chokouhmand, respectively. The close comparison of Cheesewright's low-temperature profiles for air with the high-temperature profiles from this experiment indicates that there is very little effect of variable properties on the turbulent natural convection temperature profile shape. All of the profiles in Fig. 6 show a "viscous" sublayer or "linear" region near the wall,  $z/\delta < 0.2$ , and a "logarithmic" region in the outer region of the boundary layer,  $z/\delta > 1.0$ . The temperature distribution in the "logarithmic" region is given by

$$\theta = 0.08 \ln(z/\delta) + 0.81 \quad (11)$$

Equation (11) is represented by the solid line in Fig. 6.

Comparisons were also made with turbulent boundary layer temperature profiles from other experiments for which tabular data was not readily available for plotting [21-23]. In the outer region, the "logarithmic" region, the data from the experiments of Warner and Arpaci [21], Vliet and Liu [22], and Fujii [23] agree very well with the data in Fig. 6. In the inner region, for  $z/\delta < 0.6$ , the temperature profiles from these same references agree in terms of their shape, but there is more scatter than is indicated by the data in Fig. 6, approximately  $\pm 40$  percent at  $z/\delta$  equal to 0.1. The reasons for the scatter are not clear. One possible reason is a Pr number effect. The experiments cover a Pr number range of 0.7 to 33.

The agreement of the turbulent profiles from the various experiments strongly suggests the existence of a "universal" temperature profile for turbulent natural convection. Existence of a universal profile has not been clearly

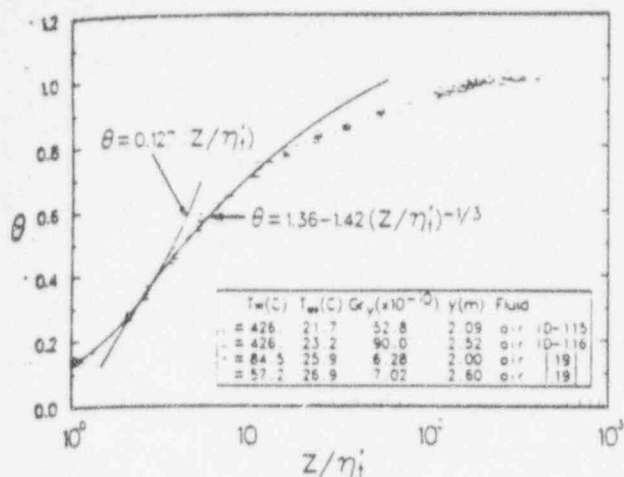


Fig. 7 Temperature profiles in a turbulent natural convection boundary layer on a vertical surface in air

established experimentally but has been theorized most recently by George and Capp [24]. George and Capp proposed dividing the boundary layer into an inner and outer region. The inner region was assumed to be a constant heat flux layer consisting of a "viscous" sublayer and a "buoyant" sublayer. The "buoyant" sublayer is between the "viscous" and "logarithmic" regions pointed out in Fig. 6. The form of the equations derived by George and Capp for the "viscous" and "buoyant" sublayers for a uniform temperature surface are, respectively

$$\theta = C_1 (z/\eta_i) \quad (12)$$

$$\theta = C_2 + C_3 (z/\eta_i)^{-1/3} \quad (13)$$

In these equations, the definition of  $\theta$  is one minus that used by George and Capp, and the terms  $C_1$ ,  $C_2$ , and  $C_3$  are functions of Pr. Based on the experimental data available, George and Capp determined  $C_1$ ,  $C_2$ , and  $C_3$  to be 0.1, 1.35, and -1.45, respectively, for air.

George and Capp theorized that the temperature profile in the outer region of the boundary layer was dependent only on  $z/\delta$ , where  $\delta$  is a length scale for the outer region of the boundary layer. Their theory showed that there should be no Pr number dependence in the outer region. George and Capp expressed the equation for the outer region as

$$\frac{T - T_\infty}{T_0} = C_4 \left( \frac{z}{\delta} \right) \quad (14)$$

where  $\delta$  was undefined. No specific form for the equation was given by their theory. An empirical fit to data is required to obtain the equation for the outer region.

Figure 6 suggests a logarithmic form for the "universal" temperature profile in the outer region of the boundary layer. Deviations of the data from equation (11) are within the uncertainty of the data available. Figure 6 also suggests  $\delta$ , as a length scale and  $T_w - T_\infty$  as a scalar for temperature in the outer region as a result of the close agreement of the various sets of data over a large range of Pr.

Using  $\delta$ , as an outer region length scale is contrary to the recommendation of George and Capp, who stated that since  $\delta$ , had "no dynamical significance," it should not be used as a length scale for the outer or inner regions. It is worth noting however, that when the Boussinesq approximation is made, the integral  $\int_0^{\delta} (T - T_\infty) dz$  appears in the integral form of the momentum equation for natural convection. The integral appears in a source term in the integral momentum equation, representing the buoyant force term in the differential momentum equation. The appearance of the integral suggests strong dynamical significance for  $\delta$ , since dividing the integral by  $T_w - T_\infty$  gives  $\delta$ .

The important points shown by Fig. 6 and equation (11) are: (i) there are no significant variable properties effects on the temperature profile shape, (ii) the temperature in the outer region appears logarithmically dependent on  $z$ , (iii)  $\delta$ , appears to be a good length scale for the outer region, and (iv) the profile appears to be independent of Pr in the outer region as suggested by George and Capp in their theory. This last point appears true for the Pr range of 0.7 to 33 based on [21-23].

The temperature profiles for air from both this experiment and Cheesewright's experiment (the same cases as shown in Fig. 6) are presented in Fig. 7 in terms of the inner region coordinate,  $z/\eta_i$ . The term  $\eta_i$  is a modified form of the inner region length scale of George and Capp. The modification, which is based on equation (8), accounts for a small shift in profile locations in these coordinates caused by variable properties effects. Also shown in this plot are the following equations

$$\theta = 0.127(z/\eta_i) \quad (15)$$

$$\theta = 1.36 - 1.42(z/\eta_i)^{-1/3} \quad (16)$$

These equations are equations (12) and (13) with coefficients modified to fit the data in Fig. 7. The coefficients in the equations are only slightly different than those derived by George and Capp on the basis of the data available to them. The figure shows that the form of the equations for a "universal" temperature profile derived by George and Capp for the inner region of the boundary layer agree very well with the data for air. The coefficients are Pr-dependent, though, since the water data of Chokouhmand, if shown, would be significantly to the right of the air data.

As a final note, equations (7) and (15) can be used to determine a heat transfer relationship for turbulent natural convection in air in a straightforward fashion

$$Nu_s = 0.10 Gr_s^{1/3} \left( \frac{T_w}{T_\infty} \right)^{-0.14} \quad (17)$$

This heat transfer relationship and the heat transfer relationship given by equation (8), determined from the independently measured boundary layer temperature profiles and surface heat transfer data, respectively, agree within 2 percent. The consistency of the independently measured boundary layer temperature profiles and the surface heat transfer data is a very good check on the experimental technique and the variable properties effects noted in this experiment.

## Conclusions

An experimental study of variable properties natural convection heat transfer in air was conducted on a large (3.02 m high by 2.95 m long), electrically heated, vertical surface. The wall temperature was varied from 60 to 520°C. The ambient temperature was approximately 20°C. Surface heat transfer coefficients were measured at 105 locations on the surface. Boundary layer mean temperature profiles were also taken. Turbulent natural convection heat transfer results show that variable properties effects on turbulent natural convection heat transfer can be correlated using the low-temperature difference correlation, if properties are evaluated at  $T_\infty$  and a small wall-to-ambient temperature ratio correction is added. This correlation is given by

$$Nu_s = 0.098 Gr_s^{1/3} \left( \frac{T_w}{T_\infty} \right)^{-0.14}$$

The correlation fits the turbulent heat transfer data taken to within  $\pm 6$  percent. The laminar variable properties heat transfer results show, as demonstrated by others, that the laminar variable properties effects for gases are small. The results also show that the location and extent of transition from laminar to turbulent flow are significantly affected by  $T_w$  for a fixed  $T_\infty$ . As  $T_w/T_\infty$  changes from 1.1 to 1.75, the



transition Gr decreases from about  $7 \times 10^4$  to  $3 \times 10^8$  when the properties in Gr are evaluated at a film temperature.

Boundary layer mean temperature profiles indicate that a "universal" temperature profile exists for turbulent natural convection. The "universal" profile for the inner region of the boundary layer for air, which includes the effects of variable properties on the profile location, is given by the following equations

$$\text{Viscous sublayer: } \theta = 0.127(z/\eta_i)$$

$$\text{Buoyant sublayer: } \theta = 1.36 - 1.42(z/\eta_i)^{-1/3}$$

The forms of the equations were taken from George and Capp. The constants in the equations, which are Pr-dependent, were determined from mean temperature profiles taken in air. The outer region of the "universal" temperature profile, based on temperature profiles from this work and temperature profiles taken in air and water from other works, has a logarithmic form.

### Acknowledgments

The authors would like to acknowledge the financial support of the Department of Energy, acting through Sandia National Laboratories, Livermore, California. In particular, we would like to thank Dr. Robert Gallagher for his attentive overview of the program and Dr. John Kraabel for his close and effective technical monitoring. This work was supported by the U.S. Department of Energy under Contract DE-AC04-76DP00789.

### References

- 1 Siebers, D. L., "Experimental Mixed Convection Heat Transfer from a Large, Vertical Surface in a Horizontal Flow." Ph.D. thesis, Department of Mechanical Engineering, Stanford University, 1983; available as Sandia National Laboratories Report No., SAND83-8225, Sandia National Laboratories, Livermore, Calif., 1983.
- 2 Carey, V. P., and Mollendorf, J. C., "Variable Viscosity Effects in Several Natural Convection Flows," *IJHT*, Vol. 23, 1980, pp. 95-108.
- 3 Shaukurullah, H., and Gebhart, B., "The Effect of Variable Properties on Laminar Natural Convection Boundary-Layer Flow Over a Vertical Isothermal Surface in Water," *Numerical Heat Transfer*, Vol. 2, 1979, pp. 215-232.
- 4 Hara, T., "Heat Transfer by Laminar Natural Convection About a Vertical Flat Plate with Large Temperature Difference," *Bull. JSME*, Vol. 1, No. 3, 1958, pp. 251-254.

- 5 Sparrow, E. M., and Gregg, J. L., "The Variable Fluid-Property Problem in Natural Convection," *ASME Transactions*, Vol. 80, 1958, pp. 869-886.
- 6 Pirovano, A., Viannay, S., and Jannot, M., "Convection Naturelle En Regime Turbulent Le Long D'Une Plaque Plane Verticale," Paper No. NC-14 1970, *Proceedings of the 4th International Heat Transfer Conference*, Paris, Versailles, France, pp. 1-12.
- 7 Clausing, A. M., "Natural Convection Correlations for Vertical Surface Including Influences of Variable Properties," *ASME JOURNAL OF HEAT TRANSFER*, Vol. 105, 1983, pp. 138-143.
- 8 Siebers, D. L., "Natural Convection Heat Transfer From an External Receiver," Sandia National Laboratories Report No. SAND78-8276, Sandia National Laboratories, Livermore, Calif., 1978.
- 9 Siegel, R., and Howell, J. R., *Thermal Radiation Heat Transfer*, McGraw-Hill, New York, 1972, p. 116.
- 10 Edwards, D. K., and Catton, I., "Radiation Characteristics of Rough and Oxidized Metals," *Advances in Thermophysical Properties at Extreme Temperatures and Pressures*, edited by Serge Gratch, ASME, 1965, pp. 174-188.
- 11 Edwards, D. K., and deVolo, N. B., "Useful Approximations for Spectral and Total Emissivity of Smooth Bare Metals," *Advances in Thermophysical Properties at Extreme Temperatures and Pressures*, edited by Serge Gratch, ASME, 1965, pp. 174-188.
- 12 Kline, S. J., and McClintock, F. A., "Describing Uncertainties in Single Sample Experiments," *Mechanical Engineering*, Vol. 75, 1953, pp. 3-8.
- 13 Sparrow, E. M., and Gregg, J. L., "Laminar Free Convection from a Vertical Plate with Uniform Surface Heat Flux," *ASME Transactions*, Vol. 78, 1956, pp. 435-440.
- 14 Churchill, S. W., and Chu, H. H. S., "Correlating Equations for Laminar and Turbulent Natural Convection From a Vertical Plate," *IJHT*, Vol. 18, 1975, pp. 1323-1328.
- 15 Ostrach, S., "An Analysis of Laminar Free-Convection Flow and Heat Transfer About a Flat Plate Parallel to the Direction of the Generating Body Force," NACA TR 1111, 1953.
- 16 Kays, W. M., and Crawford, M. E., *Convective Heat and Mass Transfer*, (2d ed.), McGraw-Hill, New York, 1980.
- 17 McAdams, W. H., *Heat Transmission*, (3d ed.), McGraw-Hill, New York, 1954, p. 258.
- 18 Gebhart, B., *Heat Transfer*, (2d ed.), McGraw-Hill, New York, 1975.
- 19 Cheesewright, R., "Turbulent Natural Convection From a Vertical Plane Surface," *ASME JOURNAL OF HEAT TRANSFER*, Vol. 90, 1968, pp. 1-8.
- 20 Chokouhmand, H., "Convection Naturelle Dans L'eau Le Long D'Une Plaque Verticale Chauffee a Densite de Flux Constante," Ph.D. thesis, A L'Universite Et Marie Curie, Paris, Rapport CEA-R-4867, 1976.
- 21 Warner, C. Y., and Arpac, V. S., "An Experimental Investigation of Turbulent Natural Convection in Air at Low Pressure Along a Vertical Heated Flat Plate," *IJHT*, Vol. 11, 1968, pp. 397-406.
- 22 Vliet, G. C., and Liu, C. K., "An Experimental Study of Turbulent Natural Convection Boundary Layers," *ASME JOURNAL OF HEAT TRANSFER*, Vol. 91, 1969, pp. 517-531.
- 23 Fujii, T., "Experimental Studies of Free Convection Heat Transfer," *Bulletin JSME*, Vol. 2, No. 8, 1959, pp. 555-558.
- 24 George, W. K., and Capp, S. P., "A Theory for Natural Convection Turbulent Boundary Layers Next to Heated Vertical Surfaces," *IJHT*, Vol. 22, 1979, pp. 813-826.

---

# STUDIES IN HEAT TRANSFER

A Festschrift for E. R. G. Eckert

---

Edited by

J. P. Hartnett  
*University of Illinois at Chicago Circle*

T. F. Irvine, Jr.  
*State University of New York at Stony Brook*

E. Pfender  
*University of Minnesota*

E. M. Sparrow  
*University of Minnesota*

Engr

● HEMISPHERE PUBLISHING CORPORATION  
Washington New York London

McGRAW-HILL BOOK COMPANY  
New York St. Louis San Francisco Auckland Bogota  
Düsseldorf Johannesburg London Madrid Mexico  
Montreal New Delhi Panama Paris São Paulo  
Singapore Sydney Tokyo Toronto

number was large at small values of  $M$ , indicating less stimulation of turbulent mixing at small injection rates.

## SUMMARY

The correlation formula derived in the analysis above,

$$\eta(z; q) = Nw(z; q)e^{(A/2)w(z)} e_2 \left[ \frac{\pi}{2}(1-z); q \right]$$

appears to represent the data given for the distribution of film cooling effectiveness on an insulated plane surface downstream of a point of lateral injection. Since it was the solution appropriate to small blowing intensities, one might expect it to be unsatisfactory for large values of  $M$ , but since the Peclet number is then small, the maximum value of  $\eta$  is also relatively small and the formula remains adequate.

Of the four empirical constants  $N$ ,  $q$ ,  $A$ , and  $k$  appearing in the derived expression for  $\eta$  when  $w(z)$  is taken to be proportional to  $e^{-kz} \sin \pi z$ , two are found to be independent of  $x/D$  while  $N$  and  $q$  are related to  $x/D$  by simple power laws. The  $q$  versus  $x/D$  relationship is, of course, the function that allows the one-dimensional Mathieu functions, with parametric  $q$ , to represent the two-dimensional effectiveness distribution that is required.

Although three values of  $M$  as well as two lateral injection angles are mentioned in Table 3, the matching of theory with data on Fig. 2 is given only for  $M = 0.5$  and  $\alpha = 35^\circ$ . The other five comparisons will be published when they are ready, together with calculations of local average values of  $\eta(z)$  for the six cases reported in [6].

## REFERENCES

1. M. Tribus and J. Klein, Forced Convection from Nonisothermal Surfaces, Heat Transfer Symp., Univ. of Michigan, p. 211, 1953.
2. J. W. Ramsey, R. J. Goldstein, and E. R. G. Eckert, A Model for Analysis of the Temperature Distribution with Injection of a Heated Jet into an Isothermal Flow, in *Heat Transfer 1970*, Elsevier, Amsterdam, 1970.
3. M. Y. Jabbari and R. J. Goldstein, Adiabatic Wall Temperature and Heat Transfer Downstream of Injection through Two Rows of Holes, ASME paper: 77-GT-50, Gas Turbine Conf., Philadelphia, March 27-31, 1977.
4. J. P. Sellers, Jr., Gaseous Film Cooling with Multiple Injection Stations, *AIAA J.*, vol. 1, pp. 2154-2156, 1963.
5. E. R. G. Eckert, Film Cooling with Injection through Holes, AGARD, Florence, Sept. 1970.
6. R. J. Goldstein, E. R. G. Eckert, V. L. Erickson, and J. W. Ramsey, Film Cooling Following Injection through Inclined Circular Holes, *Int. J. Technol.*, pp. 145-154, 1970; also Univ. of Minnesota Rept. HTL-91, 1969.
7. F. L. Ince and F. Ince, *Tables of Functions*, p. 293, Dover, New York, 1945.
8. F. L. Ince, Tables of the Elliptic-Cylinder Functions, *Proc. R. Soc. Edinburgh*, vol. 52, pp. 355-391, 1931-1932.

MAXIMILIAN GREINER

EDGAR R. F. WINTER

## Analogy Defects of Mass, Heat, and Momentum Transfer in Evaporation Boundary-Layer Flow

### NOMENCLATURE

$C$	normalized driving force $[= (x_{1w} - x_{1\infty})/(1 - x_{1\infty})]$
$c_f$	local skin friction coefficient
$c_p$	specific heat at constant pressure
$D$	binary diffusion coefficient
$F$	parameter defined by Eq. (19)
$f(\eta)$	modified stream function, Eq. (15)
$M$	mass transfer parameter, Eq. (20)
$\dot{m}_1$	mass transfer rate
$N$	parameter defined by Eq. (21)
$Nu_x$	local Nusselt number
$p$	total pressure
$p_{1,2}$	partial pressure of components
$Pr$	Prandtl number
$\dot{q}$	heat transfer rate
$\dot{q}_H$	heating rate
$R$	gas constant
$Re_x$	local Reynolds number
$Sc$	Schmidt number
$Sh_x$	local Sherwood number
$T$	temperature, K
$u$	velocity component parallel to plate
$v$	velocity component normal to plate
$W_1$	dimensionless mass fraction, Eq. (17)
$w$	mass fraction

$x$	mole fraction
$x$	coordinate distance along plate
$y$	coordinate distance normal to plate
$\alpha$	local heat transfer coefficient, Eq. (7)
$\beta$	local mass transfer coefficient, Eq. (8)
$\eta$	similarity coordinate, Eq. (14)
$\theta$	temperature, °C
$\theta$	dimensionless temperature, Eq. (17)
$\lambda$	thermal conductivity
$\mu$	dynamic viscosity
$\nu$	kinematic viscosity
$\rho$	mass density
$\tau$	dew-point temperature
$\tau_w$	shear stress at wall
$\varphi$	normalized fluid property, Eq. (18)
$\psi$	stream function Eq. (16)
$\omega$	normalized velocity, Eq. (17)

### Subscripts

Fluid properties without any subscript are related to the mixture.

0	vanishing mass transfer
1	evaporating substance
2	free-stream gas (air)
$m$	fluid composition at $x_{1,m} = 0.5 (x_{1,w} + x_{1,\infty})$ and $T_m = 0.5 (T_w + T_\infty)$
$w$	liquid surface ( $y = 0$ )
$\infty$	free stream ( $y \rightarrow \infty$ )
'	differentiation with respect to $\eta$

### INTRODUCTION

The analogy between heat and mass transfer processes provides a useful tool for the solution of mass transfer problems. The basis for this engineering technique is the similarity relations first derived by Schmidt [1] and Nusselt [2], which allow application of heat transfer solutions to mass transfer problems and vice versa. Ackermann [3], however, demonstrated that the application of analogy yields correct results only if the boundary conditions are similar and the mechanisms of heat, mass, and momentum transfer are uncoupled. In the converse case, deviations from the analogy relations arise, which have been estimated by Ackermann (film theory) [3], Eckert and Lieblein (Kármán-Pohlhausen integral technique) [4], and Schlünder (penetration theory) [5].

The objective of this contribution is to verify analytically and experimentally the applicability of the approximate solutions to heat and mass transfer problems in evaporation processes.

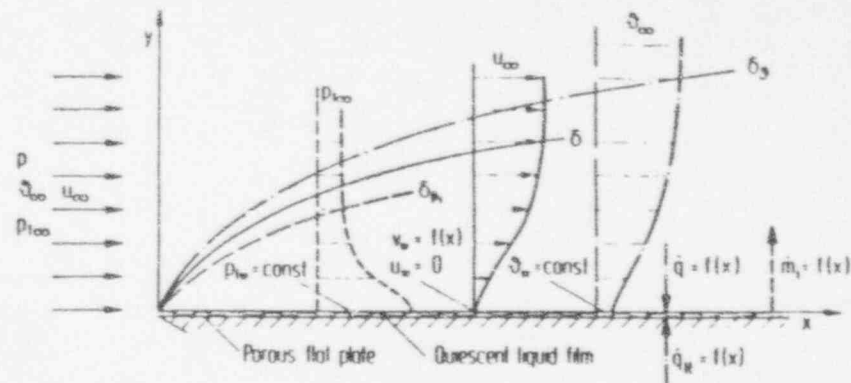


Figure 1 Physical model of boundary-layer flow with evaporation.

### PHYSICAL MODEL

The problem under investigation is illustrated in Fig. 1. A heated flat porous plate is covered by a quiescent thin liquid film (index 1) of constant surface temperature. The plate is subjected to parallel flow at zero incidence of a gas (index 2), which may contain vapor of the evaporating liquid. The pertinent flow, wall, and boundary-layer parameters for momentum, heat, and mass transfer are given in the figure.

### GOAL OF THE INVESTIGATION

If the following conditions are met

$$p_{1w} - p_{1\infty} \rightarrow 0 \quad p_{1w} \rightarrow 0 \quad T_m - T_w \rightarrow 0 \quad (1)$$

then with uncoupled transfer mechanisms the well-known Pohlhausen and Blasius relations allow the computation of heat and mass transfer and friction coefficients under laminar flow conditions with the equations

$$Nu_{x,0} = \frac{\alpha_0 x}{\lambda} = 0.332 Re_x^{1/2} Pr^{1/3} \quad (2)$$

$$Sh_{x,0} = \frac{\beta_0 x}{D} = 0.332 Re_x^{1/2} Sc^{1/3} \quad (3)$$

$$c_{f,0} = \frac{0.664}{Re_x^{1/2}} \quad (4)$$

The corresponding equations for turbulent flow are

$$Nu_{x,0} = \frac{\alpha_0 x}{\lambda} = 0.0295 Re_x^{0.8} Pr^{0.6} \quad (5)$$



$$\text{Sh}_{1,0} \frac{\beta_0 x}{D} = 0.0295 \text{Re}_x^{0.8} \text{Sc}^{0.4} \quad (6)$$

If the conditions under Eqs. (1) are not satisfied, then the above analogy relations, Eqs. (2)-(6), are no longer valid. These so-called analogy defects are the specific object of this investigation.

## ANALYSIS

The analysis is restricted to laminary boundary-layer flow. To determine the heat and mass transfer and friction coefficients  $\alpha$ ,  $\beta$ , and  $c_f$  defined by

$$\dot{q} = \alpha (T_w - T_\infty) = -\lambda \left( \frac{\partial T}{\partial y} \right)_w \quad (7)$$

$$\dot{m}_1 = \frac{\beta}{R_1 T_m} (p_{1w} - p_{1\infty}) = -\frac{D_w}{R_1 T_w} \frac{p}{p - p_{1w}} \left( \frac{\partial p_1}{\partial y} \right)_w \quad (8)$$

$$\tau_w = c_f \frac{1}{2} \rho_\infty u_\infty^2 = \mu_w \left( \frac{\partial u}{\partial y} \right)_w \quad (9)$$

the temperature, partial pressure, and velocity gradients at the wall must be computed by numerical solution of the following set of boundary-layer equations, which take into account temperature- and concentration-dependent properties:

Continuity:

$$\frac{\partial(\rho u)}{\partial x} + \frac{\partial(\rho v)}{\partial y} = 0 \quad (10)$$

Momentum:

$$\rho u \frac{\partial u}{\partial x} + \rho v \frac{\partial u}{\partial y} = \frac{\partial}{\partial y} \left( \mu \frac{\partial u}{\partial y} \right) \quad (11)$$

Diffusion:

$$\rho u \frac{\partial w_1}{\partial x} + \rho v \frac{\partial w_1}{\partial y} = \frac{\partial}{\partial y} \left( \rho D \frac{\partial w_1}{\partial y} \right) \quad (12)$$

Energy:

$$\rho u c_p \frac{\partial T}{\partial x} + \rho v c_p \frac{\partial T}{\partial y} = \frac{\partial}{\partial y} \left( \lambda \frac{\partial T}{\partial y} \right) + \rho D (c_{p1} - c_{p2}) \frac{\partial T}{\partial y} \frac{\partial w_1}{\partial y} \quad (13)$$

The thermal-diffusion and diffusion-thermal effects as well as the effect of aerodynamic heating have been neglected in Eqs. (12) and (13). Equations (11)-(13) are reduced to a set of ordinary simultaneous differential equations by a similarity transformation, introducing the variable

$$\eta = \frac{1}{2} \sqrt{\frac{u_\infty}{\nu_\infty x}} \int_0^y \frac{\rho}{\rho_\infty} dy' \quad (14)$$

and the dimensionless stream function  $f(\eta)$ , given by

$$f(\eta) = \frac{\psi}{\sqrt{\nu_\infty x u_\infty}} \quad (15)$$

The continuity equation is satisfied by the stream function  $\psi$  in terms of

$$\rho u = \rho_\infty \frac{\partial \psi}{\partial y} \quad \rho v = -\rho_\infty \frac{\partial \psi}{\partial x} \quad (16)$$

Normalizing the velocity, the mass fraction, and the temperature

$$\omega = \frac{u}{u_\infty} \quad W_1 = \frac{w_1 - w_{1w}}{w_{1\infty} - w_{1w}} \quad \theta = \frac{T - T_w}{T_\infty - T_w} \quad (17)$$

and the physical properties of the mixture

$$\varphi_\rho = \frac{\rho}{\rho_\infty} \quad \varphi_\mu = \frac{\mu}{\mu_\infty} \quad \varphi_\lambda = \frac{\lambda}{\lambda_\infty} \quad (18)$$

$$\varphi_D = \frac{D}{D_\infty} \quad \varphi_c = \frac{c_p}{c_{p\infty}} \quad \varphi_{c12} = \frac{c_{p1} - c_{p2}}{c_{p\infty}}$$

and employing the dimensionless abbreviations

$$F = 2 \int_0^\eta \omega d\eta \quad (19)$$

$$M = 2 \frac{\rho_w u_w}{\rho_\infty u_\infty} \sqrt{\text{Re}_{x,w}} \quad (20)$$

$$N = \frac{\varphi_\rho \varphi_\mu \varphi_D \varphi_{c12}}{\varphi_c \text{Sc}_\infty} (w_{1\infty} - w_{1w}) \frac{\partial w_1}{\partial \eta} \quad (21)$$

the following system of ordinary differential equations results ultimately from the similarity transformation:

$$[\varphi_\rho \varphi_\mu f'']' + f'' (F - M) = 0 \quad (22)$$

$$[\varphi_\rho \varphi_D W_1']' + W_1' \text{Sc}_\infty (F - M) = 0 \quad (23)$$

$$[\varphi_\rho \varphi_\lambda \theta']' + \theta' \text{Pr}_\infty \varphi_c (F - M + N) = 0 \quad (24)$$

In these equations the primes denote differentiation with respect to the similarity variable  $\eta$ .

The transformed boundary conditions are

$$\begin{aligned} \eta = 0: & \quad f' = 0 \quad W_1 = 0 \quad \theta = 0 \\ \eta \rightarrow \infty: & \quad f' = 2 \quad W_1 = 1 \quad \theta = 1 \end{aligned} \quad (25)$$

Formal integration of Eqs. (22)–(24) using the boundary conditions results in a set of integral equations for the determination of the velocity, concentration, and temperature field:

$$\omega = \frac{\int_0^{\eta} (1/\varphi_{\rho}\varphi_{\mu}) \exp \left[ -\int_0^{\eta} (1/\varphi_{\rho}\varphi_{\mu}) (F - M) d\eta \right] d\eta}{\int_0^{\infty} (1/\varphi_{\rho}\varphi_{\mu}) \exp \left[ -\int_0^{\eta} (1/\varphi_{\rho}\varphi_{\mu}) (F - M) d\eta \right] d\eta} \quad (26)$$

$$W_1 = \frac{\int_0^{\eta} (1/\varphi_{\rho}\varphi_{\rho}\varphi_D) \exp \left[ -\int_0^{\eta} (Sc_{\infty}/\varphi_{\rho}\varphi_{\rho}\varphi_D) (F - M) d\eta \right] d\eta}{\int_0^{\infty} (1/\varphi_{\rho}\varphi_{\rho}\varphi_D) \exp \left[ -\int_0^{\eta} (Sc_{\infty}/\varphi_{\rho}\varphi_{\rho}\varphi_D) (F - M) d\eta \right] d\eta} \quad (27)$$

$$\theta = \frac{\int_0^{\eta} (1/\varphi_{\rho}\varphi_{\lambda}) \exp \left[ -\int_0^{\eta} (Pr_{\infty}\varphi_c/\varphi_{\rho}\varphi_{\lambda}) (F - M + N) d\eta \right] d\eta}{\int_0^{\infty} (1/\varphi_{\rho}\varphi_{\lambda}) \exp \left[ -\int_0^{\eta} (Pr_{\infty}\varphi_c/\varphi_{\rho}\varphi_{\lambda}) (F - M + N) d\eta \right] d\eta} \quad (28)$$

This system of integral equations can be solved according to an iteration procedure used by Piercy and Preston [6] and extended by Schuh [7] to include mass transfer.

The thermal and transport properties of the inert gas (air) and the vapor of the evaporating substances are taken from data collections and curve-fitted, so that the temperature- and concentration-dependent physical properties of the mixtures can be computed by customary mixing rules [8].

## ANALYTICAL RESULTS

Computations were performed for the evaporation of water, methanol, toluene, and carbon tetrachloride into air. These four substances cover a range of molecular weights commonly encountered in chemical engineering processes.

The results of the numerical computations for the evaporation of these four liquids are displayed in Figs. 2–4. The transfer coefficients  $\beta$ ,  $\alpha$ , and  $c_f$  are normalized with  $\beta_0$ ,  $\alpha_0$ , and  $c_{f0}$  calculated from Eqs. (2) and (3), the fluid properties being taken at  $x_{1\infty}$  and  $T_{\infty}$ , and Eq. (4), using  $x_{1\infty}$  and  $T_{\infty}$  as the reference state. The transfer coefficients thus normalized are plotted as a function of the normalized driving force of the evaporation process,  $C = (x_{1w} - x_{1\infty})/(1 - x_{1\infty})$ . Deviations from unity represent the analogy defects.

The results, shown in Fig. 2, were obtained for zero mole fraction of the vapor in the free stream,  $x_{1\infty} = 0$ , and a free-stream temperature  $\vartheta_{\infty}$  of 100°C. In chemical engineering processes such as drying and humidification, a wide range of  $\vartheta_{\infty}$  and  $x_{1\infty}$  may occur. Therefore the influence of these parameters on the transfer coefficients was studied. The results, depicted in Figs. 3 and 4 for the systems

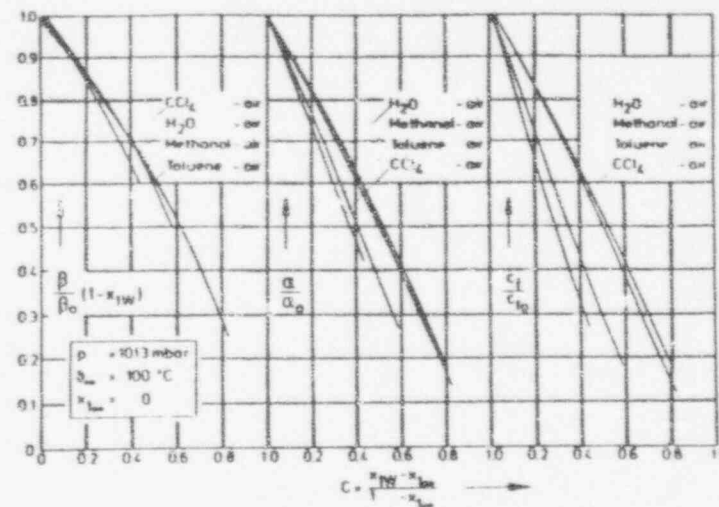


Figure 2 Normalized transfer coefficients as a function of the dimensionless driving force for the evaporation of several liquids with different molecular weights.

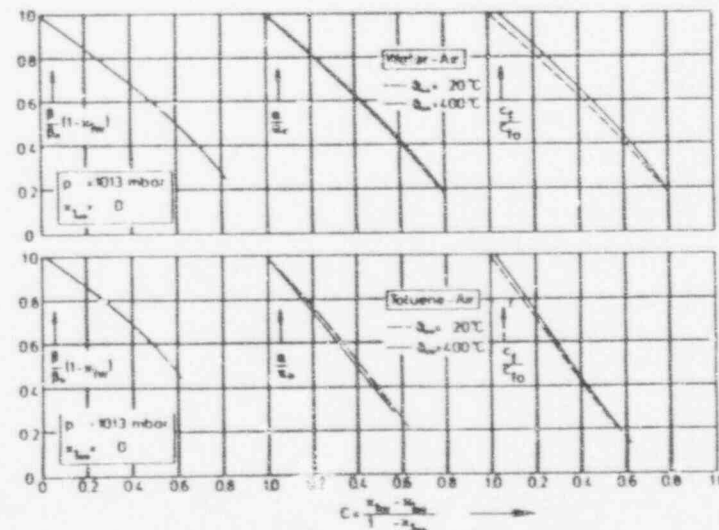


Figure 3 Normalized transfer coefficients as a function of the dimensionless driving force at different free-stream temperatures.

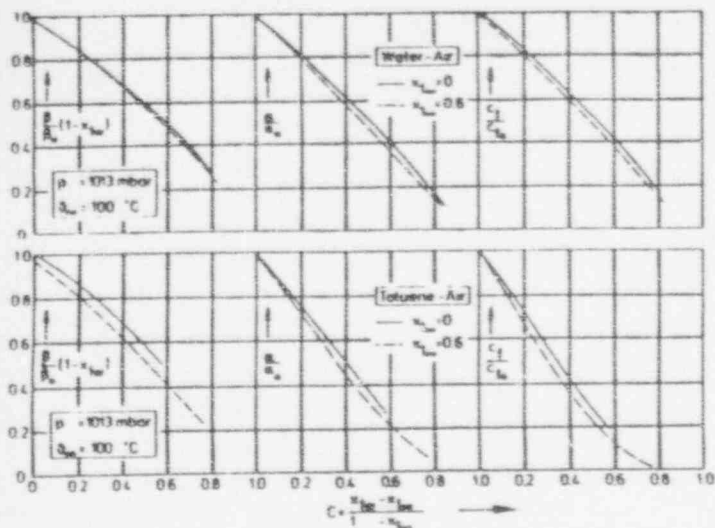


Figure 4 Normalized transfer coefficients as a function of the dimensionless driving force at different vapor contents of the free stream.

water-air and toluene-air for  $\delta_w = 20$  and  $400^\circ\text{C}$  and  $x_{1m} = 0$  and  $0.6$ , show that the behavior of all the normalized transfer coefficients as a function of  $C$  is only slightly affected by these free-stream parameters.

## APPROXIMATE SOLUTIONS

In Fig. 5, results obtained with approximate theories are compared with the exact numerical predictions of boundary-layer theory for the evaporation into air of several substances with different molecular weights.

Again, the coefficients  $\beta_0$  and  $\alpha_0$  are computed by using the Pohlhausen relations, Eqs. (2) and (3), the fluid properties now being taken at  $x_{1m}$  and  $T_m$ . Curves 1 represent the approximate theory of Ackermann [3], which was confirmed by Colburn and Drew [9]. The results of this theory, which is commonly called film theory [10], agree best with the exact numerical boundary-layer solutions for systems with almost constant density. The same holds true for the theory introduced by Eckert and Lieblein [4], curves 2, and the penetration theory [5], curves 5. Ackermann [3] extended the film theory by a factor  $A$ . This factor takes into account the influence of the "diffusing masses" but results in an overcorrection, curves 3. The deviation can be eliminated by a simple variation of Ackermann's original factor  $A$ , leading to

$$\frac{\beta}{\beta_0} (1 - x_{1w}) = A \frac{1 - C}{C} \ln \frac{1}{1 - C} \quad (29)$$

$$\frac{\alpha}{\alpha_0} = A \frac{S \ln [1/(1 - C)]}{c_{x_1} (S \ln [1/(1 - C)] - 1)} \quad (30)$$

$$S = \left( \frac{Pr_m}{Sc_m} \right)^{1/3} \frac{p}{R_1 T_m} \frac{c_{p1m}}{\rho_m c_{pm}}$$

$$A = \frac{1}{[1 + 0.2 (D_m p / \mu_m R_1 T_m) \ln (1/(1 - C))]}$$

The results obtained with these improved relations, curves 4, are in excellent agreement with the numerical solutions.

## EXPERIMENTS

For the investigation of the analogy defects in turbulent boundary-layer flow, an experimental facility including laminar investigation capabilities has been built. The core of this experimental setup is the test plate depicted in Fig. 6. This flat plate is installed horizontally in the test section of an open-loop laminar wind tunnel, in which the free-stream velocity and temperature can be adjusted continuously from 0 to 20 m/s and from ambient temperature to  $150^\circ\text{C}$ . The degree of turbulence in the free stream is less than 0.1%.

The evaporation area of the flat plate consists of six sections composed of porous, hydraulically smooth sintered plate segments, which are fabricated from sherrit nickel powder. Their mean surface roughness is  $2 \mu\text{m}$  (CLA), measured with a  $3\text{-}\mu\text{m}$  stylus. The excellent wettability features of the sintered plates serve for the generation of a very thin and continuous quiescent liquid film.

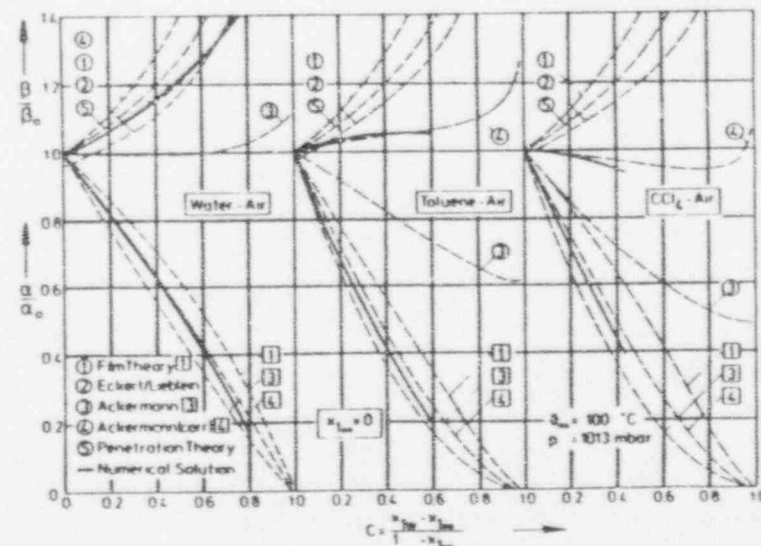


Figure 5 Comparison of the results of approximate theories with the numerical solutions of the boundary-layer equations.

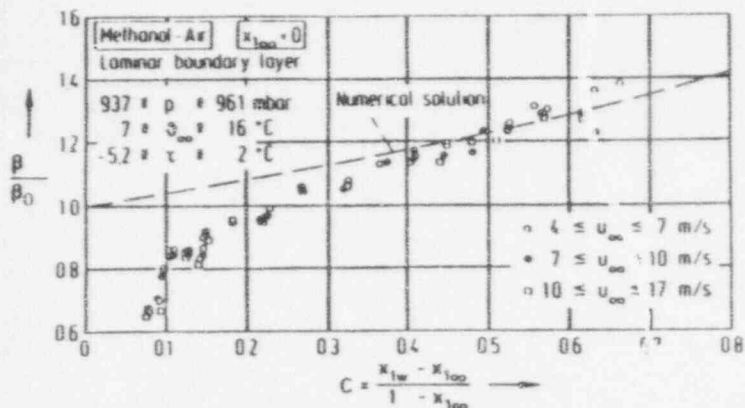


Figure 7 Mass transfer as a function of the driving force of evaporation for laminar boundary-layer flow. Evaporation was into moist air.

of approximately  $-20^\circ\text{C}$  before entering the wind tunnel are displayed in Fig. 8. Since these data, obtained for evaporation in laminar boundary layers, are in good agreement with the corresponding theoretical predictions, the experimental data measured under turbulent flow conditions (Fig. 9) should also be very reliable. The results are restricted to mass transfer in constant-density boundary-layer flow, because the molecular weights of methanol and air are nearly equal and the temperature differences across the boundary layer have been small. The experimental data are reproduced quite well by the film theory. For the case of mass transfer in boundary layers with large density gradients, however, the accuracy of the film theory is still an open question.

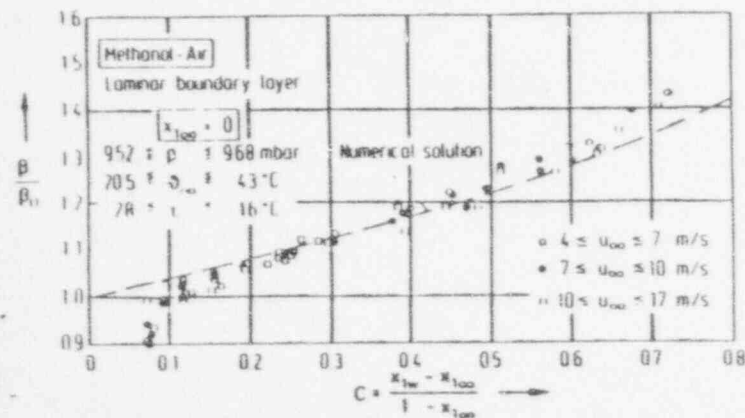


Figure 8 Mass transfer as a function of the driving force of evaporation for laminar boundary-layer flow. Evaporation was into dry air.

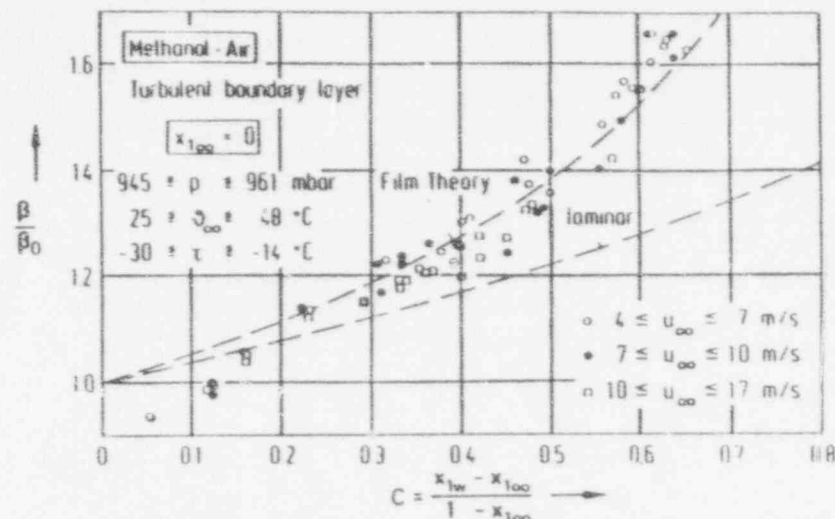


Figure 9 Mass transfer as a function of the driving force of evaporation for turbulent boundary-layer flow. Evaporation was into dry air.

## REFERENCES

1. E. Schmidt, Verdunstung und Wärmeübergang, *Gesund. Ing.*, vol. 52, pp. 525-529, 1929; reprinted in *Int. J. Heat Mass Transfer*, vol. 19, pp. 3-8, 1976.
2. W. Nusselt, Wärmeübergang, Diffusion und Verdunstung, *Z. Angew. Math. Mech.*, vol. 10, pp. 105-121, 1930.
3. G. Ackermann, Wärmeübergang und molekulare Stoffübertragung im gleichen Feld bei grossen Temperatur- und Partialdruckdifferenzen, *VDI Forschungsh.*, vol. 382, pp. 1-16, 1937.
4. E. Eckert and V. Lieblein, Berechnung des Stoffübergangs an einer ebenen, längs angeströmten Oberfläche bei grossem Teildruckgefälle, *Forsch. Ingenieurwes.*, vol. 16, pp. 33-42, 1949.
5. E. U. Schlünder, Stoffübergang bei Verdunstungs- und Absorptionsvorgängen an einer ebenen, überströmten Platte, *Chem. Ing. Tech.*, vol. 36, pp. 484-492, 1964.
6. N. A. V. Pierce and E. H. Preston, A Simple Solution of the Flat Plate Problem of Skin Friction and Heat Transfer, *Philos. Mag.*, vol. 21, pp. 995-1005, 1936.
7. H. Schuh, The Solution of the Laminar-Boundary-Layer Equation for the Flat Plate for Velocity and Temperature Fields for Variable Physical Properties and for the Diffusion Field at High Concentration, NACA Tech. Memo 1275, pp. 1-19, 1950; translated from *ZWB Forsch. Ber.*, no. 1980, 1944.
8. *VDI-Wärmeatlas*, VDI-Verlag, Düsseldorf, 1974.
9. A. P. Colburn and T. B. Drew, The Condensation of Mixed Vapors, *Trans. AIChE*, vol. 33, pp. 197-212, 1937.
10. R. B. Bird, W. E. Stewart, and E. N. Lightfoot, *Transport Phenomena*, Wiley, New York, 1960.
11. M. Greiner, Analogieeffekte bei der Verdunstung an der längs angeströmten ebenen Platte in laminarer und turbulenter Strömungsgrenzschicht, doctoral thesis, Technische Universität München, 1978.



# Mixed Convection Heat Transfer – 1987

*presented at*

THE WINTER ANNUAL MEETING OF  
THE AMERICAN SOCIETY OF MECHANICAL ENGINEERS  
BOSTON, MASSACHUSETTS  
DECEMBER 13-18, 1987

*sponsored by*

THE HEAT TRANSFER DIVISION, ASME

*edited by*

V. PRASAD  
COLUMBIA UNIVERSITY

I. CATTON  
UNIVERSITY OF CALIFORNIA, LOS ANGELES

P. CHENG  
UNIVERSITY OF HAWAII

THE AMERICAN SOCIETY OF MECHANICAL ENGINEERS  
United Engineering Center      345 East 47th Street      New York, N.Y. 10017

**ENGR**

## COMPARISON BETWEEN THEORY AND EXPERIMENT FOR TURBULENT FLOW OF AIR IN A VERTICAL TUBE WITH INTERACTION BETWEEN FREE AND FORCED CONVECTION

M. A. Cotton and J. D. Jackson  
Nuclear Engineering Laboratories  
University of Manchester  
Manchester, United Kingdom

### ABSTRACT

Heat transfer to turbulent flow in a vertical tube under conditions of mixed convection can exhibit marked departures from the behaviour found in forced convection: in ascending flow heat transfer may be either impaired with respect to forced convection levels (at moderate heat loadings) or enhanced (at high heat loadings), whereas, in descending flow, heat transfer is enhanced at all heat loadings. The present contribution reviews earlier comparisons between theoretical formulations and experimental data for turbulent mixed convection and reports numerical results obtained using a low-Reynolds-number  $k-\epsilon$  turbulence model. Direct comparison with experimental data for turbulent mixed convection heat transfer to air is made and the general picture to emerge is one of satisfactory computation of measured bulk heat transfer. In addition, approximate comparisons are made with data obtained over wide ranges of Reynolds and Grashof numbers using a buoyancy parameter which combines these groups.

### NOMENCLATURE

$A^+$	van Driest constant
$B$	buoyancy parameter
$C_p$	specific heat capacity at constant pressure
$C_{\epsilon 1}, C_{\epsilon 2}$	constants in production, sink terms of $\epsilon$ -equation
$C_\mu$	constant in constitutive equation of $k-\epsilon$ model
$D$	tube internal diameter
$D_{\text{add}}$	'additional' dissipation term in $k$ -equation
$f_2^t$	function in sink term of $\epsilon$ -equation
$f_\mu$	function in constitutive equation of $k-\epsilon$ model
$g$	magnitude of acceleration due to gravity
$g_x$	component of acceleration due to gravity in $x$ -direction
$Gr$	Grashof number based on wall heat flux, $g g_w D^4 / \lambda \nu^2$
$k$	turbulent kinetic energy
$l_m$	mixing length

$Nu$	Nusselt number, $qD/\lambda (T_w - T_b)$
$Nu_D$	Nusselt number for forced convection
$p$	pressure
$P$	rate of production of $k$ by mean flow shear
$Pr$	Prandtl number, $c_p \mu / \lambda$
$q$	wall heat flux
$r, z$	radial, axial cylindrical polar coordinates
$R$	tube internal radius
$Re$	Reynolds number, $\rho W_b D / \mu$
$Re_t$	turbulent Reynolds number
$T$	temperature (time-averaged)
$T_0$	reference temperature (upstream of the start of heating)
$v, w$	velocity components in $r, z$ -directions (fluctuating)
$\overline{vw}$	$\overline{vw} / (\tau_w / \rho)$
$V, W$	velocity components in $r, z$ -directions (time-averaged)
$y$	normal distance from wall, $R-r$
$y^+$	$y \sqrt{\tau_w / \rho} / \nu$

### Greek letters

$\beta$	coefficient of volume expansion
$\epsilon$	rate of dissipation of $k$
$\hat{\epsilon}$	modified dissipation variable
$\kappa$	von Karman constant
$\lambda$	thermal conductivity
$\mu$	dynamic viscosity
$\nu$	kinematic viscosity, $\mu/\rho$
$\rho$	density corresponding to temperature $T_0$
$\rho'$	fluctuating temperature-dependent density
$\sigma_t$	turbulent Prandtl number
$\sigma_k, \sigma_\epsilon$	turbulent Prandtl number for diffusion of $k, \epsilon$
$\tau$	shear stress

### Subscripts

$b$	bulk
$t$	turbulent
$w$	wall

### Superscripts

$-$	time-averaged
$'$	fluctuating

## INTRODUCTION

In situations where the mechanisms of forced and free convection operate simultaneously the heat transfer mode is termed 'mixed' or 'combined' convection. Turbulent flow in vertical tubes under this heat transfer regime reveals complex thermo-fluid development which produces bulk effects markedly different from those that would result if the influence of free convection were combined with that of forced convection in a simple 'additive' manner. The mixed convection regime is thus of considerable intrinsic physical interest, and, because of the possible impact that significantly modified levels of heat transfer may have upon the performance of thermal engineering systems, the problem is also of practical importance.

Investigators have obtained experimental results for turbulent mixed convection heat transfer in a number of fluids under a wide range of conditions (reviewed by Jackson and Hall [1]). The behaviour observed experimentally is that, for heated ascending flow, heat transfer (quantified in terms of Nusselt number) may be either impaired with respect to forced convection (at moderate heat loadings) or enhanced (at high heat loadings); in heated descending flow heat transfer is always enhanced by buoyancy effects. The difference between these trends and those found in laminar mixed convection should be noted: the general results found for the laminar case (in which diffusivities are purely molecular properties) are that heat transfer is enhanced in heated upflow and impaired in heated downflow. In the present work comparison is made with a body of experimental data for turbulent mixed convection heat transfer to gases: Carr, Connor and Buhr [2], Byrne and Ejiogu [3] and Steiner [4] have made measurements for ascending air flows, while Axcell and Hall [5] obtained data for a descending air flow and Easby [6] examined a descending nitrogen flow.

Jackson and Hall [1] proposed a phenomenological model of heat transfer in the turbulent mixed convection regime based upon consideration of the modified turbulent shear stress distributions which occur in the near-wall region in response to buoyancy forces. A slightly revised form of the earlier model based upon Grashof number appropriate to the uniform wall heat flux thermal boundary condition is employed in the present work. The analysis leads to a 'buoyancy parameter',  $B$ , by which the importance of mixed convection effects may be characterized:

$$B = \frac{Gr}{Re^{3.425} Pr^{0.8}} \quad (1)$$

Further analysis, in which recourse to empirical heat transfer and flow resistance correlations is made, leads to an equation for the ratio of Nusselt number for mixed convection to that for forced convection as a function of the buoyancy parameter:

$$\frac{Nu}{Nu_0} = \left[ 1 \pm \frac{B \times 10^4}{(Nu/Nu_0)^2} \right]^{0.46} \quad (2)$$

where the + sign applies to descending flow and the - sign to ascending flow.

The buoyancy parameter (equation (1)) and semi-empirical equation (equation (2)) are derived upon the assumption of a fully-developed condition, however, in ascending mixed convection flows, very long development lengths (of the order of 100 tube diameters in some cases) are found to occur both experimentally

and in the numerical study discussed below. This limits the usefulness of the semi-empirical equation in ascending flow to providing a guide to the magnitude of impairment for specified conditions; in descending flow, by contrast, development lengths are short and the equation correlates data well. It is nonetheless evident from the following comparisons of data and the  $k-\epsilon$  turbulence model that the buoyancy parameter,  $B$ , is a primary correlating parameter for flow in vertical tubes under conditions of turbulent mixed convection.

## A REVIEW OF THE APPLICATION OF TURBULENCE MODELS TO TURBULENT MIXED CONVECTION IN VERTICAL TUBES

The present numerical results are obtained using a 'low-Reynolds-number' two-equation ( $k-\epsilon$ ) turbulence model which is applicable over the entire flow domain, including the viscosity-affected near-wall region where turbulent Reynolds number,  $Re_t$ , is small. The particular formulation adopted here is that of Launder and Sharma [8], a minor re-optimization of the pioneering model of this kind due to Jones and Launder [9,10]. The selection of model type was guided by consideration of the importance of modifications which occur to the turbulent shear stress distribution in the near-wall region of mixed convection flows, identified by Jackson and Hall [1], and by the experience gained by other workers in applying different forms of turbulence closure to the problem. Earlier results obtained using turbulence models of varying complexity are reviewed below and related to the theoretical assumptions implicit in the models. The turbulence models discussed are of the 'Boussinesq viscosity' or 'turbulent viscosity' type in which Reynolds stress is related to the mean velocity gradient via turbulent viscosity,  $\mu_t$ :

$$-\overline{p'v'w'} = \mu_t \frac{\partial w}{\partial r} \quad (3)$$

### Eddy diffusivity models

The simplest approach to closure of the mean flow equation set relies upon prescription of turbulent viscosity without direct reference to spatial variations of the mean or turbulence fields. Models in which this approach is adopted are known as 'eddy diffusivity' models (note: this terminology introduces some ambiguity and care should be taken to distinguish these models from the wider class of Boussinesq viscosity models of which they form part; a better description might be 'prescribed eddy diffusivity' models).

Reichardt [11] proposed an eddy diffusivity model in which the ratio of turbulent to molecular viscosity is prescribed as a function of the universal distance coordinate,  $y^+$ . Tanaka et al. [12] examined turbulent mixed convection tube flows using a modification of Reichardt's expression in which  $y^+$  was replaced by the integral with respect to  $y$  of  $\sqrt{\tau}/\rho/\nu$  from the wall to position  $y$ . In fact, neither Reichardt's original formulation nor Tanaka's modification correctly reflect turbulence production by shear which is given as the product of local Reynolds stress and velocity gradient:

$$P = -\overline{p'v'w'} \frac{\partial w}{\partial r} \quad (4)$$

Tanaka et al. found that computed wall temperature distributions for a vertical heated tube were opposite to observed behaviour, exhibiting heat transfer

enhancement for ascending flow and impairment for descending flow.

#### Mixing length models

Prandtl's mixing length hypothesis provides the framework for a group of turbulence models in which, by contrast with eddy diffusivity models, local mean velocity gradient is incorporated in a formula for  $\nu_t$ . Mixing length models are significant on their own merits, finding wide application in turbulent flow calculation; they also have an important bearing on more detailed models which include equations for the transport of turbulence quantities. This connection is two-fold: firstly, consideration of turbulent kinetic energy transport reveals that, under the assumption of local equilibrium between production and dissipation of turbulent kinetic energy, the mixing length formulation correctly reflects turbulence production (Townsend [13]). Secondly, transport models rely in part upon mixing length results for the determination of model constants (Launder and Spalding [14]).

In the mixing length formulation it is postulated that  $\nu_t$  appearing in equation (3) may be expressed in terms of a mixing length,  $l_m$ , and mean velocity gradient as follows:

$$\nu_t = \rho l_m^2 \left| \frac{\partial W}{\partial r} \right| \quad (5)$$

Prandtl's original suggestion was that  $l$  should be proportional to distance from the wall. Numerous proposals for alternative prescriptions have been advanced: one such modification of Prandtl's linear model which has found widespread application is due to van Driest [15]. The van Driest approach makes allowance for the effect of a solid boundary upon turbulence by incorporation of an exponential damping term in the expression for mixing length:

$$l_m = \kappa y [1 - \exp(-y^+/A^+)] \quad (6)$$

Palhotra and Hauptmann [16] applied the van Driest model to turbulent mixed convection with the result that computed wall temperature distributions for heated upflow and downflow demonstrated the correct trends, indicating heat transfer impairment for upflow and enhancement for downflow. However, comparison made with the wall temperature data of Jackson and Evans Lutterodt [17] for carbon dioxide at near-critical conditions showed good agreement for downward flow but a marked absence of quantitative agreement for upward flow.

Walklate [18] tested four mixing length models against data for heated upflow of air with uniform wall heat flux obtained by Carr et al. [2]. Carr et al. numbered their tests N10 to N13 in order of increasing Grashof number and, of these, Walklate made comparisons with the lowest and highest Grashof number tests, Runs N10 and N13.

The four models used by Walklate represent various modifications of the van Driest formulation, however a detailed description of the models is not given here since the results indicate that all perform similarly. Comparison made with the heat transfer data of Carr et al. revealed large discrepancies between calculated and measured parameters.

#### One and two-equation transport models

Transport models of turbulence in which recourse is made to the turbulent viscosity concept (but not to the remainder of the mixing length formulation) have been applied to turbulent mixed convection in vertical tubes. These models employ alternative means of determining characteristic length and velocity scales to determine  $\nu_t$ . The models have two distinguishing features: firstly, the characteristic scales are determined by reference to turbulence quantities, as opposed to mean field quantities. Secondly, transport equations are introduced for the relevant quantities and  $\nu_t$  is formed, at least in part in the case of one-equation models, from differentially determined (as opposed to algebraically prescribed) scales. Thus local equilibrium is not assumed in the manner of mixing length models.

Models in which a transport equation for one of the scales (in practice the velocity scale via  $k$ -transport) is employed are termed 'one-equation' models. Axcell and Hall [5] applied a variant of Wolfshtein's [19] one-equation  $k$ - $\epsilon$  model to their data for heated descending flow of air. Anticipating the Launder and Sharma [8] model employed in the current studies, it should be noted that Wolfshtein's model is applicable over the entire flow domain, including the viscosity-affected near-wall region. The model may therefore be classed as a low-Reynolds-number model, in common with the van Driest mixing length model. Axcell and Hall's calculations were qualitatively correct, showing enhancement of heat transfer with respect to forced convection. The computed enhancement was, however, considerably less than that found experimentally.

Higher order models that have been applied with some success to turbulent mixed convection data are 'two-equation' models. These models incorporate transport effects on both the velocity and length scales forming the constitutive equation for  $\nu_t$ . The turbulence quantities most often selected to form the basis of the model are the turbulent kinetic energy,  $k$ , and its rate of dissipation,  $\epsilon$ . Walklate [18], whose mixing length results were discussed above, tested three versions of the  $k$ - $\epsilon$  model against Runs N10 and N13 of Carr et al. [2]. The first model tested consisted of a standard 'high-Reynolds-number' model in which the transport equations for  $k$  and  $\epsilon$  were solved over the region  $y^+ > 30$ , analytical 'wall functions' being employed to bridge the near-wall region and thus provide boundary conditions for the transport equations at  $y^+ = 30$ . The remaining two models were variants of a hybrid partial low-Reynolds-number treatment, in which a damping term was applied to the expression for  $\nu_t$ , following Jones and Launder [13,14], but the form of the  $k$  and  $\epsilon$  equations was unaltered from the high-Reynolds-number form (although  $k$  transport was solved over the entire flow).

Walklate found that, as a group, the  $k$ - $\epsilon$  models performed better than the mixing length models in computing turbulent mixed convection. Heat transfer computed using the partial low-Reynolds-number models showed good agreement with the data, however poorer agreement was evident when the high-Reynolds-number model was applied.

Further encouraging results using a  $k$ - $\epsilon$  model have been obtained by Abdelmeguid and Spalding [20] who combined a high-Reynolds-number model with wall functions. Computed results demonstrated the correct trends in mixed convection heat transfer, i.e. for heated upflow, impairment at low and moderate Grashof number was followed by enhancement at higher values, whereas for downflow enhancement was found for



all values of Grashof number. No comparison with experimental heat transfer data was made by Abdelmequid and Spalding, however their calculations yielded levels of impairment and enhancement lower than those evident in available data.

Two recent numerical studies of turbulent mixed convection in vertical tubes using low-Reynolds-number  $k-\epsilon$  models are particularly relevant to the present work. In the first of these Renz and Bellinghausen [21] used the Jones and Launder model to compute heat transfer to an ascending flow of a refrigerant under the conditions of an experiment by Scheidt [22] carried out near the thermodynamic critical point. The correct qualitative trends of wall temperature development were found, although there were some significant quantitative discrepancies (c.f. Malhotra and Hauptmann's [16] mixing length results for near-critical point data discussed above). It should be noted, however, that the highly variable properties of the near-critical point fluid add a further complication to the problem and make this an especially stringent test of the model. In support of this observation, it is interesting to examine the work of Tanaka et al. [23] who compared a slight variant of the Jones and Launder model against their data for heated upflow of nitrogen and found generally good agreement between measured and calculated Nusselt number.

In attempting to form an overall picture of the relative performance of the turbulence models reviewed above, it is necessary to bear in mind that such a picture is not wholly complete because of sparse comparison with (different) data and the various thermal-hydraulic formulations adopted (Axcell and Hall [5], Tanaka et al. [12], Malhotra and Hauptmann [16] and Tanaka et al. [23] assumed that a fully-developed, or 'quasi-developed' [12], condition prevailed). Nonetheless, the results of previous studies strongly indicate that  $k-\epsilon$  formulations offer an improvement over simpler models in the calculation of turbulent mixed convection. In applying  $k-\epsilon$  models particular attention should be given to the treatment of the near-wall region; Jackson and Hall [1] identified the importance of deviations from 'universal' behaviour in determining mixed convection heat transfer and Walklate [18] found that agreement with experiment was improved by the adoption of a partial low-Reynolds-number treatment.

#### PRESENT ANALYSIS: LOW-REYNOLDS-NUMBER TWO-EQUATION TURBULENCE MODEL

Calculations have been performed using the low-Reynolds-number model of Launder and Sharma [8], details of which are given below. In a physical sense the formulation of the mean equations and the turbulence model possess three characteristics which are important to the accurate computation of turbulent mixed convection heat transfer:

- (i) The formulation is for developing thermal-hydraulic conditions, a feature which is necessary if one aims to resolve the significant development effects occurring over long lengths in ascending turbulent mixed convection.
- (ii) The turbulence model is of the two-equation class, thus transport effects on both the length and velocity scales are permitted and the implicit assumption of local balance between production and dissipation of turbulent kinetic energy is absent from the model (c.f. mixing length models).

- (iii) A further important feature of the turbulence model is that it is of the low-Reynolds-number type: turbulence transport equations are solved over the entire flow domain, thus rendering empirical wall functions and associated assumptions of near-wall universality redundant.

#### Complete formulation of the mean flow and turbulence model (Launder and Sharma) equations

The mean flow equations are written in the 'thin shear' (or 'boundary layer') and Pousineux approximations. Turbulent viscosity,  $\nu_t$ , appearing in the Momentum and Energy Equations is evaluated as a function of turbulent kinetic energy,  $k$ , and the modified dissipation variable,  $\hat{\epsilon}$ , (to which the boundary condition  $\hat{\epsilon} = 0$  at  $y = 0$  applies). The turbulent kinetic energy and dissipation rate are determined from transport equations.

##### Continuity

$$\frac{1}{r} \frac{\partial (rV)}{\partial r} + \frac{\partial W}{\partial z} = 0 \quad (7)$$

##### Momentum

$$\frac{1}{r} \frac{\partial}{\partial r} (\rho r V W) + \frac{\partial}{\partial z} (\rho W^2) = - \frac{dp}{dz} + \frac{1}{r} \frac{\partial}{\partial r} [r (u + \nu_t) \frac{\partial W}{\partial r}] + [1 - B (T - T_0)] \rho g_z \quad (8)$$

where

$$g_z = \begin{cases} -g & \text{for ascending flow} \\ +g & \text{for descending flow} \end{cases}$$

##### Energy

$$\frac{1}{r} \frac{\partial}{\partial r} (\rho r V T) + \frac{\partial}{\partial z} (\rho W T) = \frac{1}{r} \frac{\partial}{\partial r} [r (\frac{u}{Pr} + \frac{\nu_t}{\sigma_t}) \frac{\partial T}{\partial r}] \quad (9)$$

##### Constitutive equation

$$\nu_t = C_\mu \frac{\rho k^2}{\nu \hat{\epsilon}} \quad (10)$$

##### k-transport

$$\frac{1}{r} \frac{\partial}{\partial r} (\rho r V k) + \frac{\partial}{\partial z} (\rho W k) = \nu_t \left( \frac{\partial W}{\partial r} \right)^2 + \frac{1}{r} \frac{\partial}{\partial r} [r (u + \frac{\nu_t}{\sigma_k}) \frac{\partial k}{\partial r}] - \rho (\hat{\epsilon} + D_c) \quad (11)$$

where

$$D_c = \begin{cases} 2 \nu k / y^2 & (y^+ < 2) \\ 2 \nu (\partial k / \partial y)^2 & (y^+ > 2) \end{cases}$$

The special form for  $D_c$  adopted in the region  $y^+ < 2$  is used because of convergence difficulties

experienced when the standard form is retained in this region.

$\hat{e}$  - transport

$$\begin{aligned} \frac{1}{r} \frac{\partial}{\partial r} (\mu r \hat{v}) + \frac{\partial}{\partial z} (\rho k \hat{e}) &= C_{\epsilon 1} \frac{\hat{e}}{T} u_{\tau} \left( \frac{\partial u}{\partial r} \right)^2 \\ &+ \frac{1}{r} \frac{\partial}{\partial r} \left[ r \left( u + \frac{u_{\tau}}{\sigma_{\epsilon}} \right) \frac{\partial \hat{e}}{\partial r} \right] \\ &- C_{\epsilon 2} f_2 \frac{\rho \hat{e}^2}{k} + \frac{2 u u_{\tau}}{r} \left( \frac{\partial u}{\partial r} \right)^2 \end{aligned} \quad (12)$$

Constants and Functions

$$C_{\mu} = 0.09; f_{\mu} = \exp(-3.4/[1 + Re_{\tau}/50]^2); Re_{\tau} = \frac{k^2}{\nu \hat{e}}$$

$$\sigma_k = 1.0; \sigma_{\epsilon} = 1.3; \quad (13)$$

$$C_{\epsilon 1} = 1.44; C_{\epsilon 2} = 1.92; f_2 = 1.0 - 0.3 \exp(-Re_{\tau}^2)$$

Turbulent Prandtl number

$$\sigma_{\epsilon} = 0.9 \quad (14)$$

Numerical solutions of the governing equations are obtained using a finite volume/finite difference scheme following Lechner [24] and the discretized parabolic equations are solved using a 'marching' solution procedure. Full details of the numerical scheme are given in Ref. [7].

## RESULTS AND DISCUSSION

Attention in the present work is focussed upon the modification of heat transfer in the mixed convection regime combined with some consideration of mean velocity profile distortion. A companion paper by the authors [25] makes detailed comparison between measured and computed mean flow and turbulence profiles.

Comparison with experimental data is made at two levels: at the first level direct comparison with data is made in which the experimental conditions are precisely replicated. At the second level experimental conditions are not reproduced exactly, but instead approximate comparisons with data are made by casting both in the form of Nusselt number normalized to the appropriate forced convection value and then plotting  $Nu/Nu_0$  as a function of the buoyancy parameter,  $B$  (equation (1)).

Figure 1 shows such an approximate comparison with data. The trends of heat transfer impairment (with maximum impairment of over 50%) and enhancement discussed above are clearly evident. Present results obtained using the Launder and Sharma low-Reynolds-number  $k-\epsilon$  model are for  $Re = 5000$  and  $Pr = 0.699$ .  $B$  is varied by increasing Grashof number over the range  $4.4 \times 10^5 < Gr < 9.0 \times 10^8$  and Nusselt number is normalized to the computed value for fully-developed forced convection at the given Reynolds and Prandtl numbers. In the main, the points plotted for ascending flow represent Nusselt number at an axial position  $z/D = 103.45$  (the location at which Carr et al [2] made their measurements), although some points in the region of maximum impairment are for higher  $z/D$  (between

$z/D = 106$  and  $z/D = 207$ ) and there is evidence that, even at such high length-to-diameter ratios, a fully-developed condition has not been attained over the range  $2.5 \times 10^{-6} < B < 5 \times 10^{-6}$  (maximum impairment occurs at  $B = 2.75 \times 10^{-6}$ ). In the case of descending flow a fully-developed condition is attained by  $z/D = 30$ . The experimental data shown on Figure 1 were obtained under a wide range of conditions: Carr et al [2] made measurements on air for  $5000 < Re < 5400$  and  $1.06 \times 10^7 < Gr < 2.22 \times 10^7$  at  $z/D = 103.45$ ; the data of Steiner [4] are for air in the ranges  $5000 < Re < 14900$  and  $9.3 \times 10^7 < Gr < 2.17 \times 10^8$  at  $z/D = 60$  and Easby's [6] descending flow data are for nitrogen at  $2100 < Re < 8300$ ,  $1.4 \times 10^5 < Gr < 6.8 \times 10^6$  and  $z/D = 83 - 159$ . In all cases,  $B$  is evaluated at the experimental conditions quoted by the authors (taking  $Pr = 0.7$  in the presentation of Steiner's and Easby's data) and experimentally-determined Nusselt number is normalized with respect to the Dittus-Boelter equation:

$$Nu_0 = 0.023 Re^{0.8} Pr^{0.4} \quad (15)$$

The ascending flow data may be considered as a group since all are for large  $z/D$  and therefore realistic comparison with the present results for  $z/D > 103.45$  may be made. Two points emerge: firstly, agreement between present numerical results and the experimental data is seen to be close and, secondly, weight is given to the statement made in the Introduction that the buoyancy parameter is a primary correlating parameter for  $Nu/Nu_0$  since the data are obtained over wide ranges of Reynolds number and Grashof number. Unfortunately, none of the three sets of experimental data include measurements for fully-developed forced convection heat transfer and an uncertainty in the comparison is consequently introduced by the use of the Dittus-Boelter equation: this uncertainty may be partly quantified by the observation that computed  $Nu_0$  at  $Re = 5000$ ,  $Pr = 0.699$  is 6.3% lower than that yielded by equation (15). It is also worth noting that direct simulation of Runs N10, N12 and N13 of Carr et al yielded discrepancies between computed values of Nusselt number and those deduced from the experimental measurements of 8%, 12% and 11% respectively (computed values being lower).

A plot of the revised form of the Jackson and Hall semi-empirical equation, equation (2), is also shown in Figure 1. Agreement between the equation, the present numerical results and the experimental data is fairly close in general, although the semi-empirical equation would appear to under-predict the degree of maximum impairment by a margin of approximately 20%.

Figure 2 shows a second approximate comparison, in this case made with experimental measurements of heat transfer obtained at low  $z/D$ . Byrne and Ejiogu [3] made measurements on a heated ascending air flow for  $1.6 \times 10^4 < Re < 1.4 \times 10^5$  and  $3.15 \times 10^{10} < Gr < 6.72 \times 10^{11}$  and Axcell and Hall [5] made measurements on the same experimental rig for a heated descending flow over the ranges  $2 \times 10^4 < Re < 1.3 \times 10^5$  and  $1.39 \times 10^{11} < Gr < 5.03 \times 10^{11}$ . Both sets of data were obtained at  $z/D = 5.5$ . Figure 2 shows computed  $Nu/Nu_0$  for ascending flow at  $z/D = 10, 20$  and  $50$  ( $Re = 5000$ ,  $Pr = 0.699$ ) and the fully-developed descending flow curve reproduced from Figure 1. The ascending flow curves demonstrate marked development effects. The distortions apparent in these curves arise in consequence of local recoveries in Nusselt number, similar to those apparent in Figure 3 (see below). A Prandtl number of 0.7 was taken in processing the

experimental data appearing on Figure 2 and measured Nusselt number is again normalized to the Dittus-Boelter equation.

The results of direct simulations of Steiner's [4] experiments on ascending air flows are shown in Figure 3. To the authors' knowledge, Steiner's results represent the only set of data for ascending mixed convection heat transfer for air in which Nusselt number development is measured. Agreement between the computed values and experimental points is acceptably close for all four cases over the full range of axial position. (Note: In Ref. [4] Steiner does not mark values on the  $z/D$  axis but it seems likely from the text of the paper that this extends from  $z/D = 0$  to  $z/D = 60$ ). It is interesting to observe the local recovery in Nusselt number occurring in the calculations and for which there is evidence in Steiner's data.

Figures 4, 5 and 6 show direct comparisons between present calculations and the data of Byrne and Ejiogu [3] for ascending flow and Axcell and Hall [5] and Easby [6] for the descending flow case. The results shown in Figures 4 and 6 would appear to indicate satisfactory computation of the experimental data, although, in examining Easby's data, this remark should be qualified by the observation that the data exhibit large scatter in relation to the relatively low enhancement levels. Comparison with Axcell and Hall's data at generally higher levels of enhancement (Figure 5) reveals by contrast computed Nusselt number enhancement consistently higher than the measured points. The cause of this discrepancy is not presently known with certainty, although, without prejudice, two clear possibilities may be identified: firstly, it may be the case that the turbulence model performs less accurately where turbulent diffusivity is increased; alternatively, experimental inaccuracies may be the primary source of error. A third interesting hypothesis is that descending mixed convection flows may, under certain circumstances, exhibit an elliptic flow structure, thereby rendering inappropriate the present parabolic formulation of the problem. This question is currently under investigation in order that the source of the discrepancy might be identified with greater certainty.

Returning to the ascending flow data of Carr et al [2], Figure 7 shows the velocity profile measurements for Run M13 together with the present computed points. The marked distortion of the profile measured by Carr et al is captured to good accuracy by the model computations. Presentation of the same data in  $W^+ - y^+$  coordinates (Figure 8) serves to indicate the pronounced departure from near-wall 'universality' evident under conditions of turbulent mixed convection. Thus, any assumptions of universality made in order to construct wall functions for use with 'high-Reynolds-number' turbulence models applied to mixed convection are clearly highly questionable.

Figure 9 provides an illustration of the inadequacy of mixing length models for the calculation of turbulent mixed convection flows. The experimental points shown are the velocity profile measurements of Run M10 of Carr et al for which profile inversion was not found. The computed curves are obtained using the Launder and Sharma low-Reynolds-number  $k - \epsilon$  model used throughout this study and a low-Reynolds-number mixing length model obtained as the product of the van Driest damping function and the Nikuradse distribution of mixing length for pipe flow:

$$\frac{i_m}{R} = [1 - \exp(-y^+/A^*)],$$

$$[0.14 - 0.08(1 - \frac{y}{R})^2 - 0.06(1 - \frac{y}{R})^4] \quad (16)$$

The profile is computed accurately by the Launder and Sharma model whereas the mixing length model incorrectly yields an off-centrelines velocity maximum, a finding in confirmation of Walklate's earlier study [18].

In conclusion, the present results and those of other workers reviewed above indicate that the low-Reynolds-number two-equation turbulence model of Launder and Sharma [8] offers significant advantages over simpler models in the calculation of turbulent mixed convection heat transfer to air in vertical tubes. There remains some uncertainty regarding the applicability of the model to descending mixed convection flows at high heat transfer enhancement levels and this question together with application of the model to other fluids (liquid metals and water) form the subjects of continuing investigations.

#### ACKNOWLEDGEMENTS

The authors would like to thank Professor B.E. Launder of the University of Manchester Institute of Science and Technology for his help and advice in the course of the theoretical study reported here and also Miss L. Yu for her assistance in performing computer runs for some of the cases shown.

#### REFERENCES

1. Jackson, J.D. and Hall, W.B. "Influences of buoyancy on heat transfer to fluids in vertical tubes under turbulent flow conditions" in "Turbulent Forced Convection in Channels and Bundles. Theory and Applications to Heat Exchangers and Nuclear Reactors" Eds. S. Kakac and D.B. Spalding, Hemisphere, New York, 1979.
2. Carr, A.D., Connor, P.A. and Euhr, H.O. "Velocity, temperature and turbulence measurements in air for pipe flow with combined free and forced convection". Trans. ASME C, J. Heat Transfer, 95, pp 445-452 (1973).
3. Byrne, J.F. and Ejiogu, E. "Combined free and forced convection heat transfer in a vertical pipe". Paper C118/71, J. Mech. E. Symposium on Heat and Mass Transfer by Combined Forced and Natural Convection, Manchester, 1971.
4. Steiner, A. "On the reverse transition of a turbulent flow under the action of buoyancy forces". J. Fluid Mech., 47, pp 503-512 (1971).
5. Axcell, B.P. and Hall, W.B. "Mixed convection to air in a vertical pipe". Paper MC-7, Proc. 6th International Heat Transfer Conference, Toronto, 1978.
6. Easby, J.P. "The effect of buoyancy on flow and heat transfer for a gas passing down a vertical pipe at low turbulent Reynolds numbers". Int. J. Heat Mass Transfer, 21, pp 791 - 801, (1978).
7. Cotton, P.A. "Theoretical studies of mixed convection in vertical tubes". Ph.D. Thesis, University of Manchester, 1987.
8. Launder, B.E. and Sharma, B.I. "Application of the energy-dissipation model of turbulence to the calculation of flow near a spinning disc". Lett. Heat Mass Transfer, 1, pp 131-138, (1974).

9. Jones, W.P. and Launder, B.E.  
"The prediction of laminarization with a two-equation model of turbulence". *Int. J. Heat Mass Transfer*, 15, pp 301-314, (1972).
10. Jones, W.P. and Launder, B.E.  
"The calculation of low-Reynolds-number phenomena with a two-equation model of turbulence". *Int. J. Heat Mass Transfer*, 16, pp 1119-1130, (1973).
11. Reichardt, H.  
"The principles of turbulent heat transfer" in "Recent advances in heat and mass transfer" Ed. J.P. Hartnett, McGraw-Hill, New York, 1961.
12. Tanaka, H., Tsuge, A., Hirata, T. and Mishiaki, N.  
"Effects of buoyancy and of acceleration owing to thermal expansion on forced turbulent convection in vertical circular tubes - criteria of the effects, velocity and temperature profiles and reverse transition from turbulent to laminar flow", *Int. J. Heat Mass Transfer*, 16, pp 1267-1288 (1973).
13. Townsend, A.A.  
"Equilibrium layers and wall turbulence" *J. Fluid Mech.*, 11, pp 97-120 (1961).
14. Launder, B.E. and Spalding, D.B.  
"Lectures in mathematical models of turbulence", Academic Press, London, 1972.
15. van Driest, E.R.  
"On turbulent flow near a wall", *J. Aero. Sci.*, 23, pp 1007-1011 and 1036 (1956).
16. Malhotra, A. and Hauptmann, E.G.  
"Heat transfer to a supercritical fluid during turbulent, vertical flow in a circular duct" Paper presented at the International Centre for Heat and Mass Transfer Symposium on Turbulent Buoyant flow in Ducts, Dubrovnik, 1976.
17. Jackson, J.D. and Evans Lutterodt, K.O.J.  
"Influence of buoyancy on heat transfer to supercritical pressure carbon dioxide in a vertical pipe" Report ME2, Nuclear Engineering Laboratories, University of Manchester, 1968.
18. Walklate, P.J.  
"A comparative study of theoretical models of turbulence for the numerical prediction of boundary layer flows", Ph.D. Thesis, UMIST, 1976.
19. Wolfshtein, N.  
"The velocity and temperature distribution in one-dimensional flow with turbulence augmentation and pressure gradient", *Int. J. Heat Mass Transfer*, 12, pp 301-318 (1969).
20. Abdelmeguid, A.P. and Spalding, D.B.  
"Turbulent flow and heat transfer in pipes with buoyancy effects", *J. Fluid Mech.*, 94, pp 383-400 (1979).
21. Renz, U. and Bellinghausen, R.  
"Heat transfer in a vertical pipe at supercritical pressure", Proc. 8th International Heat Transfer Conference, San Francisco, 1986.
22. Scheidt, F.  
Dissertation, University of Hannover, 1983.
23. Tanaka, H., Murayama, S. and Hetano, S.  
"Combined forced and natural convection heat transfer for upward flow in a uniformly heated vertical pipe", *Int. J. Heat Mass Transfer*, 30, pp 165-175 (1987).
24. Leachziner, M.A.  
"An introduction and guide to the computer code PASSABLE", UMIST report, 1982.
25. Cotton, M.A. and Jackson, J.D.  
"Calculation of turbulent mixed convection in a vertical tube using a low-Reynolds-number  $k-\epsilon$  turbulence model", 6th Symposium on Turbulent Shear Flows, Toulouse, September 1987.

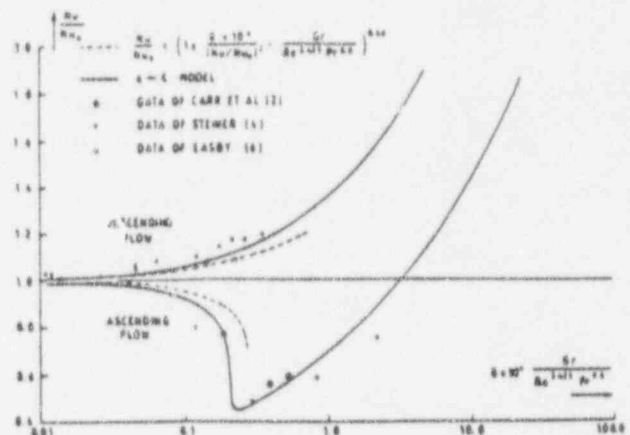


Figure 1 Heat transfer impairment and enhancement in ascending and descending turbulent mixed convection.

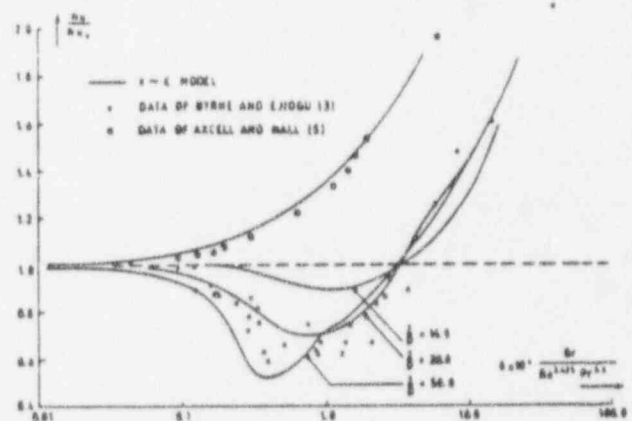


Figure 2 Development effects upon heat transfer impairment and enhancement in turbulent mixed convection.

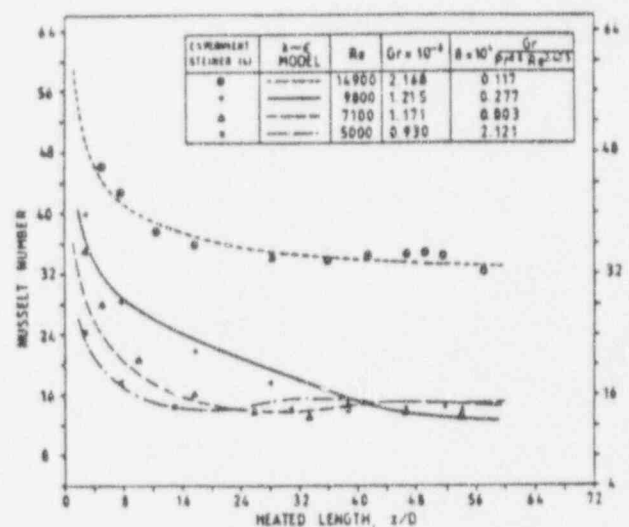


Figure 3 Nusselt number development in ascending turbulent mixed convection: direct comparison with the data of Steiner



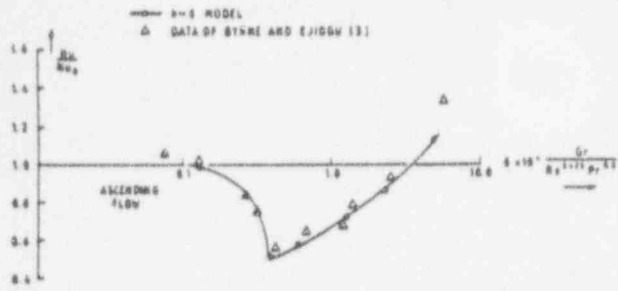


Figure 4 Ascending flow: direct comparison with the data of Byrne and Ejioqu.

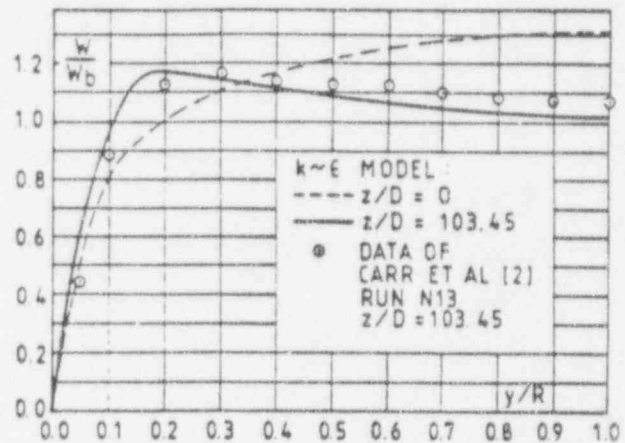


Figure 7 Velocity profile in ascending flow (Carr et al, Run N13).

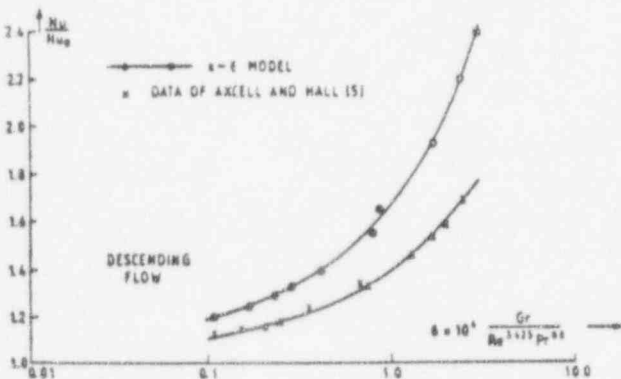


Figure 5 Descending flow: direct comparison with the data of Axcell and Hall.

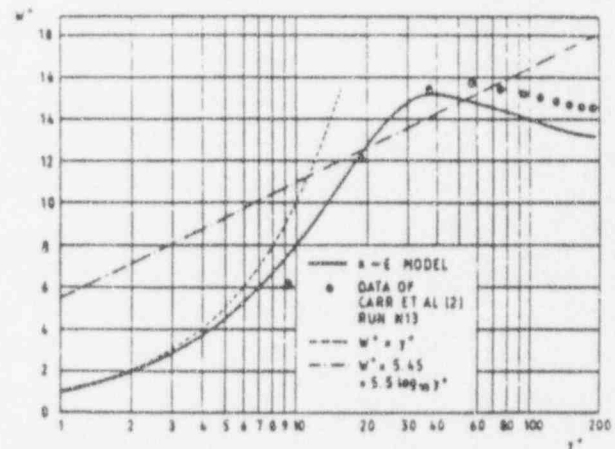


Figure 8 Velocity profile in ascending flow plotted in 'universal' coordinates (Carr et al, Run N13).

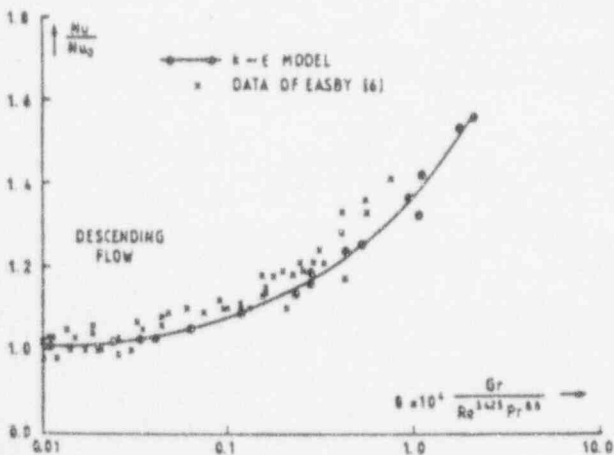


Figure 6 Descending flow: direct comparison with the data of Easby.

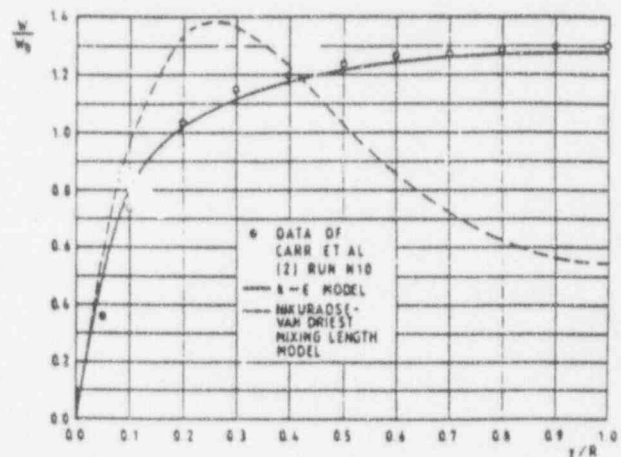


Figure 9 Velocity profile in ascending flow; comparison with a mixing length model (Carr et al, Run N10).

# MIXED CONVECTION HEAT TRANSFER — 1991 —

*presented at*

THE 28<sup>TH</sup> NATIONAL HEAT TRANSFER CONFERENCE  
MINNEAPOLIS, MINNESOTA  
JULY 28-31, 1991

*sponsored by*

THE HEAT TRANSFER DIVISION, ASME

*edited by*

DARRELL W. PEPPER  
ADVANCED PROJECTS RESEARCH INC.

BASSEM F. ARMALY  
UNIVERSITY OF MISSOURI-ROLLA

M. ALI EBADIAN  
FLORIDA INTERNATIONAL UNIVERSITY

P. H. OOSTHUIZEN  
QUEEN'S UNIVERSITY

ENGR

536-5  
Am  
2.8

## MIXED CONVECTION IN A TWO-DIMENSIONAL ASYMMETRICALLY HEATED VERTICAL DUCT

B. J. Baek

Department of Precision Mechanical Engineering  
Chonbuk National University  
Chonju, Korea

M. B. Younger, B. F. Armaly, and T. S. Chen

Department of Mechanical and Aerospace Engineering and  
Engineering Mechanics  
University of Missouri-Rolla  
Rolla, Missouri

### ABSTRACT

Measurements and predictions of mixed convection air flow in a vertical two-dimensional duct that is formed by one adiabatic wall and one uniform temperature wall are reported. Velocity distributions and wall heat flux were measured by using a Laser-Doppler Velocimeter (LDV) and a Wollaston Interferometer (WI), respectively, for different buoyancy force effects and for various inter-wall spacings. Reversed flows were observed adjacent to the adiabatic wall when the inlet air flow was restricted to a level below the natural convective value (starved flow conditions). Velocity distributions skew toward the heated wall as a result of the asymmetric heating, and the occurrence of flow reversal diminishes as the buoyancy force decreases. The occurrence of reversed flow adjacent to the adiabatic wall influenced significantly the velocity distribution in the duct, but it had only small effect on the heat transfer from the heated wall. Numerical predictions of velocity distributions and heat transfer compare well with measured values.

### NOMENCLATURE

$b$  = spacing between walls  
 $g$  = gravitational acceleration  
 $Gr_b$  =  $g\beta(T_1 - T_0)b^3/\nu^2$ , Grashof number based on  $b$   
 $Gr_x$  =  $g\beta(T_1 - T_0)x^3/\nu^2$ , Grashof number based on  $x$   
 $h_x$  =  $q_w/(T_1 - T_0)$ , local heat transfer coefficient at the heated wall  
 $k$  = thermal conductivity  
 $L$  = length of duct  
 $Nu_x$  =  $hx/k$ , local Nusselt number at the heated wall  
 $P$  = pressure  
 $Pr$  = Prandtl number  
 $q_w$  = wall heat flux at the heated wall  
 $Re_b$  =  $u_0 b/\nu$ , Reynolds number based on  $b$   
 $Re_x$  =  $u_0 x/\nu$ , Reynolds number based on  $x$   
 $S$  =  $b/L$ , dimensionless spacing between walls  
 $T$  = fluid temperature  
 $T_0$  = inlet air temperature  
 $T_1$  = temperature of heated wall (at  $y = b$ )  
 $T_2$  = temperature of unheated (adiabatic) wall (at  $y = 0$ )  
 $u$  = streamwise velocity component  
 $u_0$  = centerline streamwise velocity at the duct inlet for natural convection

$u_0$  = centerline streamwise velocity at the duct inlet  
 $v$  = transverse velocity component  
 $W$  = width of duct  
 $x$  = axial coordinate  
 $x_p$  = penetration depth of the reversed flow as measured from the exit section  
 $y$  = transverse coordinate (measured from the adiabatic wall)  
 $z$  = spanwise coordinate  
 $\alpha$  = thermal diffusivity  
 $\beta$  = volumetric coefficient of thermal expansion  
 $\rho$  = density  
 $\theta$  =  $(T - T_0)/(T_1 - T_0)$ , dimensionless temperature  
 $\nu$  = kinematic viscosity  
 $\xi$  =  $Gr_b/(Re_b^2)$ , buoyancy parameter

### INTRODUCTION

Convective heat transfer between two parallel plates is of considerable interest in many engineering designs dealing with electronic cooling and heat exchangers. The heat transfer in that geometry can take place via forced convection (Mercer et al., 1967), free convection (Sparrow and Azevedo, 1985), or mixed forced and free convection (Cebeci et al., 1982) with either symmetric (Beckett and Friend, 1982 and Wirtz and Stutzman, 1982) or asymmetric (Aung, 1972 and Quintiere and Mueller, 1973) heating condition. In addition, the geometry can be horizontal (Kamotani and Ostrach, 1976 and Emery and Gessner, 1976), inclined (Ou et al., 1976 and Azevedo and Sparrow, 1985) or vertical (Bododia and Osterle, 1962), and the flow and heat transfer phenomena can be either laminar or turbulent.

The problem of laminar mixed convection in vertical ducts has been studied extensively (Habchi and Acharya, 1986) for either symmetrically or asymmetrically heated condition. The study of mixed forced and free convection with reversed flow regions in vertical ducts, has received relatively little attention. Flow reversals have been observed inside two dimensional vertical ducts of finite length with asymmetrical heating conditions (two walls at uniform but different temperatures) in natural convection (Sparrow et al. 1984) and in mixed convection (Baek et al. 1991). The criteria for developing a reverse flow region in such flows and the extent of that reverse flow region are important for design considerations. Such criteria have

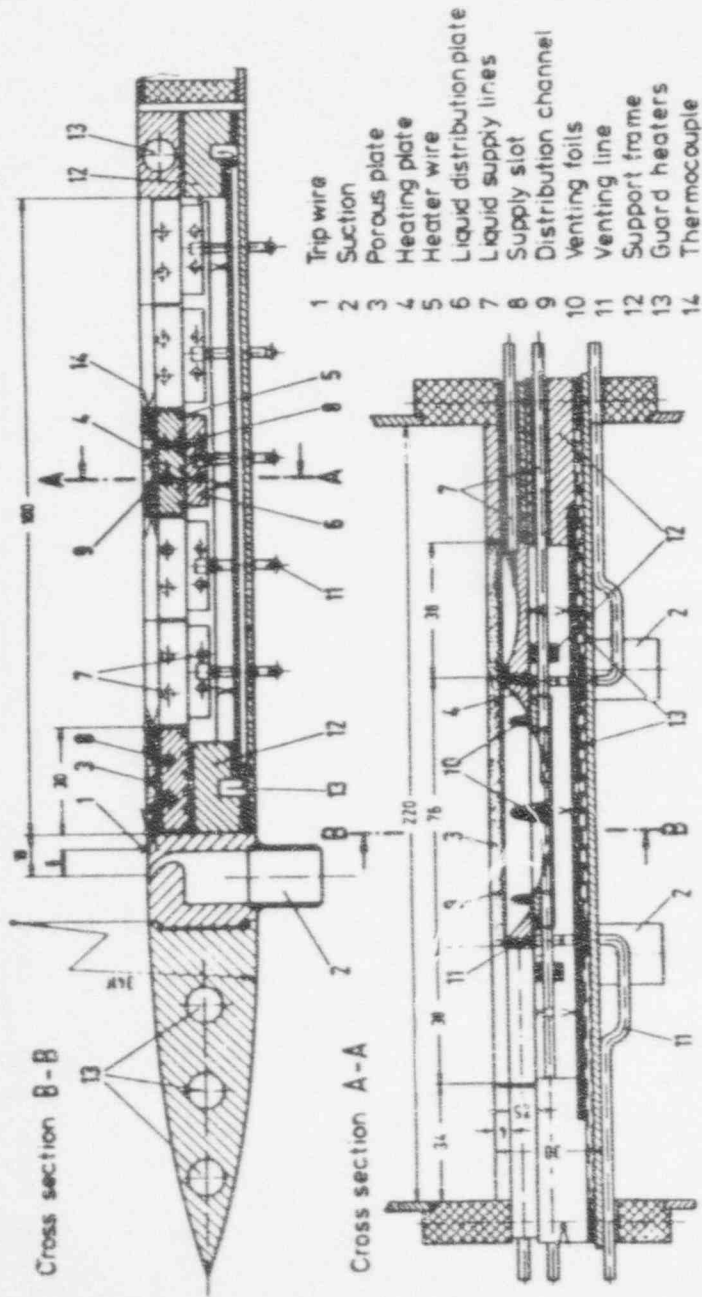


Figure 6. Longitudinal and cross-sectional views of the test plate.

To achieve controlled film temperatures, extending from the adiabatic to close to the boiling temperature of the evaporating fluid, the plate sections are heated individually by electrical heaters embedded in solid nickel plates soldered to the lower side of the porous plate segments. Each of the porous plate segments is supplied separately with degassed liquid. With the aid of a specially developed liquid supply system in combination with an optical observation device, a very thin liquid film with a constant thickness of less than  $2\ \mu\text{m}$  can be maintained on the surface of each porous plate segment. This is accomplished at any local evaporation rate.

The very thin film is a prerequisite for the achievement of high surface temperatures with exclusion of boiling. In the present case, heat fluxes of the order of  $50\ \text{kW/m}^2$  are to be transferred from the heated plate to the film surface, causing temperature gradients of approximately  $25^\circ\text{C}$  per  $0.1\ \text{mm}$ . Since the maximum temperature drop across a film  $2\ \mu\text{m}$  thick amounts to  $0.5^\circ\text{C}$ , the surface temperature to be determined exactly for the evaluation of the mass transfer coefficient can be measured within a few tenths of a degree with miniature thermocouples soldered into grooves on both sides of each section of the test plate. The temperature of the support frame and the bottom of the flat plate as well as the leading edge is controlled by liquid bath thermostats.

Velocity and thermal boundary layers originating at the leading edge of the test plate are sucked off a short distance upstream of the evaporation area, causing approximate coincidence of the lines of origin of the three boundary layers. For the experiments with turbulent boundary layers, a trip wire is installed across the flat plate  $6\ \text{mm}$  downstream of the suction slot, ensuring the existence of fully developed turbulent boundary layers obeying the  $\frac{1}{2}$  power relation along the measurement area of the dry flat plate. A detailed description of the experimental facility, the test procedure, and the data reduction is given by Greiner [11].

## EXPERIMENTAL RESULTS

The first series of experiments consisted of heat transfer measurements in laminar and turbulent boundary layer flow with the flat plate kept dry. The results (not shown here) are in very good agreement with the predictions of Eqs. (2) and (5). After the facility was checked out, experiments in which methanol was evaporated into slightly moist air under laminar flow conditions were performed. The reduced mass transfer coefficients are displayed in Fig. 7 as a function of the driving force  $C$ . They deviate from the exact numerical solution, especially at low interphase temperatures. This is due to absorption of water vapor by the methanol film. The methanol vapor pressure from the methanol-water mixture is lower than that of pure methanol. Consequently, the rate of evaporation is reduced. The vapor pressure lowering, however, was not taken into account in the data reduction process. Although in the experiments the air was quite dry, with values of the dew-point temperature  $\tau$  between  $-5$  and  $+2^\circ\text{C}$ , a deviation of 30–40% arises in the region where the analogy should be most applicable.

Results of experiments for which the air was dried to a dew-point temperature



been established for the asymmetrically heated duct with uniform wall temperatures (Baek et al. 1990). The objective of this investigation is to extend that experimental and numerical study to a two dimensional asymmetrically heated duct having one of its walls maintained at a uniform temperature while the other wall is adiabatic. Heat transfer and velocity distribution measurements and predictions are presented for various heating levels, spacings between the duct walls, and inlet flow velocities.

## EXPERIMENTAL FACILITIES AND PROCEDURE

The experimental investigation was performed in a low turbulence, open circuit, vertically aligned air tunnel. A schematic diagram of the air tunnel is shown in Fig. 1. The tunnel had a smooth converging nozzle with a contraction ratio of 18:1, a straight test section and a smooth diverging diffuser. The two dimensional duct was constructed in the test section of the air tunnel. The test section of the air tunnel had two glass windows that extended along its length to facilitate interferometric measurements of the wall heat flux and the velocity measurements by the laser-Doppler velocimeter. Plastic honeycomb and several wire screens were used in the front section of the tunnel to straighten the flow and to reduce the turbulence level. A single speed fan and a mixing chamber were attached to the tunnel entrance section to provide a forced air flow through the test section at a controlled rate. Forced flow velocities from 0.03 to 1.3 m/s could be provided through the inlet section of the duct by controlling the pressure drop across the fan and the inlet mixing chamber.

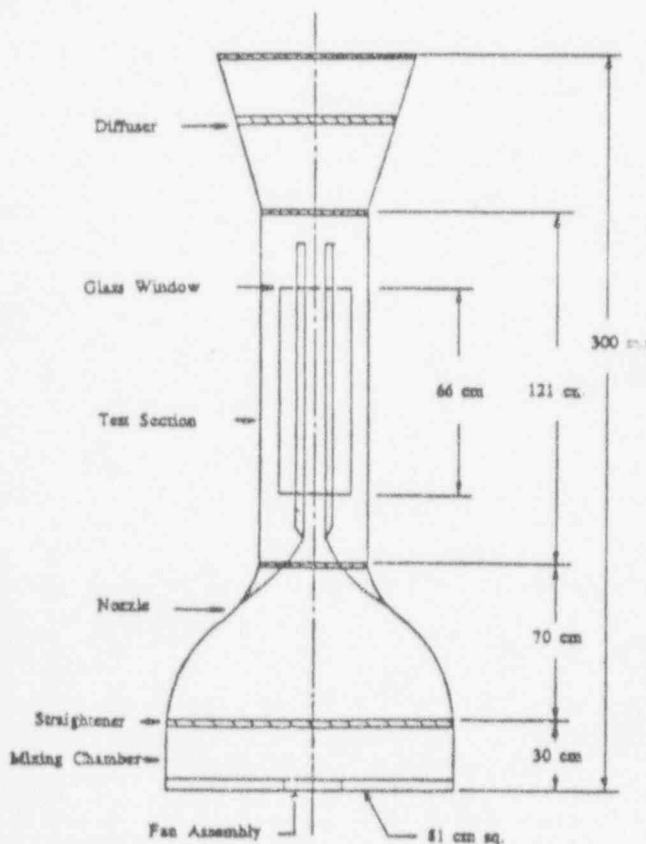


Fig. 1 Schematic diagram of air tunnel

The two-dimensional duct was formed by two plates that were placed across the width of the air tunnel. Each plate was instrumented with twelve copper-constantan thermocouples. Each thermocouple was inserted into a small hole on the back of the plate, and its measuring junction was 1 mm below the test surface. Electrical energy was supplied to the heated aluminum plate via six heating pads that were attached to the back side of the plate. The power input to each of the six heating pads was controlled by individual rheostats to maintain a uniform temperature over the entire heated test surface. The back side of the heated plate was insulated to minimize energy loss from that side. The heated plate could be maintained at uniform and constant temperature to within 0.2°C by controlling the voltage across the individual heaters. The other plate that formed the two dimensional duct was made from plexiglass and its back was insulated with styrofoam board to simulate an adiabatic surface. Thus, the electrically heated and the insulated (adiabatic) plates formed an asymmetrically heated duct which was 27.62 cm wide and 106.68 cm long, with adjustable wall spacing between 0.95 and 4.37 cm.

Velocity measurements were made using a single channel laser-Doppler velocimeter (LDV) operating in a backward scattering mode and utilizing a counter for processing the Doppler signals. The counter interfaced with a microcomputer for rapid data acquisition and reduction. Glycerin particles, two to five microns in diameter, were mixed with the inlet forced air flow to provide the scattering centers for the velocity measurements. Flow visualizations were carried out when needed by using a 15-watt collimated white light beam, 2.5 cm in diameter, and Glycerin particles as scattering centers. Heat flux measurements at the heated wall were performed by using a Wollaston Interferometer (WI) which provided a 15.24 cm diameter beam of parallel light for interferometric measurements. This type of interferometer and its use for measuring and deducing the heat flux from the interferogram were described in detail by Semas et al. (1972) and by Younger (1987). Each interferogram typically had 9 fringes terminating at the heated wall from which fringe displacements could be measured. These fringes usually spanned a length of about 9 cm of the heated wall. Heat flux measurements from each interferogram were averaged over the 9 cm length, and the average magnitude was considered as occurring at the midpoint of the interferogram. The duct was aligned with the beam of the interferometer and was moved vertically up or down to make heat flux measurements at different axial locations of the duct. All measurements, velocities and wall heat fluxes, were made after the system had reached steady state conditions. Under these conditions the temperatures of the heated and the adiabatic walls varied by less than 0.5°C during a four-hour period. The heat flux and the velocity measurements were not made simultaneously. The air properties were calculated at a mean temperature,  $(T_0 + T_1)/2$ , that is based on the inlet air temperature to the duct and the temperature of the heated wall. Flow visualizations were used to determine the onset of flow reversal and the depth of its penetration.

## NUMERICAL ANALYSIS

Predictions of the flow and temperature fields in the experimental geometry were obtained by numerically solving the governing elliptic partial differential equations. The flow was assumed to be steady, two-dimensional, laminar, and the properties were considered constant (evaluated at the average temperature  $(T_1 + T_0)/2$ ). By utilizing the Boussinesq approximation, the governing conservation equations can be listed as follows:

$$\frac{\partial u}{\partial x} + \frac{\partial v}{\partial y} = 0 \quad (1)$$

$$\frac{\partial(uu)}{\partial x} + \frac{\partial(uv)}{\partial y} = -\frac{1}{\rho} \frac{\partial P}{\partial x} + \nu \left( \frac{\partial^2 u}{\partial x^2} + \frac{\partial^2 u}{\partial y^2} \right) + g\beta(T-T_0) \quad (2)$$

$$\frac{\partial(uv)}{\partial x} + \frac{\partial(vv)}{\partial y} = -\frac{1}{\rho} \frac{\partial P}{\partial y} + \nu \left( \frac{\partial^2 v}{\partial x^2} + \frac{\partial^2 v}{\partial y^2} \right) \quad (3)$$

$$\frac{\partial(uT)}{\partial x} + \frac{\partial(vT)}{\partial y} = \alpha \left( \frac{\partial^2 T}{\partial x^2} + \frac{\partial^2 T}{\partial y^2} \right) \quad (4)$$

The applicable boundary conditions are given by

$$y = 0: u = v = 0, \partial T / \partial y = 0 \text{ or } T = T_2 \text{ (measured values)} \quad (5)$$

$$y = b: u = v = 0, T = T_1 \quad (6)$$

$$x = 0: u = u_0, v = 0, T = T_0 \quad (7)$$

$$x = L: \partial^2 u / \partial x^2 = 0, \partial v / \partial x = 0, \partial^2 T / \partial x^2 = 0 \quad (8)$$

The numerical solution of the above equations was obtained by using a finite-difference scheme, embodied in the computer code TEACH using the SIMPLE algorithm. The grid distribution in the calculation domain was non-uniform in both the longitudinal and the cross-flow coordinate directions. A large number of grid points were placed in the regions where steep variations of velocities were expected. Some of that information was deduced from the experimental observations and also from preliminary calculations using an equally spaced numerical grid. It was established from comparisons of predicted velocity distributions using different grid density at different axial locations that, for the range of parameters examined in this study, a grid density of  $N_x \times N_y = 90 \times 60$  is sufficient for providing a grid-independent solution.

## DISCUSSION OF RESULTS

The two-dimensional nature of the flow was verified by measuring the streamwise velocity distribution at the midplane between the two walls,  $y = b/2$ , across the width of the tunnel in the spanwise,  $z$ , direction for isothermal flow conditions. These results reveal a constant velocity across 80% of the duct's width, thus confirming the two dimensional nature of the flow away from the side walls. All reported streamwise velocity distributions in the transverse  $y$  direction were measured along the midplane (spanwise direction,  $z = 0$ ) of the duct's width. The inlet velocity profile was measured and was found to be uniform over 90% of the cross section. This justified the use of the measured centerline inlet velocity as the inlet conditions in the numerical model. The uncertainty associated with temperature measurements was determined to be  $0.2^\circ\text{C}$  and with the velocity measurements 1 percent. Similarly, in order to establish the accuracy level of the Wollaston Interferometer for measuring the local surface heat flux, local heat transfer rate from a single vertical heated plate was measured under natural convective conditions. The experimental and analytical results,  $Nu_x = 0.508Pr^{1/4}(0.952 + Pr)^{-1/4}Gr_x^{1/4}$ , are compared in Fig. 2 in terms of  $Nu_x$  vs.  $Gr_x$ . These results indicate that the present Wollaston Interferometer setup could be used to measure the local surface heat flux to within an accuracy level of  $\pm 5\%$ .

The measured and predicted local heat transfer coefficient,  $h_x$ , for natural convection at the heated wall of the duct are

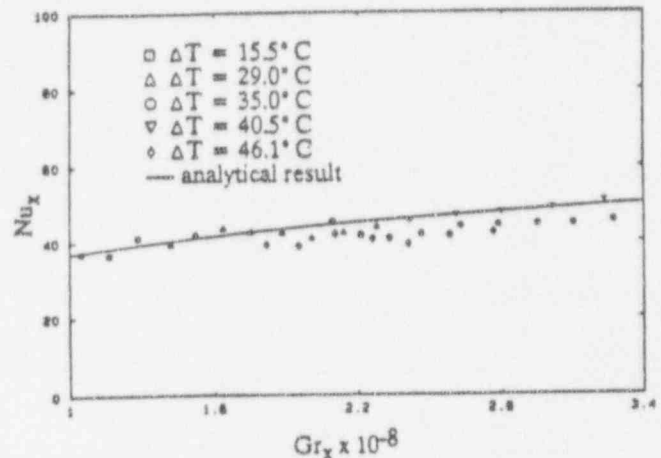


Fig. 2 Heat transfer from a vertical, heated, constant temperature plate by natural convection

presented in Fig. 3 as a function of the axial distance  $x$ . Measurements at axial locations of  $x = 38, 55$  and  $69$  cm, for heating conditions of  $(T_1 - T_0) = 24, 30, 38, 46^\circ\text{C}$ , and for duct wall spacings of  $b = 0.95, 1.91, 3.18$ , and  $4.37$  cm, were made to cover a wide range of the laminar natural convection domain in this geometry,  $10 < (b/L)Gr_bPr < 10,000$ . The results in Fig. 3a and 3b are for a duct spacing of  $b = 1.91$  cm, while those in Fig. 3c are for a duct spacing of  $b = 4.37$  cm. The temperature difference,  $(T_1 - T_0)$ , is  $24^\circ\text{C}$  in Fig. 3a and  $46^\circ\text{C}$  in Fig. 3b and 3c. Each experimental point in these figures represents the average from a single Wollaston Interferometer interferogram taken at a given axial location. The dotted line on these figures represents the predictions for a single uniformly heated vertical plate under natural convection conditions (Ostrach, 1953), and the solid line represents the predictions for the asymmetrically heated duct with conditions corresponding to the experimental geometry.

The heat transfer coefficient results in Figs. 3a - 3c indicate a good agreement between the predicted and measured values. It is also clear from the figure that for some thermal conditions, Fig. 3a, the local heat transfer coefficient at the heated wall in the vertical duct could be smaller than the local heat transfer coefficient at a single uniformly heated vertical plate under the same thermal condition. For these thermal conditions, the thermal boundary layer adjacent to the heated wall becomes relatively large in comparison to the wall spacing, and beyond some point along the length of the duct the bulk temperature becomes relatively high, causing thermal saturation. In that region the heat transfer coefficient decreases at a rate faster than what occurs for the single uniformly heated plate. The adiabatic wall that forms the duct also helps to form a chimney effect that increases the velocity adjacent to the heated plate as compared to that of the single uniformly heated plate, and thus causes an increase in the heat transfer coefficient. This can be seen by comparing the results of Fig. 3a with those in Fig. 3b. In that case an increase in wall temperature increases the chimney effects and thus increases the heat transfer rate as compared with the single uniformly heated plate results. Similarly, the results in Fig. 3b and Fig. 3c illustrate that an increase in the duct wall spacing decreases the chimney effect and thus decreases the heat transfer rate. It should be noted that if the adiabatic wall is removed sufficiently away from the heated plate, i.e. if the wall spacing of the duct is increased, then the duct geometry becomes equivalent to the vertical uniformly heated plate case. This limiting flat plate condition appears to occur when  $(b/x)Gr_bPr > 7000$ . For cases when  $(b/x)Gr_bPr < 200$  in Fig. 4, the heat transfer from the heated wall of the duct could be smaller than the single uniformly heated vertical flat

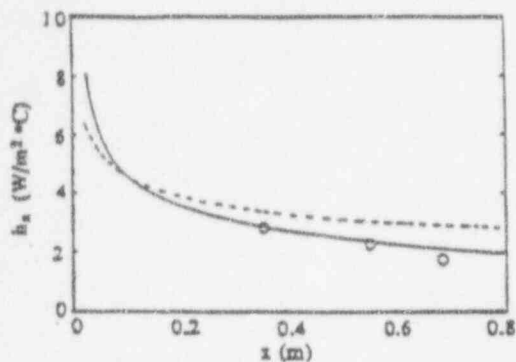


Fig. 3a  $\Delta T = 24^\circ\text{C}$ ,  $u_0 = 0.31\text{ m/s}$  and  $b = 1.91\text{ cm}$

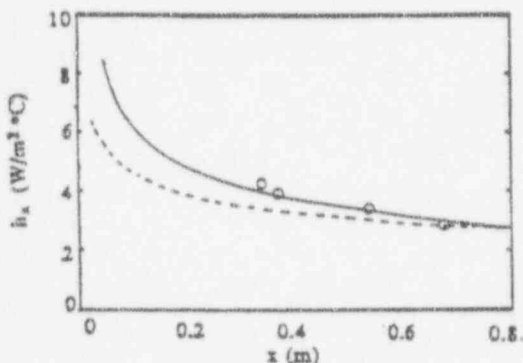


Fig. 3b  $\Delta T = 46^\circ\text{C}$ ,  $u_0 = 0.41\text{ m/s}$  and  $b = 1.91\text{ cm}$

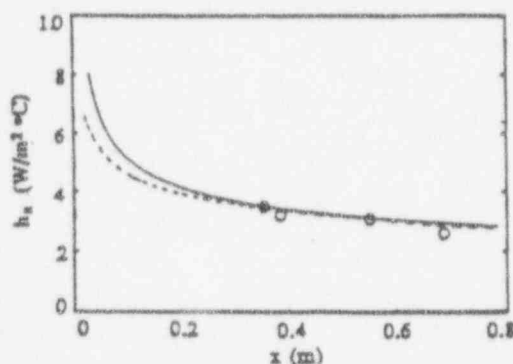


Fig. 3c  $\Delta T = 46^\circ\text{C}$ ,  $u_0 = 0.21\text{ m/s}$  and  $b = 4.37\text{ cm}$

(o experimental results, — predicted result,  
— single vertical plate result)

Fig. 3 Heat transfer coefficient along the heated wall of the duct

plate values along the length of the duct due to thermal saturation and boundary layer interaction with the adiabatic wall. Reversed flow from the exit section of the duct was not observed in the experimental geometry for the experimental conditions in natural convection flow.

The measured heat transfer results for the heated wall of the duct under mixed convection conditions are presented in terms of  $Nu_x/Re_x^{1/2}$  vs.  $Gr_x/Re_x^2$  in Fig. 5, and they are compared with the natural and the forced convection heat transfer limits for a single vertical uniformly heated plate. The results in this figure were generated by using the asymmetrically heated duct with wall spacings of  $b = 3.18$  and  $1.91\text{ cm}$  and the inlet velocity was larger than what would develop under naturally convective conditions, i.e. not under a starved flow condition, and where the boundary layer adjacent to the heated wall of the

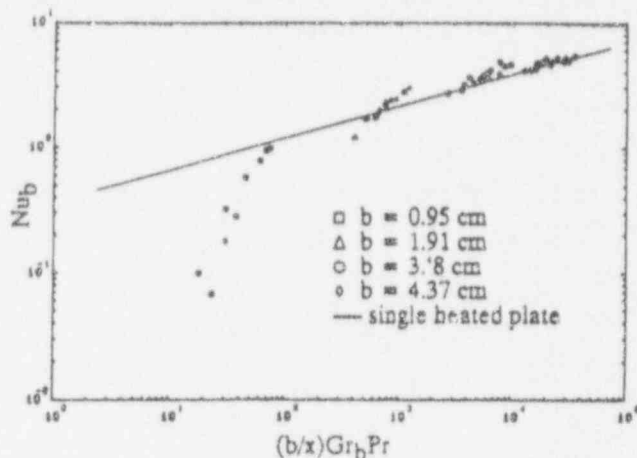


Fig. 4 Nusselt number for the heated wall in natural convection

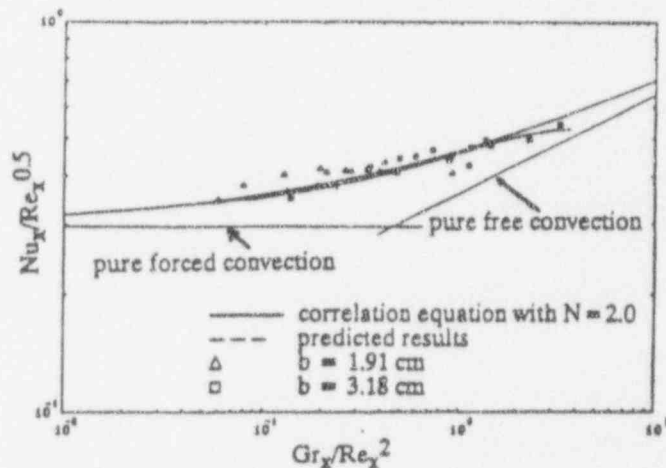


Fig. 5 Correlated mixed convection local Nusselt number for the heated wall in a vertical duct.

duct is smaller than the duct wall spacing. The results for this regime can be correlated by the following relation.

$$Nu_x/Re_x^{0.5} = [(0.296)^N + (0.359(Gr_x/Re_x)^{0.25})N]^{1/N} \quad (9)$$

The value of  $N = 2.0$  seems to give the best correlation for the data. This form is similar to the one proposed by Chen et al. (1986) for mixed convection adjacent to heated flat plate where the value of  $N$  for that case was 3. Note that the experimental Reynolds number was calculated based on  $u_0$  which is the center line velocity at the inlet section of the duct.

Measurements of heat transfer in the starved convection regime, where the centerline velocity at the inlet section of the duct was lower than the induced value by natural convection, are presented in Fig. 6. The heat transfer coefficient is presented in that figure as a function of the flow restriction ratio  $u_0/u_D$ . For some of the starved flow conditions, the asymmetric heating (buoyancy forces) accelerates the flow at some point along the duct length to a level higher than what can be provided by the fixed inlet flow condition. Thus additional mass flow rate must be provided to that section of the duct via a reversed flow from the top section (normally an exit section) of the duct to satisfy the conservation of mass and momentum. The reverse flow starts at the exit section of the duct and flows downward adjacent to the cooler adiabatic wall. The penetration depth of that reversed flow depends on the level of the

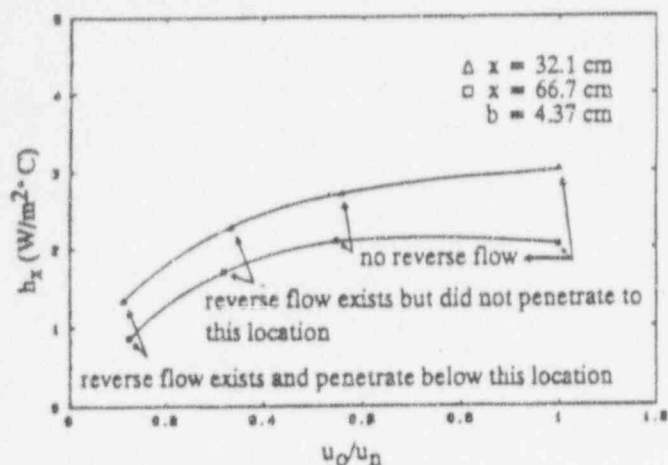


Fig. 6 Heat transfer coefficient for the heated wall in the starved convection flow regime,  $\Delta T = 30^\circ\text{C}$

starved flow condition as dictated by the geometry, heating level and the fixed inlet velocity. The results presented in Fig. 6 correspond to measurements at an axial location of  $x = 32.1$  and  $66.7$  cm when the duct spacing is  $b = 4.37$  cm and the temperature difference is  $(T_1 - T_0) = 30^\circ\text{C}$ . The measurements in that figure represent starved flow conditions with and without a reversed flow region. For the case when a reverse flow occurs at the exit section of the duct, measurements of heat transfer inside and outside the reversed flow region are identified and presented in the figure. The data indicate that reverse flow will occur when the starved flow satisfies the conditions of  $u_0/u_n < 0.5$ . From the available but limited set of experimental data, it also appears that the heat transfer from the heated wall depends more strongly on the level of starved flow conditions ( $u_0/u_n$ ) when the reverse flow occurs, i.e. when  $u_0/u_n < 0.5$ .

Flow visualizations were carried out to determine the occurrence of the reversed flow and its penetration depth under starved flow conditions. The results show that reverse flow will occur in the duct when  $u_0/u_n < 0.5$ . The penetration depth increases rapidly as the starved flow condition increases, and reaches its maximum value for the experimental geometry at about  $0.7 - 0.8$  meters (70 - 80% of the duct's height) when  $u_0/u_n < 0.2$ , where it remains approximately constant as the degree of starved flow condition continues to increase. When the penetration depth ceases to increase with increasing buoyancy,  $u_0/u_n < 0.2$ , the transition from laminar to turbulent flow starts to occur to balance the momentum and mass conservation requirements.

Measurements of the velocity distribution in the asymmetrically heated duct were performed using one component LDV system and they were not done simultaneously with the previously reported heat transfer measurements. They were, however performed on the same experimental duct. Measurements and predictions of velocity distributions in the mixed and starved flow regimes are presented in Figs. 7 through 11. The numerically predicted values, which are presented by solid lines in these figures, are in very good agreement with measured values. Measurements and predictions are presented at different axial locations, for different inlet velocities and different heating (buoyancy force) levels to explore the effects of the various parameters on the final results. The characteristic flow behaviors consist of a skewed velocity distribution toward the heated wall, with the level of skewness increasing as the level of buoyancy force increases, as shown in Figs. 7 and 8. The difference between the conditions of Figs. 7 and 8 is that the temperature difference was increased from  $25$  to  $40^\circ\text{C}$  while maintaining everything else constant,  $u_0 = 0.15$  m/s and  $b = 3.17$  cm. These two figures also show that as the buoyancy (heating)

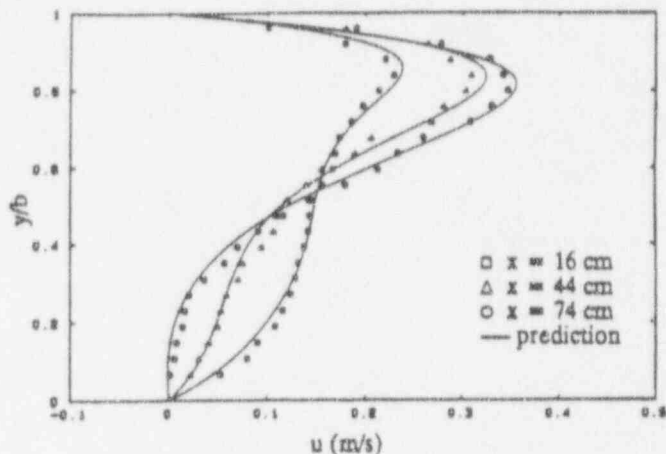


Fig. 7 Axial velocity distributions in the duct for starved convection flow,  $\Delta T = 25^\circ\text{C}$ ,  $u_0 = 0.15$  m/s, and  $b = 3.17$  cm

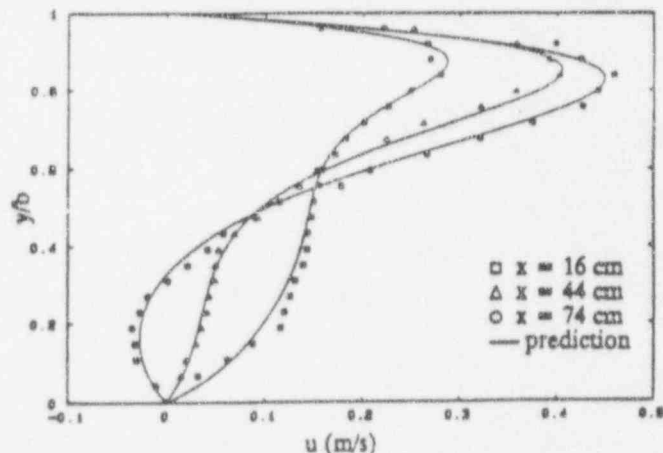


Fig. 8 Axial velocity distributions in the duct for starved convection flow,  $\Delta T = 40^\circ\text{C}$ ,  $u_0 = 0.15$  m/s, and  $b = 3.17$  cm

level increases for a fixed geometry and inlet velocity, a starved flow regime could develop in the duct, causing a reversed flow to occur along the cooler adiabatic wall of the duct.

The effects of duct wall spacing on the velocity distributions under natural convection conditions are shown in Figs. 9 and 10 where the heated wall temperature was maintained constant at  $25^\circ\text{C}$  and the wall spacing was changed from  $b = 3.17$  cm in Fig. 9 to  $b = 1.91$  cm in Fig. 10. When the duct wall spacing is decreased from  $b = 3.17$  cm in Fig. 9 to  $b = 1.91$  cm in Fig. 10, the naturally induced velocity at the center of the inlet section of the duct increased from  $u_0 = 0.25$  m/s to  $u_0 = 0.40$  m/s due to the chimney effects. The increase in velocity reduces the relative influence of the buoyancy force on the velocity distribution, and thus the skewness of the velocity distribution toward the heated wall decreases as observed in Figs. 9 and 10. When the inlet velocity is increased by forced flow to a value of  $u_0 = 0.9$  m/s while holding the other conditions of Fig. 10 constant, the buoyancy force effects decrease even further, and the skewness in the velocity distribution diminishes further as shown in Fig. 11. It is important to note that by utilizing the adiabatic boundary condition,  $\partial T/\partial y = 0$  at  $y = 0$ , the numerical code provided predictions for the velocity distribution that agree favorably with measured values when there is no reverse flow in the duct, i.e. in the natural or mixed convection regime (Fig. 9 - Fig. 11). But for the starved flow conditions, where reverse flow appears in the duct, the use of the adiabatic



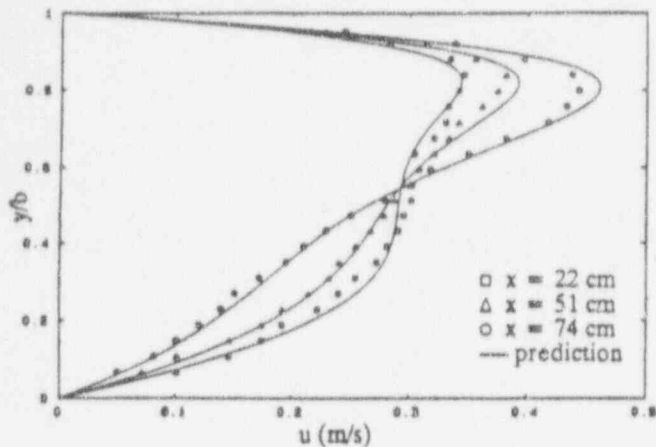


Fig. 9 Axial velocity distributions in the duct for natural convection flow  $\Delta T = 25^\circ\text{C}$ ,  $u_0 = 0.25$  m/s, and  $b = 3.17$  cm

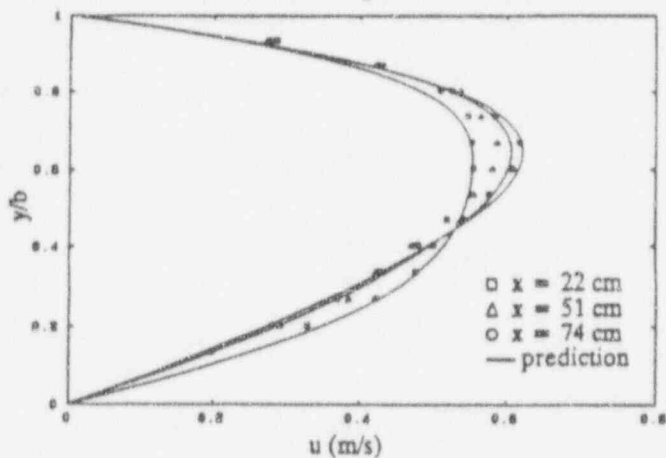


Fig. 10 Axial velocity distributions in the duct for natural convection flow  $\Delta T = 25^\circ\text{C}$ ,  $u_0 = 0.40$  m/s, and  $b = 1.91$  cm

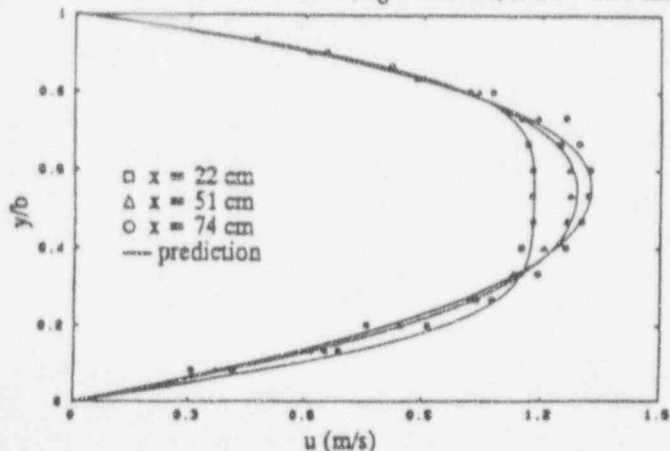


Fig. 11 Axial velocity distributions in the duct for mixed convection flow  $\Delta T = 25^\circ\text{C}$ ,  $u_0 = 0.90$  m/s, and  $b = 1.91$  cm

boundary condition in the numerical code produces results that deviate significantly from measured data in the reversed flow region. For that reason measured adiabatic wall temperatures were used as the boundary condition in the numerical code for that flow domain (Fig. 7 - Fig. 8). The velocity in the reversed flow region is normally very small and its magnitude is very sensitive to the wall temperatures. Thus small deviations from the adiabatic condition in the experimental apparatus affect

significantly the magnitude of the velocity in the reverse flow as shown in Fig. 12 where a sample of the results from Fig. 7 are presented and compared for the two stated boundary conditions.

Measurements of the temperature distribution inside the duct were not performed but they were predicted by the numerical code and a sample is presented in Fig. 13. The fluid temperature and the adiabatic wall temperature increase as the axial distance increases, because of the added energy from the heated wall. The reversed flow could not be detected from the measurements of the temperature distribution.

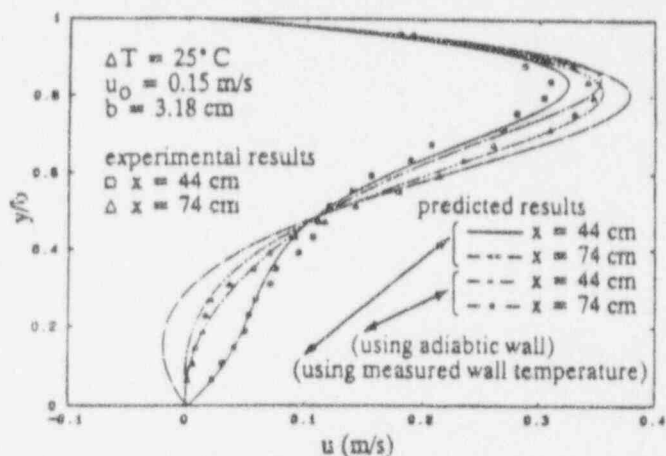


Fig. 12 Sensitivity of numerical solution to boundary conditions in the starved flow regime

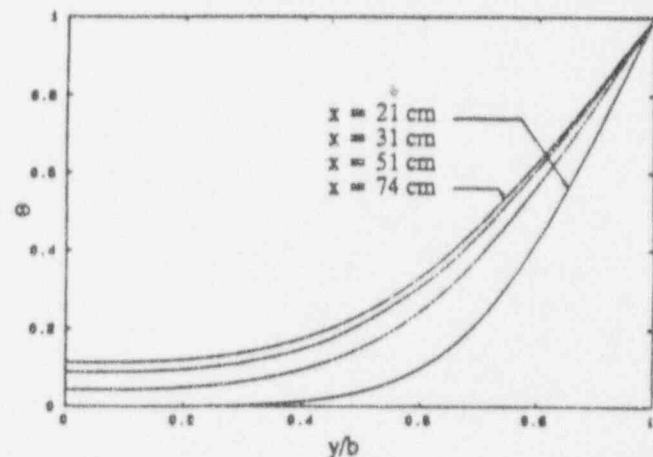


Fig. 13 Dimensionless temperature distributions in the duct for starved flow,  $\Delta T = 46^\circ\text{C}$ ,  $u_0 = 0.41$  m/s, and  $b = 1.91$  cm

## CONCLUSION

In the present study, velocity and wall heat flux measurements are reported for mixed convection air flow in a vertical two-dimensional duct that is formed by one adiabatic wall and one uniformly heated wall. Results are reported for different buoyancy force effects by varying the heated wall temperature, inlet air velocity and wall spacing. The numerically predicted velocity distribution and wall heat flux compare well with measured-values. The velocity distributions are found to skew toward the heated wall as the buoyancy force increases. A starved flow regime could develop in the duct, at high buoyancy levels, causing a reverse flow to occur along the cooler adiabatic wall of the duct. For the natural convection case a reduc-

tion in the duct wall spacing, while keeping all the other conditions constant, will produce an increase in the naturally induced inlet velocity due to the chimney effect. This causes the buoyancy force effects to decrease and decreases the skewness of the velocity distributions. For the mixed convection case, a simple correlation was developed for predicting with reasonable accuracy the local mixed convection Nusselt number as a function of the Grashof and Reynolds numbers. Measurements of the wall heat flux show that the heat transfer rate is sensitive to the level of starved flow condition,  $u_0/u_n$ , in the region where  $u_0/u_n < 0.5$ . Reverse flow will occur in the duct adjacent to the adiabatic wall when  $u_0/u_n < 0.5$ . The penetration depth of the reverse flow will increase rapidly as the buoyancy level increases through the decrease of the starved flow parameter,  $u_0/u_n$ , but it reaches a limiting value when  $u_0/u_n < 0.2$ . Higher buoyancy levels will not cause an increase in the penetration depth but will cause a transition from laminar to turbulent flow.

#### ACKNOWLEDGEMENT

The study reported in this paper was supported in part by the National Science Foundation under the grants NSF MEA-8300785 and NSF CTS-8923010.

#### REFERENCES

- Aung, W., 1972, "Fully Developed Laminar Free Convection Between Vertical Plates Heated Asymmetrically," *International Journal of Heat and Mass Transfer*, Vol. 15, pp. 1577-1580.
- Azevedo, L. F. A., and Sparrow, E. M., 1985, "Natural Convection in Open-Ended Inclined Channels," *Journal of Heat Transfer*, Vol. 107, pp. 893-901.
- Baek, B. J., Palaski, D. A., Armaly, B. F., and Chen, T. S., 1990, "Mixed Convection in an Asymmetrically Heated Vertical Parallel-Plate Duct Flow," *Proceedings in 9th International Heat Transfer Conference*, Vol. 2, pp. 369-374.
- Beckett, P. M., and Friend, I. E., 1982, "Combined Natural and Forced Convection Between Parallel Walls: Developing Flow at Higher Rayleigh Numbers," *International Journal of Heat and Mass Transfer*, Vol. 27, pp. 611-621.
- Bodoia, J. R. and Osterle, J. F., 1962, "The Development of Free Convection Between Heated Vertical Plates," *Journal of Heat Transfer*, Vol. 84, pp. 40-44.
- Cebeci, T., Khattab, A. A., and Lamont, R., 1982, "Combined Natural and Forced Convection in Vertical Ducts," *Heat Transfer 82. Proceedings of the 7th International Heat Transfer Conference*, Vol. 3, pp. 419-424.
- Chen, T. S., Armaly, B. F., and Ramachandran, N., 1986, "Correlations of Mixed Convection Flows on Vertical, Inclined, and Horizontal Flat Plates," *Journal of Heat Transfer*, Vol. 108, pp. 835-840.
- Emery, A. F., and Gessner, F. B., 1976, "The Numerical Prediction of Turbulent Flow and Heat Transfer in the Entrance Region of a Parallel Plate Duct," *Journal of Heat Transfer*, Vol. 98, pp. 594-600.
- Habchi, S., and Acharya, S., 1986, "Laminar Mixed Convection in a Symmetrically or Asymmetrically Heated Vertical Channel," *Numerical Heat Transfer*, Vol. 9, pp. 605-618.
- Kamotani, Y., and Ostrach, S., 1976, "Effect of Thermal Instability on Thermally Developing Laminar Channel Flow," *Journal of Heat Transfer*, Vol. 98, pp. 62-66.
- Mercer, W. E., Pearce, W. M., and Hitchcock, J. E., 1967, "Laminar Forced Convection in the Entrance Region Between Parallel Flat Plates," *Journal of Heat Transfer*, Vol. 89, pp. 251-256.
- Ostrach, S., 1953, "An Analysis of Laminar Free Convection Flow and Heat Transfer about a Flat Plate Parallel to the Generating Body Force," NACA Rept. 1111, Washington, D.C.
- Ou, J., Cheng, K. C., and Lin, R., 1976, "Combined Free and Forced Laminar Convection in Inclined Rectangular Channels," *International Journal of Heat and Mass Transfer*, Vol. 19, pp. 277-283.
- Quintiere, J., and Mueller, W. K., 1973, "An Analysis of Laminar Free and forced Convection Between Finite Vertical Parallel Plates," *Journal of Heat Transfer*, Vol. 95, pp. 53-59.
- Sernas, V., Fletcher, L. S., and Jones, J. A., 1972, "An Interferometric Heat Flux Measuring Device," *I. S. A. Transactions*, Vol. 11, No. 4, pp. 346-357.
- Sparrow, E. M., Chrysler, G. M., and Azevedo, L. F. A., 1984, "Observed Flow Reversals and Measured-Predicted Nusselt Numbers for Natural Convection in a One-Sided Heated Vertical Channel," *Journal of Heat Transfer*, Vol. 106, pp. 325-332.
- Sparrow, E. M., and Azevedo, L. F. A., 1985, "Vertical-Channel Natural Convection Spanning Between The Fully-Developed Limit and the Single-Plate Boundary-Layer Limit," *International Journal of Heat and Transfer*, Vol. 28, pp. 1847-1859.
- Wirtz, R. A., and Stutzman, R. J., 1982, "Experiments on Free Convection Between Vertical Plates with Symmetric Heating," *Journal of Heat Transfer*, Vol. 104, pp. 501-507.
- Younger, M. B., 1987, "Experimental Measurements of Natural and Mixed Convective Heat Transfer in an Asymmetrically Heated Parallel-Plate Channel," *M.S. Thesis, Mechanical Engineering Department, University of Missouri-Rolla*.

# MIXED CONVECTION HEAT TRANSFER — 1991 —

*presented at*

THE 28TH NATIONAL HEAT TRANSFER CONFERENCE  
MINNEAPOLIS, MINNESOTA  
JULY 28-31, 1991

*sponsored by*

THE HEAT TRANSFER DIVISION, ASME

*edited by*

DARRELL W. PEPPER  
ADVANCED PROJECTS RESEARCH INC.

BASSEM F. ARMALY  
UNIVERSITY OF MISSOURI-ROLLA

M. ALI EBADIAN  
FLORIDA INTERNATIONAL UNIVERSITY

P. H. OOSTHUIZEN  
QUEEN'S UNIVERSITY

ENGR

536.85  
American  
1991

## MIXED CONVECTIVE HEAT TRANSFER CHARACTERISTICS OF A DOWNWARD TURNING BUOYANT CEILING JET

Kamlesh Kapoor and Yogesh Jaluria  
Department of Mechanical and Aerospace Engineering  
Rutgers, State University of New Jersey  
New Brunswick, New Jersey

### ABSTRACT

An experimental investigation has been carried out on the mixed convective heat transfer characteristics of a buoyant ceiling jet turning downward at a corner. Such flows are frequently encountered in buoyancy driven transport in enclosed regions, such as those associated with thermal energy storage problems and enclosure fires. However, very little work has been done on the basic heat transfer mechanisms in such flows, particularly on the local heat flux distributions over the ceiling and the vertical wall near the corner. In this study, a two-dimensional horizontal jet of heated air is discharged adjacent to the underside of an isothermal horizontal plate whose other end is attached to an isothermal vertical plate, making a right angle corner with it. The distance between the jet discharge and the corner could be varied. Extensive heat flux measurements were carried out for different inflow conditions of the jet. The variation of the local heat transfer rate along the ceiling and the vertical wall shows a minimum followed by a recovery, as the flow turns at the corner. The average Nusselt numbers for the horizontal surface and the vertical walls are obtained as functions of the mixed convection parameter  $Gr/Re^2$  which is also known as the Richardson number  $Ri$  of the discharged ceiling jet. The total heat transfer rate to the isothermal ceiling and the vertical wall by the jet flow is also obtained. The study brings out several basic considerations in the thermal transport from a buoyant jet to the isothermal surface over which it flows, including the effects of opposing buoyancy for the vertical wall.

### NOMENCLATURE

$A_0$  cross sectional area of the slot through which the heated air jet is discharged  
 $C_p$  specific heat of the fluid at constant pressure  
 $D$  width of the slot for jet discharge  
 $g$  magnitude of gravitational acceleration  
 $Gr$  Grashof number,  $g\beta(T_0 - T_\infty)D^3/\nu^2$   
 $h$  local heat transfer coefficient,  $q/(T_0 - T_s)$   
 $k$  thermal conductivity of air  
 $L$  horizontal distance between ceiling jet discharge and corner

$Nu_D$  Nusselt number based on  $D$ ,  $hD/k$   
 $\Delta Nu_D$  difference between the maximum and the minimum value of  $Nu_D$  at the corner  
 $q$  local heat transfer flux to the surface  
 $Q$  total net heat transfer to the isothermal surface from the heated jet flow  
 $Q_{IN}$  total thermal energy input by the ceiling jet,  $\rho_0 U_0 A_0 C_p (T_0 - T_\infty)$   
 $Re$  Reynolds number,  $U_0 D/\nu$   
 $Ri$  Richardson number,  $Ri = Gr/Re^2$   
 $T_0$  discharge temperature of the ceiling jet  
 $T_s$  temperature of the isothermal surface  
 $T_\infty$  temperature of the surroundings  
 $U_0$  discharge velocity of the ceiling jet  
 $W$  width of the horizontal and vertical plates  
 $x$  horizontal coordinate distance, measured from the slot  
 $\bar{x}$  distance along the two surfaces from the slot  
 $y$  vertical coordinate distance measured downward from the slot  
 $z$  transverse coordinate distance  
 Greek symbols  
 $\beta$  coefficient of thermal expansion of the fluid  
 $\nu$  kinematic viscosity of the fluid  
 $\delta_p$  penetration distance of the jet flow, measured downward from the slot  
 $\rho_0$  density of air at the jet discharge  
 $\theta$  dimensionless temperature,  $\theta = (T - T_\infty)/(T_0 - T_\infty)$

### INTRODUCTION

Buoyant jets are of considerable importance in many practical problems. For example, heat rejection to the atmosphere and to water reservoirs, heat extraction and thermal energy storage involve buoyant jet flows. Similarly, at the early stages of



fire growth in an enclosure, the ceiling jet driven by the fire plume turns downward at the corners and generates a wall flow with opposing thermal buoyancy. The flow and heat transfer characteristics of vertical buoyant jets have been considered in the literature. But very little work has been reported on the flow of a downward turning buoyant ceiling jet. This is the problem considered in the present paper, which reports a detailed experimental investigation on the heat transfer characteristics of such flows. Interest lies mainly in the transport processes in the vicinity of the corner and in the negatively buoyant flow that arises after the turn.

Laminar buoyant jets have received considerable attention in the literature, as reviewed by Jaluria (1986). Vertical jets with a small amount of thermal buoyancy are considered in many investigations. However, turbulent buoyant jets have been studied more extensively because of their practical relevance, see the reviews by Chen and Rodi (1979) and List (1982). Goldman and Jaluria (1986) carried out a detailed experimental study of vertically discharged, negatively buoyant, wall jets. They obtained the flow characteristics of a two-dimensional wall jet, with the buoyancy force acting in the direction opposite to that of the flow, in an isothermal environment. An insulated surface was employed to simulate the wall. The penetration distance  $\delta_p$ , which characterizes the downward penetration of the flow, was obtained and related to the inflow conditions of the jet in terms of the mixed convection parameter  $Gr/Re^2$ , defined later. This parameter is also often known as the Richardson number  $Ri = Gr/Re^2$ , where  $Ri$  is defined in terms of the discharge velocity, temperature and slot width, as defined in the nomenclature. The penetration distance  $\delta_p$  was found to decrease with an increase in  $Gr/Re^2$ , indicating the effect of increasing thermal buoyancy.

The fluid entrainment into the flow was also measured and was found to increase with  $Gr/Re^2$  over the investigated range of 0.01 to 0.15. Jaluria and Kapoor (1988) extended this  $Gr/Re^2$  range to 0.6 and found that very large flow rates are indeed entrained into the jet flow due to the large horizontal spread of the flow particularly near the stagnation region. Kapoor and Jaluria (1989) have reported a detailed experimental investigation on the heat transfer characteristics of such two-dimensional negatively buoyant wall jets in isothermal media. A heated jet was discharged vertically downward adjacent to a water cooled, isothermal, aluminum plate. The local heat transfer flux was measured over the plate for various values of the mixed convection parameter  $Gr/Re^2$ , ranging from 0.05 to 1.05. It was found that the total heat transfer rate from the jet to the isothermal surface decreases with an increase in  $Gr/Re^2$  due to the decrease in the penetration distance and the consequent reduction in the heat transfer area with increasing buoyancy effects. The effect of the wall temperature on the jet penetration distance was also determined and it was found that the penetration distance decreases with an increase in the wall temperature. This was due to the decrease in the heat transfer rate which results in a higher buoyancy level in the jet flow and, hence, smaller penetration distance.

The penetration of vertical buoyant jets into thermally stratified media has also been investigated by many workers. Jaluria (1982) obtained a numerical solution to the problem of penetration of a laminar vertical plane jet into a thermally stratified environment. Kapoor and Jaluria (1991a) have carried out an experimental investigation on the flow and thermal characteristics of a plane turbulent wall jet in a two-layer thermally stable environment. The penetration distance  $\delta_p$  in the stably stratified medium was found to be larger than that in an isothermal medium at the lower temperature level. Again, this behavior is expected from the increased opposing buoyancy effect in the latter case. The mass flow rate penetrating downward across the interface between the two layers was estimated and compared with the jet inlet mass flow rate. The heat transfer to the isothermal surface was also measured for several wall temperatures and jet discharge conditions.

The flow and heat transfer due to a horizontal buoyant ceiling jet has also been considered by several investigators. Most of these studies have been concerned with enclosure fires. Alpert (1975) studied the flow generated by the fire plume driven ceiling jet. The characteristics of a ceiling jet were investigated by Cooper (1986,1987). He developed analytical estimates to predict the spread and entrainment into the ceiling jet. Alpert (1971) and You and Faeth (1978) have measured steady state velocity and temperature profiles in ceiling jets. Transient ceiling jet characteristics were investigated by Veldman et al. (1975) and Motevalli et al. (1987). Transient temperature and velocity distributions were measured in the ceiling jet flow caused by a fire plume impinging on a ceiling. Cooper (1982,1989), in a theoretical investigation, obtained the heat transfer from a ceiling jet to the horizontal boundary. He developed an algorithm to predict the thermal response of the ceiling, for a variety of realistic constructions, to different fire scenario.

It is seen from the above review of the relevant literature that, although many studies have been carried out on vertical and ceiling jets, no effort has been made to study the heat transfer characteristics of a downward turning buoyant ceiling jet, particularly near the corner. In this paper, an experimental study is carried out on the heat transfer behavior of a horizontal two-dimensional buoyant ceiling jet as it turns downward at the corner. The results presented here consist largely of temperature and local heat transfer data. Detailed velocity measurements were also undertaken but are not presented here for conciseness. The flow characteristics, including entrainment, will be the subject of an accompanying paper (Kapoor and Jaluria, 1991b).

In this paper, the jet penetration distance and the thermal field were measured. The local heat transfer flux to the horizontal and vertical plates was measured extensively over the range of  $0.02 \leq Gr/Re^2 \leq 0.6$ . From these heat flux measurements, the heat transfer from the ceiling jet to the ceiling and to the vertical wall is obtained. The distance between the jet discharge and the corner,  $L$ , has been varied in the experiments to determine the effect of the parameter  $L/D$  on the heat transfer rates. Results are presented for three values of  $L/D$ . The basic heat transfer characteristics of the downward turning jet are emphasized and some relevant aspects of the resulting flow are also reported. The heat transfer in the vicinity of the corner is important in the simulation of these flows. Similarly, the resulting negatively buoyant flow is important in the modeling of enclosure fires to study the changing environment in a room.

## EXPERIMENTAL ARRANGEMENT

Figure 1 shows a sketch of the experimental arrangement. A blower sends ambient air, over a wide range of flow rates, through a heated copper tube. The blower is fixed at the bottom of a vertical duct which is 1.35 m high and 0.3m x 0.3m in cross section. To ensure uniform flow and a low level of turbulence in the duct, a honeycomb section and three very fine screens are provided at the entrance. Two very fine screens, which are 0.3m apart from each other, are provided in the central portion of the duct. This arrangement provides a very low level of turbulence, with intensities usually less than 0.5%, in the duct and a fairly uniform flow, with a variation of less than 5% in the velocity is obtained across the duct width. The copper tube, which is 5 cm in diameter and 1 m in length, is heated by means of three fiberglass insulated heaters which are wrapped around it. The electric energy input to each of the heaters is varied by means of power controllers. A two-dimensional diffuser, whose width could be varied, is fixed to the copper tube. Several diffuser designs were considered to ensure uniform two-dimensional flow at the exit. Velocity and temperature measurements across the diffuser exit showed fairly uniform distributions. The variations in the temperature and velocity were less than about 3°C and 2 cm/s, generally giving rise to values that were less than 2 and 5 percent of the mean values, respectively. The copper tube was provided with an insulation jacket, which consists of an inner layer of

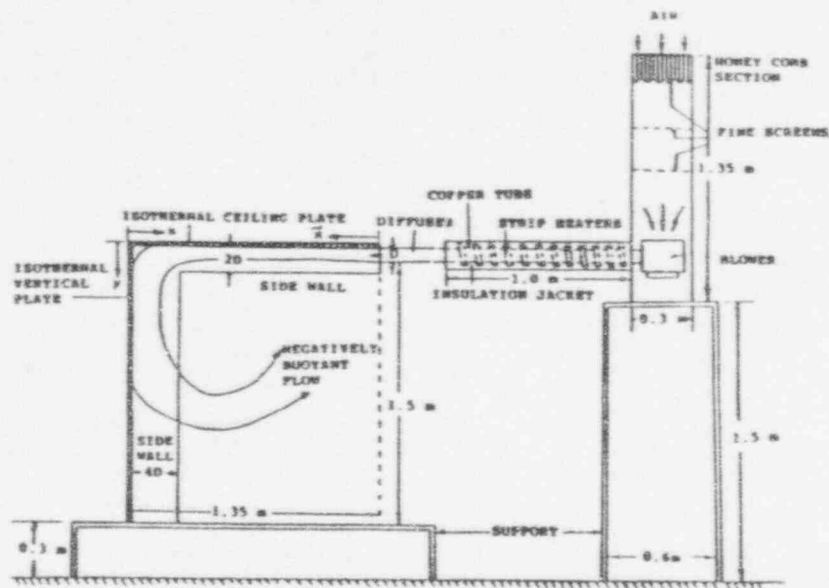


Fig. 1. Experimental arrangement for the study of the mixed convection flow of a heated, two-dimensional ceiling jet discharged horizontally into an enclosure.

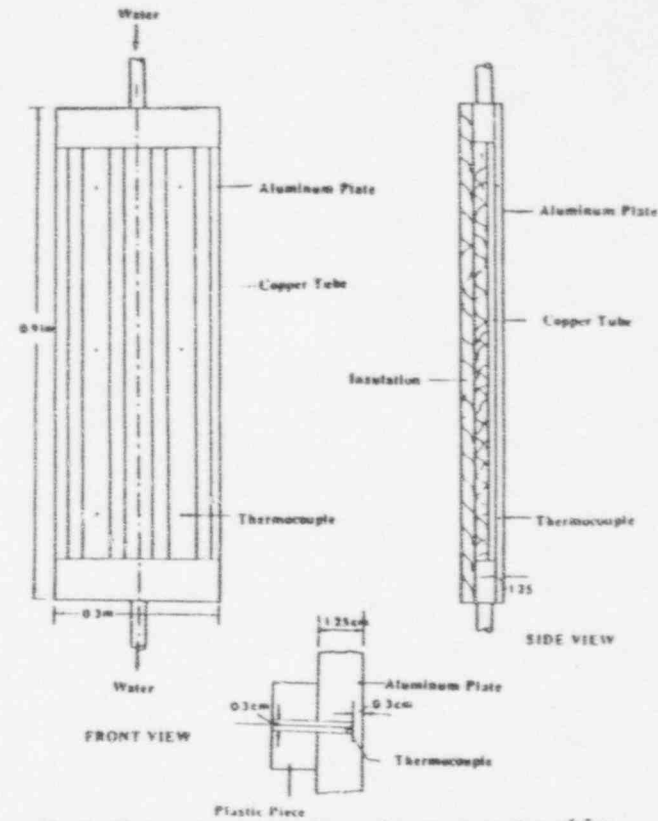


Fig. 2. Sketch of the experimental arrangement used for simulating isothermal horizontal and vertical surfaces.

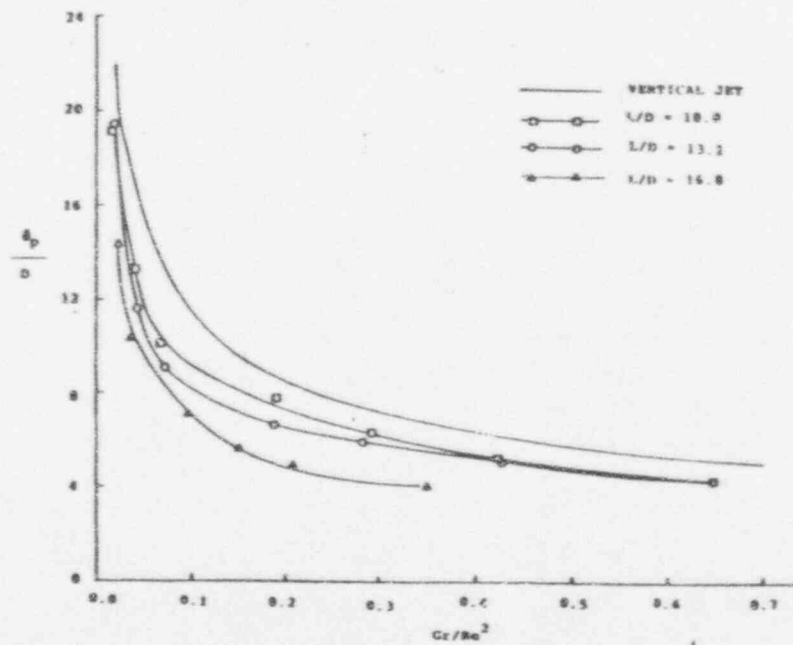


Fig. 3. Variation of the penetration distance  $\delta_p$  with the mixed convection parameter  $Gr/Re^2$ .

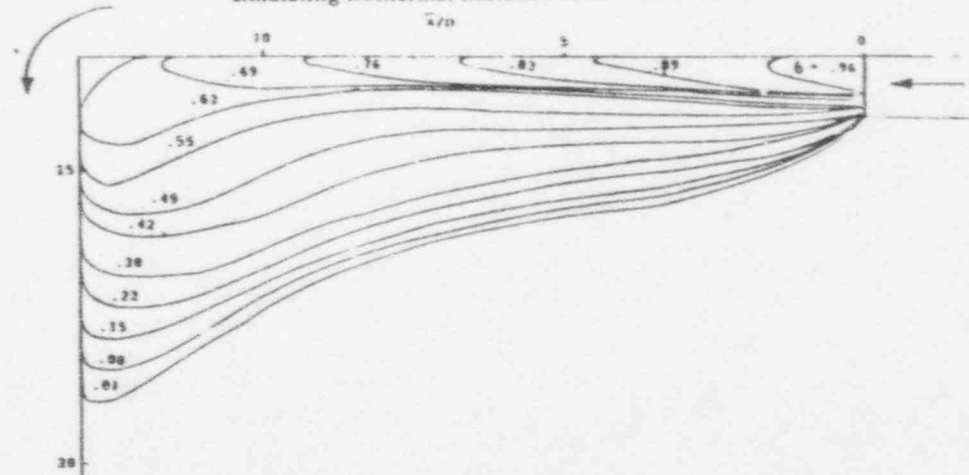


Fig. 4. Experimentally obtained isotherms for a downward turning buoyant ceiling jet at  $Gr/Re^2 = 0.303$ .

fiberglass tape and outer layer of glass wool

The discharge temperature of the jet  $T_0$  could be varied up to 150°C and the discharge velocity could be adjusted between 0.3 and 2.5 m/s. Thus, a fairly wide range of the governing parameters,  $Re$  and  $Gr$ , based on the inlet conditions, could be obtained with the present experimental arrangement. The maximum values for the Grashof number  $Gr$  and the Reynolds number  $Re$ , obtained in the present experiments, were 3500 and  $10^6$ , respectively. The discharge velocity of jet was obtained by measuring the velocity distribution at the exit of the diffuser. A calibrated DANTEC hot wire sensor was kept horizontally at the exit of the diffuser to measure the velocity distribution there. The hot wire was calibrated by using a special calibration facility which was designed to calibrate the sensor at small velocity levels, ranging from 0 to 0.5 m/s, and for a desired flow direction. The details of the calibration method and of the velocity measurements are given by Tewari and Jaluria (1990).

The discharge temperature of the jet was measured using a rake of five thermocouples located across the diffuser. The average of five temperatures was then taken as the jet discharge temperature  $T_0$ . As mentioned earlier, the temperature distribution across the diffuser exit was very uniform. A maximum variation of 30°C was measured over the range of  $Gr/Re^2$  employed in the present experiments. For further details on this system, see Goldman and Jaluria (1986) and Kapoor and Jaluria (1989).

The heated, two-dimensional jet of air, was discharged horizontally adjacent to the isothermal surfaces, as shown in Fig. 1. A water cooled aluminum plate represents the ceiling of an enclosure. Another water cooled vertical aluminum plate was fixed to the ceiling plate, thus forming a 90° corner. The horizontal distance  $L$  between the corner and the jet discharge could be varied from about 0.6m to 1.0m by moving the jet slot along the ceiling plate. The width of the jet could also be varied. In the present experiment, most of the measurements were taken at  $D = 0.065m$  and  $0.0506m$ . Thus, this arrangement allowed a change in  $L/D$  from 10 to approximately 20.

The sides of the flow region were kept partially open in order to avoid thermal stratification. Extensive data were taken without any side walls, and it was found that the jet flow was confined to a maximum value of about  $2D$  from the ceiling and of about  $4D$  from the vertical wall throughout the range of  $Gr/Re^2$ . Based on these experimental observations, as shown in Fig. 1, the sides were closed up to  $2D$  and  $4D$  from the ceiling and vertical wall, respectively, in order to avoid entrainment close to the wall flows and, thus, maintain the two-dimensionality of the flow. However, the results near the midplane were found to be essentially independent of the side walls. Thus, the results presented here are not affected by the edge flow or the side walls. All experimental results reported in this paper are with the sidewalls partially closed, as outlined above, and closely represent physical two-dimensional flows encountered in practical situations such as enclosure fires.

The water cooled aluminum ceiling and vertical plates are identical in design. As shown in Fig. 2, four rectangular copper tubes, each 2.5 cm x 1.25 cm in cross section, were fixed along the length of the plate. It was made sure that the surface contact between the aluminum plate and copper tubes was excellent. Water from an outside source enters at the top of the vertical plate and the water coming out of the arrangement for this plate was allowed to enter at one end of the ceiling plate. Water coming out of the other end of the ceiling plate was allowed to drain into a sink. The temperature of the water entering the vertical plate was maintained at a desired value by mixing hot and cold water streams. Twelve thermocouples were embedded in the plate to monitor plate temperatures. For further details on the plate assembly, see Kapoor and Jaluria (1989). A fairly uniform temperature distribution was found over the plate surface. The

maximum temperature difference measured between any two embedded thermocouples on the two plates was always less than 1.0°C, giving an error of less than 3% in the plate temperature data.

The heat transfer from the hot jet to the ceiling and vertical plate was measured by using microfoil heat flow sensors (RdF type 20472-3). Each of the heat flux sensors was 15mm x 0.3mm in surface area and 0.3mm in thickness, and could easily be attached to the plate. The typical distance between two heat flux sensors along the ceiling and vertical plate was approximately 5.0 cm except near the corner where the sensors were placed typically 1 cm from each other. This arrangement provided detailed distributions of the heat transfer flux along the ceiling and the vertical plate. The electric output (in millivolts) from the heat flux sensor was converted into heat flux (in  $W/m^2$ ) with the help of individual calibration curves supplied by the manufacturer and verified in the laboratory by employing surfaces with known heat flux inputs. The accuracy of the measured heat flux was estimated to be very high, with an estimated error of less than 3% in the present experiments. The fluctuations in the heat flux were found to be less than 10% in most of the cases and may be attributed to the turbulent flow over the surfaces. The output of the heat flux sensors were constantly monitored on a strip chart recorder and all the heat flux data were collected by using a Keithley data acquisition system. Thus, the errors in the reported Nusselt and Richardson numbers were estimated to be less than 5% and 3%, respectively. The temperatures were measured by copper-constant thermocouples. Considerable care had to be exercised to obtain accurate and repeatable data. In general, the repeatability was very high, being within 5% for most measurements reported here.

## RESULTS AND DISCUSSIONS

The height  $D$  of the two-dimensional, wide, slot discharging the jet is generally taken as the characteristic dimension for a jet in an extensive environment (Jaluria, 1980; Gebhart et al. 1988). The dimensionless governing parameters in the present experiment are the Reynolds number  $Re$ , the Grashof number  $Gr$  and the Richardson number  $Ri$ , which is also often known as the mixed convection parameter,  $Gr/Re^2$ . The heat transfer at the ceiling and vertical wall may be presented in terms of the Nusselt number  $Nu_D$ . These dimensionless quantities are defined as follows:

$$Re = \frac{U_0 D}{\nu}, \quad Gr = \frac{g\beta(T_0 - T_s)D^3}{\nu^2} \quad (1)$$

$$Ri = \frac{g\beta(T_0 - T_s)D}{U_0^2}, \quad Nu_D = \frac{hD}{k} \quad (2)$$

where  $U_0$  and  $T_0$  are the velocity and temperature at the discharge of the jet,  $g$  the magnitude of the gravitational acceleration,  $\beta$  the coefficient of thermal expansion of the fluid,  $h$  the local convective heat transfer coefficient, and  $\nu$  the kinematic viscosity of air at the discharge temperature  $T_0$ . Thus,  $h$  is given by  $h = q/(T_0 - T_s)$  where  $q$  is the measured local heat flux and  $T_s$  is the surface temperature.

The data consist mainly of the temperature distributions in the jet flow and of the local heat flux measurements along the ceiling and the vertical wall for different values of the jet discharge conditions such as temperature and flow rates. The results are presented for  $L/D = 10, 13.1$  and  $16.5$  and the mixed convection parameter  $Gr/Re^2$  or  $Ri$  was varied from 0.02 to 0.65 in the present experiments. Some of the typical experimental results obtained in this study are presented here.



The buoyant horizontal ceiling jet, after losing some of its momentum and thermal energy to the ceiling, reaches the corner and turns downward along the vertical wall and behaves like a negatively buoyant wall jet, as studied by Goldman and Jaluria (1986). The hot jet flow penetrates to a finite distance  $\delta_p$  in the enclosure, due to the opposing buoyancy. It then turns upward and flows out of the enclosure. In this process, the jet flow entrains significant amounts of fluid from the ambient medium, resulting in a much larger flow rate out of the enclosure, as compared to the discharged flow rate.

The penetration distance  $\delta_p$ , which represents the downward penetration distance of the thermal effects in the flow, is defined as the vertical distance at which a sharp increase in the temperature level is seen as one proceeds from bottom to the top of the enclosure (Kapoor and Jaluria, 1989). The variation of the penetration distance  $\delta_p$  with the mixed convection parameter  $Gr/Re^2$  for  $L/D = 10, 13.1, 16.5$  and  $20.5$ , is shown in Fig. 3. The ceiling and the vertical wall temperatures are kept the same and are very close to the ambient temperature (within  $\pm 10^\circ C$ ). It is seen from the figure that the penetration, in general, decreases with an increase in the mixed convection parameter  $Gr/Re^2$ . These results are similar to those of a negatively buoyant vertical jet. The results for a vertical jet are also shown in the figure. The penetration distance was found to be smaller for the higher value of  $L/D$  at a given  $Gr/Re^2$ . It was found that the velocity level decreases at a much faster rate than the thermal energy along the ceiling plate as the flow approaches the corner. Hence, the jet flow has, relatively, smaller momentum, while retaining a larger amount of its thermal energy after it turns downward at the corner. This results in a smaller penetration distance for the higher value of  $L/D$ . The velocity data are not presented here for brevity. But the flow field measurements agreed closely with the results from the temperature and heat flux data (Kapoor and Jaluria, 1991b).

Appropriate correlations may be obtained to calculate the non-dimensional penetration distance  $\delta_p/D$  as a function of  $Gr/Re^2$  for various values of  $L/D$ . A general correlating equation to calculate  $\delta_p/D$ , incorporating both  $L/D$  and  $Gr/Re^2$  as input parameters, is

$$\frac{\delta_p}{D} = 13.07 (L/D)^{-0.54} (Gr/Re^2)^{-0.41} \quad (3)$$

Other correlating equations for different thermal conditions such as the vertical negatively buoyant jet have been obtained earlier (Goldman and Jaluria, 1986).

In order to understand the basic nature of the resulting transport processes, detailed measurements of the thermal field across the enclosure were carried out. The thermal field was mapped very closely, by using a rake of thermocouples which was placed at the midpoint of the depth ( $z$  direction) of the enclosure. From these temperature measurements, the corresponding isotherms were determined by interpolation. Figure 4 shows a typical set of isotherms for  $Gr/Re^2 = 0.303$ . It is seen from this figure that the horizontal buoyant ceiling jet loses thermal energy as it moves along the ceiling and turns down at the corner along the vertical wall. As expected, the jet flow loses thermal energy as it penetrates downward to a finite distance  $\delta_p$ , as discussed earlier, and then rises upward due to thermal buoyancy and finally escapes out of the enclosure. It is seen from the isotherms that the ceiling jet flow starts turning downward before reaching the corner. This shows that the ceiling jet flow separates from the ceiling some distance before the corner and reattaches to the vertical wall downstream. This indicates the presence of a small recirculation zone in the corner. This conclusion was also confirmed by the velocity profiles measured near the ceiling and vertical plates. The flow separation at the corner is also confirmed by the corresponding heat flux measurements on the ceiling and vertical walls.

As mentioned earlier, the local heat transfer rate from the jet to the isothermal ceiling and vertical wall was measured by using heat flux meters. These heat flux gages were fixed at about 5.0 cm apart from each other along the midplane of the ceiling and vertical plates. In order to measure detailed heat flux distributions at the corner, the sensors were fixed more closely (up to 1 cm) at the ceiling and vertical plate near the corner. The temperature of the ceiling and vertical plates was kept the same and close to the ambient temperature (within  $\pm 10^\circ C$ ). Extensive heat transfer data has been obtained for  $0.02 \leq Gr/Re^2 \leq 0.65$  and  $L/D = 10, 13.1$  and  $16.5$ . Only a few of the typical results are shown here for conciseness.

Figure 5 shows the variation of measured heat flux  $q$  (in  $W/m^2$ ) along the ceiling and the vertical plate for  $Gr/Re^2 = 0.0435$  and  $L/D = 10$ . It is seen from the figure that the local heat transfer rate decreases along the ceiling plate and reaches its lowest value just before the corner. It is seen to increase sharply as the jet flow turns downward at the corner and reaches its maximum value just below the corner on the vertical wall. The local heat transfer flux is then seen to decrease gradually along the vertical wall and to become almost zero further downstream. The penetration distance  $\delta_p$  has also been shown in the figure. As implied by isotherms in Fig. 4, the jet flow separates from the ceiling plate and reattaches to the vertical wall at the corner. Fig. 5 further confirms the existence of a small recirculation zone in the corner.

Figure 6 shows the variation of the local Nusselt number  $Nu_D$  along the ceiling and the vertical plate for four values of  $Gr/Re^2$  and for  $L/D = 10$ . The local Nusselt number is defined as  $Nu = hD/k$ , where  $h = q/(T_o - T_s)$ . The basic trends are similar to those observed in Fig. 4. The dimensionless local heat transfer rates, in terms of the Nusselt number, are seen to be higher for the smaller values of  $Gr/Re^2$ . It should be mentioned here that the measured value of local heat flux  $q$  is smaller at the lower value of  $Gr/Re^2$ . Higher values of  $Nu_D$  are obtained because of still smaller value of  $(T_o - T_s)$ . It is seen from the figure that, in general, the local heat transfer rate first decreases along the ceiling plate, then increases at the corner and again decreases along the vertical plate, becoming almost zero at some location downstream. The penetration distance  $\delta_p$  has also been marked on the figure. The decrease in  $Nu_D$  along the ceiling and the wall is obviously due to the increasing boundary layer thickness of the flow (Jaluria, 1980).

It is seen in Fig. 6 that the recovery in the local heat transfer rate at the corner depends upon the value of  $Gr/Re^2$ . The recovery in the local heat flux was found to be larger for the smaller values of  $Gr/Re^2$ . Figure 7 shows variation of this heat transfer recovery, expressed in terms of  $\Delta Nu_D$ , defined as the difference between the maximum and the minimum values of the local  $Nu_D$  at the corner, with  $Gr/Re^2$ . It is seen from Fig. 7 that the heat transfer recovery factor,  $\Delta Nu_D$ , decreases sharply up to a value of  $Gr/Re^2 = 0.05$ . This is followed by a gradual decrease as the value of  $Gr/Re^2$  is increased to 0.435. This is an expected result because, at the lower value of  $Gr/Re^2$ , the ceiling jet flow has relatively larger momentum before it turns downward at the corner. Therefore, it separates from the ceiling plate at a larger distance from the corner and reattaches itself to the vertical wall at a larger distance below the corner. This suggests that at the smaller value of  $Gr/Re^2$ , the size of recirculation region at the corner is larger than that found at the higher values of  $Gr/Re^2$ . Hence, at the smaller value of  $Gr/Re^2$ , the separated ceiling jet flow has to travel a larger distance at the corner before it reattaches itself to the vertical wall, resulting in a higher heat transfer recovery factor.

The variation of the average Nusselt number  $\bar{Nu}_D$  for the ceiling plate with  $Gr/Re^2$  for  $L/D = 10, 13.1$  and  $16.5$  is shown in Fig. 8. As defined earlier,  $\bar{Nu}_D = \bar{h}D/k$  where  $\bar{h} = Q_{ceiling}/(T_o - T_s) \cdot W \cdot L$ . Here,  $W$  and  $L$  are the width and the length of the ceiling plate,



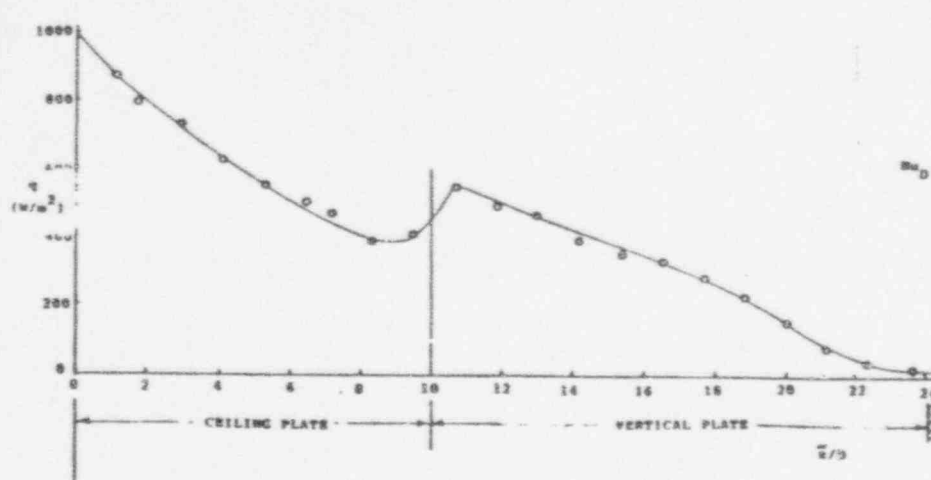


Fig. 5. Variation of the local heat transfer flux with distance  $\bar{x}$  from the slot, along the ceiling plate and the vertical wall.

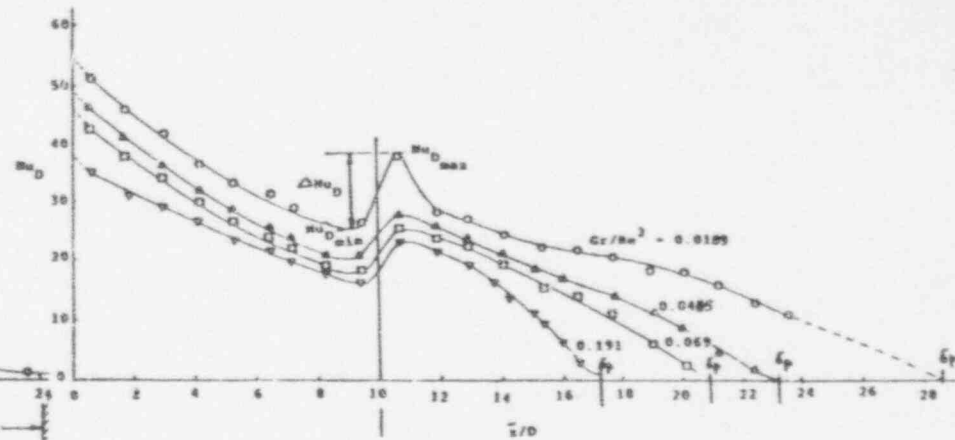


Fig. 6. Distribution of the local Nusselt number  $Nu_D$  over the ceiling and the vertical wall for  $Gr/Re^2 = 0.0189, 0.0435, 0.069$  and  $0.191$  at  $L/D = 100$ .

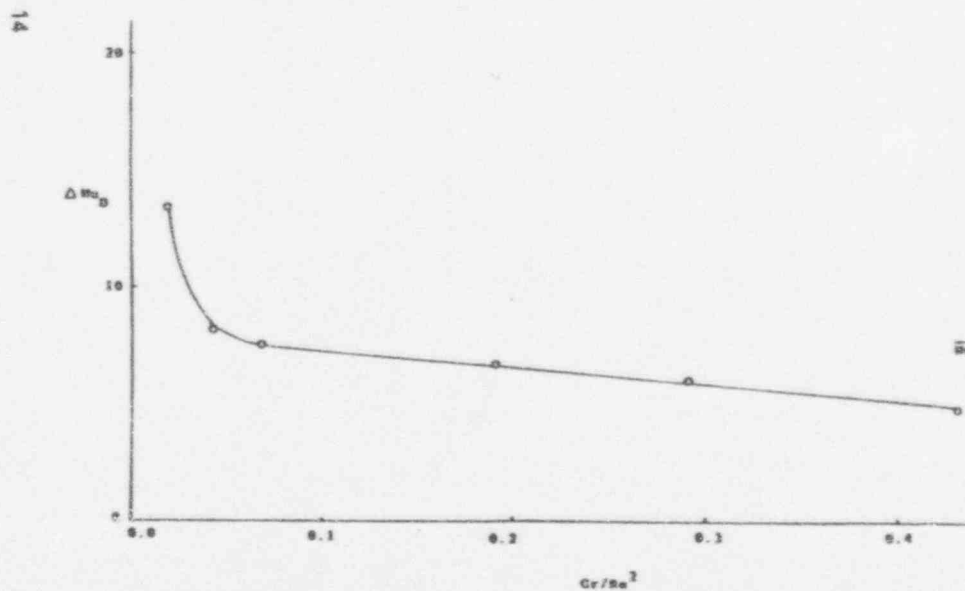


Fig. 7. Variation of heat transfer recovery factor  $\Delta Nu_D$  at the corner with  $Gr/Re^2$  at  $L/D = 100$ .

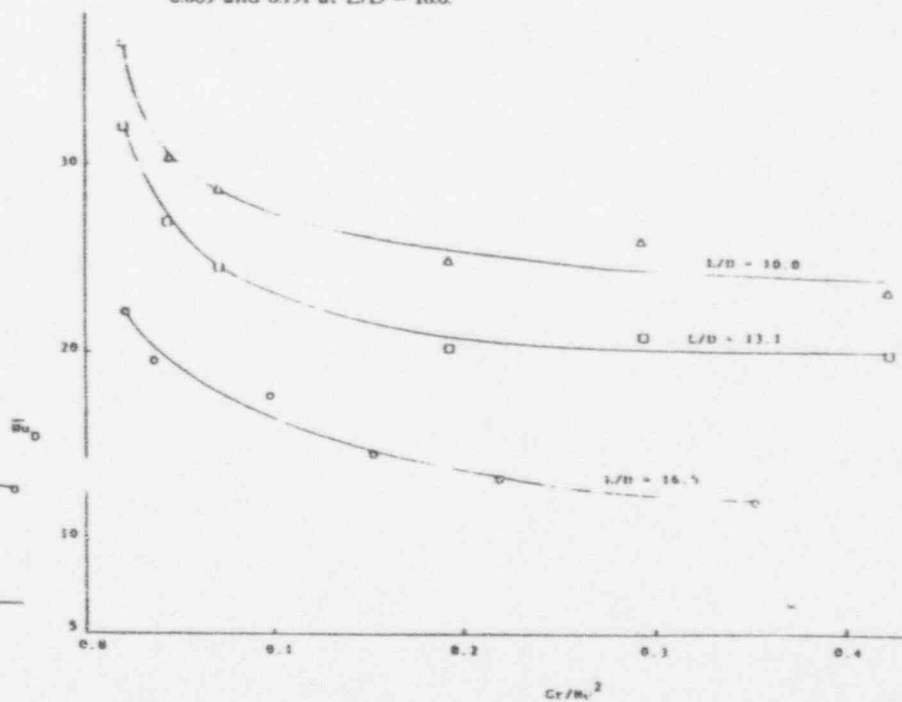


Fig. 8. Variation of the average Nusselt number  $\bar{Nu}_D$  with  $Gr/Re^2$  for the ceiling plate at different values of  $L/D$ .

respectively. The total net heat transfer rate to the ceiling  $Q_{\text{ceiling}}$  was obtained by integrating the measured heat flux over the length of the ceiling plate. It is seen from this figure that the average Nusselt number decreases with an increase in  $Gr/Re^2$ . This is due to the fact that, while the net heat transfer to the ceiling plate  $Q_{\text{ceiling}}$  increases with  $Gr/Re^2$ , the jet temperature difference  $(T_0 - T_s)$  increases more rapidly than  $Q_{\text{ceiling}}$ . This results in a lower average heat transfer coefficient and hence a lower value of  $\bar{Nu}_D$  at higher  $Gr/Re^2$ . Figure 8 shows that the average Nusselt number was also found to be larger for the lower value of  $L/D$ . As discussed earlier, the definitions of  $\bar{Nu}_D$  and  $\bar{h}$  are

$$\bar{Nu}_D = \frac{\bar{h}D}{k} \quad \text{where} \quad \bar{h} = \frac{Q_{\text{ceiling}}}{(T_0 - T_s) \cdot W \cdot L} \quad (4)$$

$$\bar{Nu}_D = \frac{Q_{\text{ceiling}} \cdot D}{k(T_0 - T_s) \cdot W \cdot L} \quad (5)$$

This equation can also be written as

$$\bar{Nu}_D = \frac{Q_{\text{ceiling}}}{k(T_0 - T_s) \cdot W \cdot (L/D)} \quad (6)$$

As seen later in this paper,  $Q_{\text{ceiling}}$  was found to be larger at the higher value of  $L/D$ , the corresponding value of  $\bar{Nu}_D$  calculated from Eqn. (5) was lower due to presence of  $(L/D)$  in the denominator.

Figure 9 shows variation of the average Nusselt number  $\bar{Nu}_D$  for the vertical plate. In this case, the average heat transfer coefficient  $\bar{h} = Q_{\text{wall}} / (T_0 - T_s) \cdot W \cdot \delta_p$ . Here,  $Q_{\text{wall}}$  is the net heat transfer from the jet flow to the vertical wall up to the corresponding penetration distance  $\delta_p$ . The basic trends of the results are similar to those discussed in the case of the ceiling plate.

The average Nusselt number  $\bar{Nu}_D$  for both the ceiling and the vertical wall can be expressed as

$$\bar{Nu}_D = \frac{\bar{h}D}{k} \quad \text{where} \quad \bar{h} = \frac{Q_{\text{ceiling}} + Q_{\text{wall}}}{(T_0 - T_s) \cdot W \cdot (L + \delta_p)} \quad (7)$$

The variation of the average Nusselt number  $\bar{Nu}_D$  for both the ceiling and the vertical wall with  $Gr/Re^2$  is shown in Fig. 10. The results show the average heat transfer rate from the jet flow to the ceiling and the vertical wall. The basic trends, as expected, are a combination of individual results for the ceiling and the vertical wall, as shown in Figs. 8 and 9, respectively.

All these results may also be expressed in terms of correlating equations to indicate the dependence of  $\bar{Nu}_D$  on  $Gr/Re^2$  and  $L/D$ . There is also a weak additional dependence on  $Re$ . However, for such turbulent mixed convection flows, the dependence on  $Gr/Re^2$  is much stronger than that on either  $Gr$  or  $Re$  and the results may be expressed fairly accurately in terms of the mixed convection parameter. Thus, over the ranges  $0.02 < Gr/Re^2 < 0.65$  and  $10 < L/D < 20$ , the experimental results are well correlated by the equations:

$$(\bar{Nu}_D)_{\text{ceiling}} = 250.47(Gr/Re^2)^{-0.15}(L/D)^{-1.0} \quad (8)$$

$$(\bar{Nu}_D)_{\text{wall}} = 82.77(Gr/Re^2)^{-0.25}(L/D)^{-0.8} \quad (9)$$

$$(\bar{Nu}_D)_{\text{ceiling+wall}} = 61.35(Gr/Re^2)^{-0.09}(L/D)^{-0.5} \quad (10)$$

The correlation coefficients for these equations are larger than 0.95, indicating a fairly close approximation of the data with these equations.

Figure 11 shows the variation of  $Q_{\text{ceiling}}$  and  $Q_{\text{wall}}$  with  $Gr/Re^2$  for  $L/D = 10$ . In this figure,  $Q$  is non-dimensionalized by the total thermal energy input by the ceiling jet  $Q_{\text{IN}}$ , which is calculated as follows

$$Q_{\text{IN}} = \rho_0 U_0 A_0 C_p (T_0 - T_s) \quad (11)$$

It is seen from this figure that  $Q_{\text{ceiling}}$  increases with an increase in  $Gr/Re^2$ . This is an expected result because at the higher value of  $Gr/Re^2$ , the ceiling jet has a relatively larger amount of thermal energy which results in larger heat transfer rate to the ceiling plate. However, the net heat transfer to the vertical wall was found to decrease gradually with an increase in  $Gr/Re^2$ . This is due to the fact that at a higher value of  $Gr/Re^2$ , the flow penetration  $\delta_p$  is smaller. Thus, the thermal transport area is smaller on the vertical wall. Similar results were found in the case of a negatively buoyant vertical jet. Figure 11 also shows the total heat transfer to the ceiling and vertical wall.  $Q_{\text{total}}$  is the sum of  $Q_{\text{ceiling}}$  and  $Q_{\text{wall}}$ , as discussed earlier.

The effect of  $L/D$  on the total heat transfer is shown in Fig. 12. It is seen from this figure that the total heat transfer rate is larger at the higher value of  $L/D$ . This is due to the corresponding surface area of the ceiling plate being larger, which results in greater heat transfer.

The results presented here indicate the basic heat transfer processes associated with the heated ceiling jet which turns downward to give rise to a vertical negatively buoyant wall jet. The flow over the wall is very similar to that of a heated, downward, jet discharged adjacent to the wall. However, the transport over the ceiling, or the horizontal boundary, substantially affects the conditions obtained at the corner and thus the wall jet. The overall transport is determined by the inlet conditions, characterized by the mixed convection parameter  $Gr/Re^2$ , and by the horizontal distance  $L/D$  over which the heated jet interacts with the ceiling. The observed trends are found to agree with earlier work on ceiling jets and on wall jets and with the underlying physical mechanisms.

## CONCLUSIONS

A detailed experimental study has been carried out to investigate the basic heat transfer characteristics of a heated, horizontal, ceiling jet which turns downward at a corner to become a wall jet with opposing thermal buoyancy. Such buoyant ceiling jets are frequently encountered in many practical problems, such as enclosure fires and thermal energy storage systems. A heated two-dimensional jet of air is discharged horizontally adjacent to the underside of an isothermal ceiling plate. An isothermal vertical plate is fixed to the other end of this horizontal plate, making a right angle corner. The distance between the corner and location of jet discharge was varied, along with the width of slot through which the jet is discharged and the inlet velocity and the temperature of the jet. The discharged ceiling jet turns downward at the corner and then penetrates along the vertical wall to a finite distance as a negatively buoyant jet. In this study, the heat transfer characteristics of the resulting flow is reported. The following are the major conclusions of the study:

1. The local heat flux measurements on the ceiling and the vertical wall and the isotherms obtained in the flow indicate that the jet flow separates from the ceiling just before the corner and reattaches itself to the vertical wall at some distance below the corner. These results indicate the existence of a small recirculation zone at the corner.

2. A minimum in the heat transfer rate arises just upstream of the corner. This value recovers downstream, attaining a maximum just below the corner and then decaying downstream.

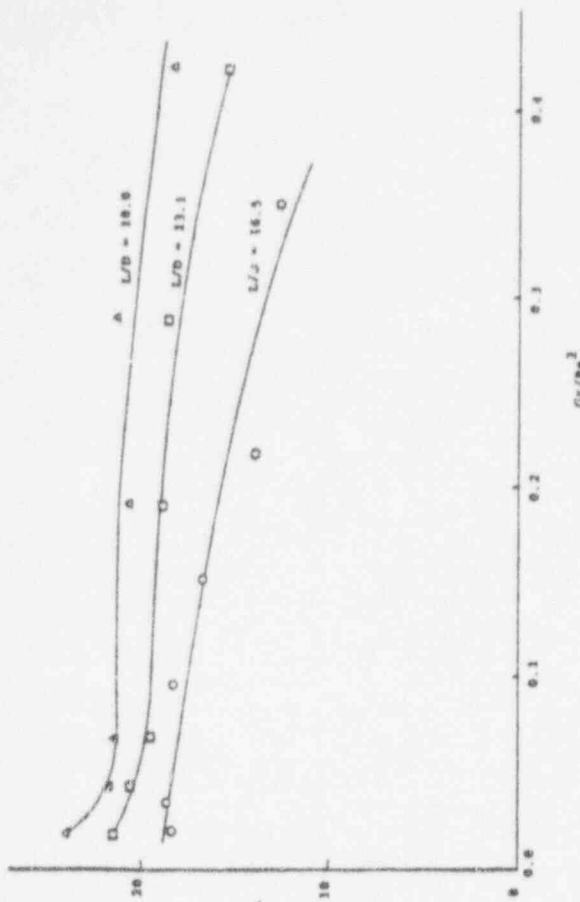


Fig. 10. Variation of the average Nusselt  $\overline{Nu}_D$  with  $Gr/Re^2$  for the total heat transfer from the ceiling and the vertical wall.

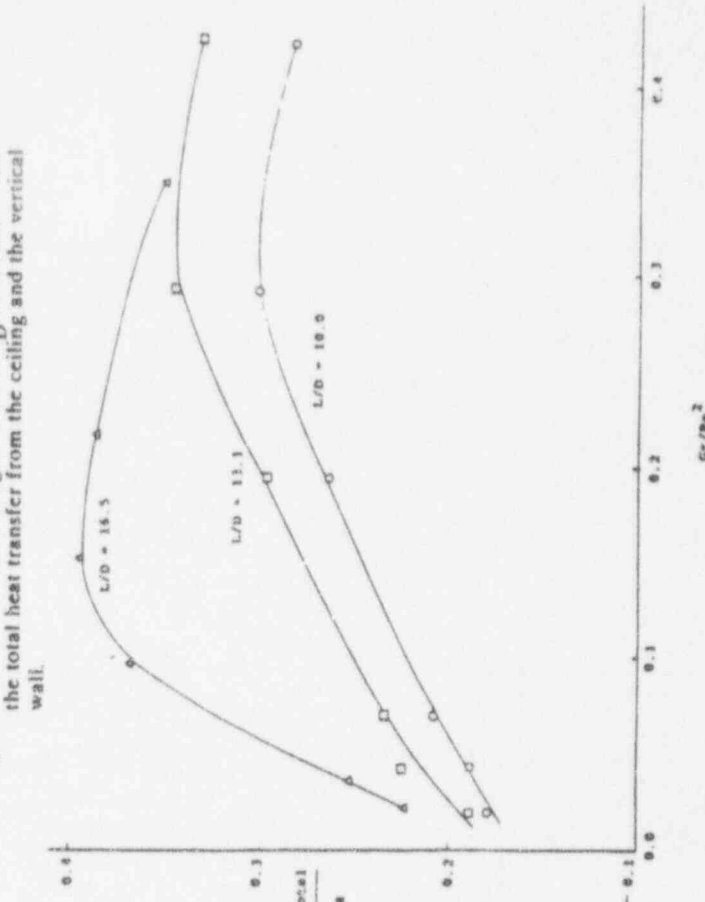


Fig. 12. Variation of the total heat transfer rate  $Q_{total}$  from the downward turning ceiling jet to the two isothermal surfaces with  $Gr/Re^2$ , at  $L/D = 100, 131$  and  $165$ .

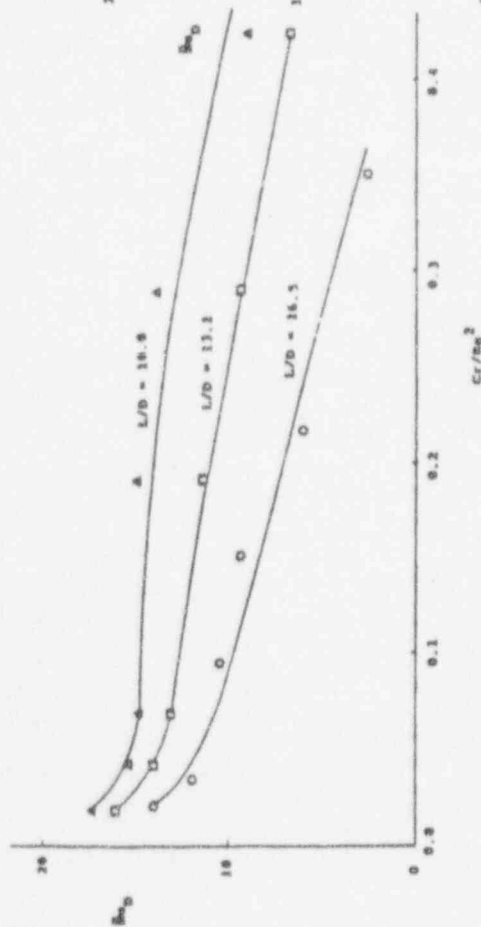


Fig. 9. Variation of the average Nusselt number  $\overline{Nu}_D$  with  $Gr/Re^2$  for the vertical wall at different values of  $L/D$ .

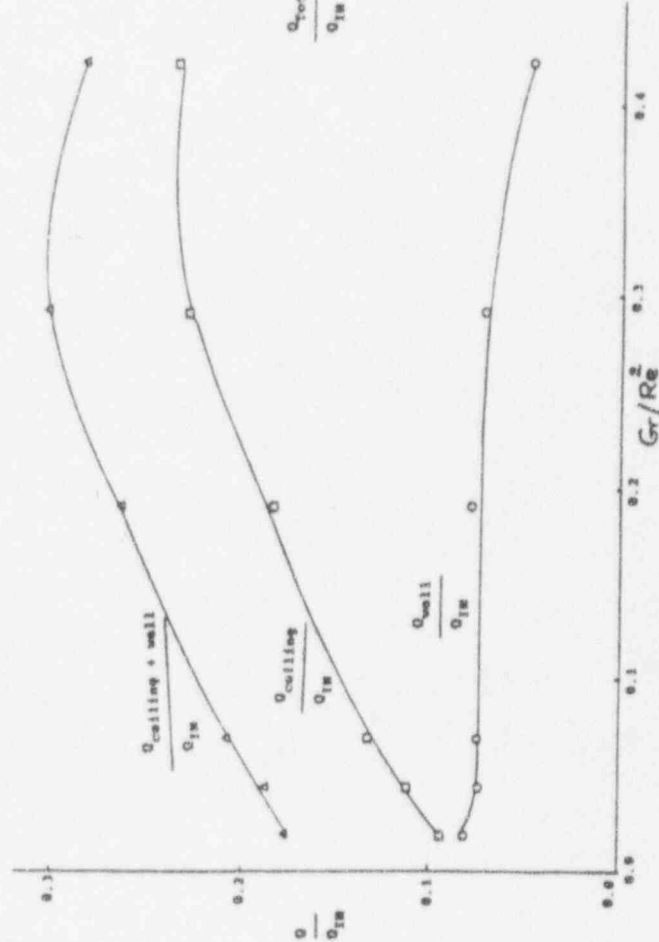


Fig. 11. Variation of net heat transfer rate  $Q$  to the ceiling and the vertical wall with  $Gr/Re^2$  for  $L/D = 100$ .